UPGRADING OF THE PUERTO RICO STORM SURGE ATLAS

(BY INCLUSION OF DYNAMIC WAVE SETUP, WAVE RUNUP, AND OVERTOPPING)

Submitted to the

Puerto Rico Coastal Zone Management Program/NOAA

and the

Department of Natural and Environmental Resources of Puerto Rico

by

Jaime Reniel Calzada

and

Aurelio Mercado-Irizarry

FEBRUARY 2020

SCOPE OF WORK

To be clear and precise, here we define the storm surge (also known as the storm tide) as the **stillwater** anomalous sea surface elevation due to the superposition of the wind, pressure, and (static) wave setups (see Figures 1 and 2). Wave setup can be divided into a (quasi) static component and a dynamic component. The dynamic component is also known as infragravity waves (periods above 25 sec up to a few minutes); some people call them "sneaker waves". The high frequency part of the wind wave spectrum is defined as wind waves with periods up to about 25 seconds. Between 26 seconds and up to about 3-5 minutes comes the infragravity wave spectrum. The gradient of the wave momentum radiation stresses produces (static) wave setup, which raises sea level in the nearshore, and contributes to the storm surge. The quasi-static part of the wave setup is typically known simply as wave setup, with time scale of tens of minutes. It is known that it can contribute a large percentage of the overall storm surge. At the same time, the dynamic wave setup, with time scales of up to 3-5 minutes, can also be present and further increase the water elevation on time scales shorter than the static wave setup. In both cases, the increased sea surface elevation serves as a ramp for the high frequency waves moving inland, thus allowing them to dissipate their energy further inland.

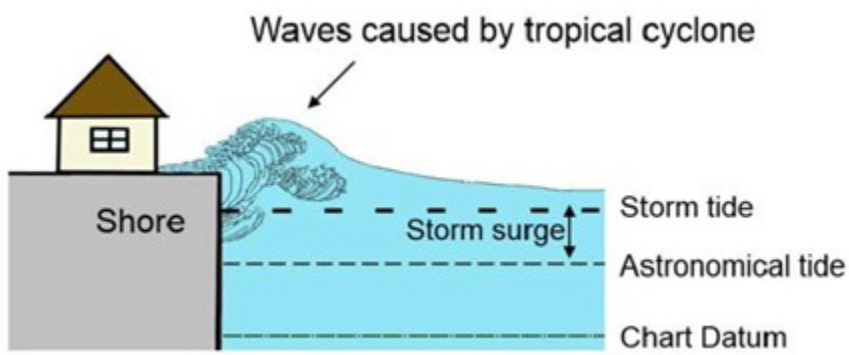

Figure 1 – Schematic showing the concept of storm surge plus high-frequency waves propagating on top of the storm surge. The case shown here is where the storm surge does not overtop the seawall but wave crashing against the seawall still cause flooding inland.

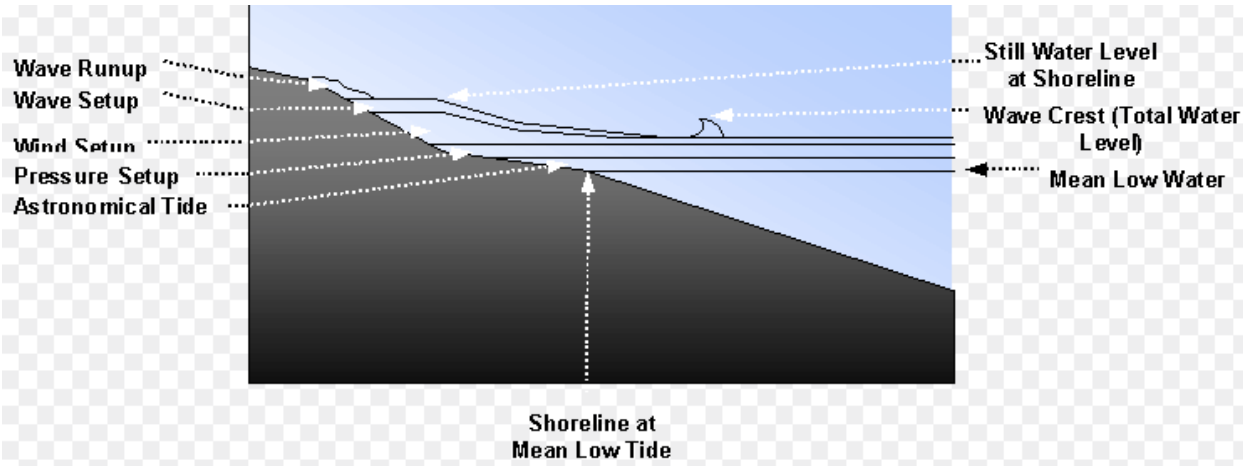

Figure 2 - This figure summarizes what has been described up to now. Storm surge models evaluate the flooding due to (see legend on left side of the figure) astronomical tide, pressure setup, wind setup, and (static) wave setup. With the model we are using (XBeach) we are additionally adding (see legend on right hand side of figure) wave crest elevations, wave runup, and overtopping. The (maximum) wave crest elevations will be given relative to the local terrain elevation. They are similar to FEMA's Base Flood Elevations (BFE), but the BFE are given along 1-D transects, and relative to MSL. These transects can be separated by several kilometers, sometimes missing important locations.

Figure 3 shows a schematic of what we are describing.

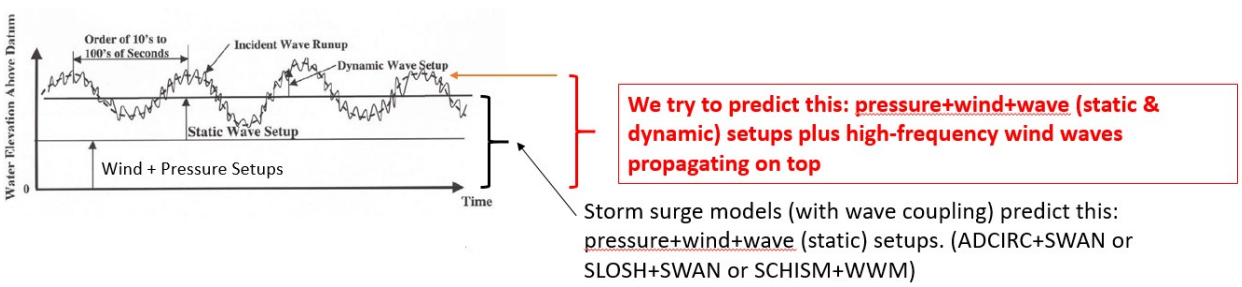

Figure 3 – Schematic illustrating the breakup of the overall water depth into

Islands like Puerto Rico have very narrow shelves, which serve to protect against high storm surges (Mercado, 1994), but not offering the same level of protection against wave energy like the wide, and shallow, continental shelves (see Figure 4). In the (tropical) island situation, if there are no protecting fringing reefs, the wave energy is mostly dissipated right against the shoreline, a shoreline which is displaced inland due to the storm surge. Consequently, dunes and any type of coastal infrastructure, will suffer the direct effect of wave breaking, erosion, wave runup and overtopping. We can safely say that in Puerto Rico the coastal damage due to the storm surge is secondary to the damage due to wave action. This has been corroborated in all landfalling hurricanes that have affected the island, and was recently verified by the passage of Hurricanes Irma (2018), Maria (2018), and the extratropical storm Riley (2018). Thus the importance of being able to model these processes.

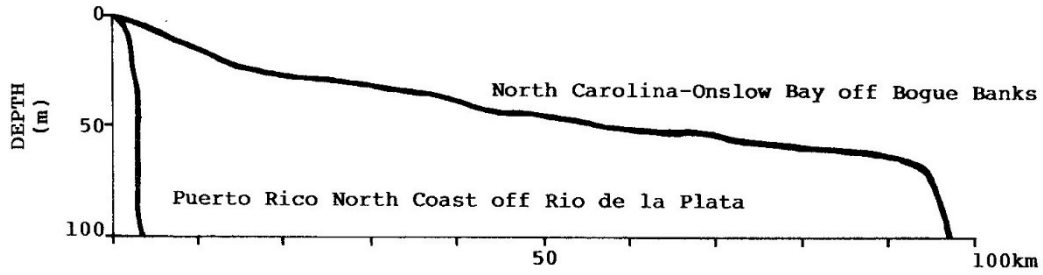

Figure 4 – Profile of depth vs distance off North Carolina versus a typical one off the north coast of Puerto Rico. The North Carolina profile explains the occurrence of large storm surges, while the Puerto Rico profile explains the small storm surges around the island. In the case of Puerto Rico wind waves can reach the coastline without much dissipation, thus producing large runups and overtopping. Taken from Mercado, 1994.

This was nicely quantified by Rodriguez et al. (1994) with Hurricane Hugo in 1989. Figure 5 shows the route followed by Hugo during its closest approach to the island. Figure 6 shows the measured storm surge and runups at the six locations shown inside parenthesis in Figure 5. The data nicely illustrates the disparity between storm surge and wave runup measurements.

That wave runup and overtopping can do a lot of damage even in the absence of a direct hurricane hit is

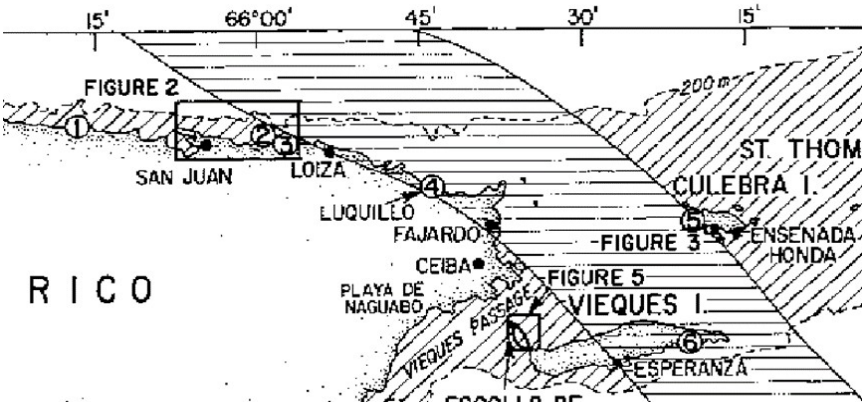

Figure 5 – Route followed by Hurricane Hugo in 1989 during its closest approach to Puerto Rico. The eastern part of the main island is shown together with its two island municipalities (Vieques and Culebra). Six numbers inside parenthesis are shown, where storm surge and wave runup were measured.

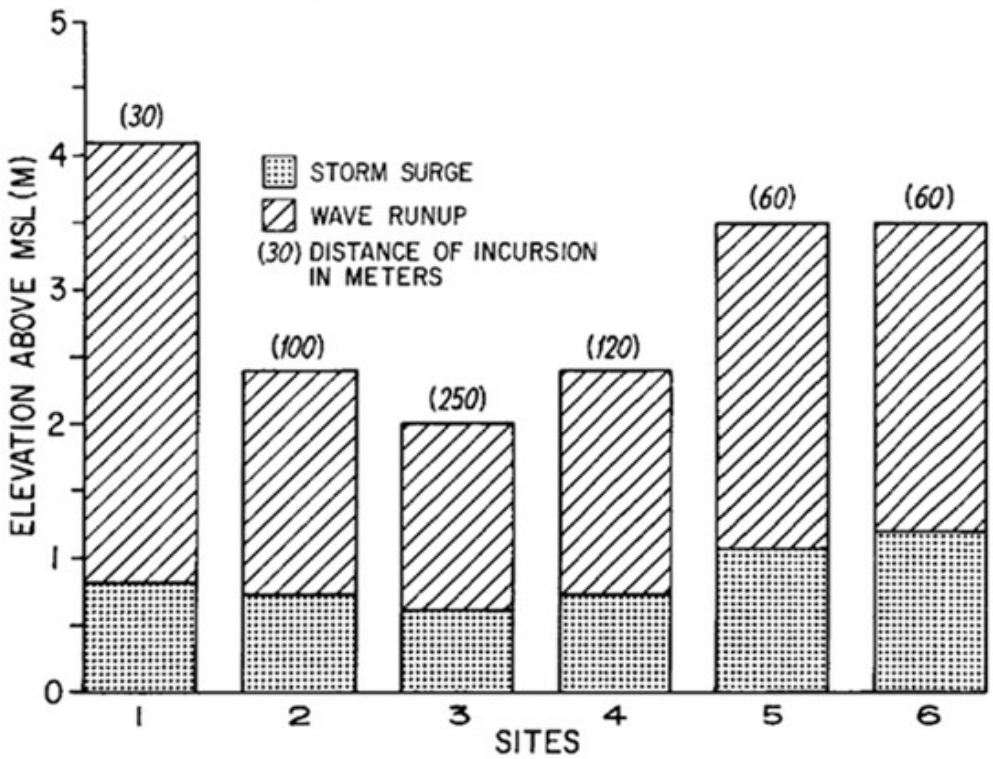

Figure 6 – Storm surge and wave runups measured by Rodriguez et al. (1994) at the six locations shown in Figure 4. Quoting from Rodriguez et al., "Storm surge was similar for the six sites, but wave runup varied as a function of location due to the variability of the coastal geomorphology, both due to the bottom profile and horizontal shoreline variability. Landward incursion of storm water is given by the values in parenthesis at the top of each column. Coastal flooding was severe in low lying areas (sites 2, 3, 4). Although storm wave swash was greater in steeper profile areas (sites 1, 5, 6), overall incursion was less."

demonstrated by the damage produced by extratropical storm Riley in March 2018. Wave periods as long as 17 sec were measured at a CariCOOS wave period. Figure 7 shows a schematic of the beach profile just north of Pico de Piedra, Aguada, a coastal city located at the west coast of Puerto Rico. The highway lies several meters above the sea surface. At the most, of the three storm surge components (wind + pressure + static wave

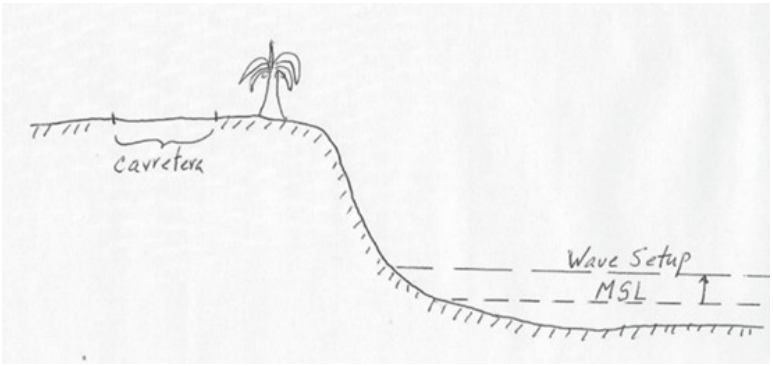

setups) only static wave setup could happen at the site since there was no wind nor atmospheric pressure anomaly at the moment.

Figure 7 - Schematic of beach profile at Pico de Piedra, Aguada. Since the coastal damage was due to extra-tropical storm Riley, only wave setup is drawn as a potential sea level increase factor. The photo shown in Figure 5 was taken from across the street (carretera) looking seaward.

Figure 8 (a snapshot from a video) shows the effects of wave overtopping (right snapshot) that happened at some instant after minutes without nothing happening (left snapshot). What is seen is consistent with the presence of an infragravity (or sneaker) wave reaching the site.

Figure 8 – Two frames of a video taken when an apparent sneaker wave overtopped the beach profile shown in Figure 7.

Figure 9 – Four snapshots from a video taken at Montones beach, in Isabela, during the Riley event in March 2018. Video provided by Dr. Sandra Cruz Pol.

Also related with extratropical storm Riley, Figure 9 shows a sequence of four snapshots from a video documenting what seem to be sneaker waves attacking coastal infrastructure in Isabela, Puerto Rico, at the north coast. The infrastructure was constructed inside the so-called “servidumbres”, which is a 20 meters wide zone adjacent to the inland limit of the so-called “zona maritime-terrestre”. This infrastructure lies outside the reach of the storm surge (stillwater) elevation.

The message from all of this is that in islands like Puerto Rico, if one does not include wave runup and overtopping in coastal flood mapping, one is highly underestimating the coastal flooding and damage potential. And this includes the potential presence of infragravity, or sneaker, waves.

This is illustrated in Figure 10 where the left image shows a coastal flood map in which no wave runup/overtopping was included versus what happens when overtopping/runup is included (right image). ***It is the scope of this project to prepare the first set of storm surge maps for Puerto Rico which include the effects of wave runup and overtopping as part of the overall storm surge. The potential presence of infragravity wave dynamics has not been investigated, but the model (XBeach) has been shown elsewhere that it is capable of simulating them. This will be investigated later.***

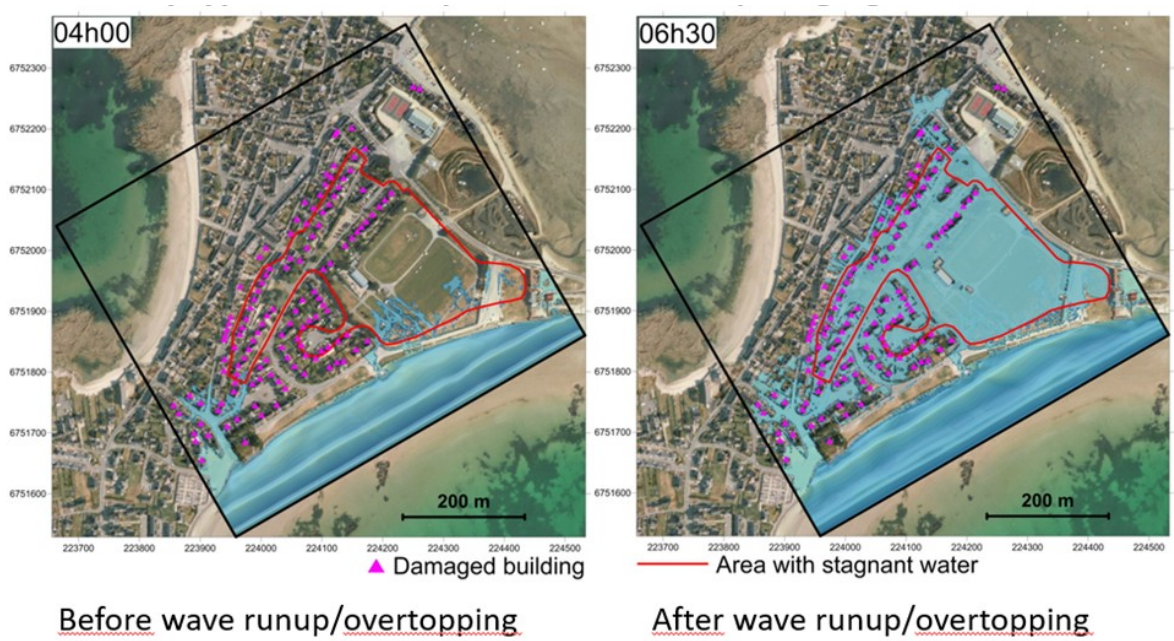

Figure 10 – Image of coastal flooding with (left image) and no (right image) wave runup/overtopping.

PREVIOUS WORK

The island of Puerto Rico lies in the hurricane alley of the Caribbean Sea. It is therefore important to have estimates of the inland flooding capabilities of storm surges due to hurricanes for multiple reasons. The Federal Emergency Management Agency (FEMA) produces storm surge flood maps based on the so-called 100-, and 500-years surges, something which can be useful for insurance purposes, but knowing the potentially floodable areas due to category 1 to 5 (Saffir-Simpson scale) hurricanes is a very useful planning, emergency, and design, tool. Typically, in the Atlas the storm surge model is run several times along parallel tracks covering the whole island, for hurricanes covering the five Saffir-Simpson scales, and maximum storm surge elevations are stored for each computational cell.

The first version of the Puerto Rico Storm Surge Atlas was prepared in the early 1990s using the National Weather Service SLOSH model (Mercado, 1994). The SLOSH model only computed wind and pressure setup, and recognizing the important contribution of wave setup (Kim et al., 2010; Hoeke et al. 2015), the static version of this component was added “after the fact” using “back-of-the-envelope” estimates of the static component of the wave setup. This same model had been used previously to prepare the Flood Insurance Rate Maps (FIRM) for a Flood Insurance Study (FIS) sponsored by the Federal Emergency Management Agency (FEMA) (Mercado, 1994), and a short explanation of the

methodology involved is warranted (as it was carried out in the 1980's and 1990s). In the preparation of the FIRMs wave runup and overtopping is included, but in a very simplified way. One dimensional transects are obtained at several locations along the island's coastline (see Figure 11 for the northeast quadrant of the island), and wave runup, and overtopping (if warranted), is carried along these transects using very simple FORTRAN programs (RUNUP.FOR and WHAFIS.FOR - Wave Height Analysis for Flood Insurance Studies). The results are then interpolated for the coastline sections in between the transect locations. No wave refraction and diffraction is considered.

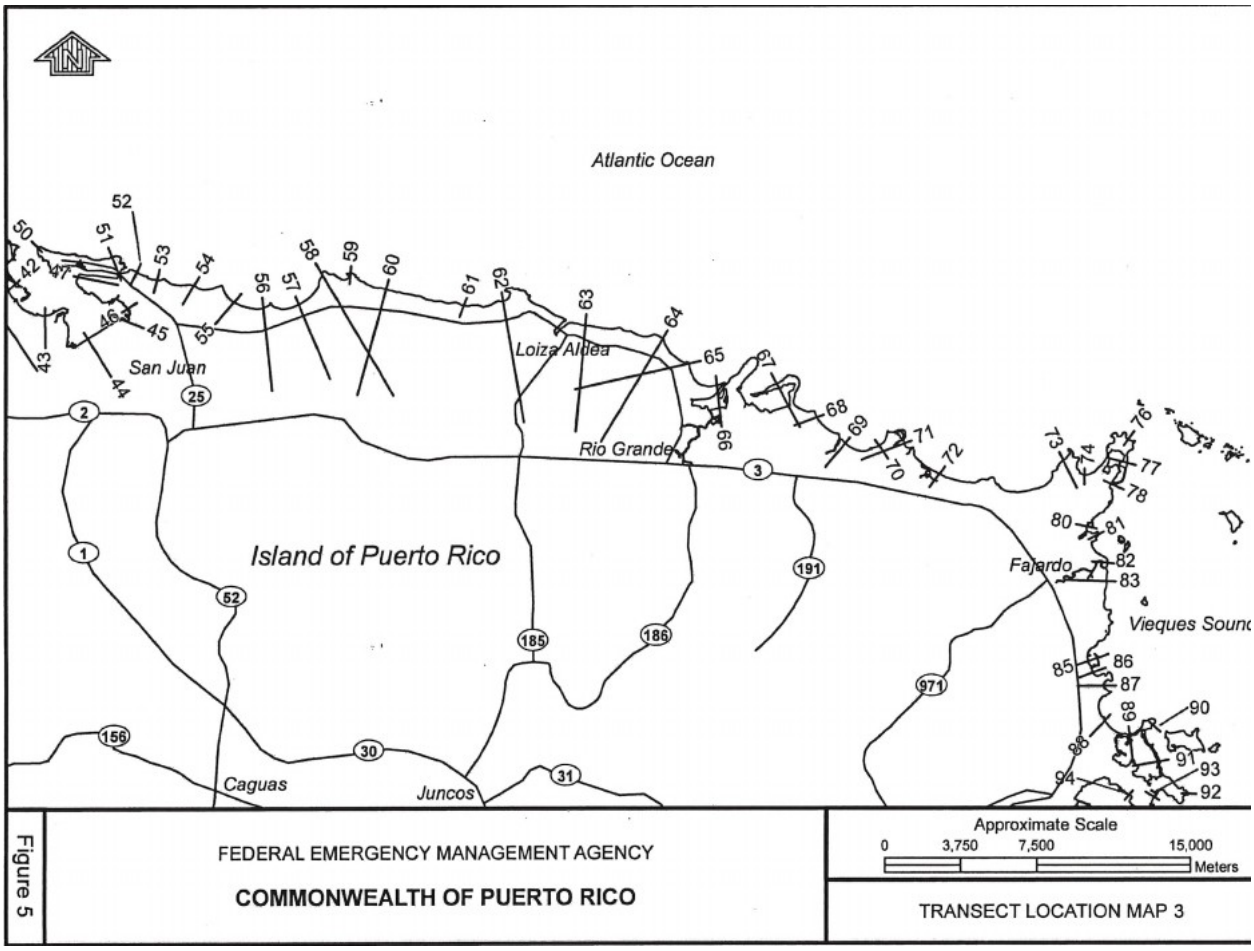

Figure 11 – Figure showing the locations where wave transformation analysis, and runup/overtopping/erosion, transects were located in the June 2007 Flood Insurance Study.

It should be mentioned that FEMAs methodology also includes the possibility of dune erosion/breaching, if required. The model used in this study (XBeach) also has the physics for modeling beach, and dune, erosion, but this was not considered in the study concerning this report.

The coastline of Puerto Rico is very convoluted, and the application of the transect methodology to compute wave runup and overtopping would require thousands of

transects. The island's coastline is not at all like the kilometers-long quasi-straight beaches seen in the continental United States. In the FIRMs that were available until 2007 only 263 transects were used, and results interpolated in-between transects. The transect separation can exceed several kilometers, making the interpolation of wave effects in between transects close to black magic. This is very dangerous since almost all of our coastline is highly populated. As an example, no transects were located in Punta Miquillo, Rio Grande. As a matter of fact, the presently valid FIRMs are also based on just the same number of transects.

This methodology required improvement, and in 2015 the Puerto Rico Storm Surge Atlas was upgraded by using high-resolution bathymetry and topography, and including static wave setup. This was done using the coupled version of ADCIRC and (unstructured) SWAN models (Dietrich et al., 2012). Now the anomalous stillwater due to wind setup, pressure setup, and static wave setup, were computed in the modeling. The Atlas can be seen at

http://coastalhazards.uprm.edu/downloads/Storm%20Surge%20Modeling%20in%20Puerto%20Rico%20in%20Support%20of%20Emergency%20Response-V10.pdf – the study report is titled "Storm Surge Modeling in Puerto Rico in Support of Emergency Response, Risk Assessment, Coastal Planning and Climate Change Analysis", by Jose Benitez and Aurelio Mercado, 2015.

The 2015 Atlas (and maps) can also be seen at https://www.caricoos.org/map/storm-surge - CariCOOS, and at

http://drnamzc.maps.arcgis.com/apps/webappviewer/index.html?id=ab48c72f102b440ab021e59c3f1f2cdb (DRNA/CZMP)

But there was still missing the inclusion of dynamic wave setup, due to infragravity waves, and wave runup and overtopping.

Recognizing that in tropical islands like Puerto Rico storm surges tend to be relatively small, and that most of the coastal damage is due to wave action, it is the purpose of this project to map up to where wave action penetrates on top of the storm surge which, with some exceptions, should extend further inland than up to where the storm surge (stillwater) penetrates, as was documented by Rodriguez et al., 1994 (see Figure 6).

OBJECTIVE OF THE PROJECT

As we have seen, in tropical islands storm surges are relatively small due to the deep waters reaching close to shore. Almost all of the coastal damage, and flooding, is due to wave runup and overtopping. People living along the north coast of Puerto Rico attest that the extratropical storm Riley (with long-period swells) did more coastal damage

than hurricane Maria. Storm surge maps, as the ones that were prepared by Benitez and Mercado (2015), using the coupled ADCIRC and SWAN models, do not include runup and overtopping, although static wave setup is included using the radiation stresses computed by the SWAN wave model, which are fed automatically to the circulation model, ADCIRC, to estimate the static wave setup component.

Therefore, in order to carry out a more accurate estimate of coastal flooding and damage, one needs to include wave runup and overtopping (see Figure 2). Over the years the transect-based 1-D parametric models have been developed for this purpose, but it has been shown that they are not accurate. Especially so in a tropical island with such an inhomogeneous, convoluted, coastline, surrounded in many places by fringing reefs and cemented sand dunes, with very irregular bottoms and shoreline geometry. Therefore, a phase-resolving wave model will be used in two-dimensions, not one-dimension as has been used elsewhere even for the XBeach model.

WAVE MODEL

Directly quoting from https://oss.deltares.nl/web/xbeach/,

> "XBeach is a two-dimensional model for wave propagation, long waves and mean flow, sediment transport and morphological changes of the nearshore area, beaches, dunes and backbarrier during storms. It is a public-domain model that has been developed with major funding from the US Army Corps of Engineers, Rijkswaterstaat and the EU, supported by a consortium of UNESCO-IHE, Deltares (formerly WL|Delft Hydraulics), Delft University of Technology and the University of Miami."

For validation information, please see https://oss.deltares.nl/web/xbeach/validation. There are many more references where validation tests are presented.

The model is updated constantly. In our case we used version 1.23.5387M XBeachX BETA release. It was run in its phase-resolving, non-hydrostatic, mode. It should be emphasized that the model used (XBeach) is capable of including dynamic wave setup (a.k.a., infragravity waves). We have not had the time to test for the presence of dynamic wave setup. But since the model was run in its non-hydrostatic version (which is very time consuming), it has included in it the full spectrum of wave dynamics which is capable of simulating, and this includes infragravity, or sneaker, waves.

WIND MODEL

Since we will be using wind forcing, it is important to mention the type of wind forcing that XBeach uses:

$$\tau_{sx} = \rho_a C_d W \|W\|$$

$$\tau_{sx} = \rho_a C_d W \|W\|$$

where τ_s id the wind stress, ρ_a is the air density, C_d is the wind drag coefficient, and W is the wind speed. The default value of Cd was used, 0.002. Although recent research (Soloviev et al., 2017) hints that C_d is a function of wind speed (see Figure 12), the value of 0.002 seems to be a reasonable one for all wind speeds used.

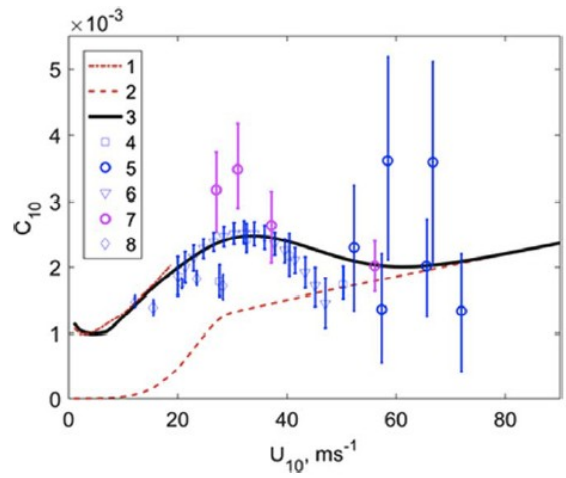

Figure 12 – Air-sea wind drag coefficient as a function of wind speed at 10 meters elevation (Soloviev et al., 2017). The XBeach default value of 0.002 was used in this study.

METHODOLOGY

XBeach is a very complicated model, still in development, with many variables as input, and as output. Most of the input variables have default values, and it is recommended by the developers to, as much as possible, use default values.

The following is an example of the input parameter file (PARAMS.txt) that the model requires as input. As will be shown below, twenty-seven computational grids were used to cover the whole island at 3 meters' resolution (wave runup is very site sensitive). It only shows the input variables of relevance for this project. Only a very small fraction of the total.

*Sample **PARAMS.txt** file (given as input to the model in our computer cluster, where the model was run in parallel using 600 CPU processing elements. The words inside square brackets next to the variable briefly describe the purpose of the variable.)*

```
%%%
```

%%%

Cd = 0.0030 [wind drag coefficient]
windv = 55.5600 [Wind velocity, in case of stationary wind; in m/s; here is where we decide upon the hurricane category]
windth = 90.0000 [Nautical wind direction, in case of stationary wind]

%%% Output variables %%%%

dynamic). So it looks as if our results will contain a double contribution from both wind and static wave setup. But to a good approximation we can assume that the zs0 value contains negligible contributions from wind and static wave setup since the outer boundary (the deep water boundary) lies in deep water (more about this in the next paragraph), where the wind and static setups are very small. The only non-negligible setup contribution in the adopted zs0 value should be the pressure setup, which is exactly the one that XBeach does not include. The wind and wave setups (static and dynamic) are computed by XBeach.

Since the model is forced by, amomg others, wind waves, in the *params.txt* file the name of a file is given (jonswap.txt) where information is supplied to the model about the principal wave statistics used to force the model. A sample jonswap.txt file is given below.

Sample **jonswap.txt** file:
Hm0 = 13.6263 [significant wave height for model forcing]
Tp = 15.20307568 [peak wave period of the time series used for model forcing]
mainang = 180.0000 [main wave train direction]
gammajsp = 3.3 [Jonswap Peak Enhancement factor]
s = 15.414032 [diretional spectrum spreading factor]
fnyq = 0.1600 [Nyquist frequency for the wave sepctrum]
tma = 1 [includes finite-depth effects into the Jonswap spectrum, convertig it to a TMA spectrum]

Another limitation of phase resolving non-linear shallow water models has to be mentioned. These are shallow water models that are improved by introducing dispersive effects, which strict shallow water models do not iinclude. By including dispersive effects shallow water models can be started from deeper waters. In the case of XBeach this was done by introducing a non-hydrostatic pressure component to a shallow water model. But, in any case, the models have a deep water limit, which is given by setting a maximum value of kh, where k is the wavenumber (2pi/wavelength), and h is the local water depth. In the case of XBeach this maximum value is $(kh)_{max} \approx 1$. Once k_{max} is decided upon, one can determine the h_{max} that can be used. In our case it was decided to set a maximum depth of 60 m. But the computational grid is extended (with a constant value of 60 m) further offshore of the location of the 60 m isobath in order to allow for several waves (corresponding to the peak wave period, Tp) to fit between the outer boundary (where the input waves are generated) and the location of the 60 m isobath. The grid boxes shown in Figure 21 satisfy this requirement. As a consequence, all depths deeper than 60 m are set equal to 60 m (until the outer boundary is reached). Figures 26 and 27 show a 3-d plot, and contour plot, of the bathymetry/depth given to XBeach for grid 2, where one can see what was just discussed above.

The wave spectrum assigned to the outer boundary (deep water) of each grid is constructed assuming a TMA spectrum, with the significant wave height, Hm0, which is also obtained from the SWAN results obtained by Benitez & Mercado (2015), for each hurricane category. The same for the Peak Wave Period, Tp. The main wave propagation direction is assumed to be perpendicular to the main trend of the coastline (along the wind forcing).

The setup of the model is that the x-axis points towards shore, and the y-axis follows a right-handed coordinate system. The model is run in UTM units, meters. The results are then transformed to geographic, WGS84 degrees, coordinates.

The hurricane parameters used are obtained from Table 1 in Benitez & Mercado (2015) (for this project only the Vmax column was used):

Table 1 – Hurricane statistics used for the five Saffir-Simpson categories.

Cat	Central pressure (mb)	RMW (nm)	Vf (kn)	Vmax (kn	Separation between tracks (nm)
1	980	25	10	78	5
2	969	25	10	92	5
3	950	20	10	108	5
4	926	15	10	131	5
5	900	10	10	150	5

The Vmax values (maximum wind speed; column 5) are used for the “windv” input parameter in PARAMS.txt. Seeking to get worst case results, the wind direction “windth” was taken as perpendicular to the main trend of the coastline. Note that the category 5 scale has no upper bound, so we set it at 150 knots (173 mph; sustained winds). In hindsight, this upper limit now seems too low. Note that the wind speeds are in knots and that, for each hurricane category (except category 5, which has no upper bound), the wind speed value used does not correspond to the maximum wind speed in the given hurricane category. Vmax was determined by the following equation: Vmax = 0.75x(wind speed range for a given category) + minimum wind speed in that range. For example, for a category 3, whose winds vary between 96 and 112 kn, Vmax = 0.75(112 - 96) + 96 = 108 kn. For a category 2 it comes out as Vmax = 0.75(95 - 83) + 83 = 92 kn.

To summarize,

- XBeach was run inside each of the grid boxes shown in Figure 21, at 3 x 3 meters resolution.
- An initial, spatially uniform, anomalous sea surface elevation was applied all over the grid. The value applied was obtained from Benitez & Mercado (2015). This initial sea surface elevation produced what we can call *passive flooding*, like the

so-called bathtub flooding used for sea level rise flood mapping. This flooding is there right from the start of the computations

- The Significant Wave Height and Peak Wave Period used to construct the forcing wave spectrum (a TMA spectrum) were also obtained from the results of Benitez & Mercado (2015).
- The maximum water depth allowed in the computational grid was 60 m.
- The non-hydrostatic XBeach version was used, and it was run in 640 processing elements cluster.
- The length of simulation time carried out for each computational grid was 3900 seconds, of which the first 300 seconds corresponds to spin up time.

DATA SOURCE

Figure 13 below shows the data sources which were used to prepare the computational grids at 3 m by 3 m resolution. Due to the high resolution required for running XBeach in nonhydrostatic mode, the island was broken up into several computational grids as shown in Figure 21. All of the data is based on high-

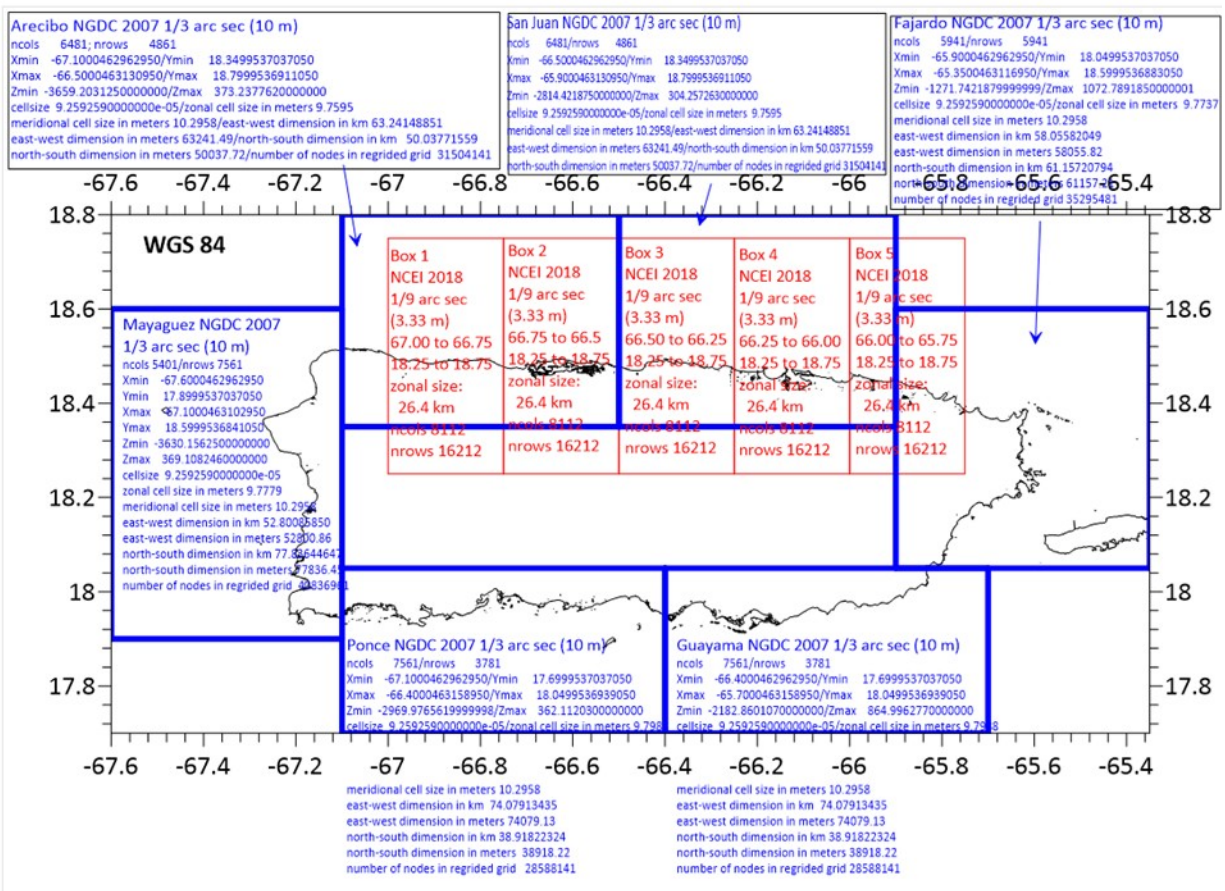

Figure 13 – Schematic showing the outline, and basic statistics, of the Digital Elevation Models (DEMs) used in this study.

resolution Lidar data obtained over the years, and which is bare earth. For tsunami flood mapping purposes, the National Geophysical Data Center (NGDC), now known as the National Centers for Environmental Information (NCEI), had made available six DEMs at 1/3 arc sec (approximately 10 m) resolution covering all of the coastline of the main island of Puerto Rico (see blue boxes in Figure 13). Recently, five 1/9 arc seconds (approximately 3.33 m) resolution were prepared for the north coast of the island (see red boxes in Figure 13). For the grids shown in Figure 21 that fall completely within the red boxes, the 1/9 arc seconds data was used, interpolated from 3.33 m down to 3 m. For the rest of the island not covered by the 1/9 arc seconds DEMs, the only option was to use the 10 m DEMs interpolated down to 3 m.

It is important to emphasize that, no matter the model, flooding results are as good as the input topography supplied. The maps in the areas outside the red boxes in Figure 13 are of 10 m resolution, which will be interpolated to 3.3 meters (1/9 arc seconds) in order to be consistent with the topography given inside the red boxes. Although this is not the correct way of doing this, there is no other choice if we want to run the non-hydrostatic XBeach model. This can be seen for Grid 12 (Fajardo area; see Figure 21 for an outline of the computational grids), for which not even the large marinas are “seen” by the model. As an example, Figure 14 shows Sunbay Marina in Fajardo. The red curve shows the z = 0 m elevation contour prepared using the input topographic/bathymetric data given to XBeach, showing that the Marina is not represented in the modeling (the painted areas are the coastline areas flooded by the model, with elevations given as sea surface elevation above the local terrain elevation). It is quite possible that the 1/9 arc seconds DEM for Fajardo will show the marinas. Meanwhile, anyone wishing to model hurricane effects on these marinas will have to supply detailed bathymetry/topography and re-do the modeling again. The same holds for Puerto Chico (Figure 15), Isleta Marina (Figure 16), and El Conquistador (Figure 17). The only marina in the Fajardo area that seems to be (almost) completely “seen” by the model is Puerto del Rey, Fajardo (see Figure 18).

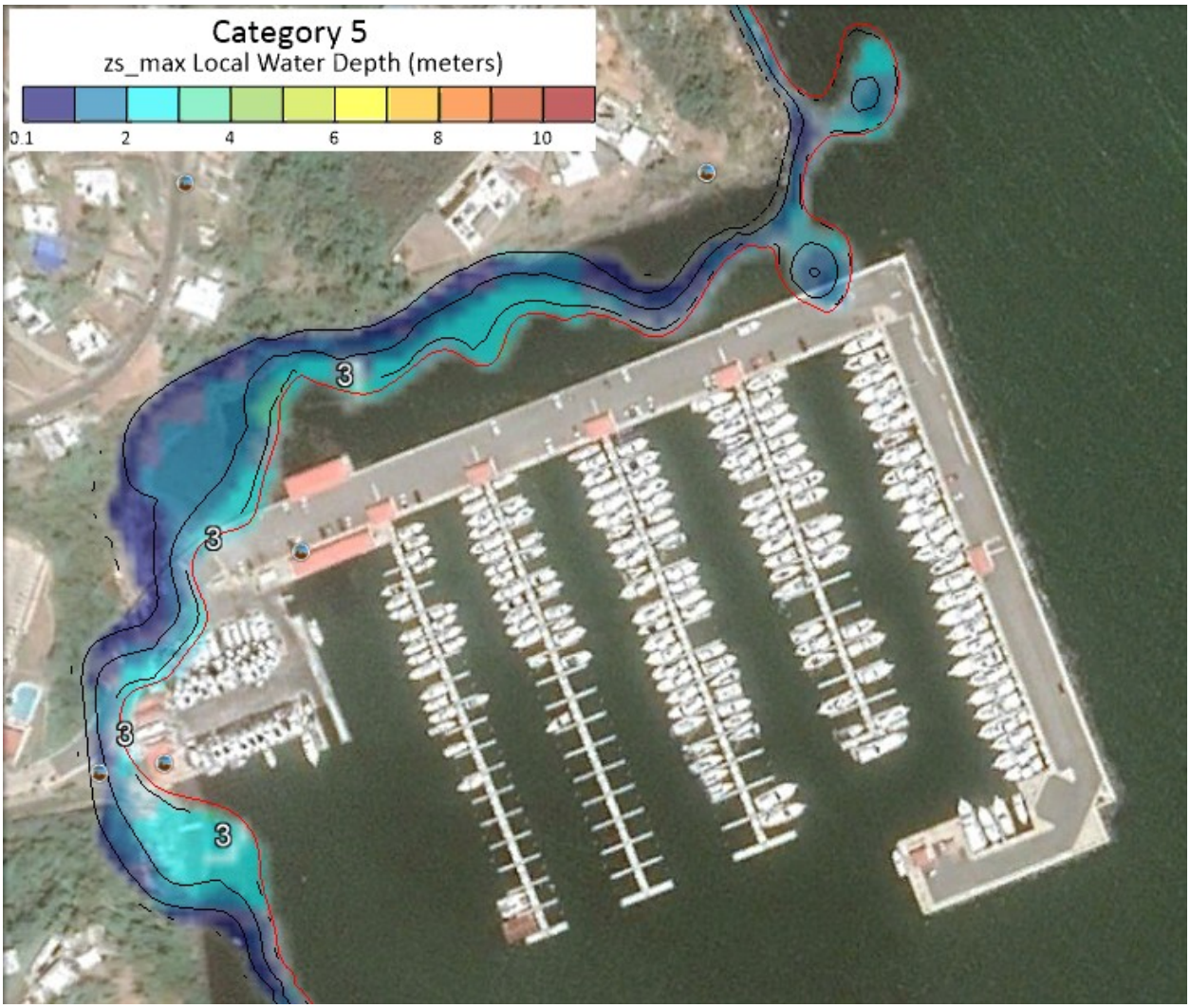

Figure 14 – Sunbay Marina in Fajardo, showing that the marina is not resolved by the DEM used. The original DEM has a resolution of 1/3 arc seconds (≈ 10 m), and it was interpolated to 1/9 arc seconds (≈ 3.33 m).

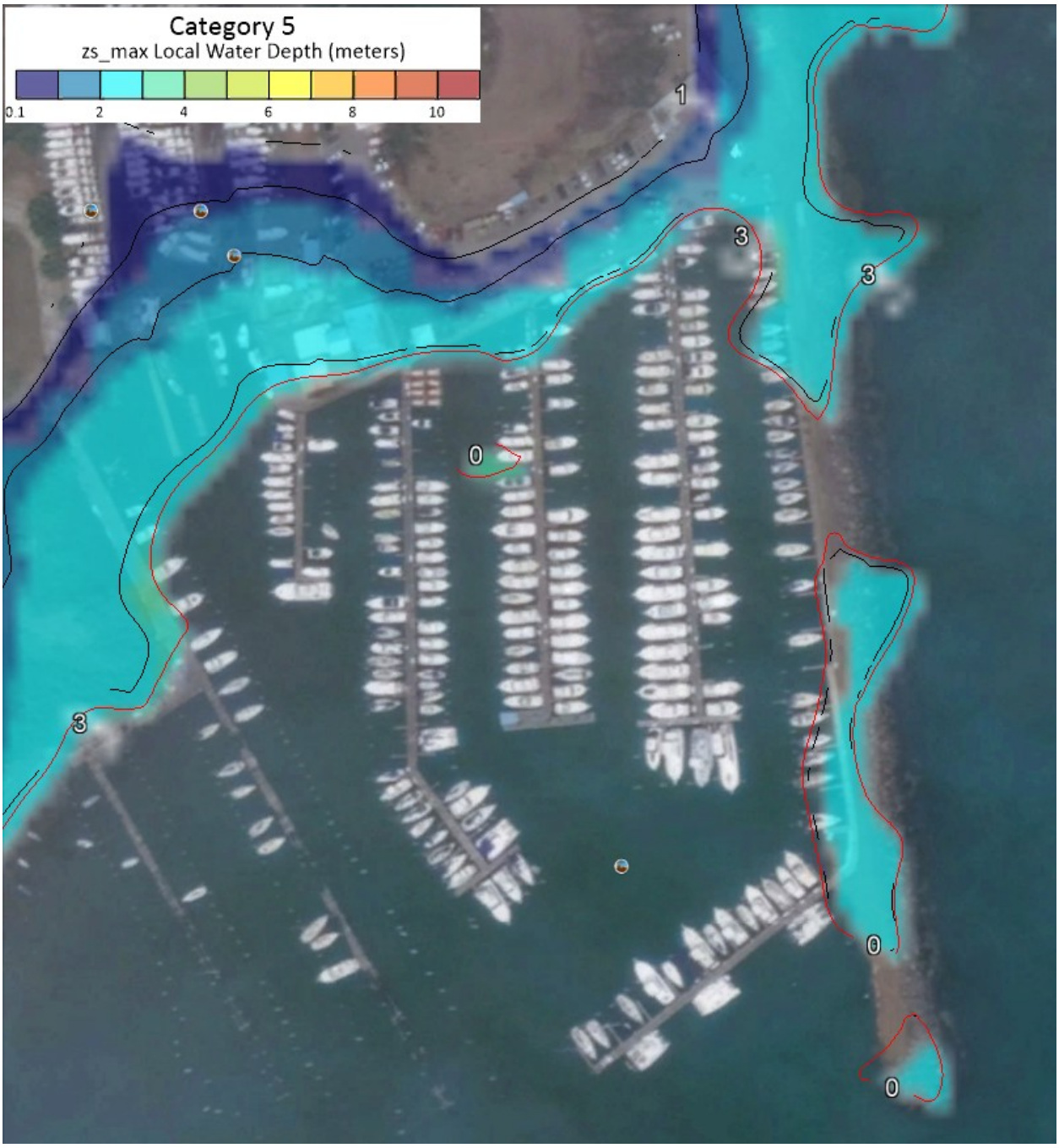

Figure 15 - Marina Puerto Chico, Fajardo. The marina is partly resolved by the DEM used. The original DEM has a resolution of 1/3 arc seconds (≈ 10 m), and it was interpolated to 1/9 arc seconds (≈ 3.33 m).

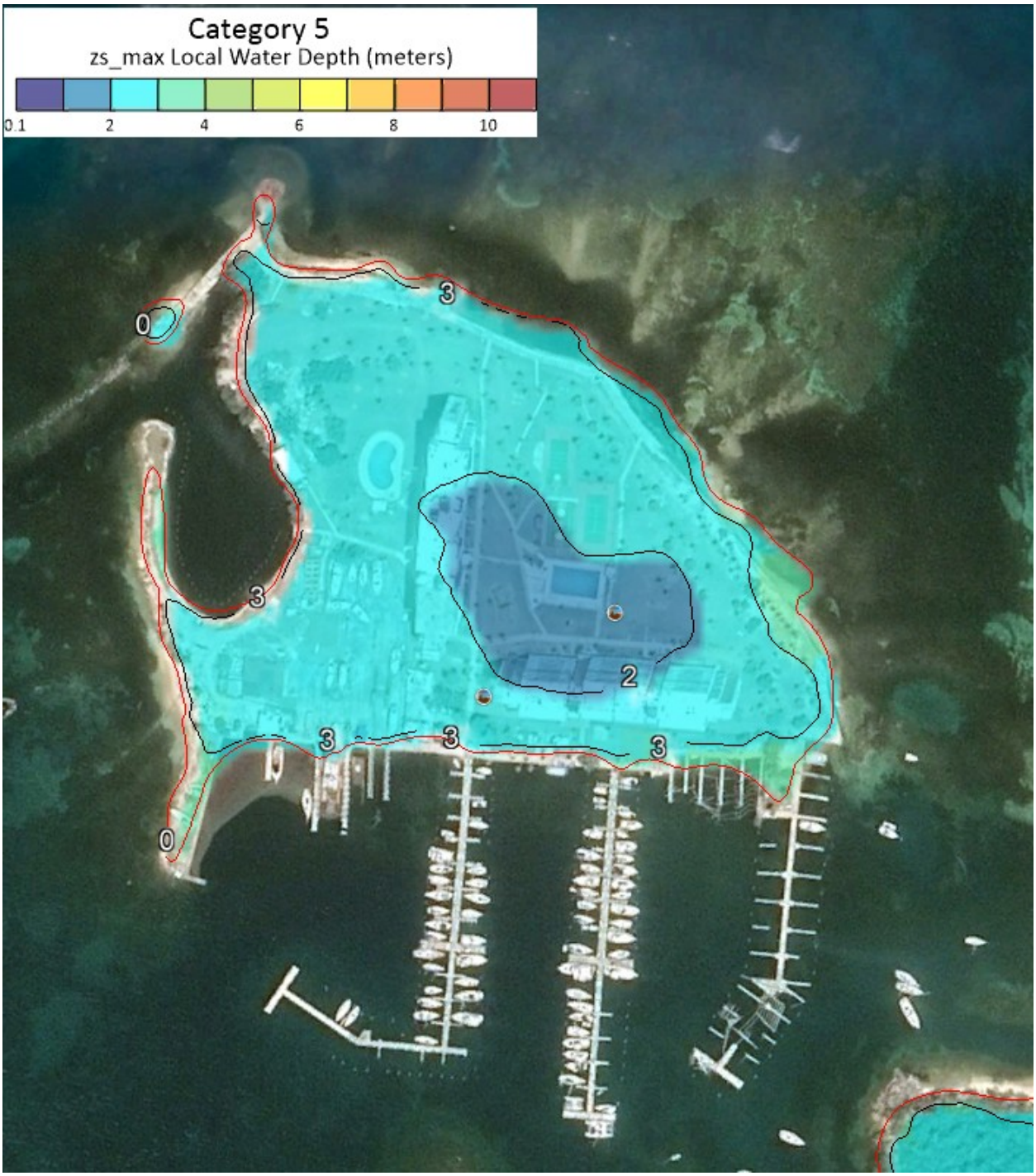

Figure 16 – Isleta Marina, Fajardo. The docks obviously are not "seen" by the model.

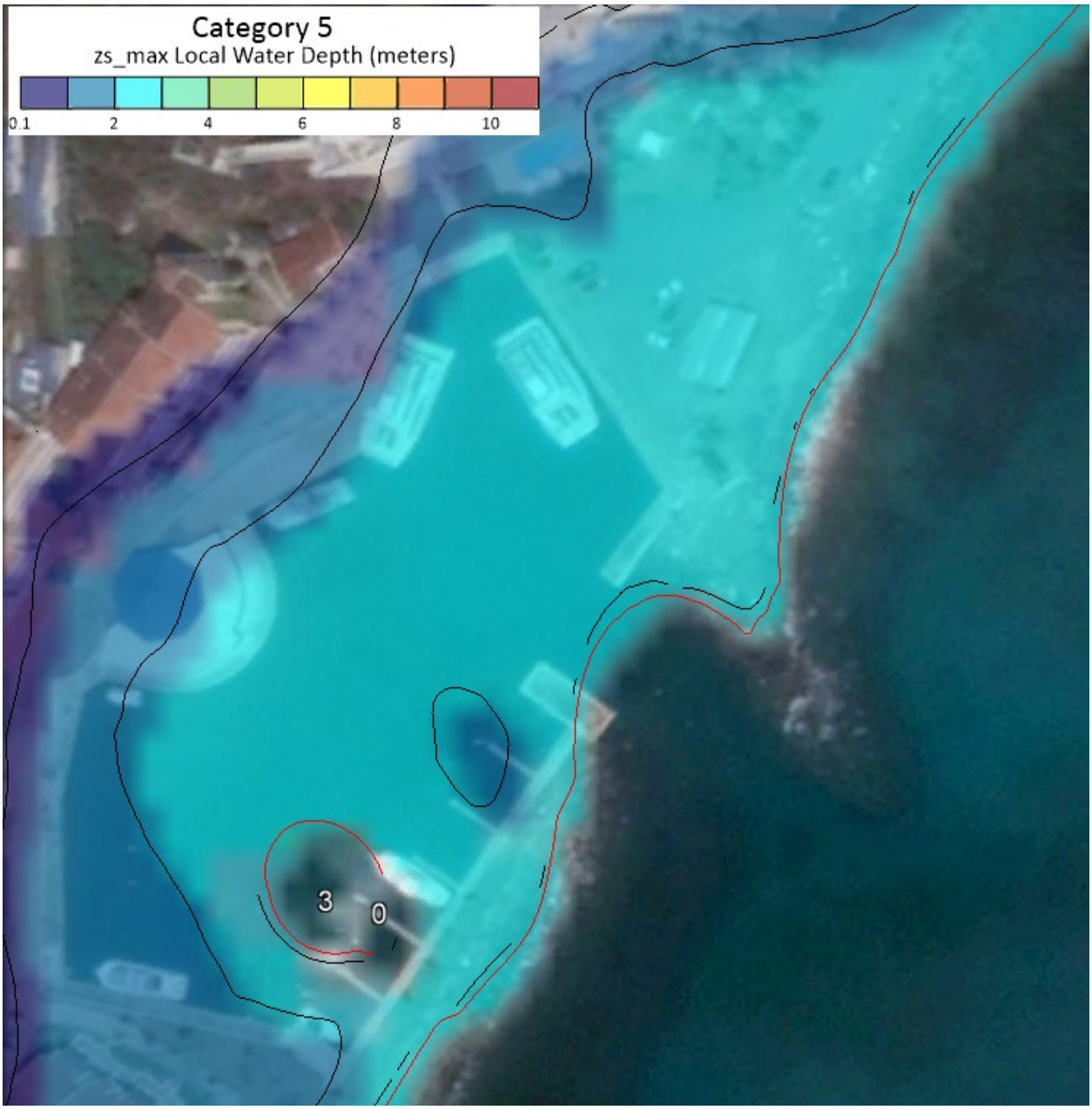

Figure 17 – Marina El Conquistador Hotel, Fajardo, showing that the marina is not resolved by the DEM used. The original DEM has a resolution of 1/3 arc seconds (≈ 10 m), and it was interpolated to 1/9 arc seconds (≈ 3.33 m).

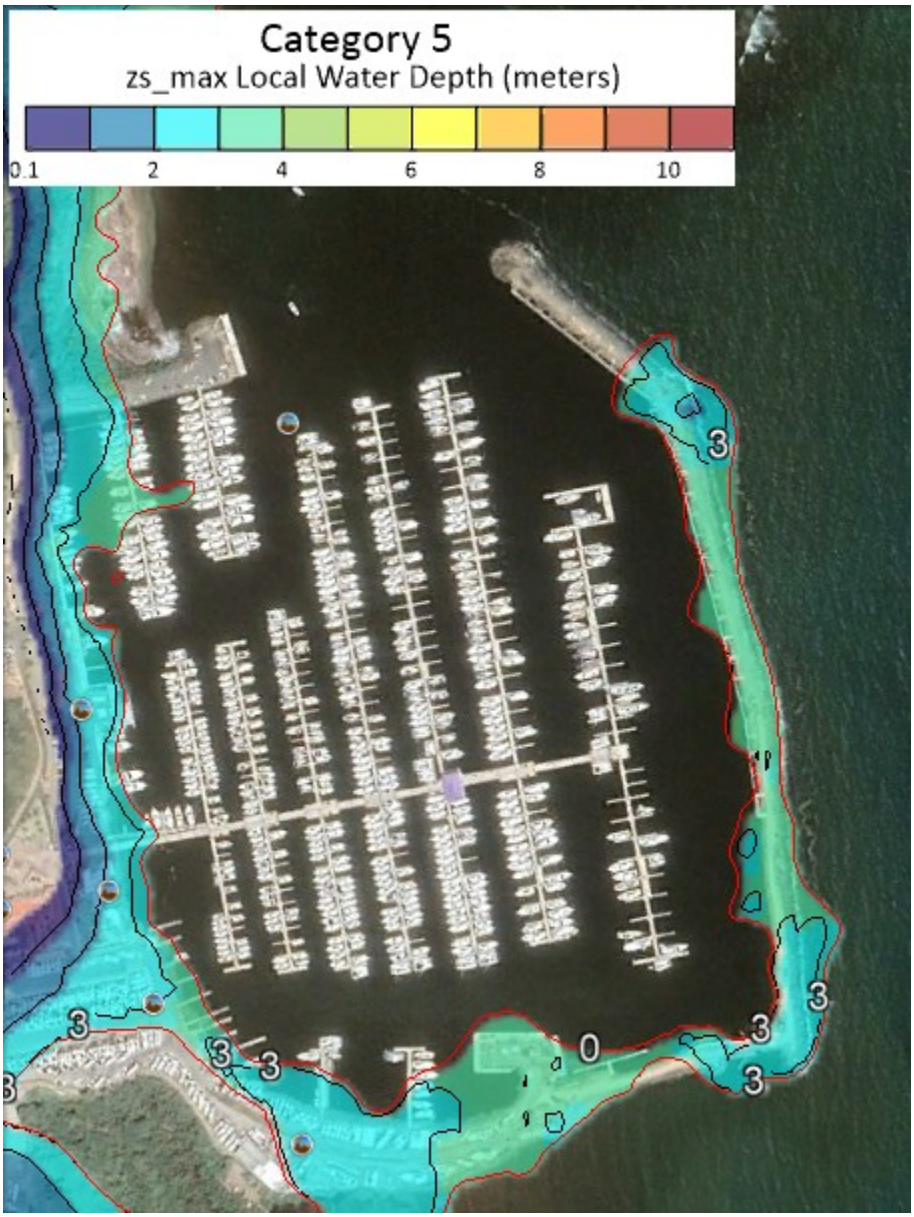

Figure 18 – Marina Puerto del Rey, Fajardo. The marina is partly resolved by the DEM used. The original DEM has a resolution of 1/3 arc seconds (≈ 10 m), and it was interpolated to 1/9 arc seconds (≈ 3.33 m).

MANNING COEFFICIENTS

Frictional dissipation can play a very important factor in the shoreward propagation, and inland penetration, of wave energy, especially whenever there are mangroves and coral reefs. XBeach has the capability to handle spatially variable Manning coefficients by means of an input file, *friction.txt*, that is supplied for each computational grid. That is, each computational cell can be assigned a Manning coefficient according to information appearing in https://coastalscience.noaa.gov/project/benthic-habitat-mapping-puerto-rico-virgin-islands/, for benthic habitats, and

https://gis1.usgs.gov/csas/gap/viewer/land_cover/Map.aspx, for type of land use. In this study all computational cells were assigned a Manning of 0.03, the same as for the tsunami flood mapping done for Puerto Rico using NOAA's MOST tsunami model, with the exception of mangrove (assigned a Manning of 0.145; Rahdarian and Niksokhan, 2017) and (linear) coral reefs areas (assigned a Manning of 0.05). This was carried out by a script that assigned those Manning values inside the polygons enclosing the mangrove and linear reef areas.

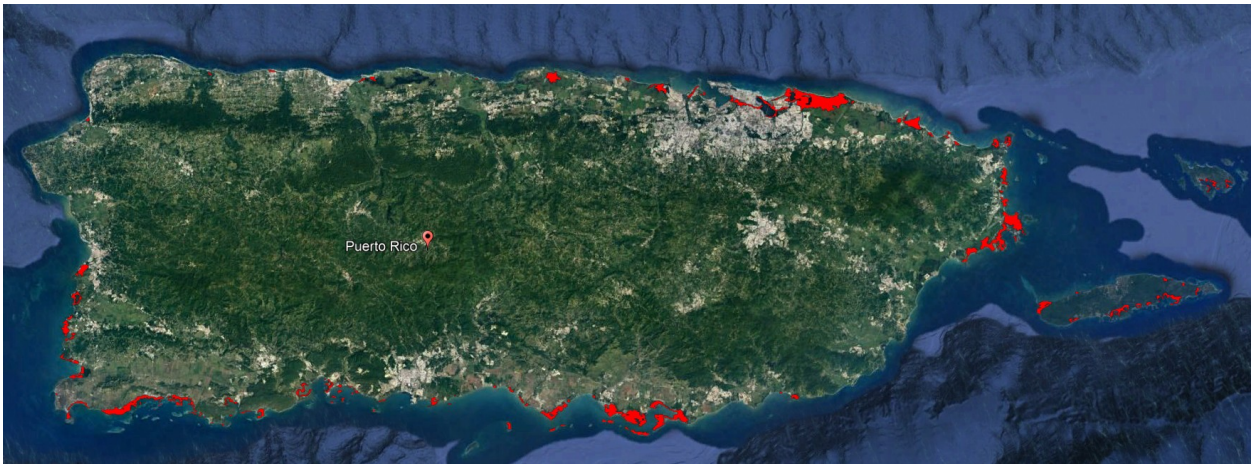

Figure 19 – Google Earth image showing, in red, areas containing mangroves, according to the USGS. For these areas the Manning coefficient at the computational nodes falling inside was given a value of 0.145.

Figure 20- Google Earth image showing, in white, areas containing the reef type called "linear reefs", according to https://coastalscience.noaa.gov/project/benthic-habitat-mapping-puerto-rico-virgin-islands/. All these areas were assigned a Manning of 0.05.

Finally, it was decided not to increase the Manning coefficient (above 0.03) for urban areas because when the wave runup overtops the highest elevation in the profile (but remember we are running XBeach in 2-D mode) the water flows downhill by gravity (which XBeach models) through streets and open areas, which are obviously smooth

areas. A summary of the methodology is described next (for mangroves; the same holds for reefs).

1. Go to the USGS National Land Use file and extract the closed polygons delimiting mangrove areas all over Puerto Rico. This was done using Surfer V 16. Figure 19 shows the case for mangroves. The extracted polygons consist of an ascii file containing the individual polygons, separated by a metadata line containing information about the number of polygon vertices that follow, plus some extra information. There are tens of individual polygons inside this asci file.

2. The above file was edited by replacing the (separating) metadata line with a line containing just the string “NaN NaN”.

3. A Matlab script was prepared that made use of the Matlab script in_polygon.m. This script is supplied the bounding polygons and the eastings and northings of each computational node in the computational grid. The program will evaluate if a given computational node falls inside, or outside, the polygons. If the node falls outside that polygon it will be assigned a Manning coefficient of 0.03 (the default Manning value used). If the computational node falls inside the polygon, then a Manning value corresponding to mangroves is assigned to the node. For the grids shown in Figure 21 that fall completely within the red boxes, the 1/9 arc seconds data was used, interpolated from 3.33 m down to 3 m. For the rest of the island not covered by the 1/9 arc seconds DEMs, the only option was to use the 10 m DEMs interpolated down to 3 m.

4. The final result is a raster file containing a Manning value of 0.03 all over the file, with the 0.03 replaced by 0.145 where there are mangroves.

5. This is then repeated using the reef’s polygons. Figure 20 shows the reef’s locations.

COMPUTATIONAL GRIDS

Figure 21 shows the outline of the computational grids into which the island was broken up. Shapefiles and kmz files will be prepared of the maximum sea surface elevation obtained for each grid and a set

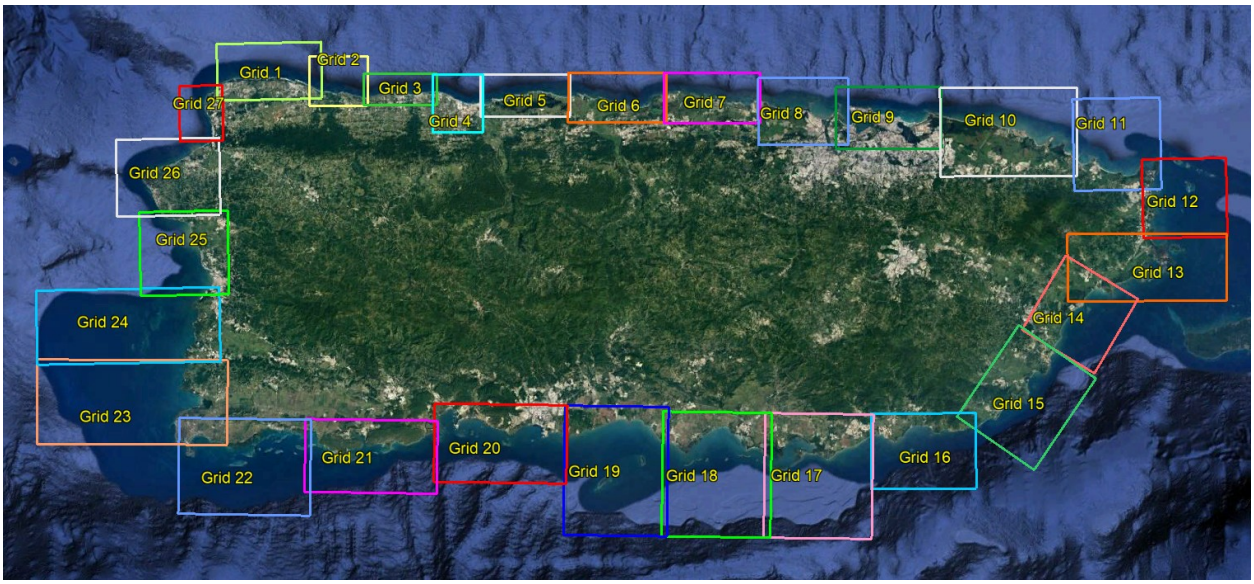

Figure 21 – Schematic showing outline boxes of the XBeach computational grids prepared up to now. The grid generation started from the northwest (Aguadilla) moving eastward (Grid 1).

of figures will be presented:

1. A Google Earth (GE) image of the outline of the grid and depth contours in meters. The shoreline is shown in red. The wave forcing for the model is done along the offshore, deep water, boundary, and the main wave direction is taken as perpendicular to this boundary.
2. An image of color-classified frictional Manning coefficients: red are mangroves (Manning = 0.145), orange are reefs (Manning = 0.05), and the rest of the grid is painted with a yellow hue where the Manning coefficient is asset at 0.03.
3. A 3-d plot of the bathymetry/topography as supplied to the model.
4. A 2-d filled contour plot of the same bathymetry/topography.

Figures 22 to 129 show the images referenced above for each of the 27 computational grids.

GRID 1 (AGUADILLA TO ISABELA)

Figure 22 – Outline of computational Grid 1 overlaid on top of Google Earth, showing depth contours, in meters. Mean Sea Level Shoreline is outlined by the red curve. Contours up to 59 m are shown. Deeper waters are set to a constant depth of 60 m. The wavemaker is located at the top boundary and waves propagate south.

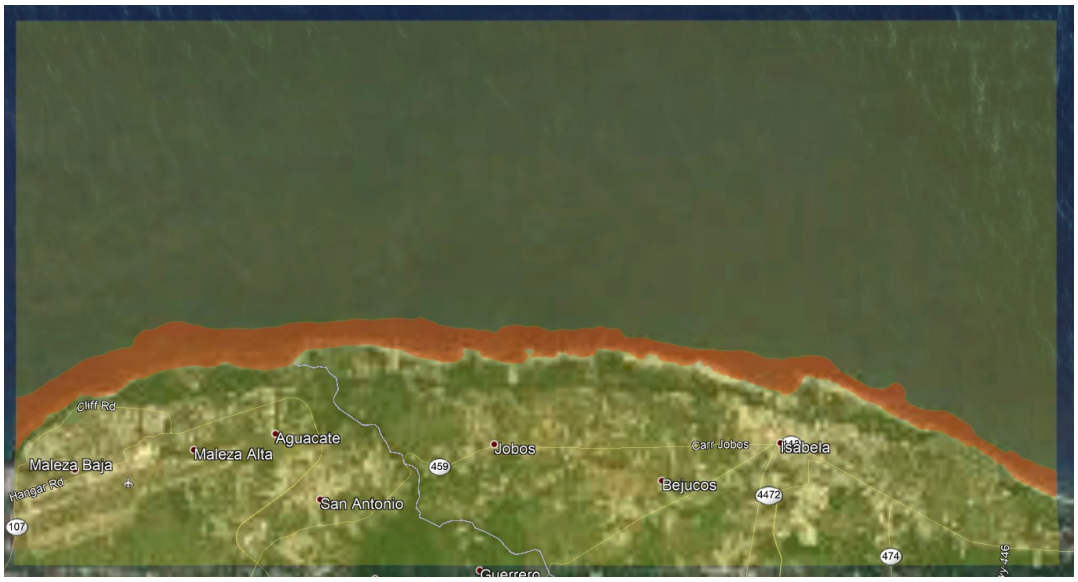

Figure 23 – Image of color-classified frictional Manning coefficients for Grid 1. Red are mangroves (Manning = 0.145), orange are reefs (Manning = 0.05), and the rest of the grid is painted with a yellow hue where the Manning coefficient is set at 0.03.

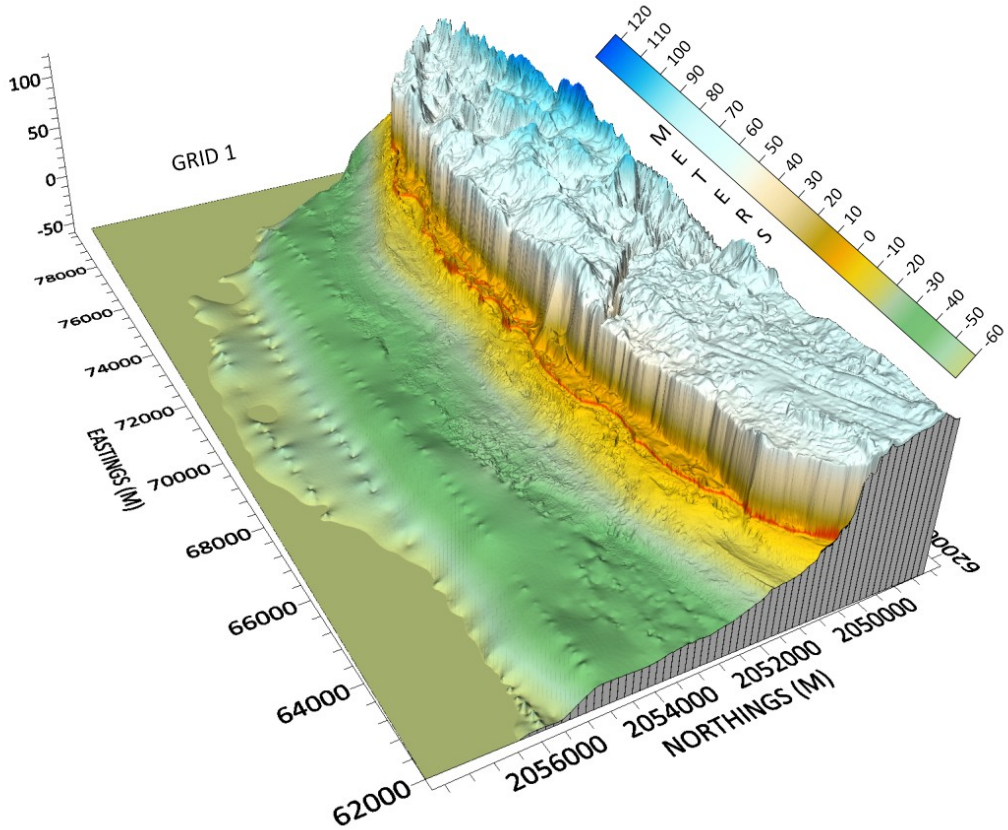

Figure 24 – 3D plot of bathymetry/topography supplied to Grid 1. Red curve is the MSL shoreline.

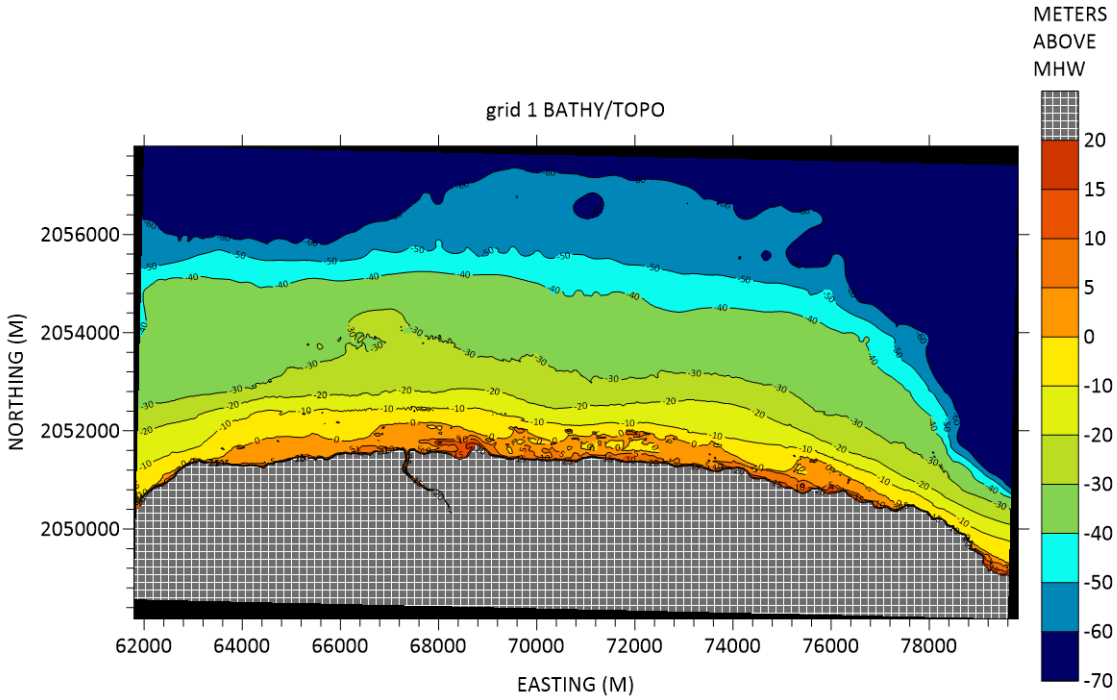

Figure 25– 2D plot of bathymetry/topography supplied to Grid 1. Red curve is the MSL shoreline. Wavemaker is located at the northern boundary and waves propagate southward.

GRID 2 (ISABELA TO QUEBRADILLAS)

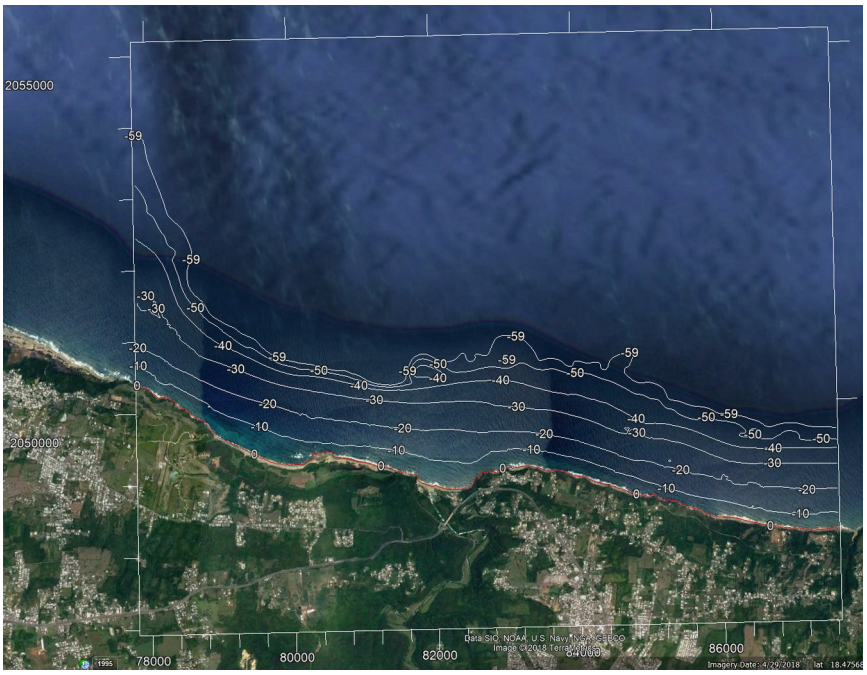

Figure 26 – Outline of computational Grid 2 overlaid on top of Google Earth, showing depth contours, in meters. Mean Sea Level Shoreline is outlined by the red curve. Contours up to 59 m are shown. Deeper waters are set to a constant depth of 60 m. The wavemaker is located at the top boundary and waves propagate south.

Figure 27 – Image of color-classified frictional Manning coefficients for Grid 2. Red are mangroves (Manning = 0.145), orange are reefs (Manning = 0.05), and the rest of the grid is painted with a yellow hue where the Manning coefficient is set at 0.03.

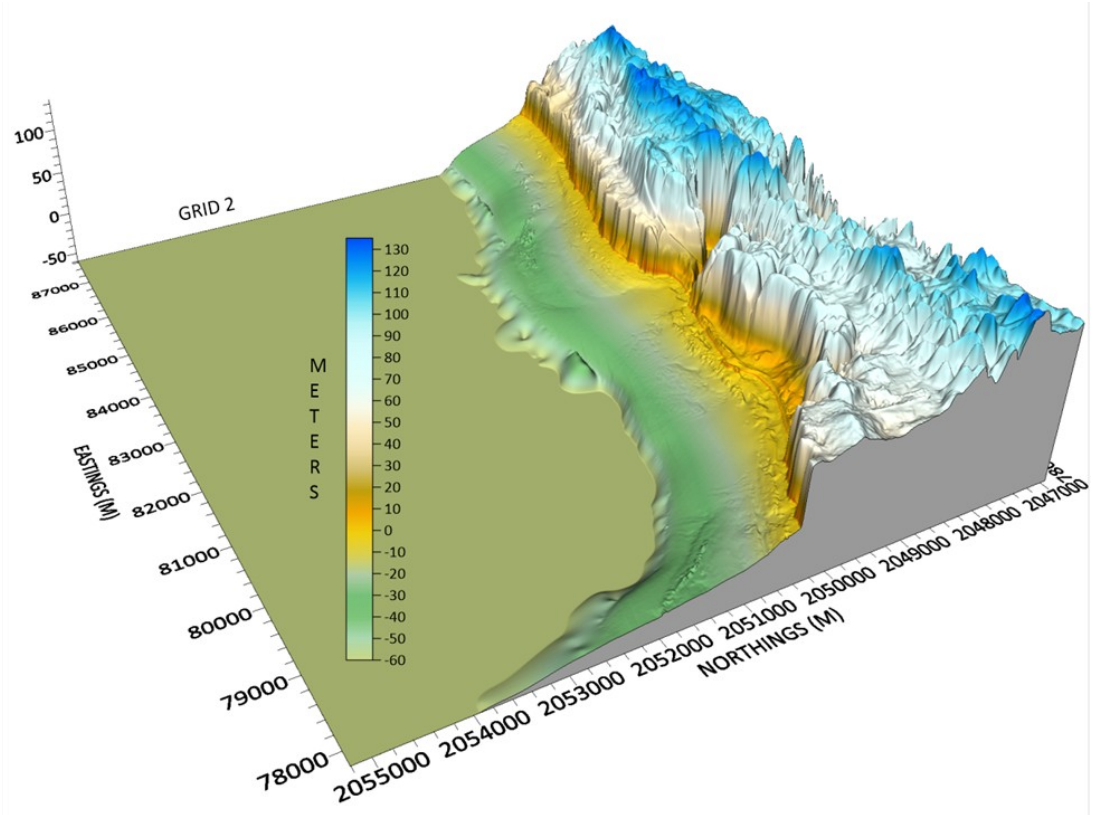

Figure 28– 3D plot of bathymetry/topography supplied to Grid 2. Red curve is the MSL shoreline.

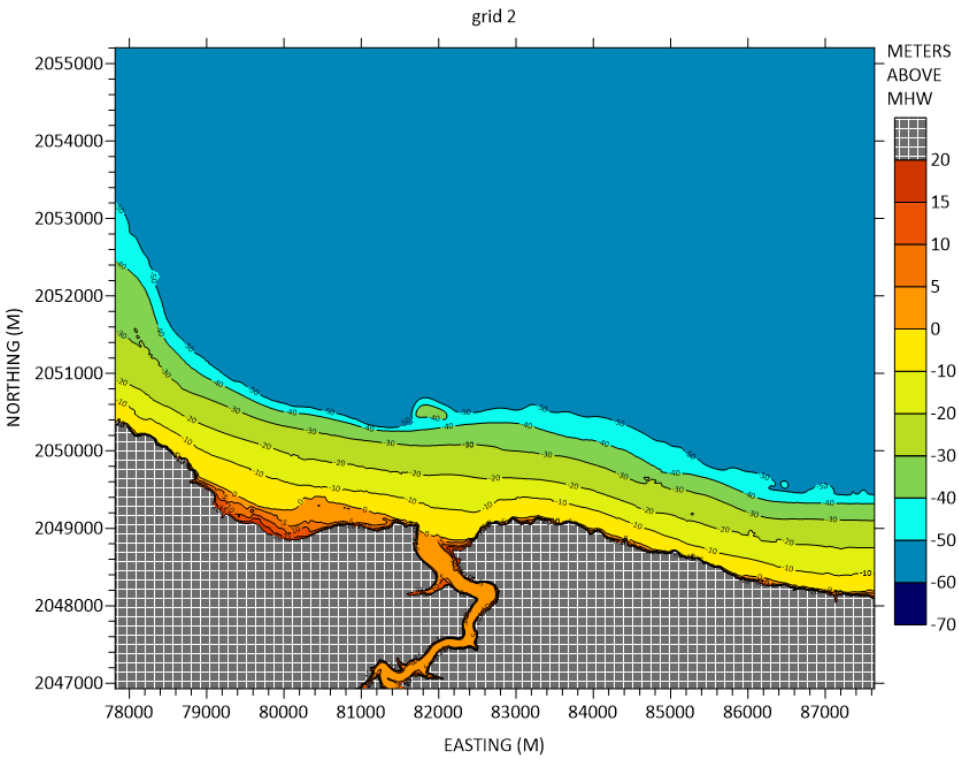

Figure 29– 2D plot of bathymetry/topography supplied to Grid 2. Red curve is the MSL shoreline. Wavemaker is located at the northern boundary and waves propagate southward.

GRID 3 (CAMUY TO HATILLO)

Figure 30 – Outline of computational Grid 3 overlaid on top of Google Earth, showing depth contours, in meters. Mean Sea Level Shoreline is outlined by the red curve. Contours up to 59 m are shown. Deeper waters are set to a constant depth of 60 m. The wavemaker is located at the top boundary and waves propagate south.

Figure 31 – Image of color-classified frictional Manning coefficients for Grid 3. Red are mangroves (Manning = 0.145), orange are reefs (Manning = 0.05), and the rest of the grid is painted with a yellow hue where the Manning coefficient is set at 0.03.

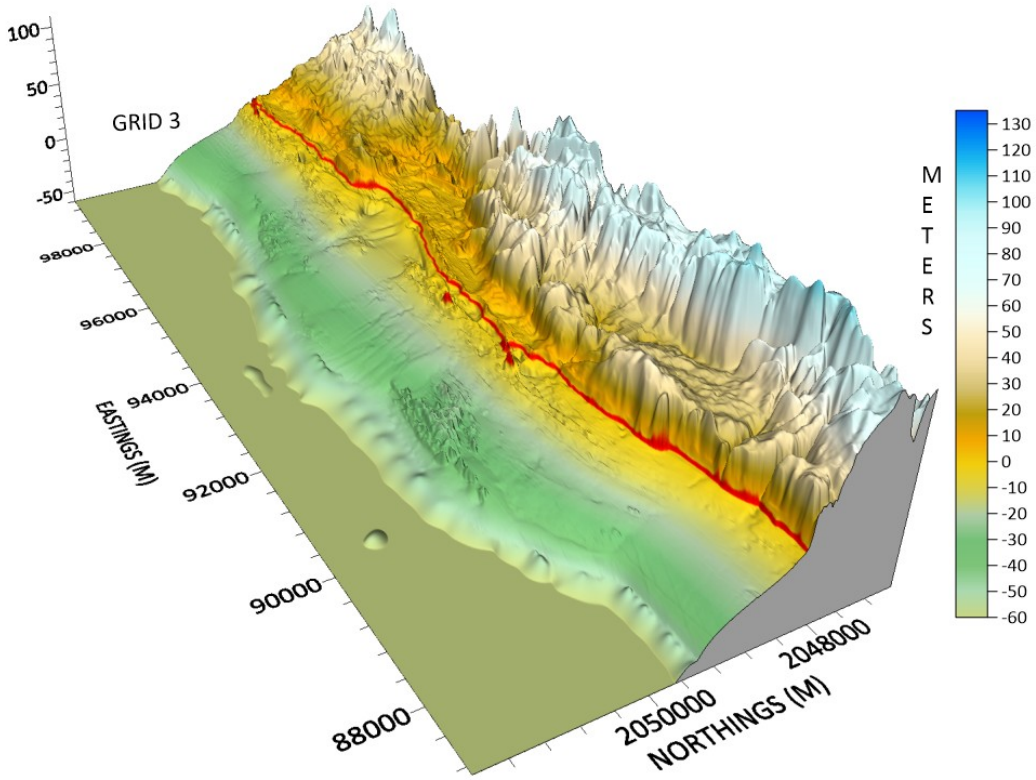

Figure 32– 3D plot of bathymetry/topography supplied to Grid 3. Red curve is the MSL shoreline.

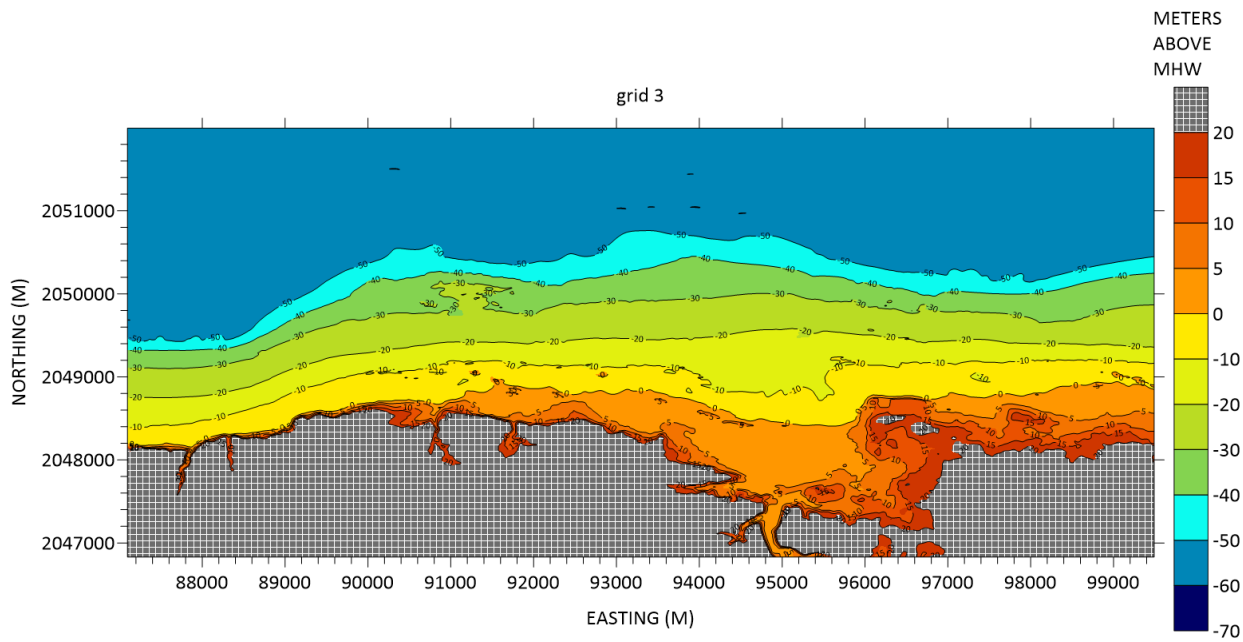

Figure 33– 2D plot of bathymetry/topography supplied to Grid 3. Red curve is the MSL shoreline. Wavemaker is located at the northern boundary and waves propagate southward.

GRID 4 (ARECIBO)

Figure 34 – Outline of computational Grid 4 overlaid on top of Google Earth, showing depth contours, in meters. Mean Sea Level Shoreline is outlined by the red curve. Contours up to 59 m are shown. Deeper waters are set to a constant depth of 60 m. The wavemaker is located at the top boundary and waves propagate south.

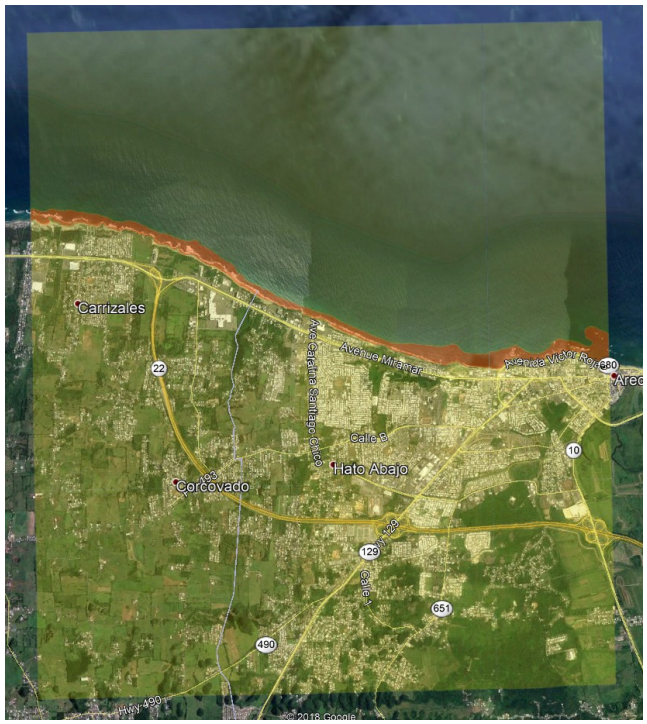

Figure 35 – Image of color-classified frictional Manning coefficients for Grid 4. Red are mangroves (Manning = 0.145), orange are reefs (Manning = 0.05), and the rest of the grid is painted with a yellow hue where the Manning coefficient is set at 0.03.

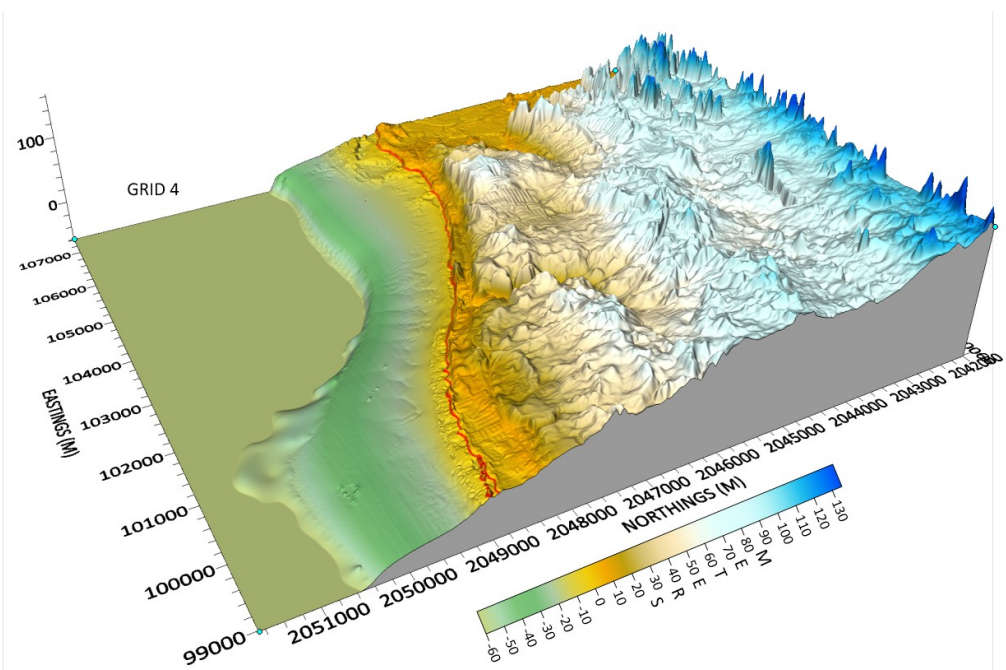

Figure 36– 3D plot of bathymetry/topography supplied to Grid 4. Red curve is the MSL shoreline.

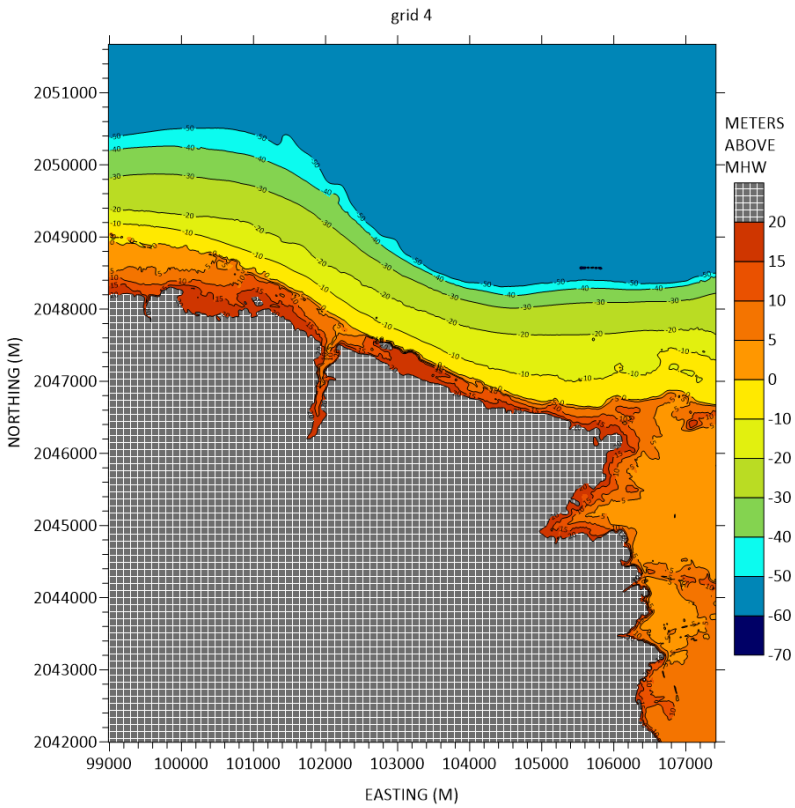

Figure 37– 2D plot of bathymetry/topography supplied to Grid 4. Red curve is the MSL shoreline. Wavemaker is located at the northern boundary and waves propagate southward.

GRID 5 (ARECIBO TO BARCELONETA)

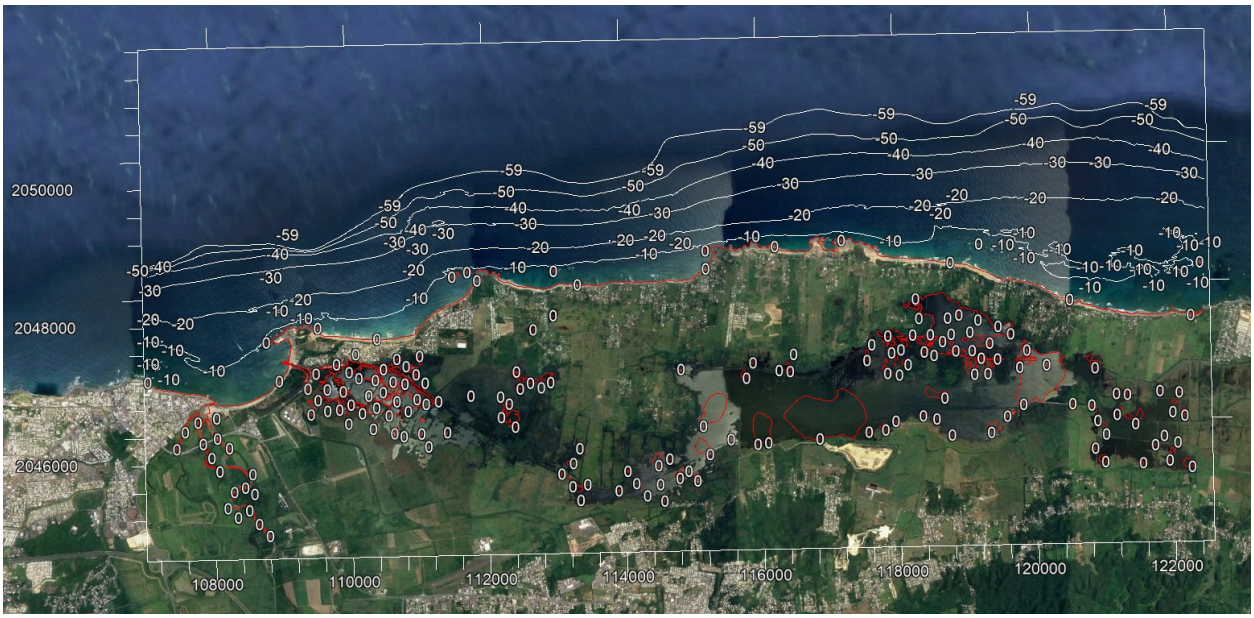

Figure 38 – Outline of computational Grid 5 overlaid on top of Google Earth, showing depth contours, in meters. Mean Sea Level Shoreline is outlined by the red curve. Contours up to 59 m are shown. Deeper waters are set to a constant depth of 60 m. The wavemaker is located at the top boundary and waves propagate south.

Figure 39 – Image of color-classified frictional Manning coefficients for Grid 5. Red are mangroves (Manning = 0.145), orange are reefs (Manning = 0.05), and the rest of the grid is painted with a yellow hue where the Manning coefficient is set at 0.03.

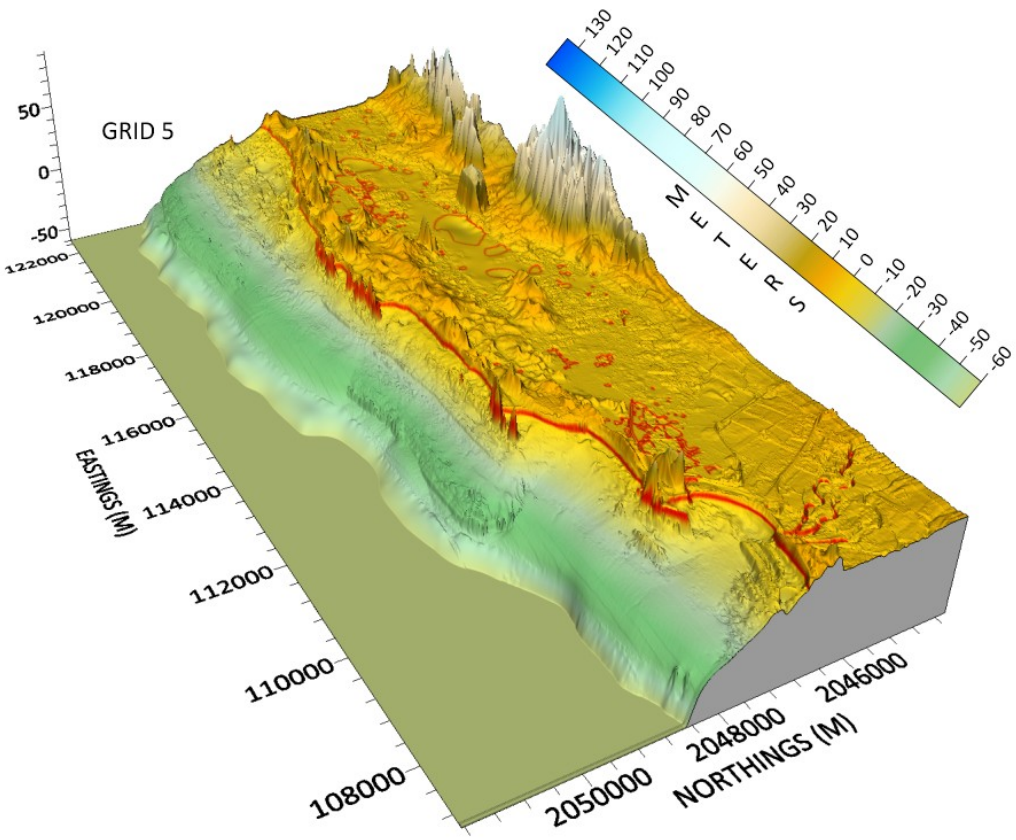

Figure 40– 3D plot of bathymetry/topography supplied to Grid 5. Red curve is the MSL shoreline.

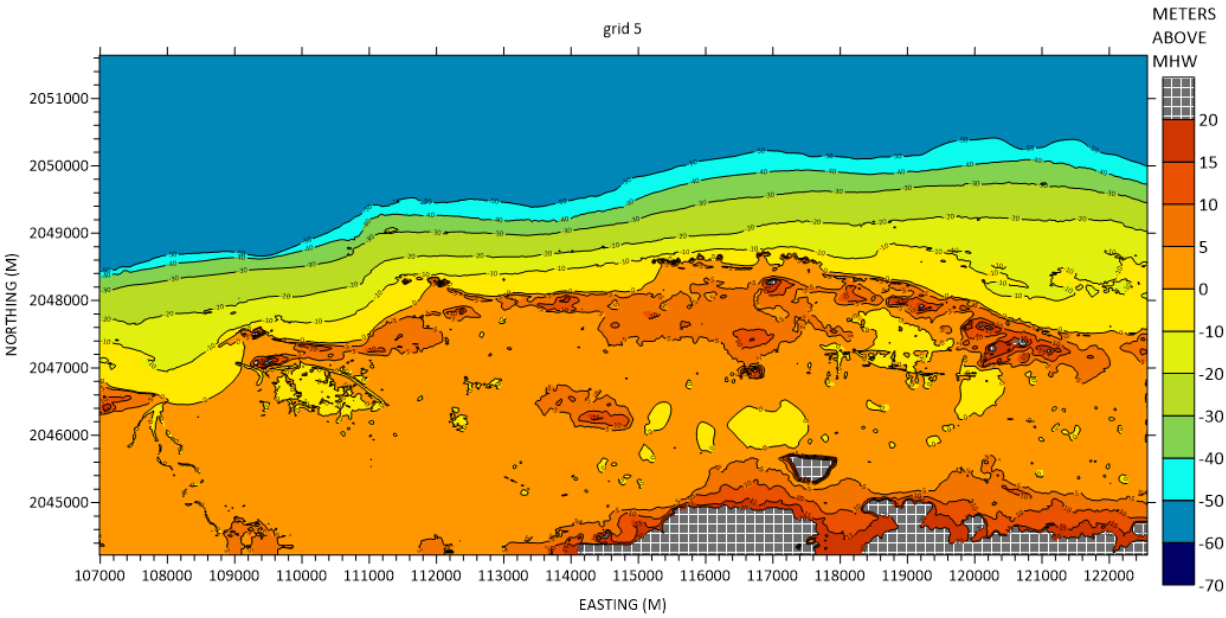

Figure 41– 2D plot of bathymetry/topography supplied to Grid 5. Red curve is the MSL shoreline. Wavemaker is located at the northern boundary and waves propagate southward.

GRID 6 (BARCELONETA TO VEGA BAJA)

Figure 42 – Outline of computational Grid 6 overlaid on top of Google Earth, showing depth contours, in meters. Mean Sea Level Shoreline is outlined by the red curve. Contours up to 59 m are shown. Deeper waters are set to a constant depth of 60 m. The wavemaker is located at the top boundary and waves propagate south.

Figure 43 – Image of color-classified frictional Manning coefficients for Grid 6. Red are mangroves (Manning = 0.145), orange are reefs (Manning = 0.05), and the rest of the grid is painted with a yellow hue where the Manning coefficient is set at 0.03.

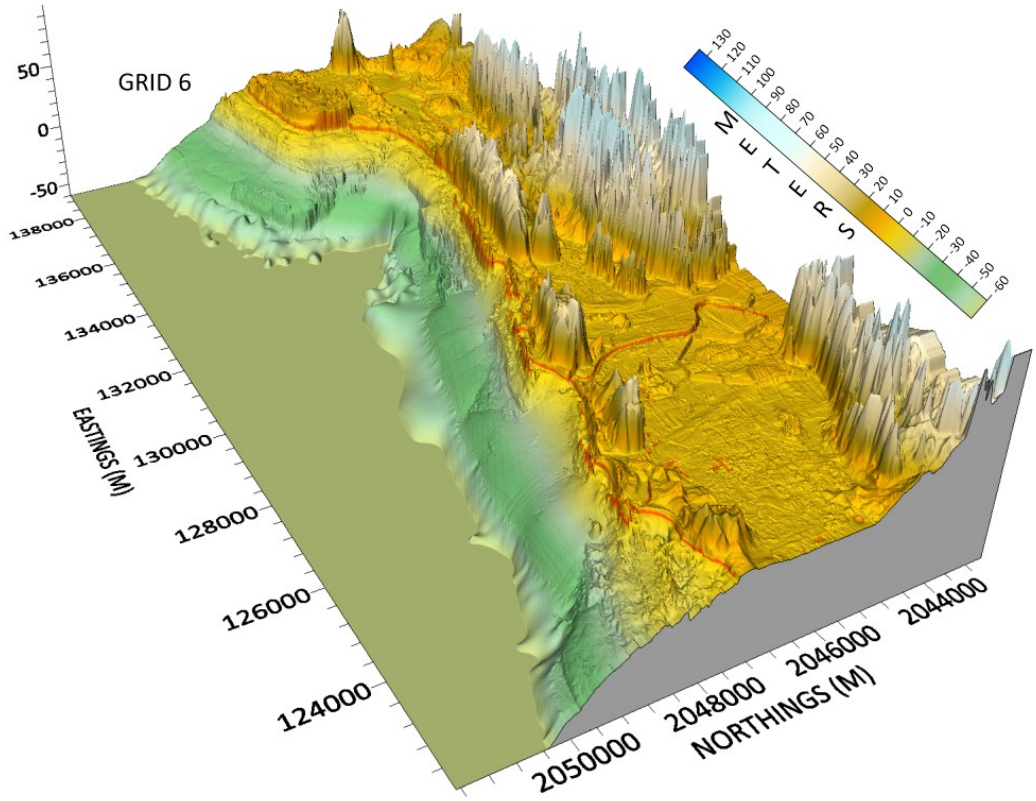

Figure 44– 3D plot of bathymetry/topography supplied to Grid 6. Red curve is the MSL shoreline.

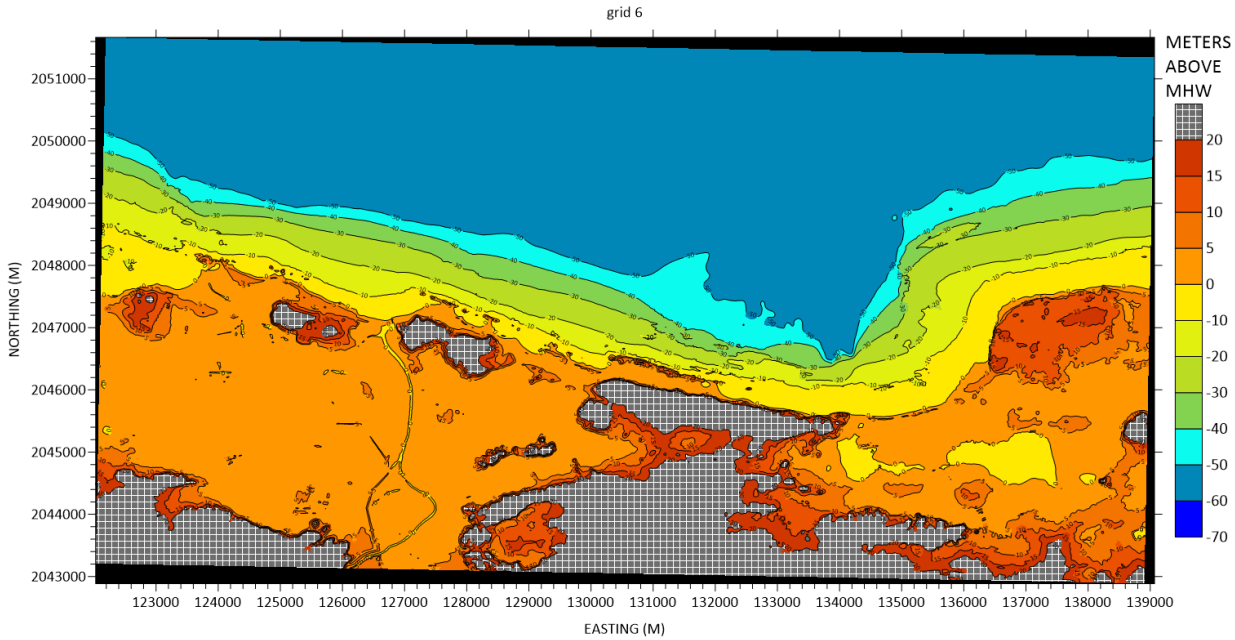

Figure 45– 2D plot of bathymetry/topography supplied to Grid 6. Red curve is the MSL shoreline. Wavemaker is located at the northern boundary and waves propagate southward.

GRID 7 (VEGA BAJA TO DORADO)

Figure 46 – Outline of computational Grid 7 overlaid on top of Google Earth, showing depth contours, in meters. Mean Sea Level Shoreline is outlined by the red curve. Contours up to 59 m are shown. Deeper waters are set to a constant depth of 60 m. The wavemaker is located at the top boundary and waves propagate south.

Figure 47 – Image of color-classified frictional Manning coefficients for Grid 7. Red are mangroves (Manning = 0.145), orange are reefs (Manning = 0.05), and the rest of the grid is painted with a yellow hue where the Manning coefficient is set at 0.03.

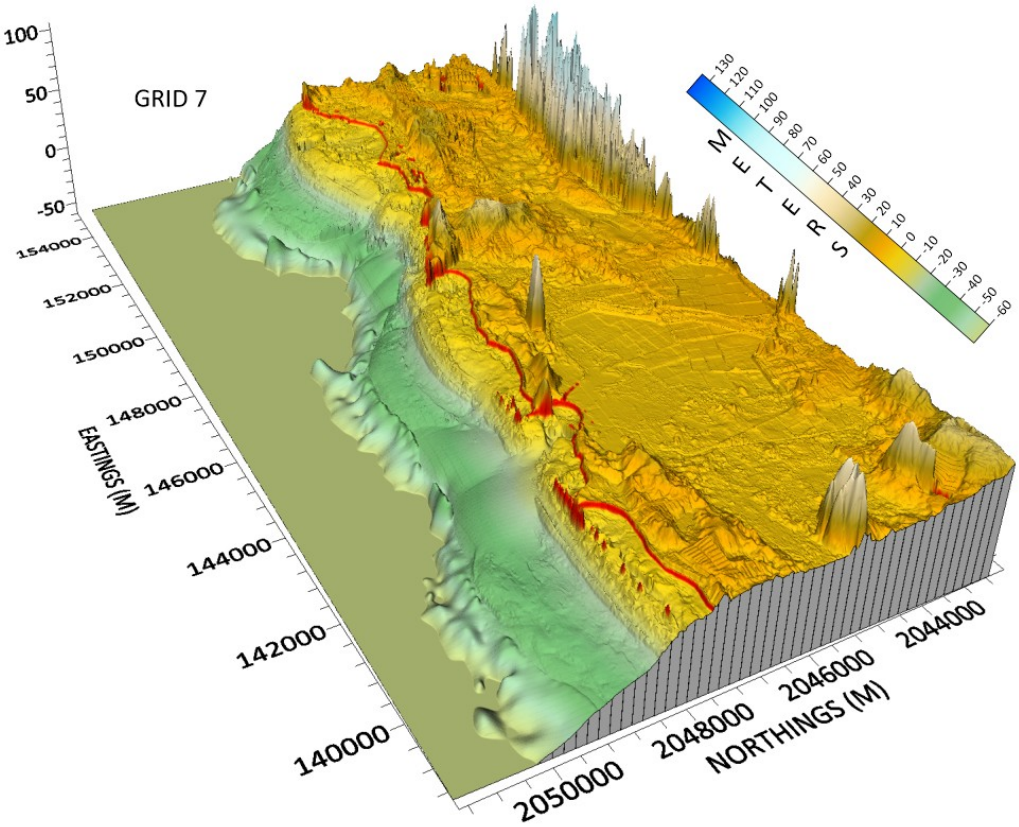

Figure 48– 3D plot of bathymetry/topography supplied to Grid 7. Red curve is the MSL shoreline.

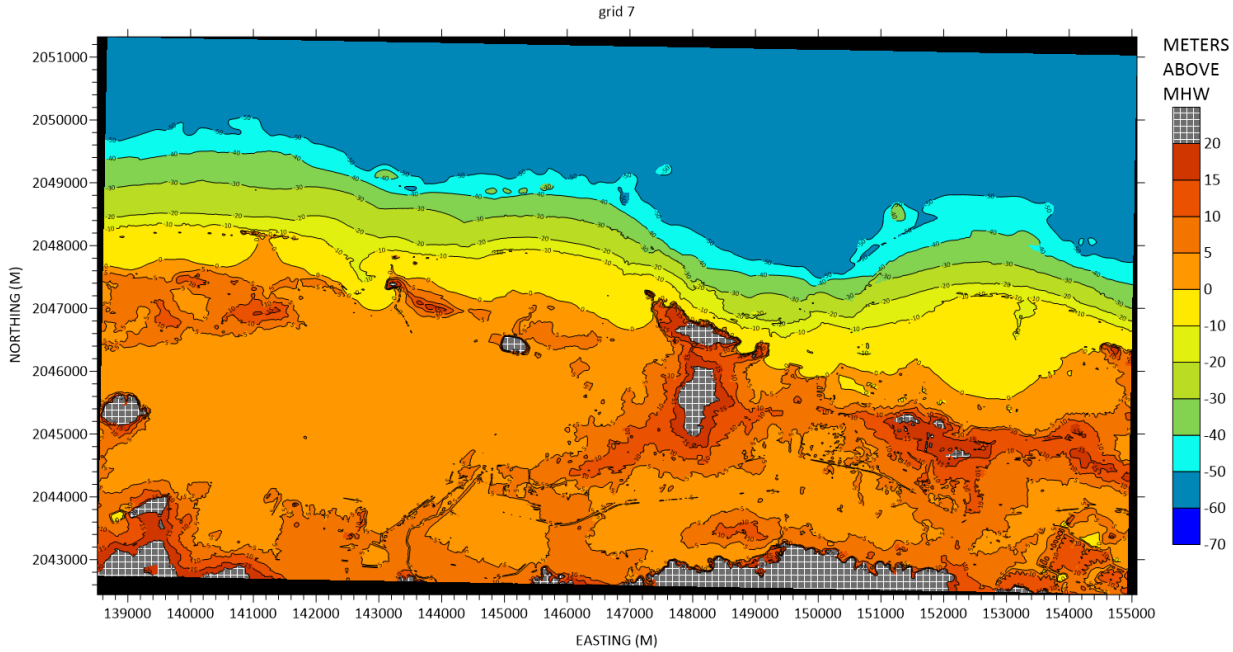

Figure 49– 2D plot of bathymetry/topography supplied to Grid 7. Red curve is the MSL shoreline. Wavemaker is located at the northern boundary and waves propagate southward.

GRID 8 (DORADO TO CATAÑO)

Figure 50 – Outline of computational Grid 8 overlaid on top of Google Earth, showing depth contours, in meters. Mean Sea Level Shoreline is outlined by the red curve. Contours up to 59 m are shown. Deeper waters are set to a constant depth of 60 m. The wavemaker is located at the top boundary and waves propagate south.

Figure 51 – Image of color-classified frictional Manning coefficients for Grid 8. Red are mangroves (Manning = 0.145), orange are reefs (Manning = 0.05), and the rest of the grid is painted with a yellow hue where the Manning coefficient is set at 0.03.

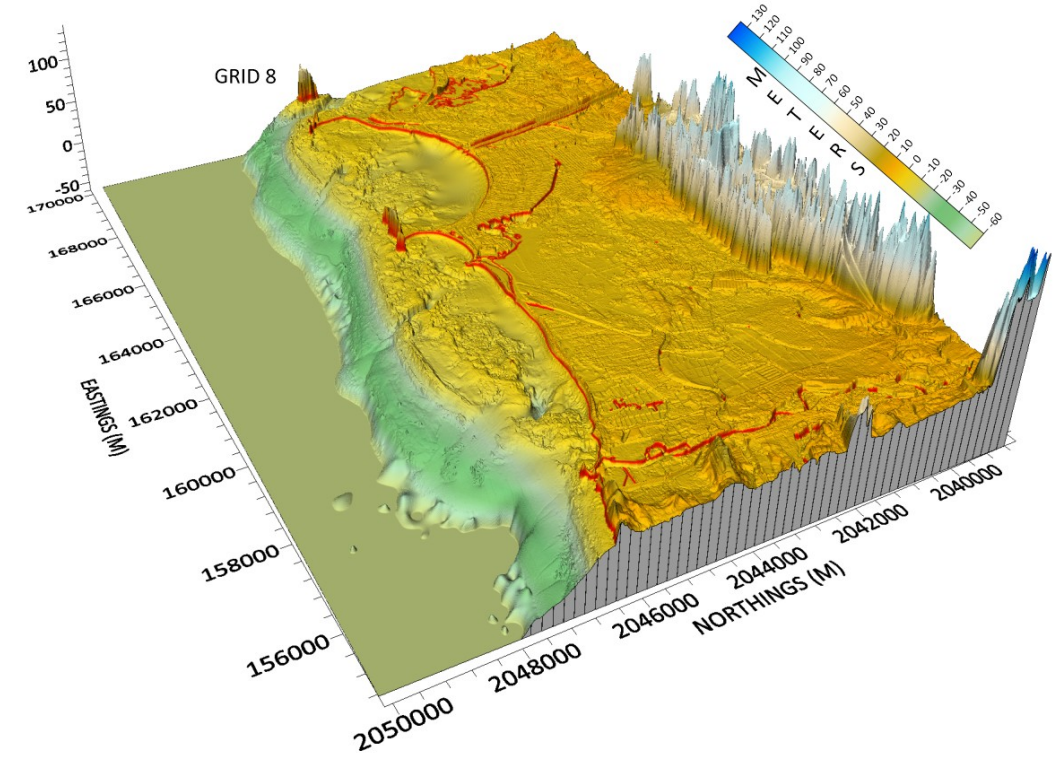

Figure 52– 3D plot of bathymetry/topography supplied to Grid 8. Red curve is the MSL shoreline.

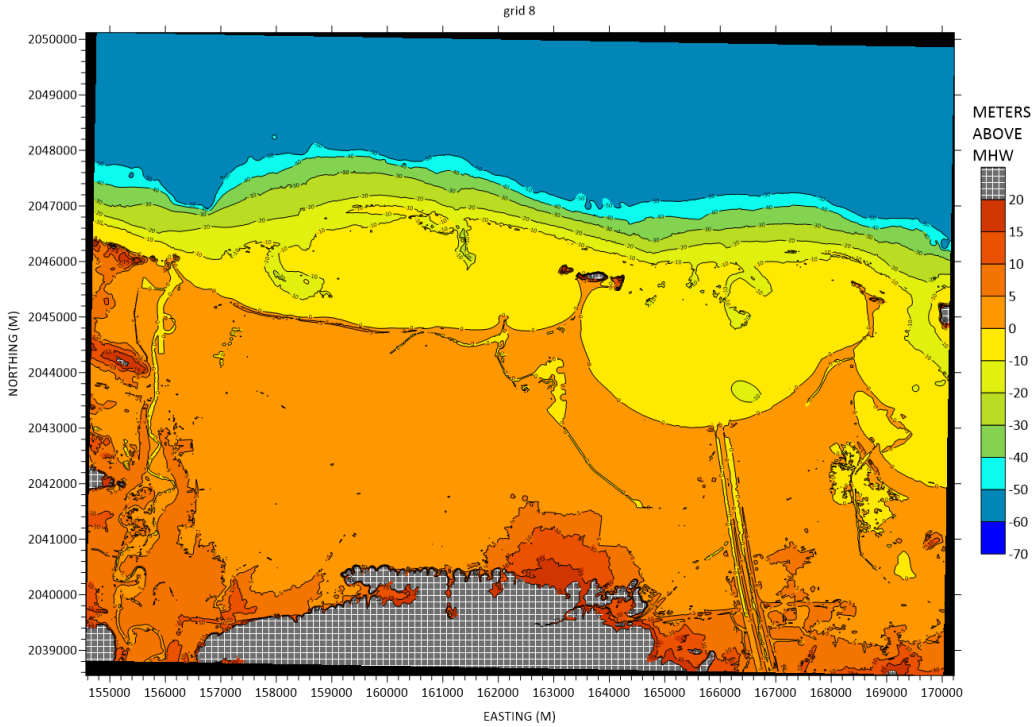

Figure 53– 2D plot of bathymetry/topography supplied to Grid 8. Red curve is the MSL shoreline. Wavemaker is located at the northern boundary and waves propagate southward.

GRID 9 (SAN JUAN METROPOLITAN AREA)

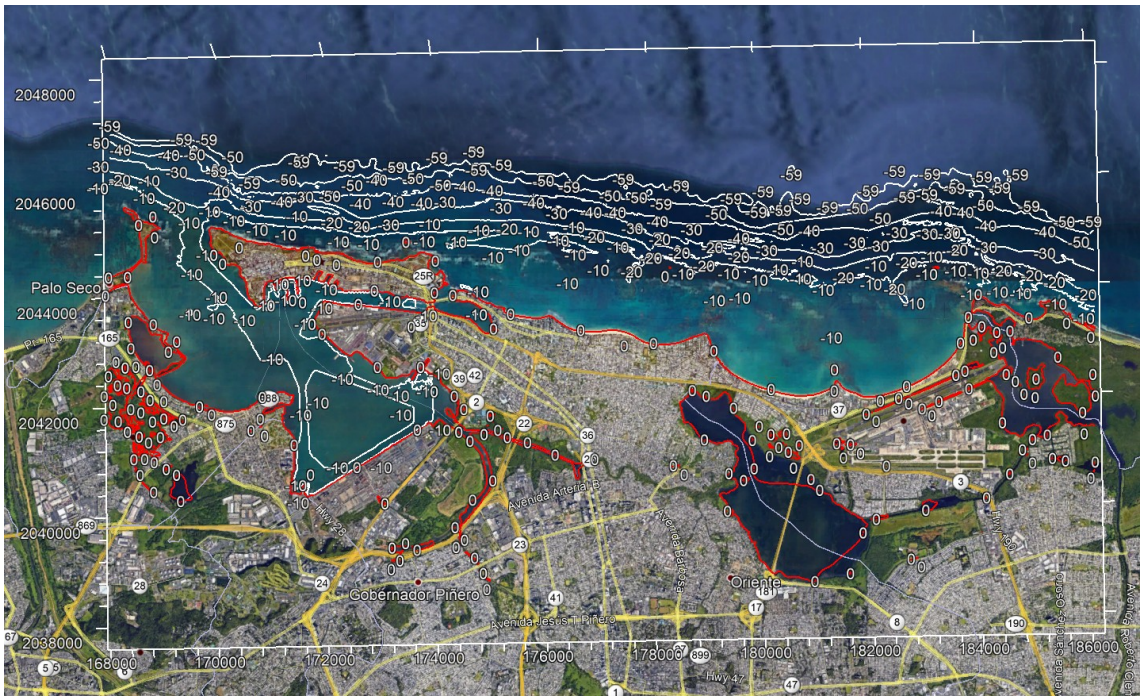

Figure 54 – Outline of computational Grid 9 overlaid on top of Google Earth, showing depth contours, in meters. Mean Sea Level Shoreline is outlined by the red curve. Contours up to 59 m are shown. Deeper waters are set to a constant depth of 60 m. The wavemaker is located at the top boundary and waves propagate south.

Figure 55 – Image of color-classified frictional Manning coefficients for Grid 9. Red are mangroves (Manning = 0.145), orange are reefs (Manning = 0.05), and the rest of the grid is painted with a yellow hue where the Manning coefficient is set at 0.03.

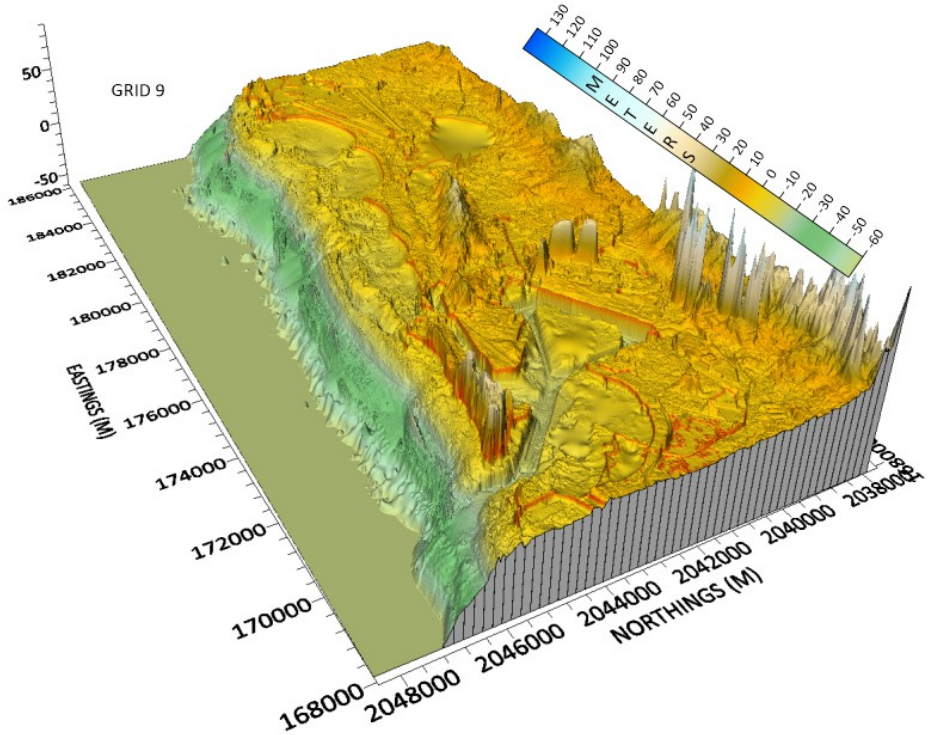

Figure 56– 3D plot of bathymetry/topography supplied to Grid 9. Red curve is the MSL shoreline.

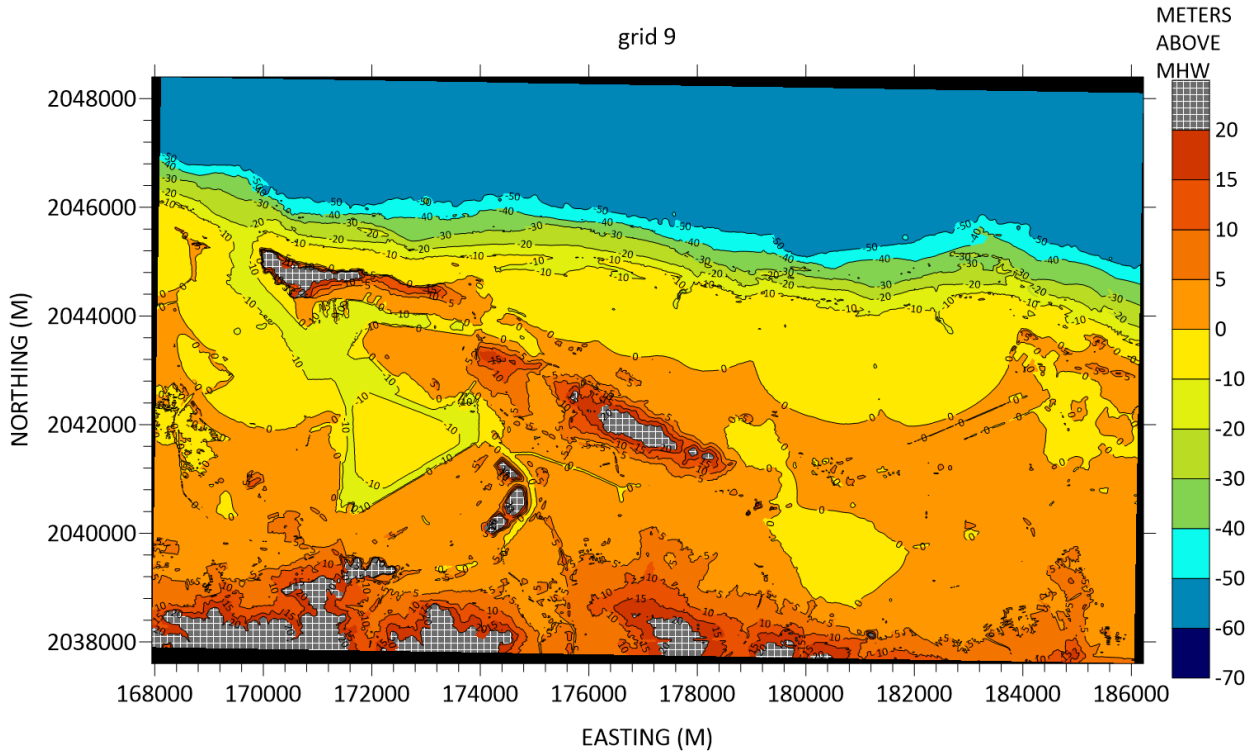

Figure 57– 2D plot of bathymetry/topography supplied to Grid 9. Red curve is the MSL shoreline. Wavemaker is located at the northern boundary and waves propagate southward.

GRID 10 (CAROLINA TO RIO GRANDE)

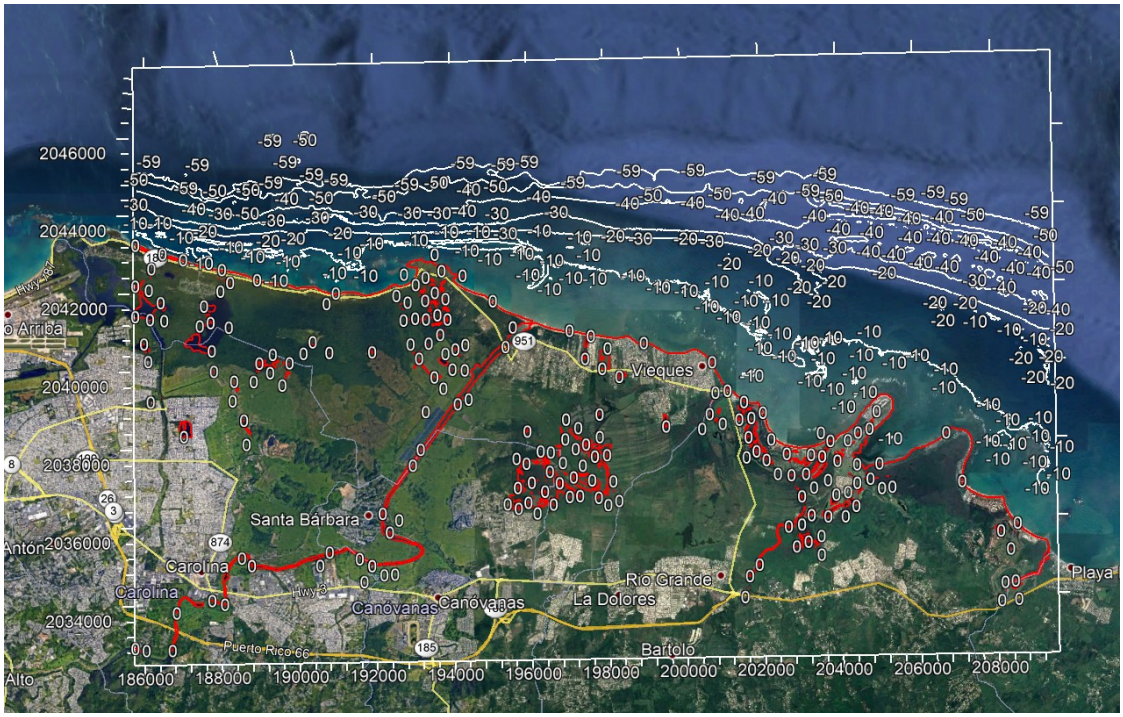

Figure 58 – Outline of computational Grid 10 overlaid on top of Google Earth, showing depth contours, in meters. Mean Sea Level Shoreline is outlined by the red curve. Contours up to 59 m are shown. Deeper waters are set to a constant depth of 60 m. The wavemaker is located at the top boundary and waves propagate south.

Figure 59 – Image of color-classified frictional Manning coefficients for Grid 10. Red are mangroves (Manning = 0.145), orange are reefs (Manning = 0.05), and the rest of the grid is painted with a yellow hue where the Manning coefficient is set at 0.03.

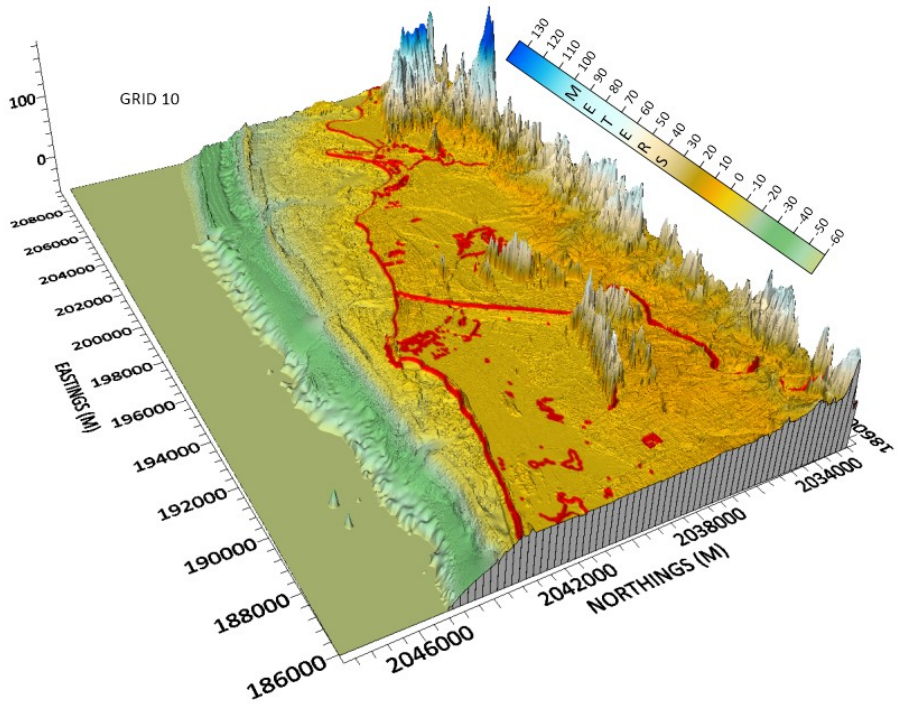

Figure 60 – 3D plot of bathymetry/topography supplied to Grid 10. Red curve is the MSL shoreline.

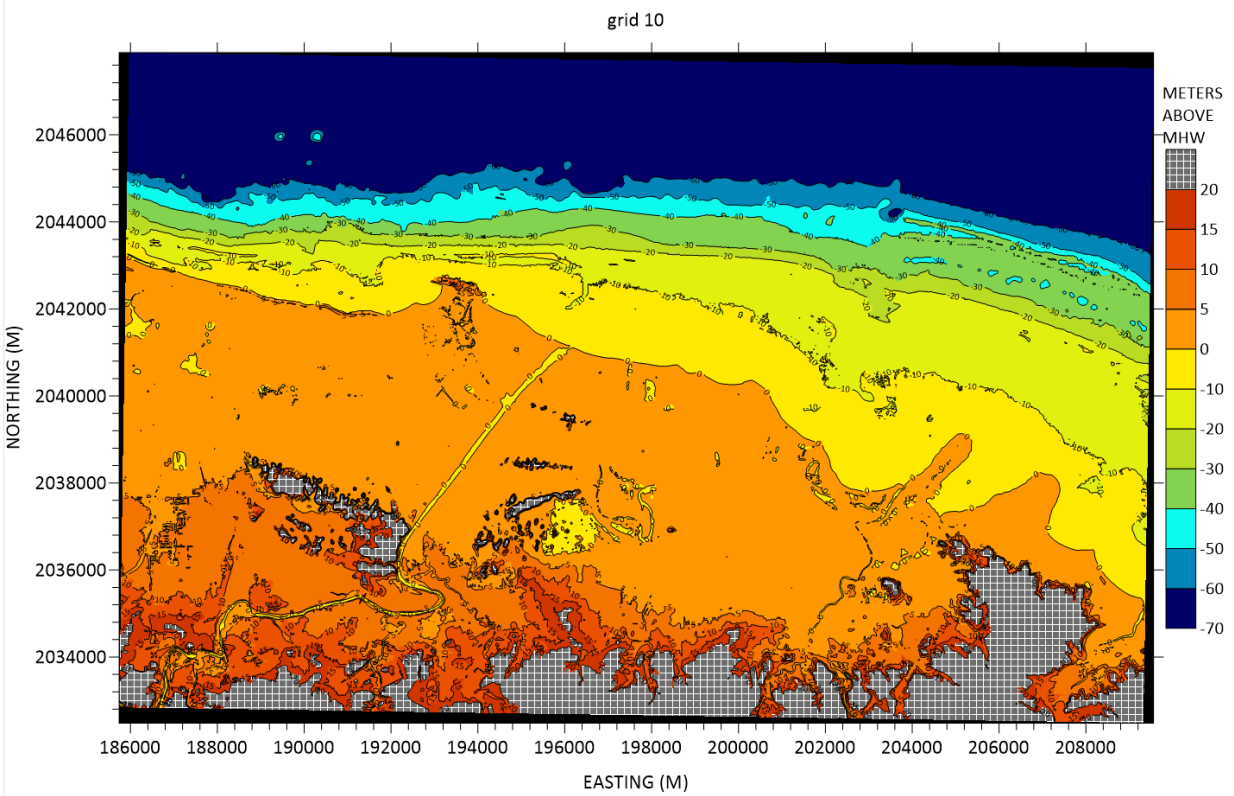

Figure 61 – 2D plot of bathymetry/topography supplied to Grid 10. Red curve is the MSL shoreline. Wavemaker is located at the northern boundary and waves propagate southward.

GRID 11 (LUQUILLO TO FAJARDO)

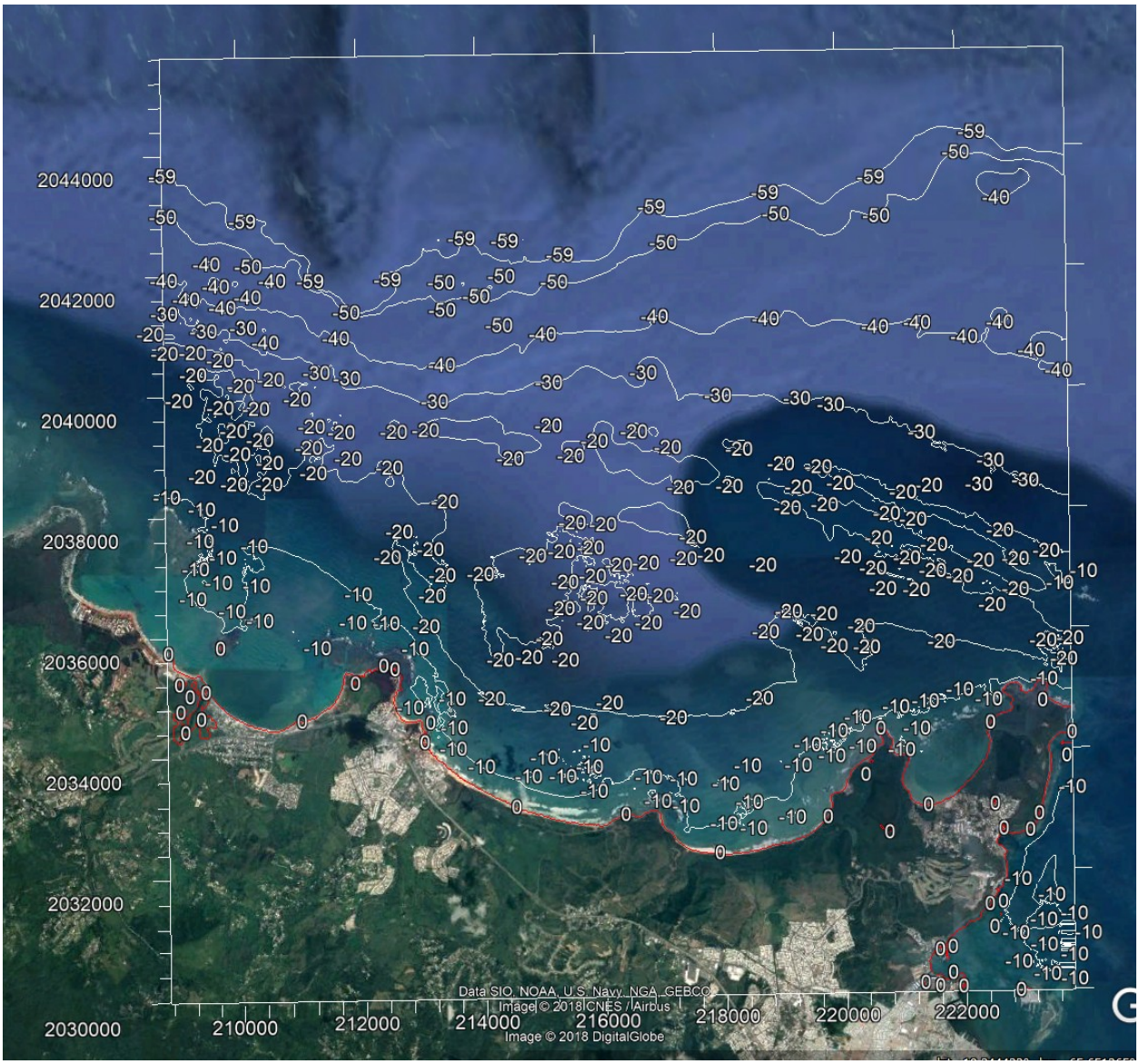

Figure 62 – Outline of computational Grid 11 (Fajardo area) overlaid on top of Google Earth, showing depth contours, in meters. Mean Sea Level Shoreline is outlined by the red curve. Contours up to 59 m are shown. Deeper waters are set to a constant depth of 60 m. For this grid wave forcing is given along the north boundary, propagating southward. Another grid will be used for the Fajardo area, facing eastwards. That is, wave forcing will be given along the eastward boundary. Results southward of Las Cabezas de San Juan should not be used. This area will be covered in Grid 12.

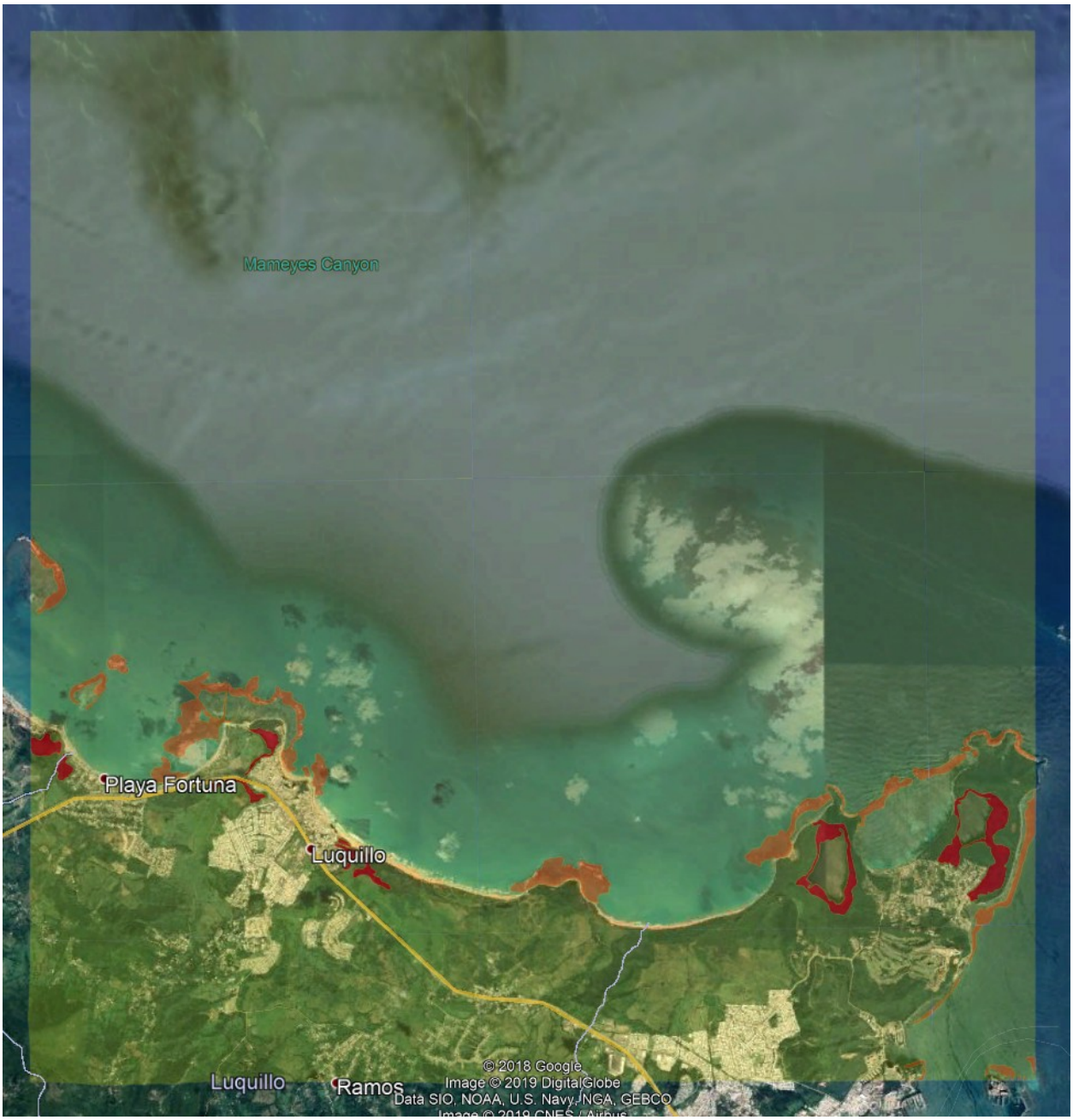

Figure 63 – Image of color-classified frictional Manning coefficients for Grid 11. Red are mangroves (Manning = 0.145), orange are reefs (Manning = 0.05), and the rest of the grid is painted with a yellow hue where the Manning coefficient is set at 0.03.

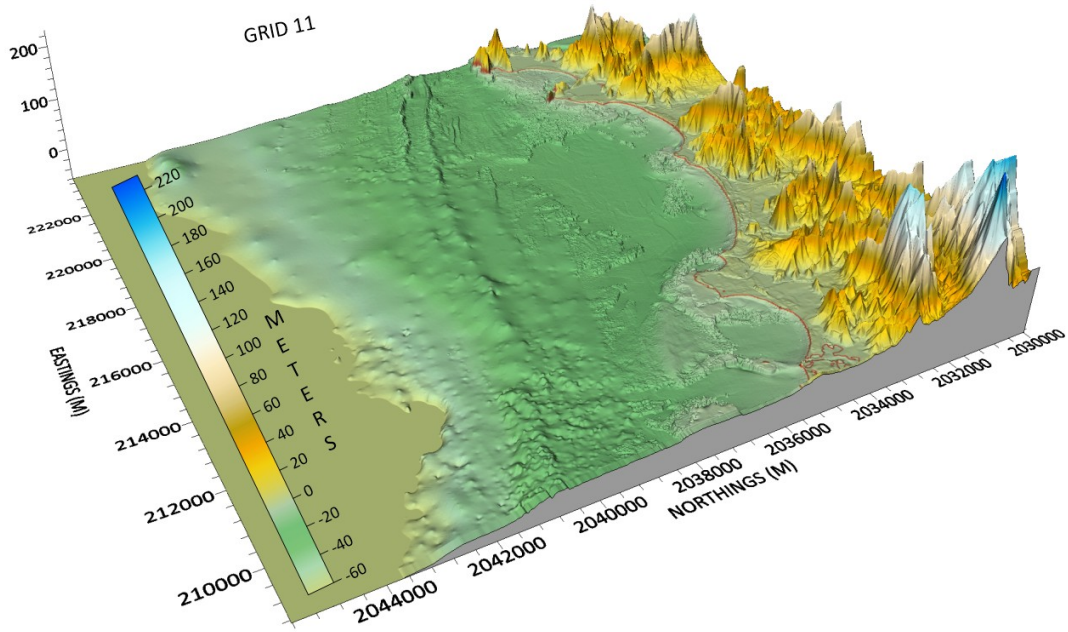

Figure 64 — 3D plot of bathymetry/topography supplied to Grid 11. Red curve is the MSL shoreline. Looking from the northeast.

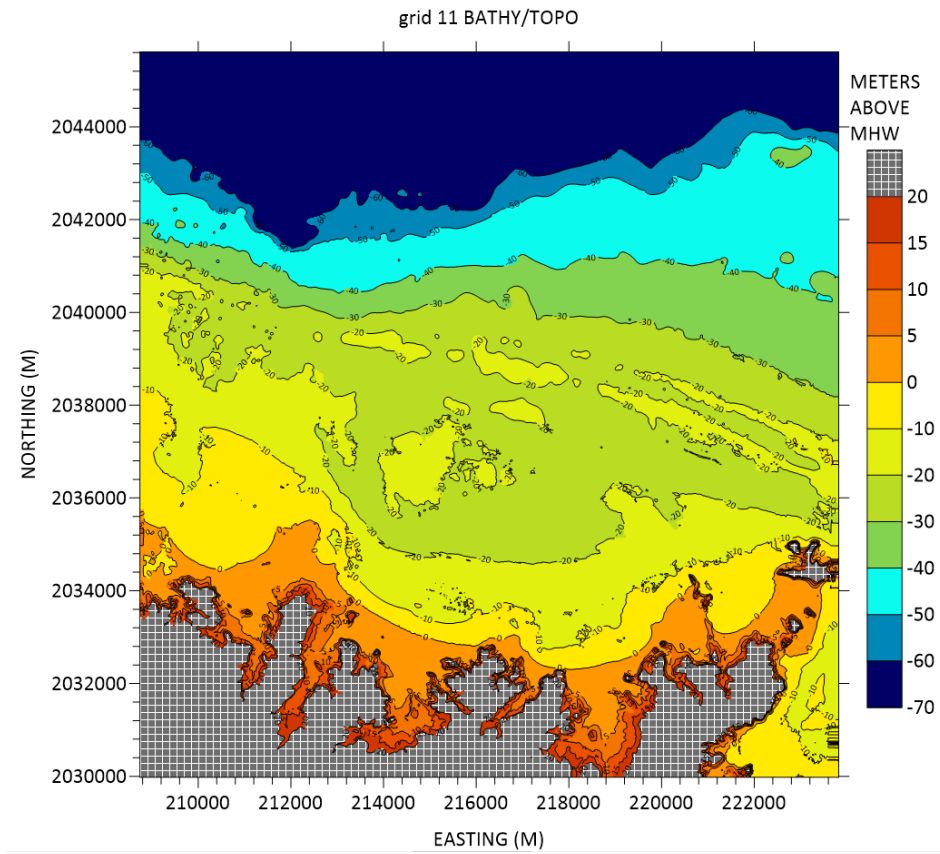

Figure 65 — 2D plot of bathymetry/topography supplied to Grid 11. Red curve is the MSL shoreline. Wavemaker is located at the northern boundary and waves propagate southward.

GRID 12 (FAJARDO TO CEIBA)

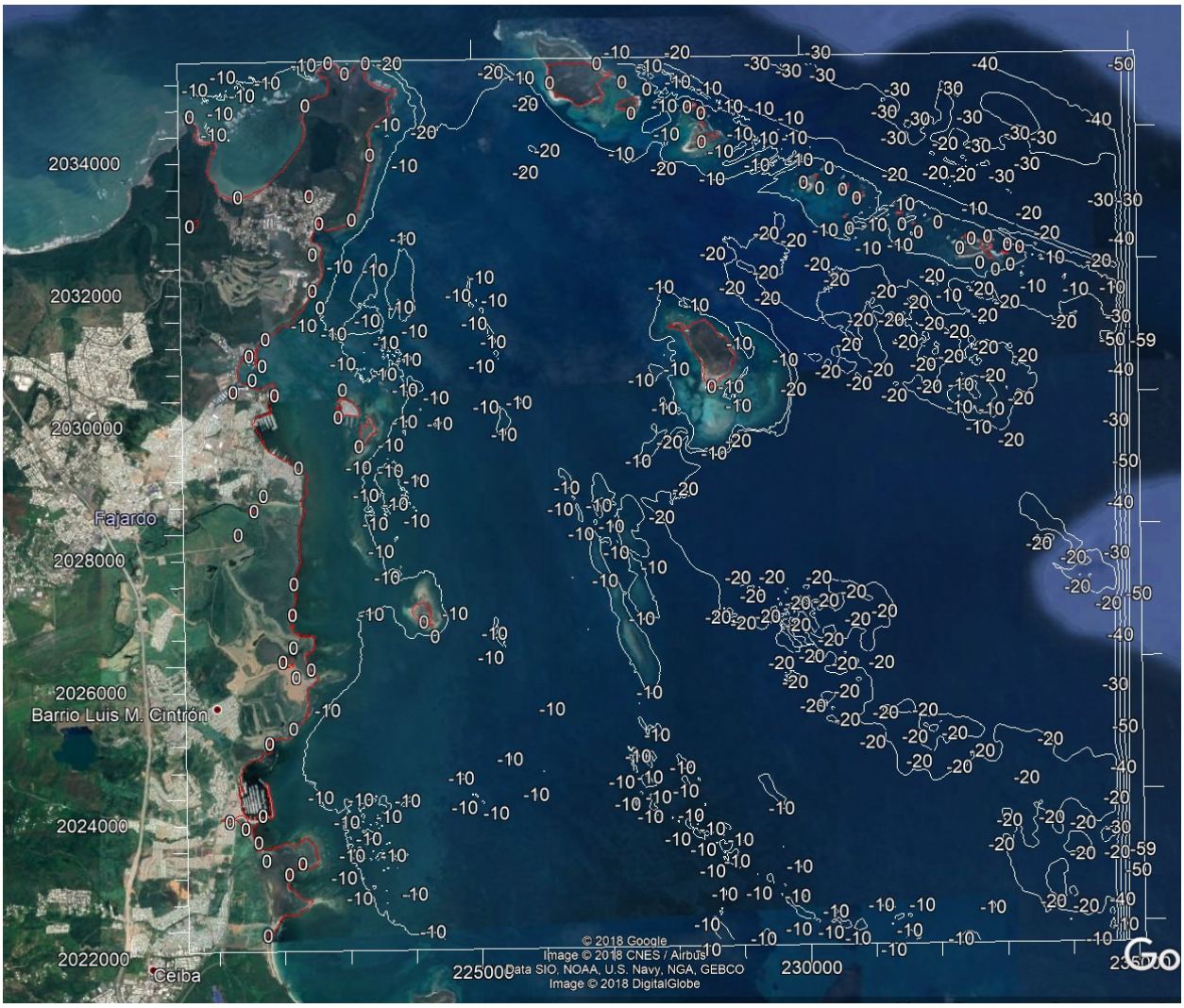

Figure 66 – Outline of computational Grid 12 overlaid on top of Google Earth, showing depth contours, in meters. Mean Sea Level Shoreline is outlined by the red curve. Contours up to 59 m are shown. Deeper waters are set to a constant depth of 60 m. The wavemaker is located at the right boundary and waves propagate westward.

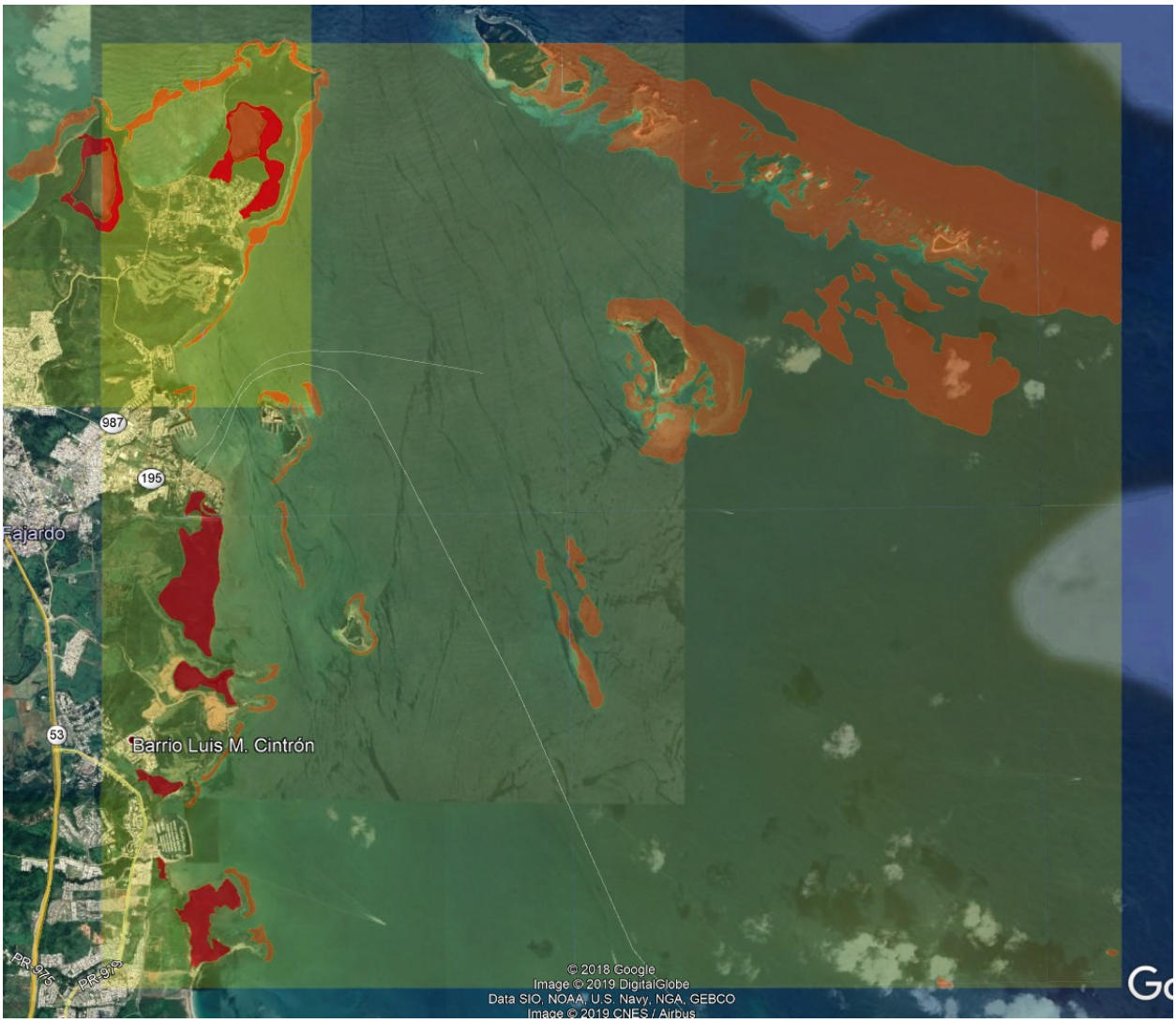

Figure 67 – Image of color-classified frictional Manning coefficients for Grid 12. Red are mangroves (Manning = 0.145), orange are reefs (Manning = 0.05), and the rest of the grid is painted with a yellow hue where the Manning coefficient is set at 0.03.

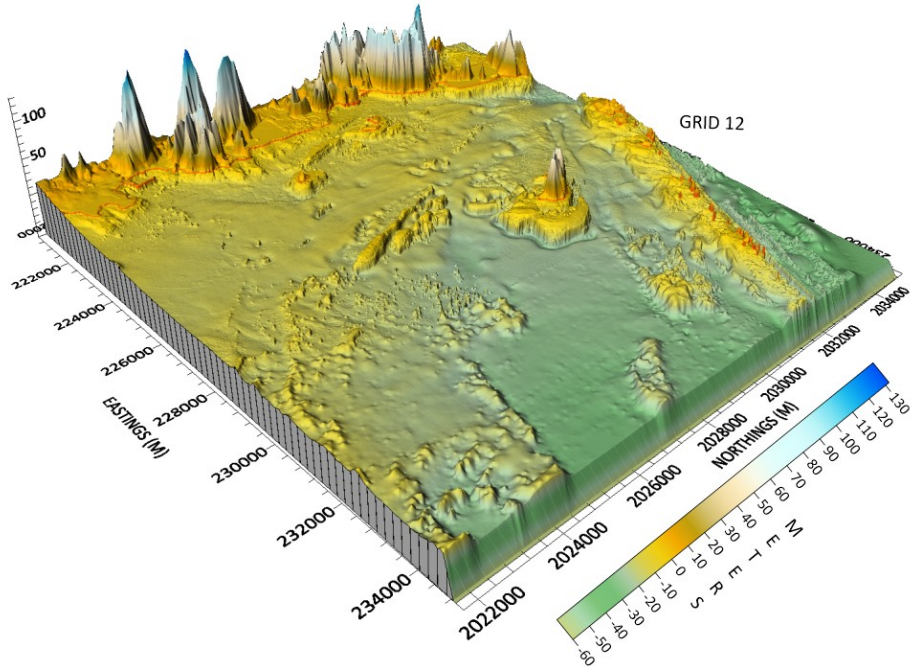

Figure 68 – 3D plot of bathymetry/topography supplied to Grid 12. Red curve is the MSL shoreline. Looking from the southeast.

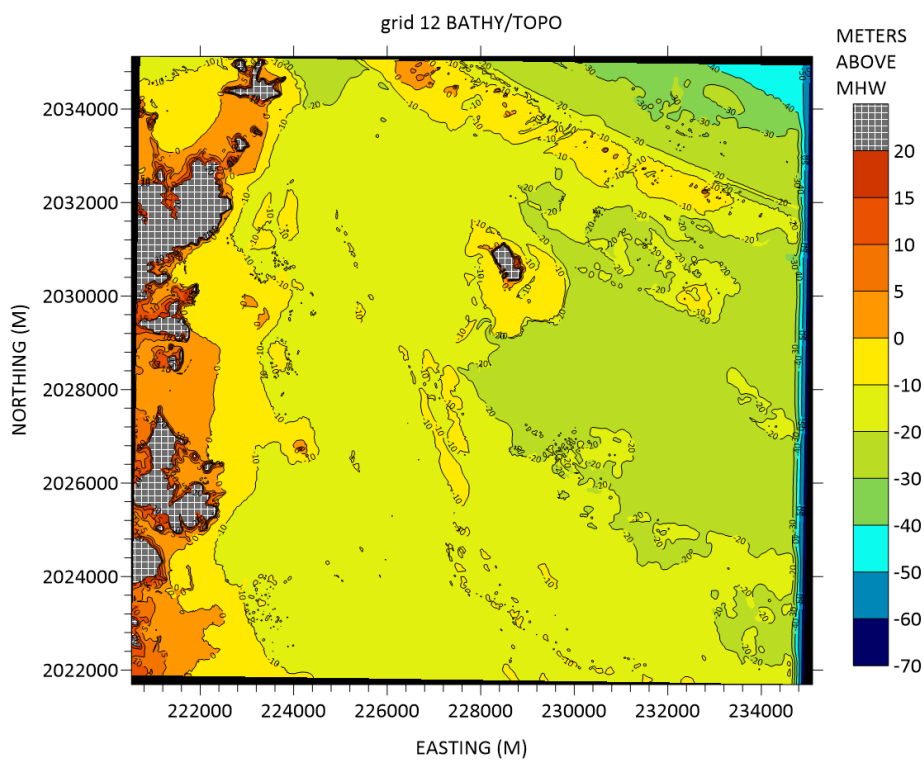

Figure 69 — 2D plot of bathymetry/topography supplied to Grid 12. Red curve is the MSL shoreline. Waves are sent along the eastern boundary towards the west.

GRID 13 (CEIBA TO NAGUABO)

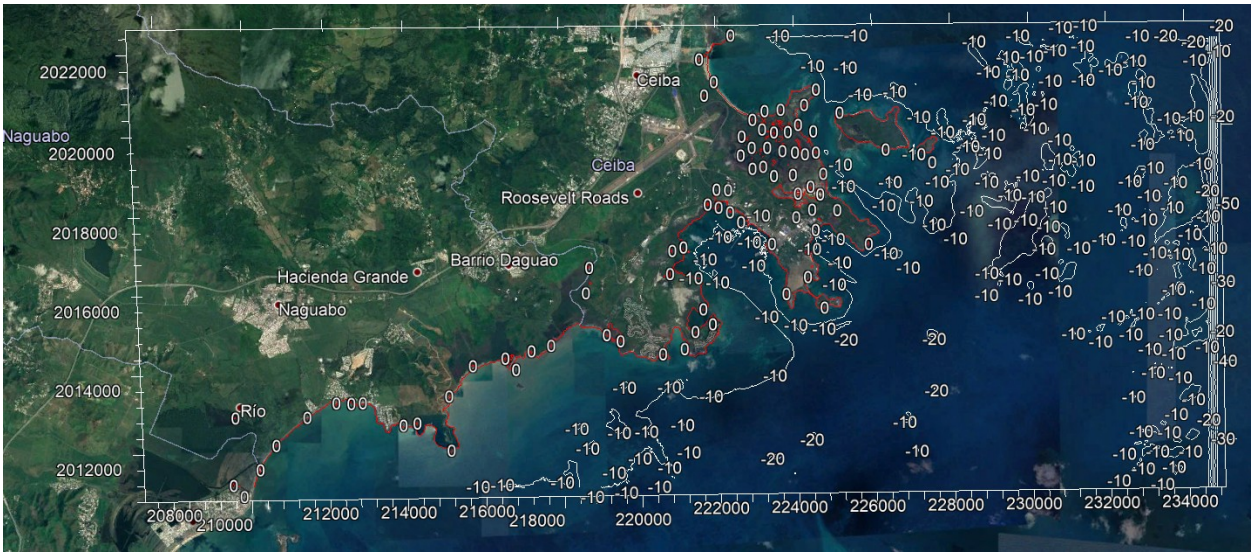

Figure 70 – Outline of computational Grid 13 overlaid on top of Google Earth, showing depth contours, in meters. Mean Sea Level Shoreline is outlined by the red curve. Contours up to 59 m are shown. Deeper waters are set to a constant depth of 60 m. The wavemaker is located at the right boundary and waves propagate westward.

Figure 71 – Image of color-classified frictional Manning coefficients for Grid 13. Red are mangroves (Manning = 0.145), orange are reefs (Manning = 0.05), and the rest of the grid is painted with a yellow hue where the Manning coefficient is set at 0.03.

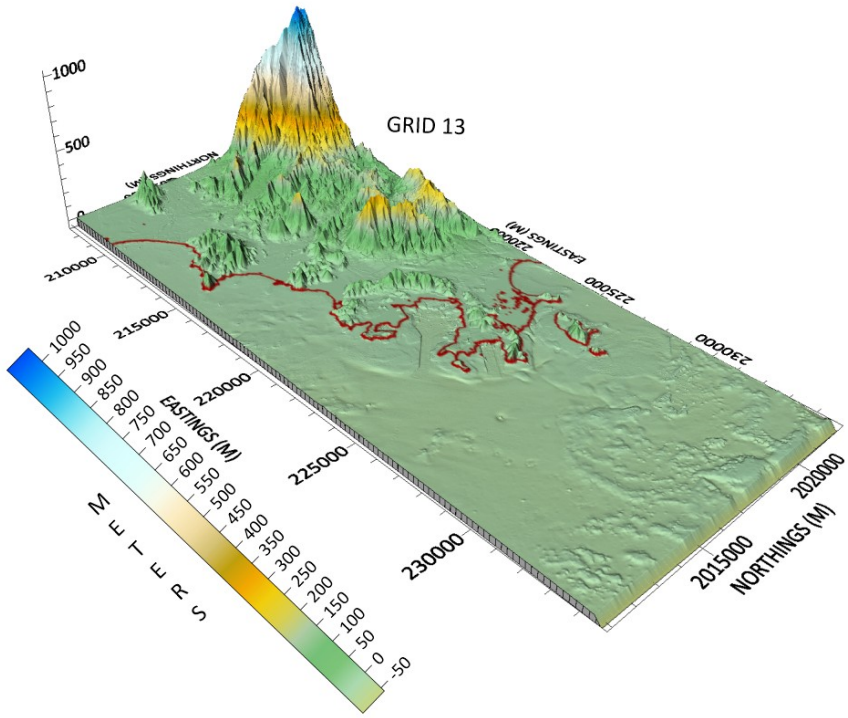

Figure 72 –23D plot of bathymetry/topography supplied to Grid 13. Red curve is the MSL shoreline.

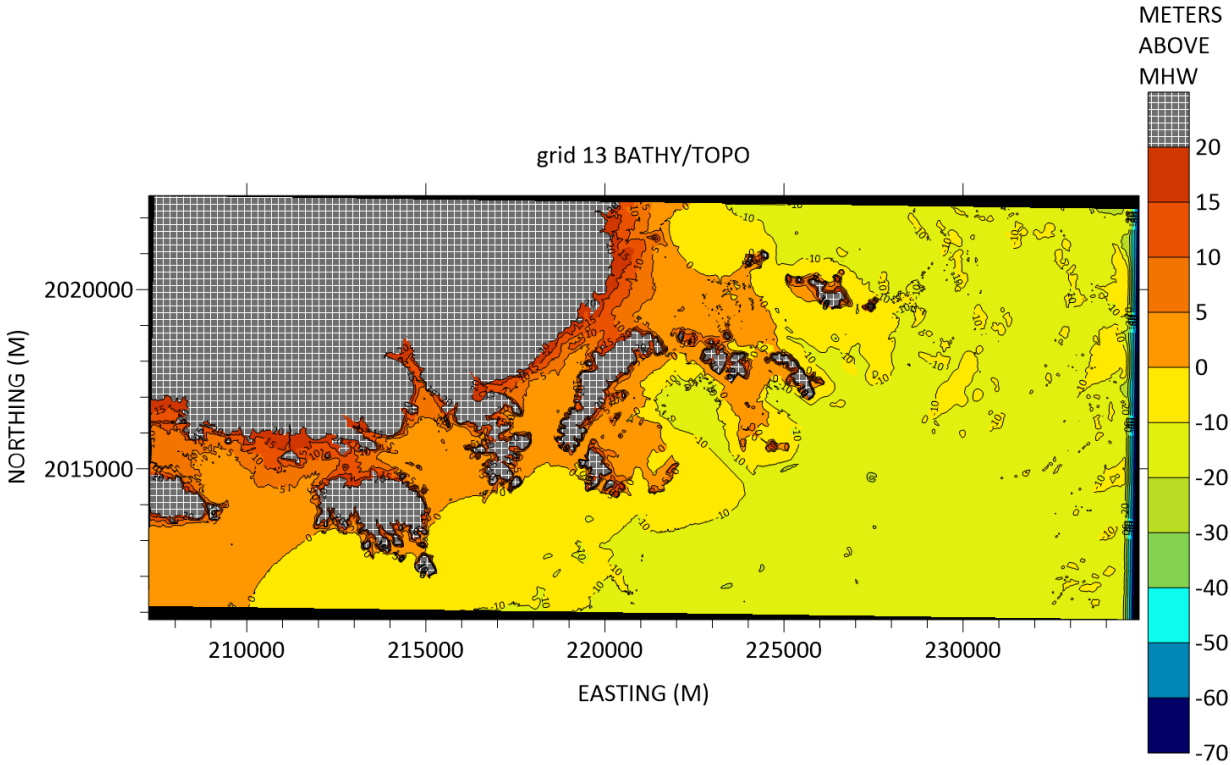

Figure 73– 2D plot of bathymetry/topography supplied to Grid 13. Red curve is the MSL shoreline. Wavemaker is located at the right boundary and waves propagate to the west.

GRID 14 (NAGUABO TO HUMACAO)

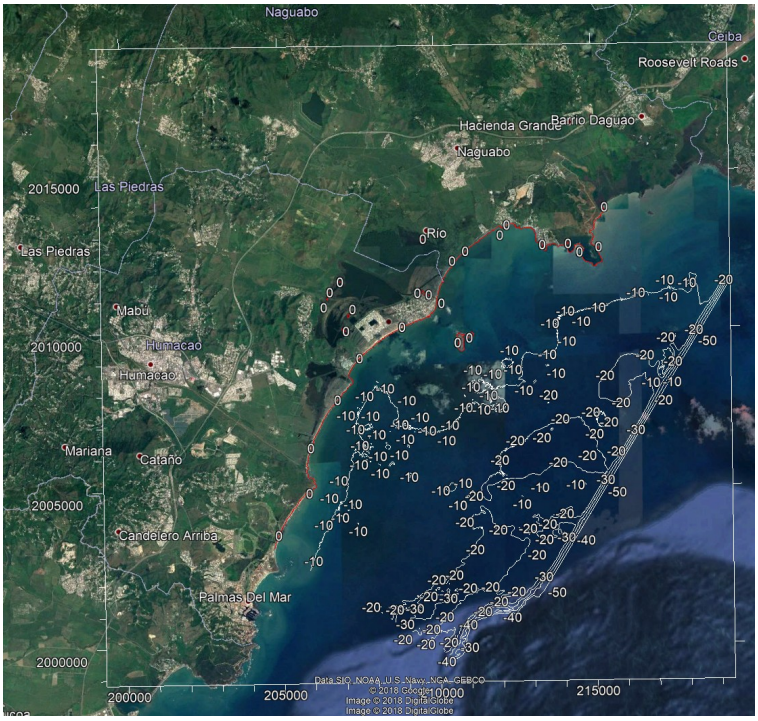

Figure 74 – Outline of computational Grid 14 overlaid on top of Google Earth, showing depth contours, in meters. Mean Sea Level Shoreline is outlined by the red curve. Contours up to 59 m are shown. Deeper waters are set to a constant depth of 60 m. . The wavemaker is located at the southeast (see Figure 75) and waves propagate northwestward (along the grid's x-axis).

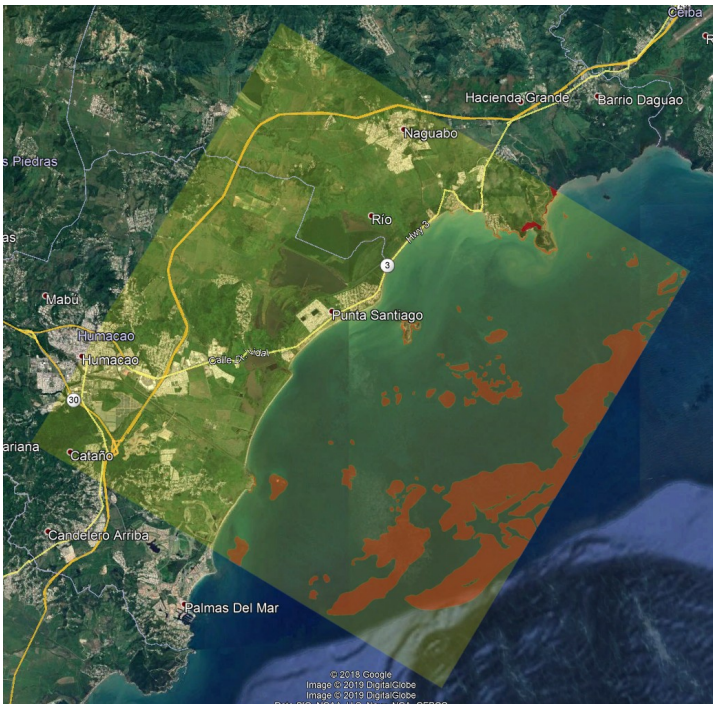

Figure 75 – Image of color-classified frictional Manning coefficients for Grid 14. Red are mangroves (Manning = 0.145), orange are reefs (Manning = 0.05), and the rest of the grid is painted with a yellow hue where the Manning coefficient is set at 0.03.

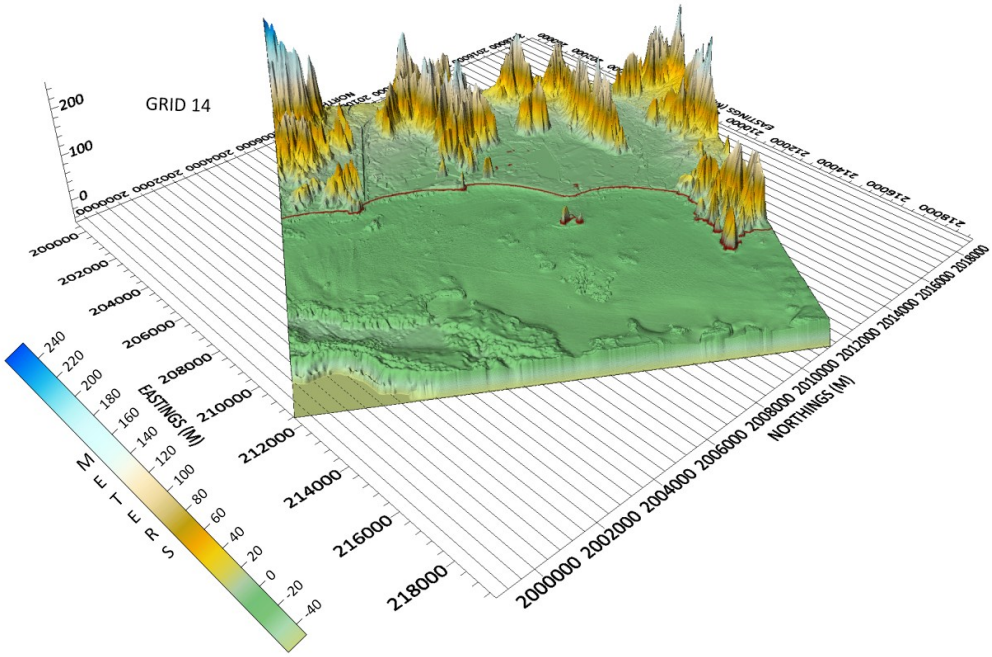

Figure 76 – 3D plot of bathymetry/topography supplied to Grid 14. Red curve is the MSL shoreline.

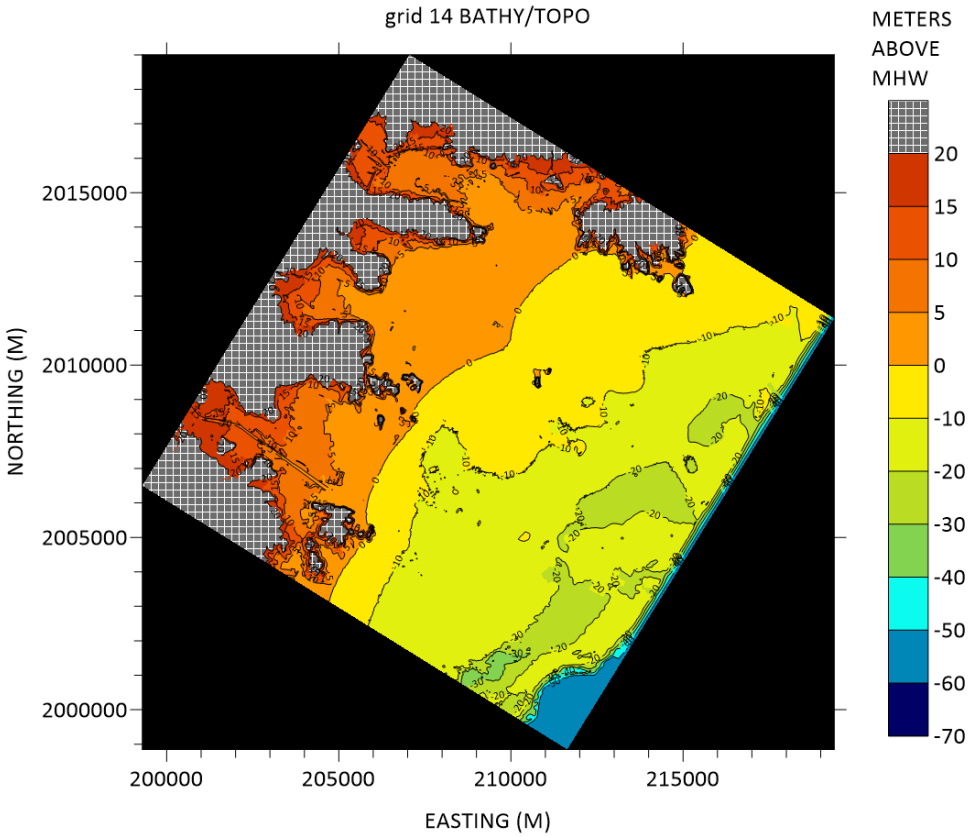

Figure 77– 2D plot of bathymetry/topography supplied to Grid 14. Red curve is the MSL shoreline. Wavemaker is located at the southeast boundary and propagate to the northwest.

GRID 15 (HUMACAO TO MAUNABO)

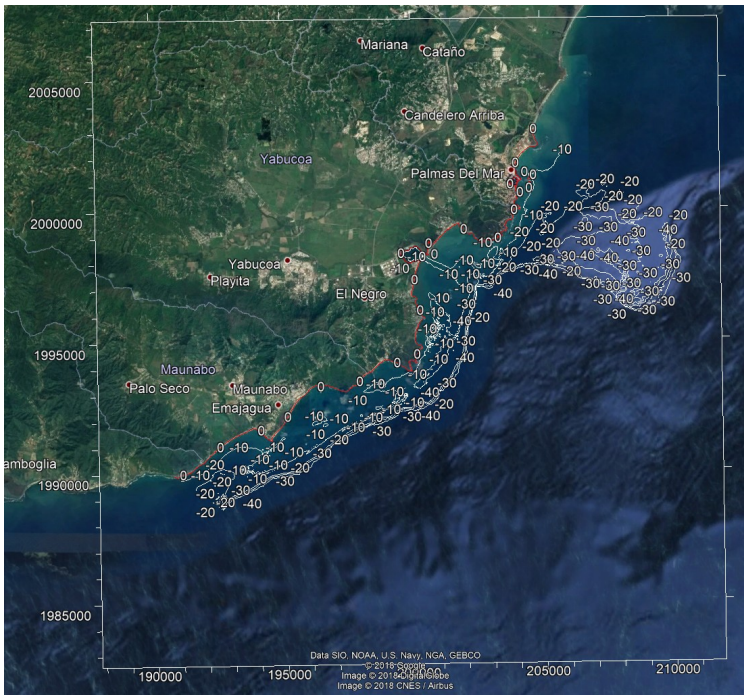

Figure 78 – Outline of computational Grid 15 overlaid on top of Google Earth, showing depth contours, in meters. Mean Sea Level Shoreline is outlined by the red curve. Contours up to 59 m are shown. Deeper waters are set to a constant depth of 60 m. The grid is rotated clockwise as shown in Figure 79 for the runs.

Figure 79 – Image of color-classified frictional Manning coefficients for Grid 15. Red are mangroves (Manning = 0.145), orange are reefs (Manning = 0.05), and the rest of the grid is painted with a yellow hue where the Manning coefficient is set at 0.03.

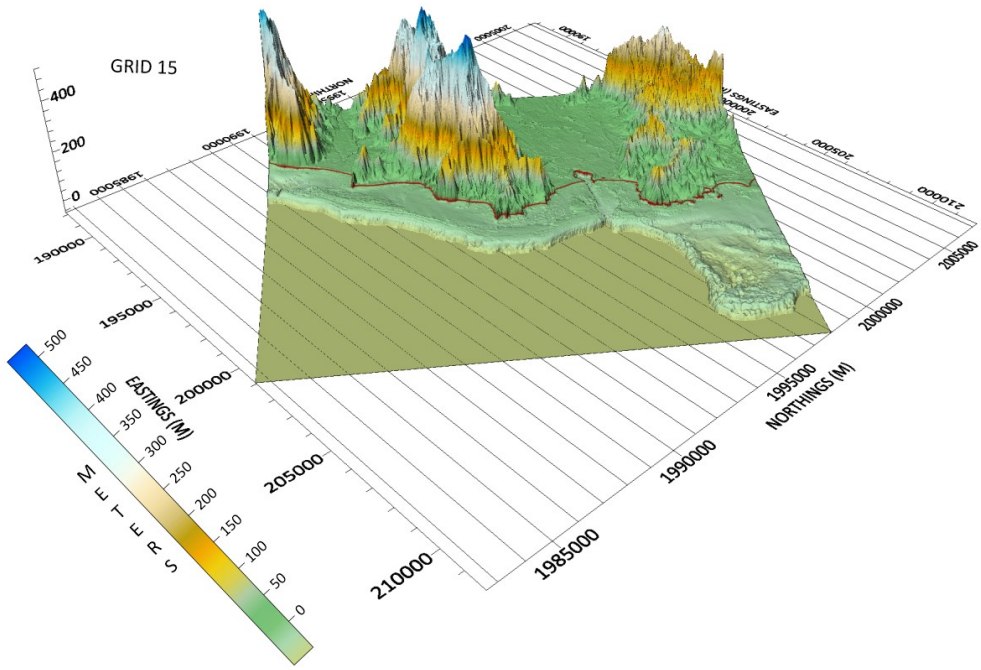

Figure 80– 3D plot of bathymetry/topography supplied to Grid 15. Red curve is the MSL shoreline.

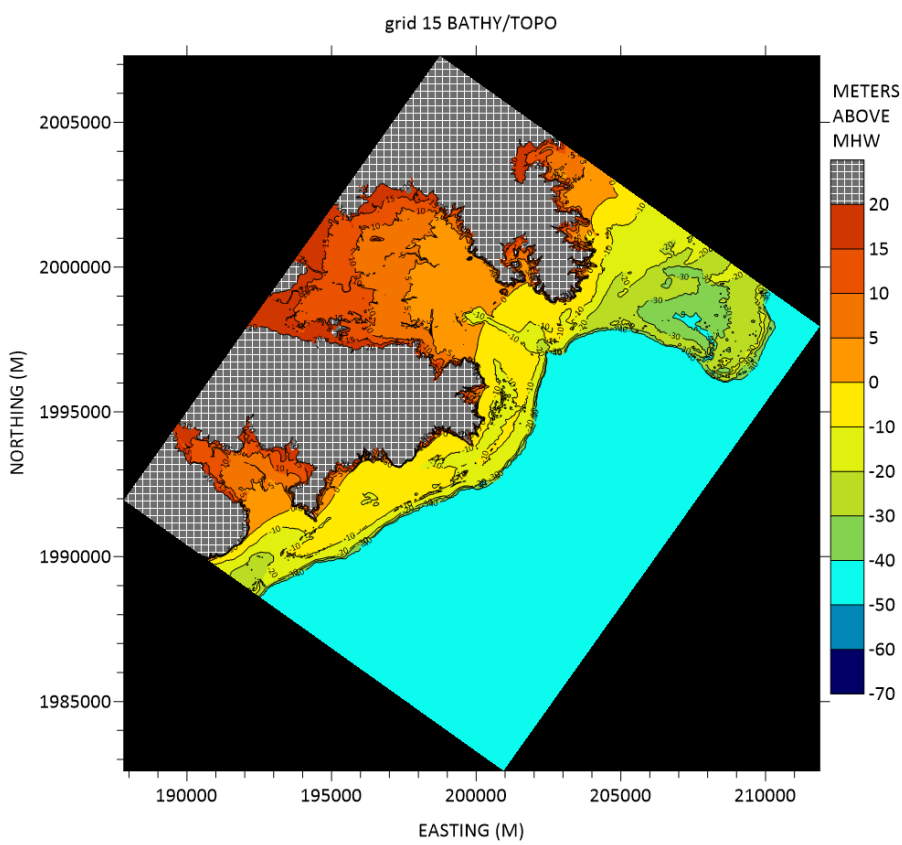

Figure 81– 2D plot of bathymetry/topography supplied to Grid 15. Red curve is the MSL shoreline. Wavemaker is located at southeastern boundary and propagate to the northwest.

GRID 16 (PATILLAS TO ARROYO)

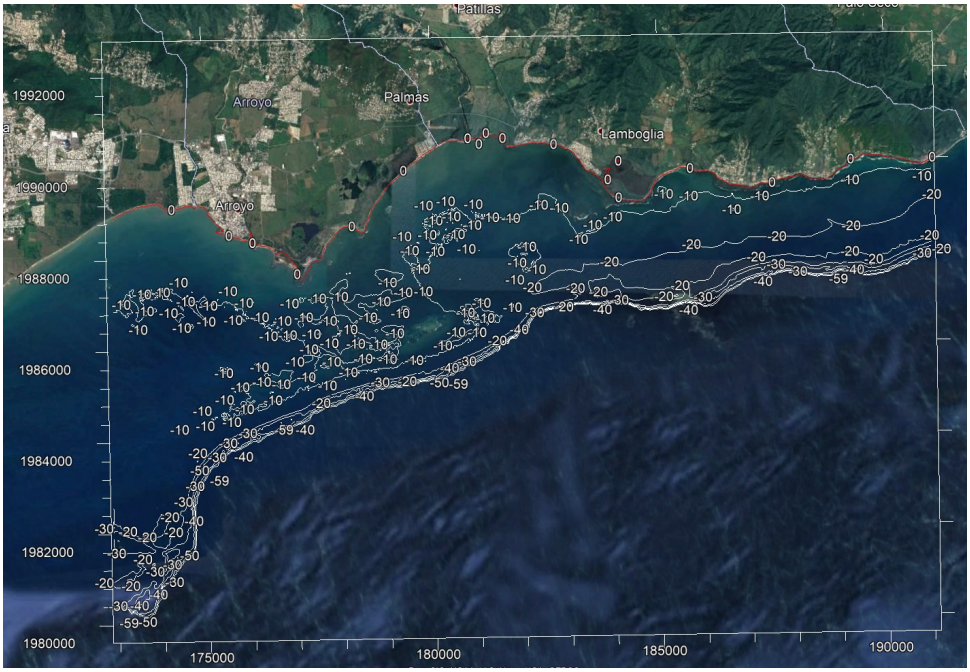

Figure 82 – Outline of computational Grid 16 overlaid on top of Google Earth, showing depth contours, in meters. Mean Sea Level Shoreline is outlined by the red curve. Contours up to 59 m are shown. Deeper waters are set to a constant depth of 60 m. The wavemaker is located at the bottom boundary and waves propagate northward.

Figure 83 – Image of color-classified frictional Manning coefficients for Grid 16. Red are mangroves (Manning = 0.145), orange are reefs (Manning = 0.05), and the rest of the grid is painted with a yellow hue where the Manning coefficient is set at 0.03.

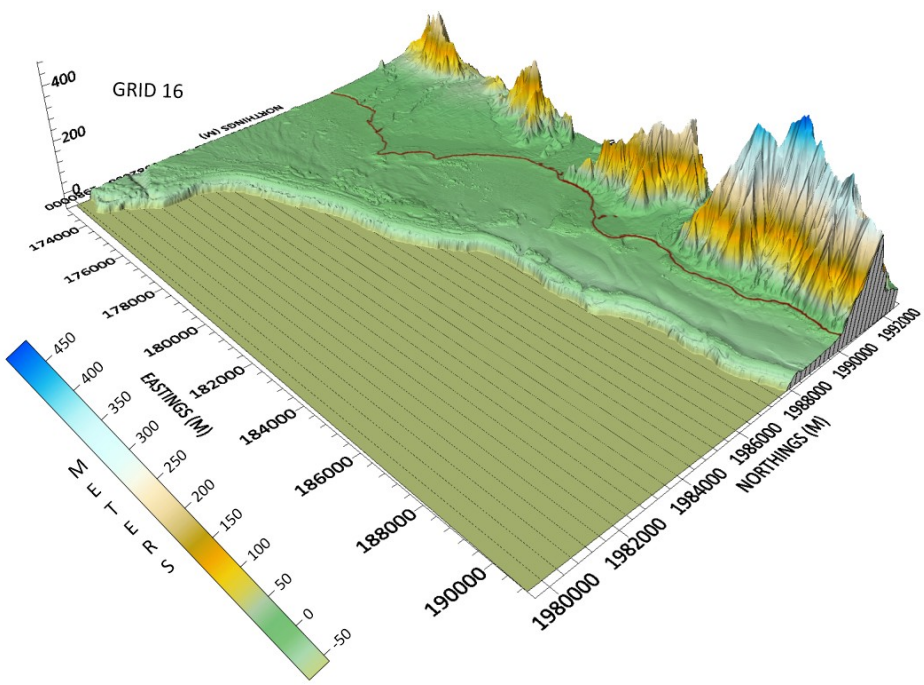

Figure 84 – 3D plot of bathymetry/topography supplied to Grid 16. Red curve is the MSL shoreline.

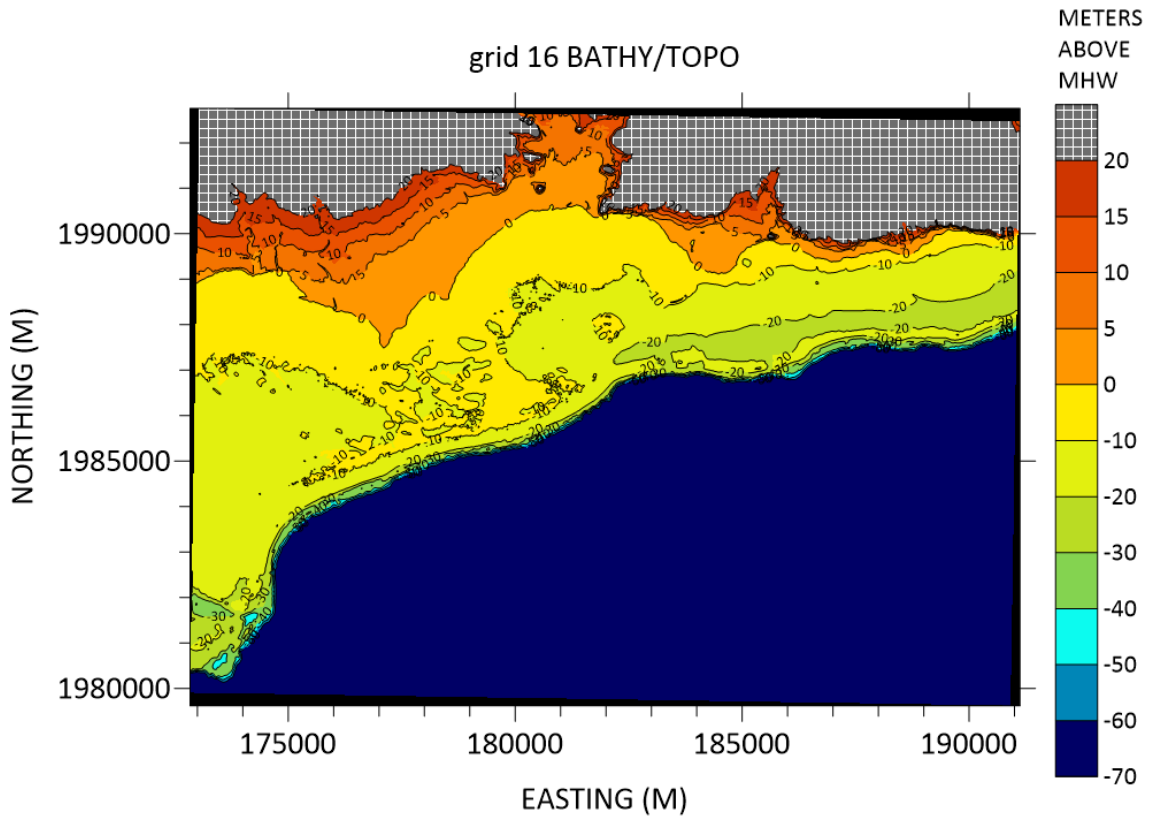

Figure 85 – 2D plot of bathymetry/topography supplied to Grid 16. Red curve is the MSL shoreline. Wavemaker is at the southern boundary and waves propagate northward.

GRID 17 (GUAYAMA TO SALINAS)

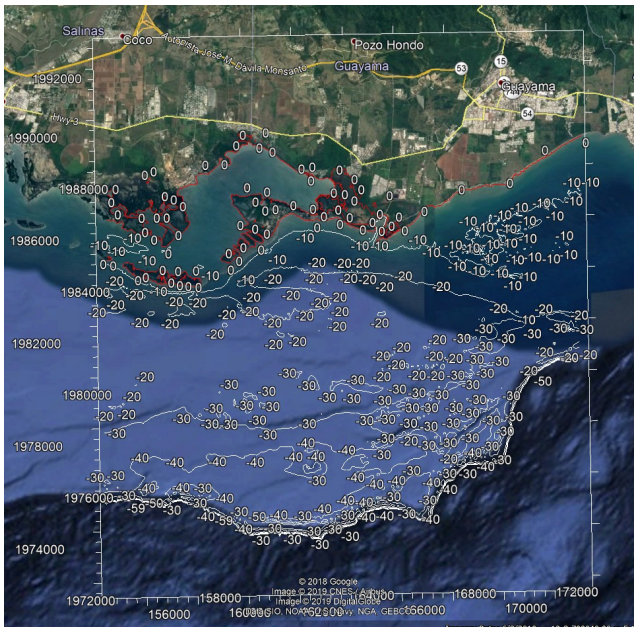

Figure 86 – Outline of computational Grid 17 overlaid on top of Google Earth, showing depth contours, in meters. Mean Sea Level Shoreline is outlined by the red curve. Contours up to 59 m are shown. Deeper waters are set to a constant depth of 60 m. The wavemaker is located at the bottom boundary and waves propagate northward.

Figure 87 – Image of color-classified frictional Manning coefficients for Grid 17. Red are mangroves (Manning = 0.145), orange are reefs (Manning = 0.05), and the rest of the grid is painted with a yellow hue where the Manning coefficient is set at 0.03.

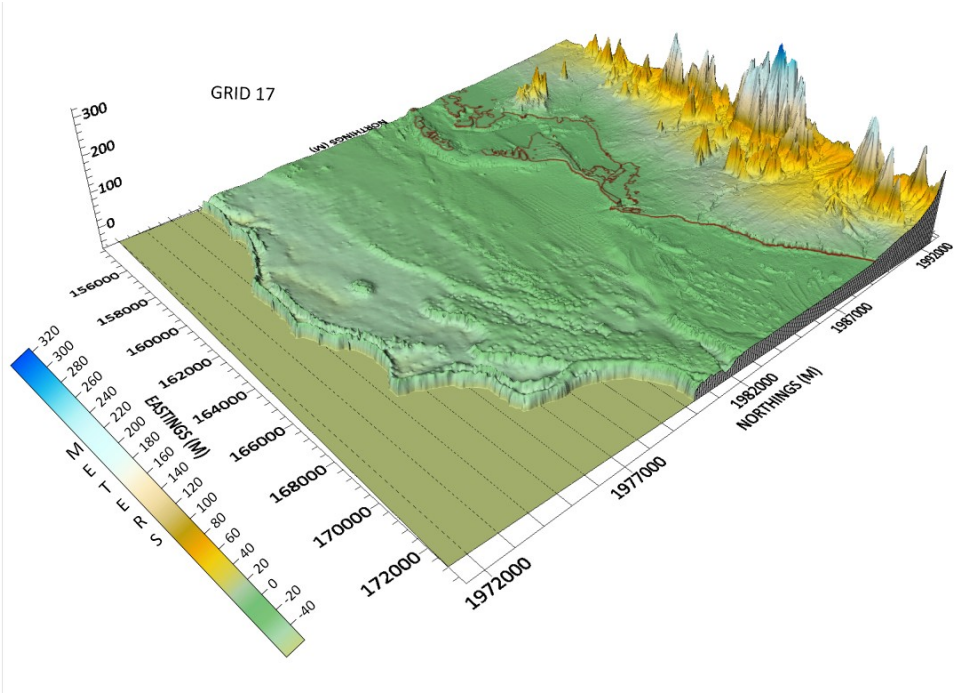

Figure 88 – 3D plot of bathymetry/topography supplied to Grid 17. Red curve is the MSL shoreline.

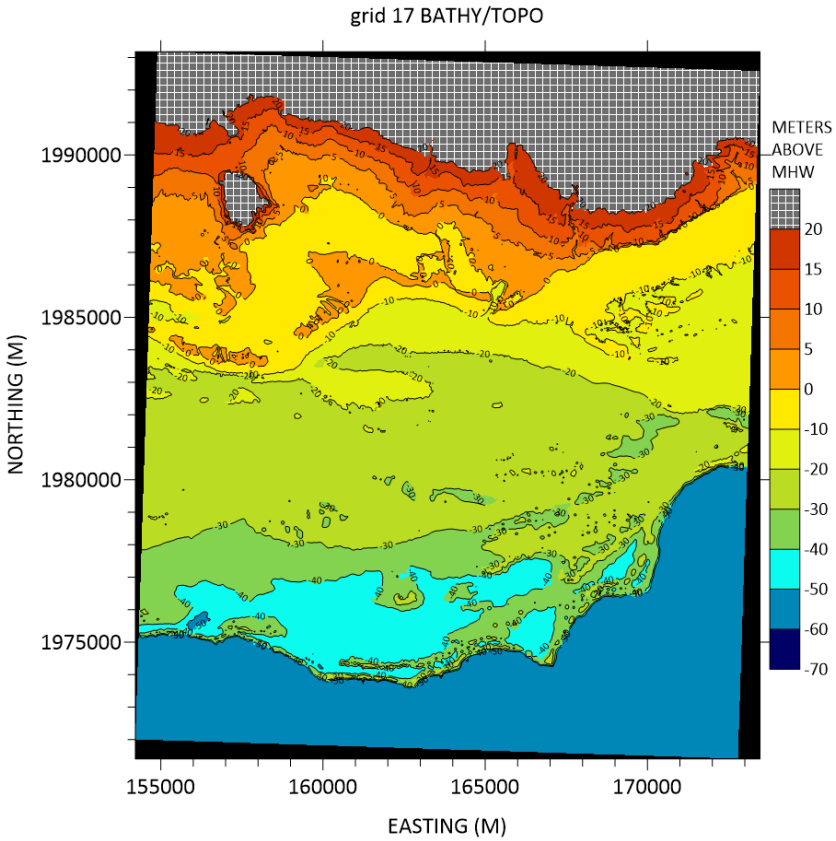

Figure 89 – 2D plot of bathymetry/topography supplied to Grid 17. Red curve is the MSL shoreline. Wavemaker is at the southern boundary and waves propagate northward.

GRID 18 (SALINAS TO SANTA ISABEL)

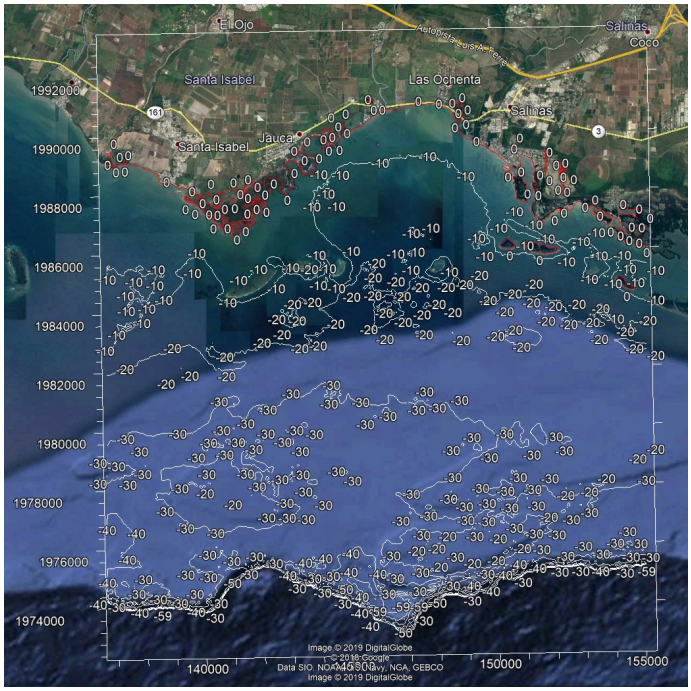

Figure 90 – Outline of computational Grid 18 overlaid on top of Google Earth, showing depth contours, in meters. Mean Sea Level Shoreline is outlined by the red curve. Contours up to 59 m are shown. Deeper waters are set to a constant depth of 60 m. The wavemaker is located at the bottom boundary and waves propagate northward.

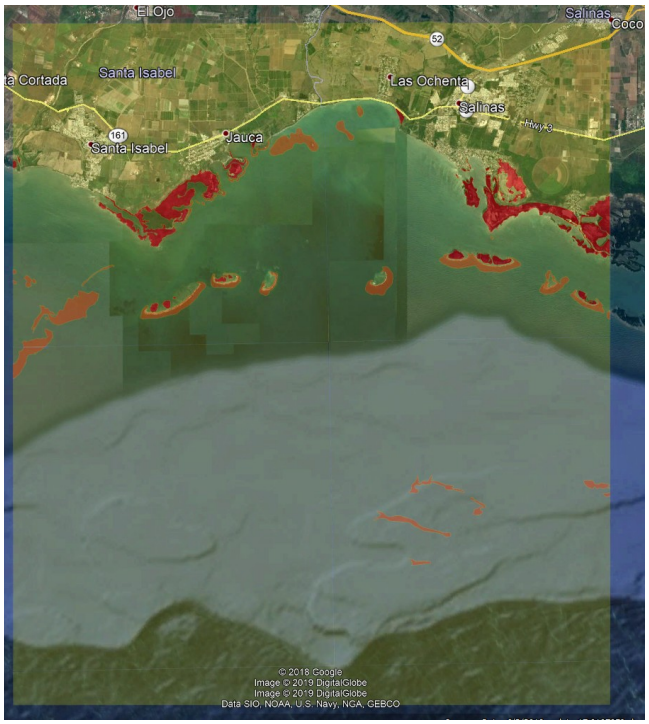

Figure 91 – Image of color-classified frictional Manning coefficients for Grid 18. Red are mangroves (Manning = 0.145), orange are reefs (Manning = 0.05), and the rest of the grid is painted with a yellow hue where the Manning coefficient is set at 0.03.

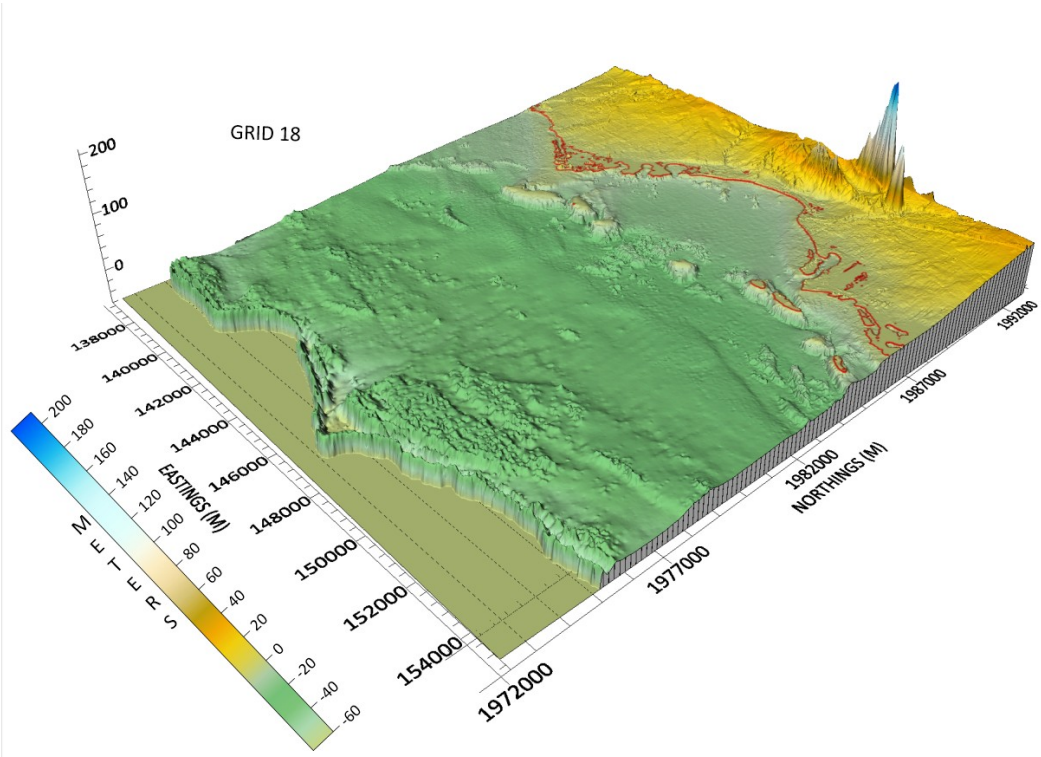

Figure 92 – 3D plot of bathymetry/topography supplied to Grid 18. Red curve is the MSL shoreline.

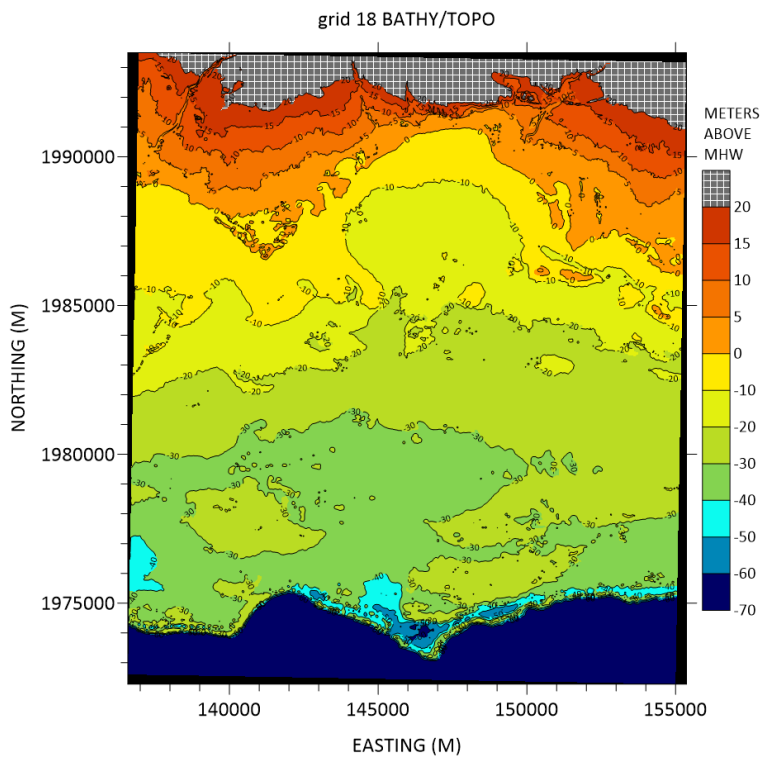

Figure 93– 2D plot of bathymetry/topography supplied to Grid 18. Red curve is the MSL shoreline. Wavemaker is at the southern boundary and waves propagate northward.

GRID 19 (SANTA ISABEL TO PONCE)

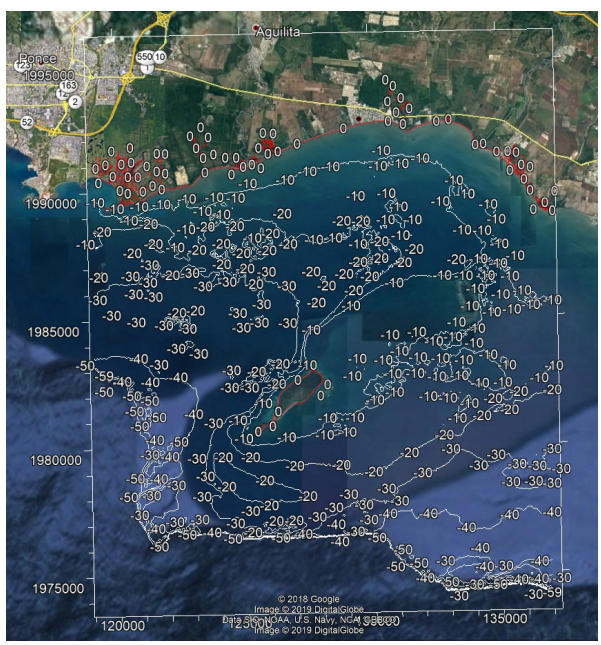

Figure 94 – Outline of computational Grid 19 overlaid on top of Google Earth, showing depth contours, in meters. Mean Sea Level Shoreline is outlined by the red curve. Contours up to 59 m are shown. Deeper waters

are set to a constant depth of 60 m. The wavemaker is located at the bottom boundary and waves propagate northward.

Figure 95 - Image of color-classified frictional Manning coefficients for Grid 19. Red are mangroves (Manning = 0.145), orange are reefs (Manning = 0.05), and the rest of the grid is painted with a yellow hue where the Manning coefficient is set at 0.03.

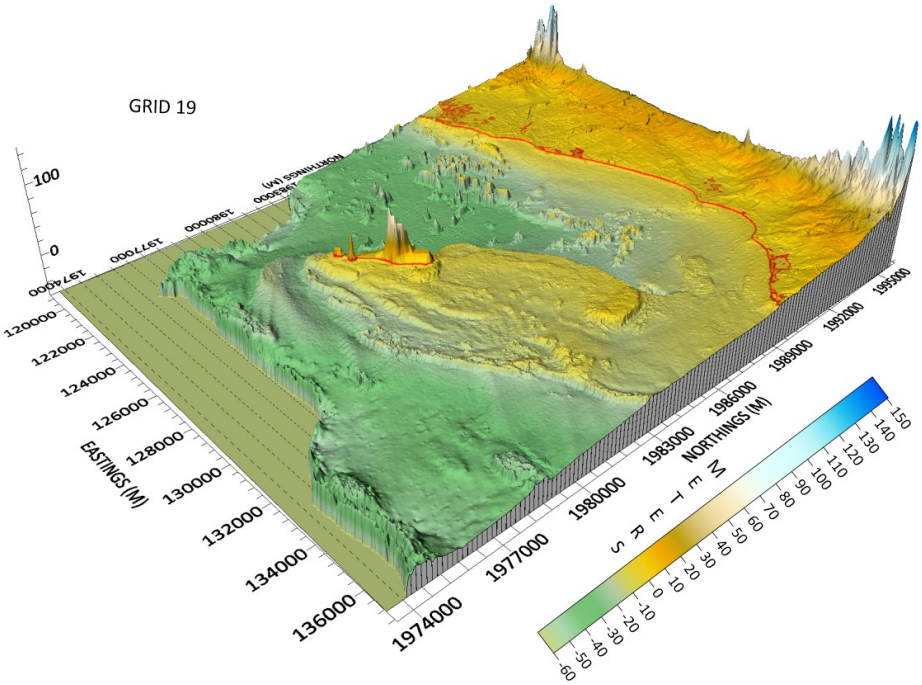

Figure 96 – 3D plot of bathymetry/topography supplied to Grid 19. Red curve is the MSL shoreline.

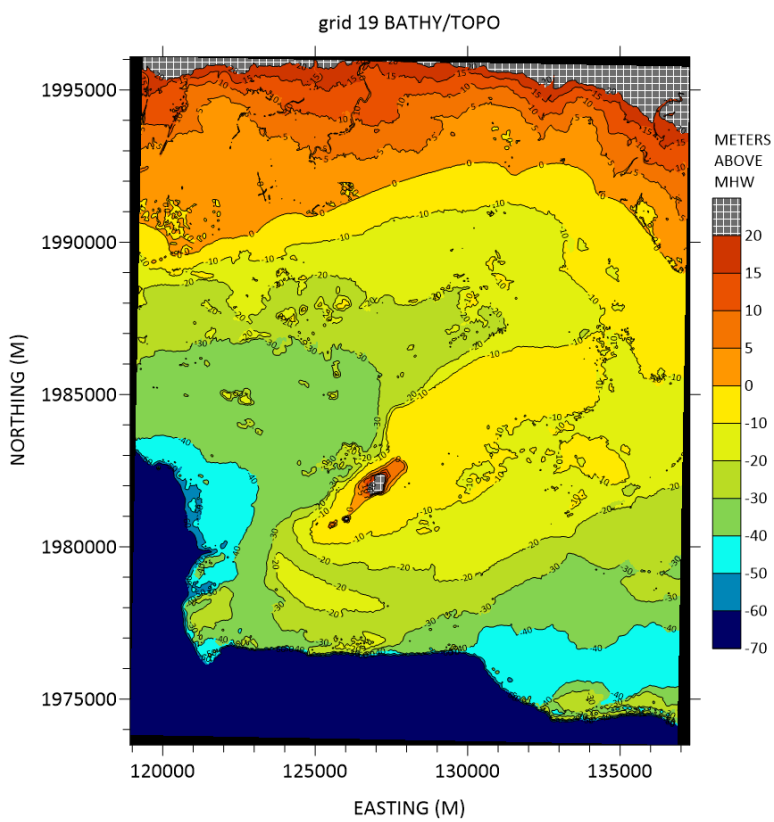

Figure 97 – 3D plot of bathymetry/topography supplied to Grid 19. Red curve is the MSL shoreline. Wavemaker is at the southern boundary and waves propagate northward.

GRID 20 (PONCE TO GUAYANILLA)

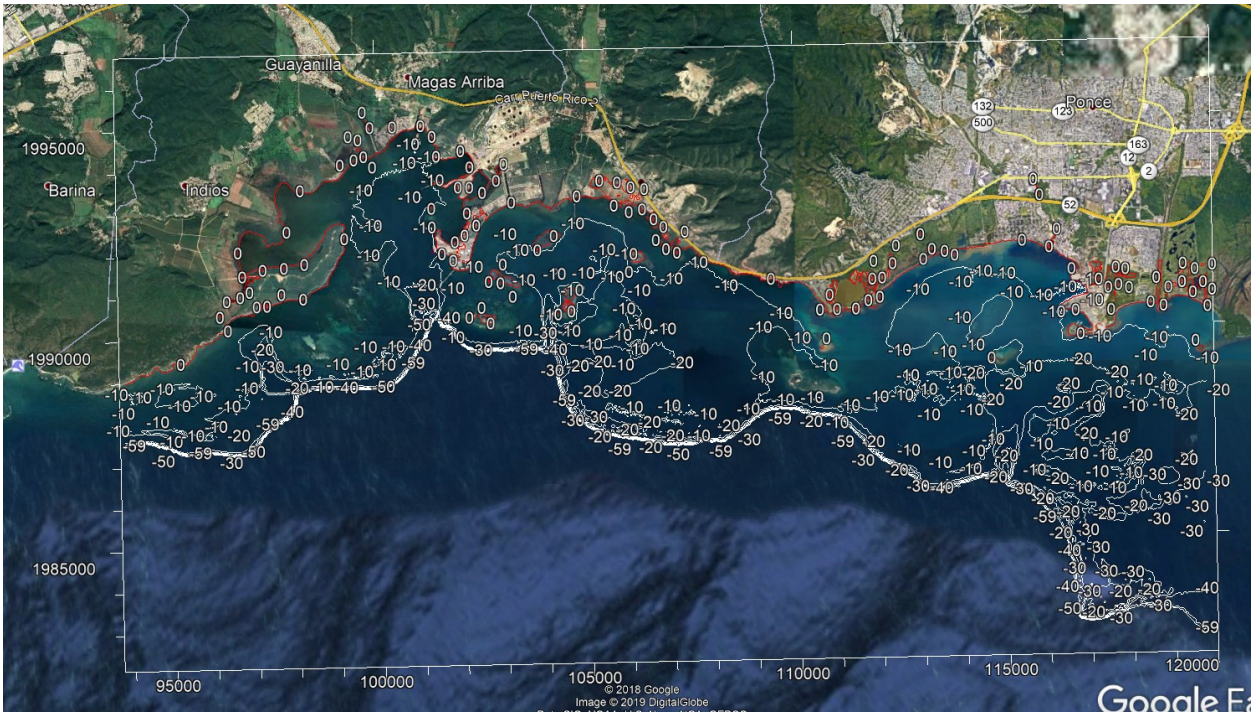

Figure 98 – Outline of computational Grid 20 overlaid on top of Google Earth, showing depth contours, in meters. Mean Sea Level Shoreline is outlined by the red curve. Contours up to 59 m are shown. Deeper waters are set to a constant depth of 60 m. The wavemaker is located at the bottom boundary and waves propagate northward.

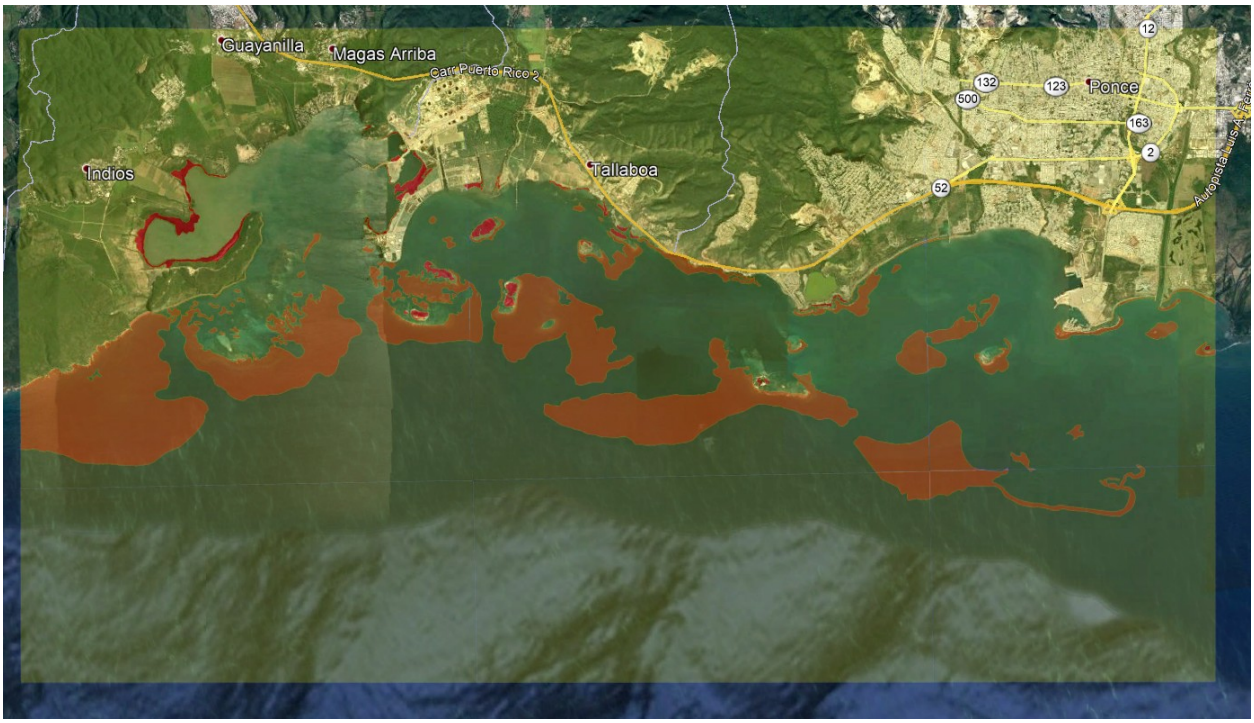

Figure 99 - Image of color-classified frictional Manning coefficients for Grid 20. Red are mangroves (Manning = 0.145), orange are reefs (Manning = 0.05), and the rest of the grid is painted with a yellow hue where the Manning coefficient is set at 0.03.

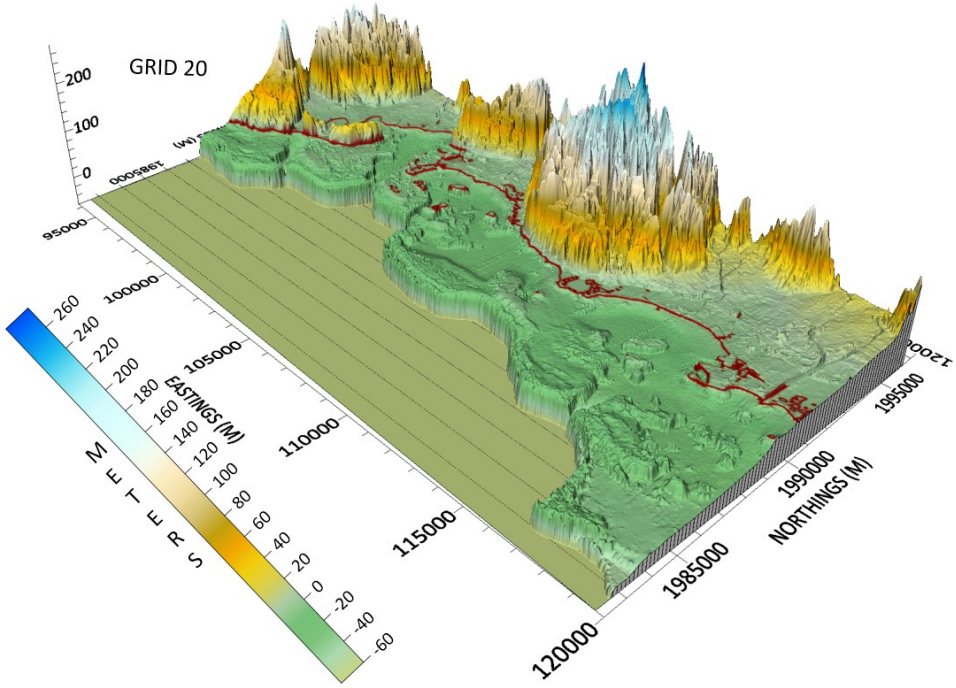

Figure 100 – 3D plot of bathymetry/topography supplied to Grid 20. Red curve is the MSL shoreline.

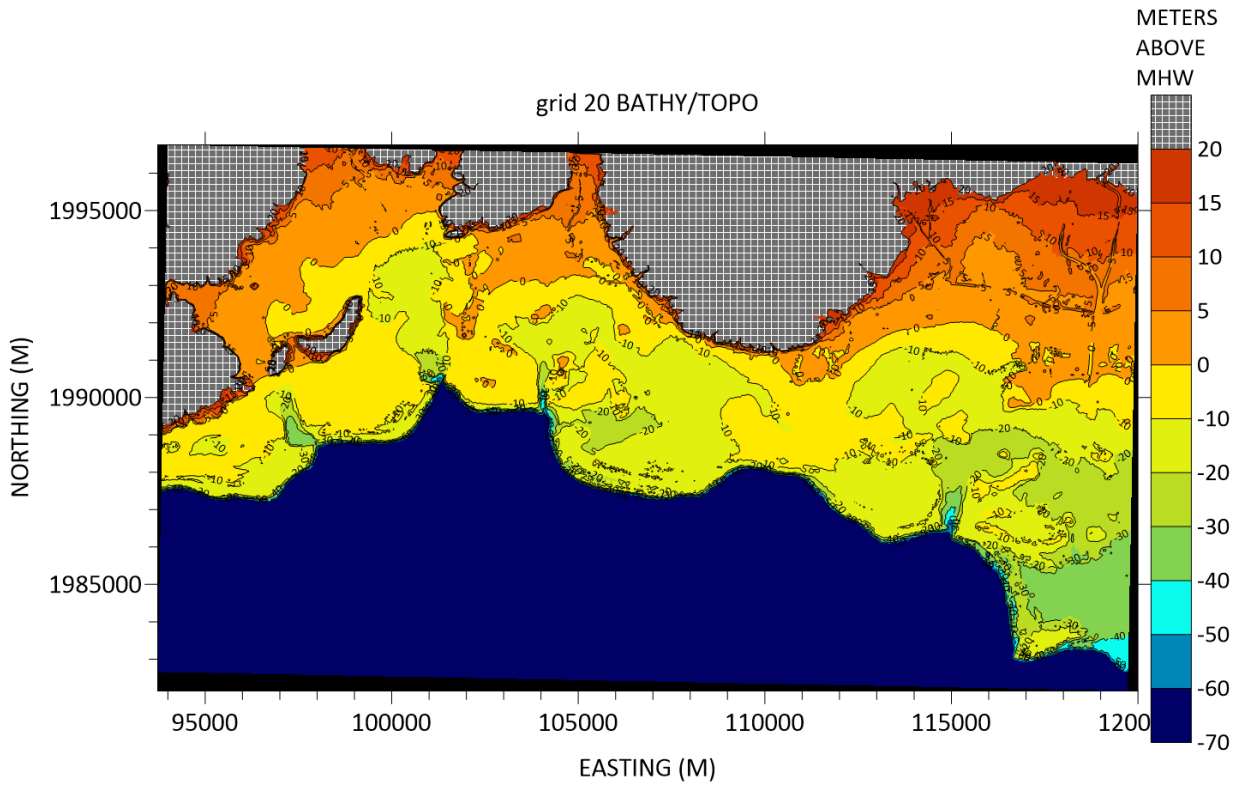

Figure 101 – 2D plot of bathymetry/topography supplied to Grid 20. Red curve is the MSL shoreline. Wavemaker is at the southern boundary and waves propagate northward.

GRID 21 (GUAYANILLA TO LAJAS)

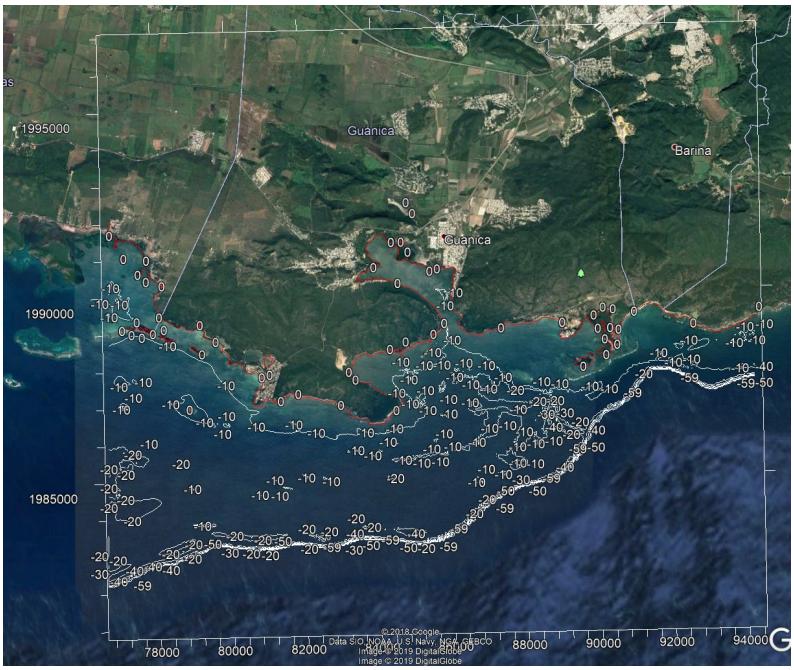

Figure 102 – Outline of computational Grid 21 overlaid on top of Google Earth, showing depth contours, in meters. Mean Sea Level Shoreline is outlined by the red curve. Contours up to 59 m are shown. Deeper waters are set to a constant depth of 60 m. The wavemaker is located at the bottom boundary and waves propagate northward.

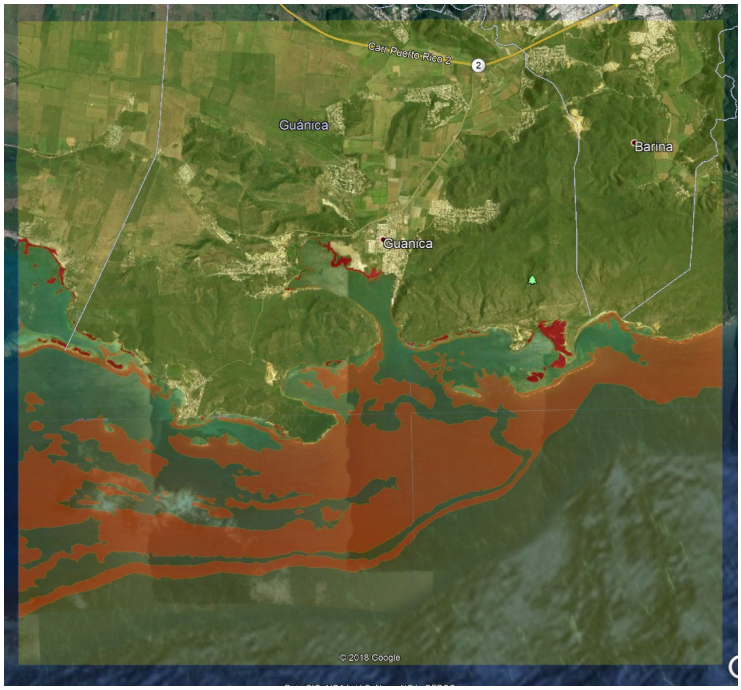

Figure 103 - Image of color-classified frictional Manning coefficients for Grid 21. Red are mangroves (Manning = 0.145), orange are reefs (Manning = 0.05), and the rest of the grid is painted with a yellow hue where the Manning coefficient is set at 0.03.

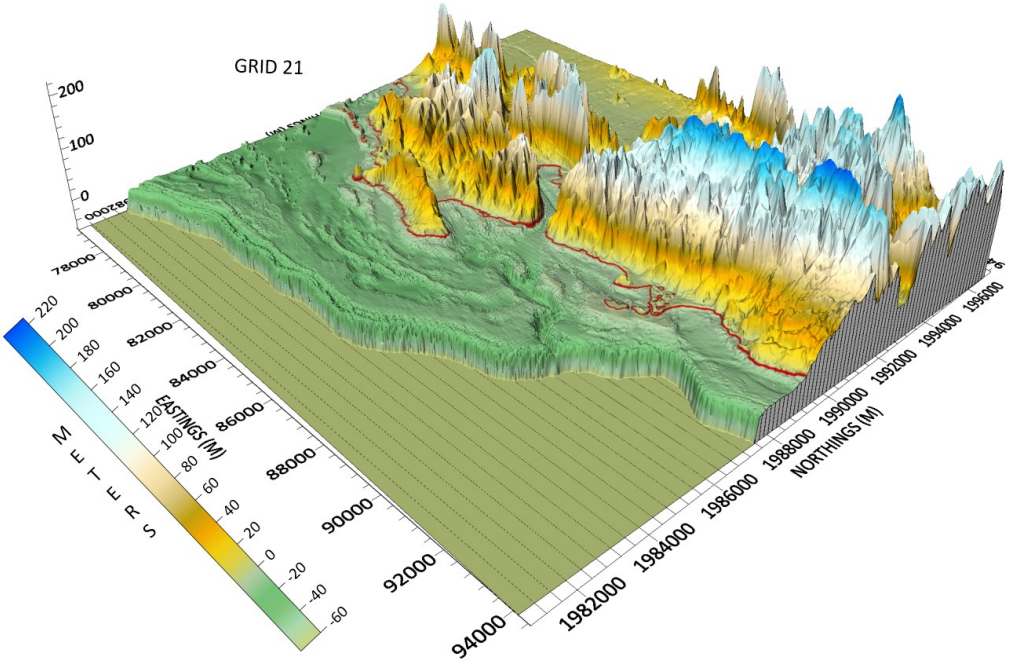

Figure 104 – 3D plot of bathymetry/topography supplied to Grid 21. Red curve is the MSL shoreline.

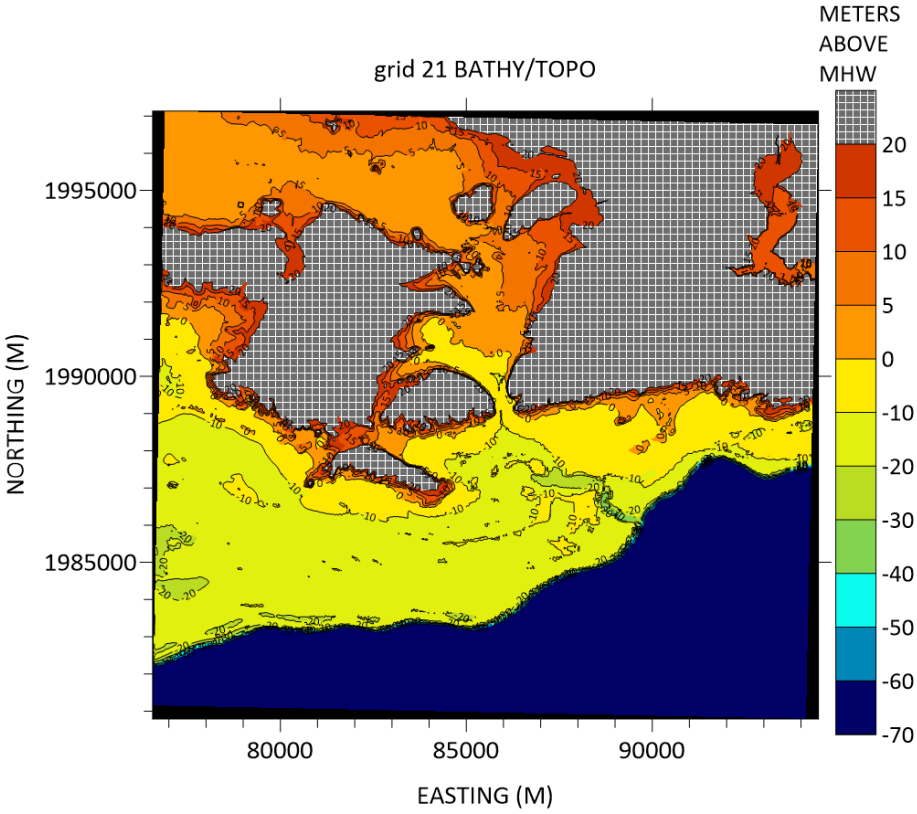

Figure 105 – 2D plot of bathymetry/topography supplied to Grid 21. Red curve is the MSL shoreline. Wavemaker is at the southern boundary and waves propagate northward.

GRID 22 (LAJAS TO CABO ROJO)

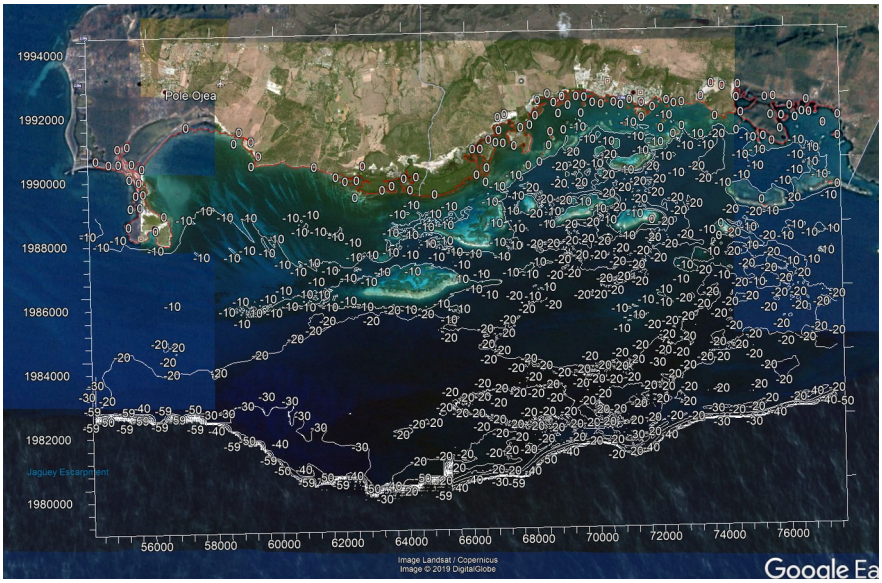

Figure 106 – Outline of computational Grid 22 overlaid on top of Google Earth, showing depth contours, in meters. Mean Sea Level Shoreline is outlined by the red curve. Contours up to 59 m are shown. Deeper waters are set to a constant depth of 60 m. The wavemaker is located at the bottom boundary and waves propagate northward.

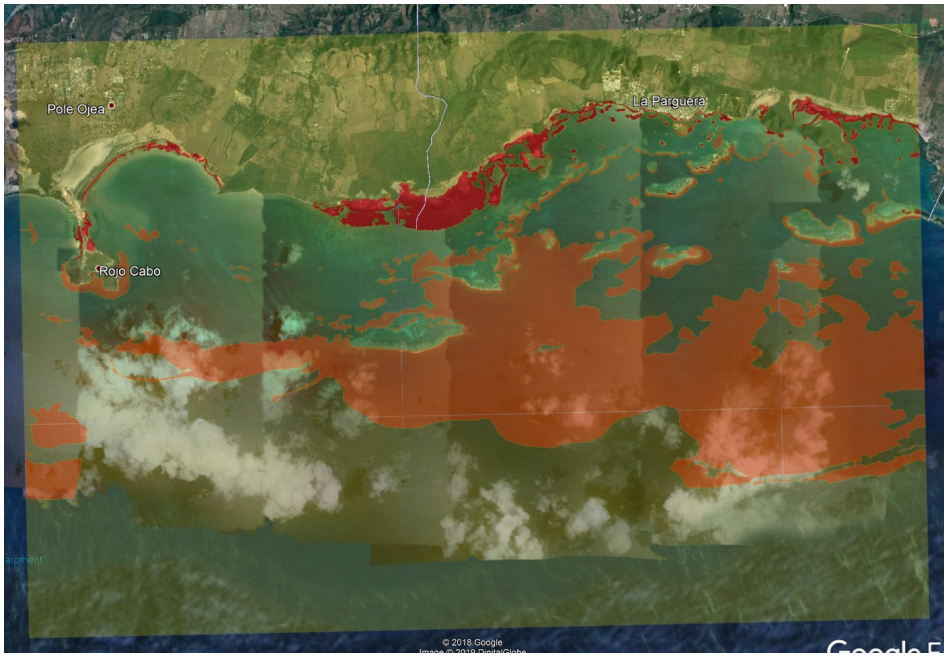

Figure 107 - Image of color-classified frictional Manning coefficients for Grid 22. Red are mangroves (Manning = 0.145), orange are reefs (Manning = 0.05), and the rest of the grid is painted with a yellow hue where the Manning coefficient is set at 0.03.

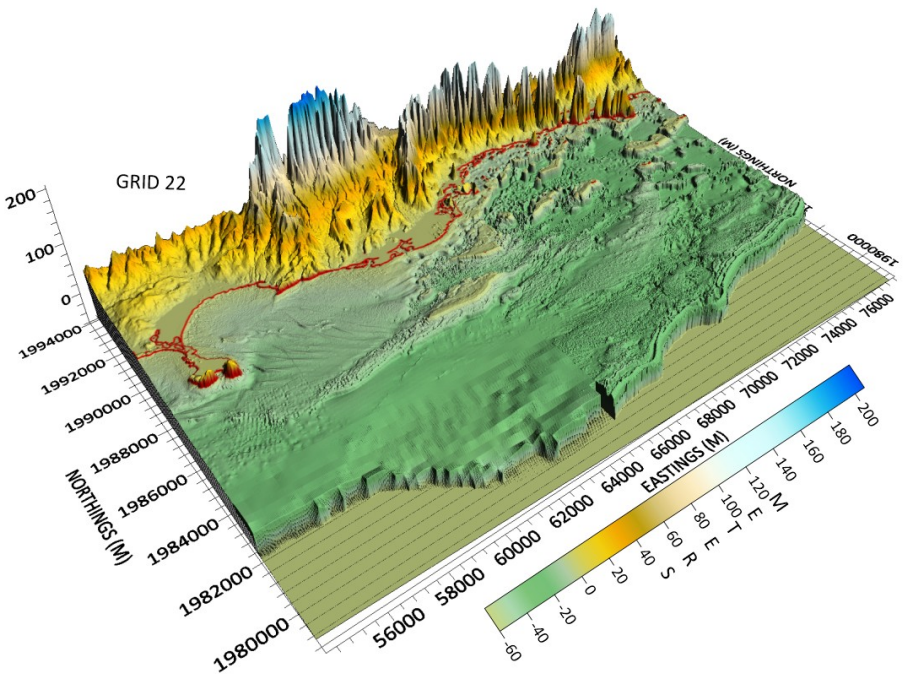

Figure 108– 3D plot of bathymetry/topography supplied to Grid 22. Red curve is the MSL shoreline.

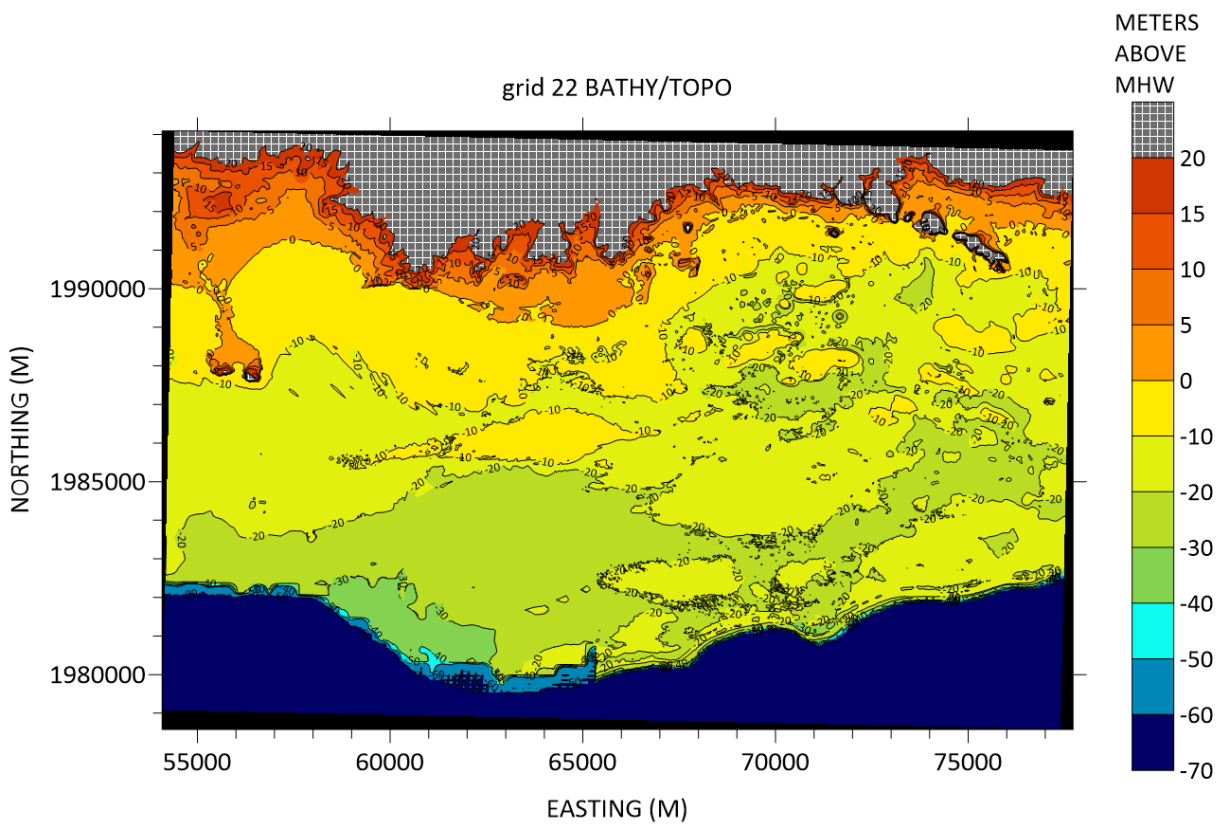

Figure 109 - 2D plot of bathymetry/topography supplied to Grid 22. Red curve is the MSL shoreline. Wavemaker is at the southern boundary and waves propagate northward.

GRID 23 (CABO ROJO)

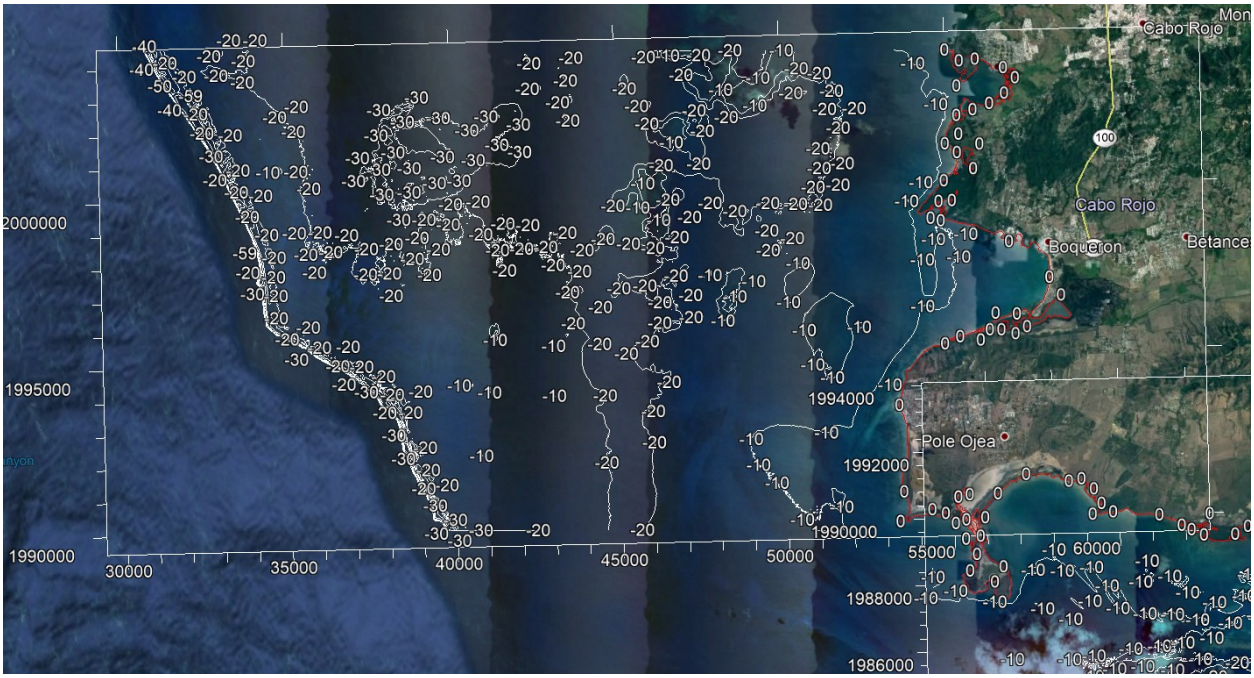

Figure 110 – Outline of computational Grid 23 overlaid on top of Google Earth, showing depth contours, in meters. Mean Sea Level Shoreline is outlined by the red curve. Contours up to 59 m are shown. Deeper waters are set to a constant depth of 60 m. The wavemaker is located at the left boundary and waves propagate eastward (to the right). The outline of grid 22 is shown at the bottom right corner.

Figure 111 - Image of color-classified frictional Manning coefficients for Grid 22. Red are mangroves (Manning = 0.145), orange are reefs (Manning = 0.05), and the rest of the grid is painted with a yellow hue where the Manning coefficient is set at 0.03.

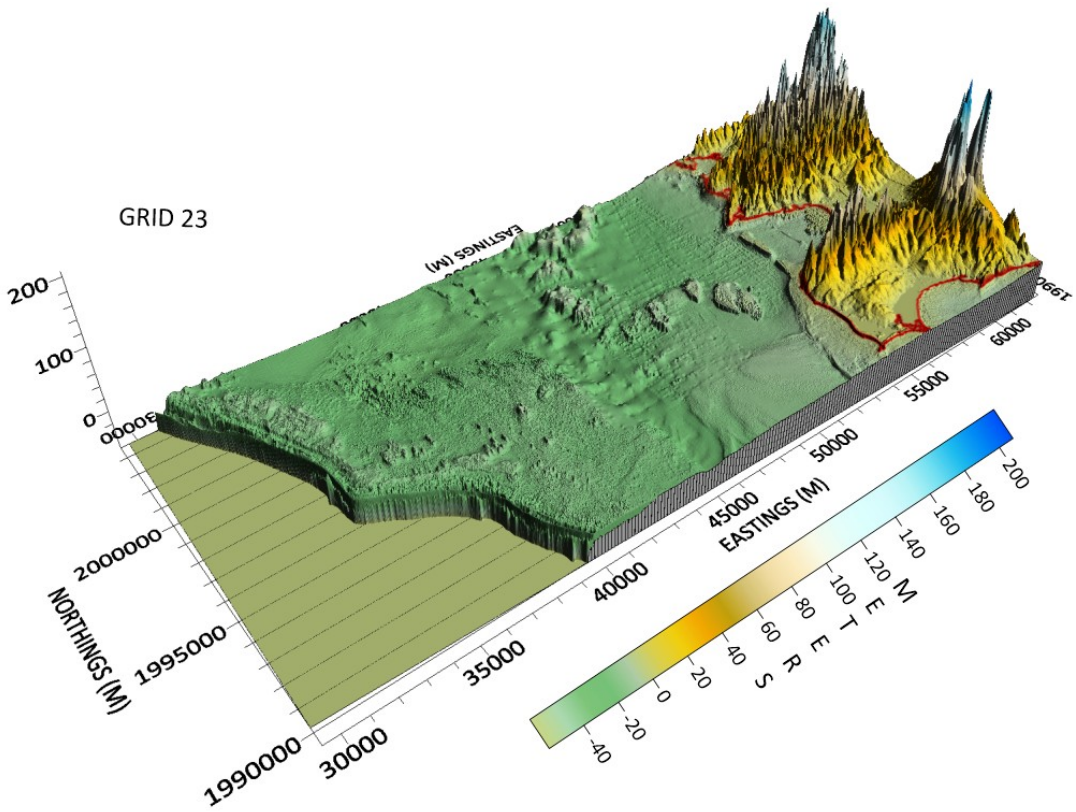

Figure 112 – 3D plot of bathymetry/topography supplied to Grid 23. Red curve is the MSL shoreline.

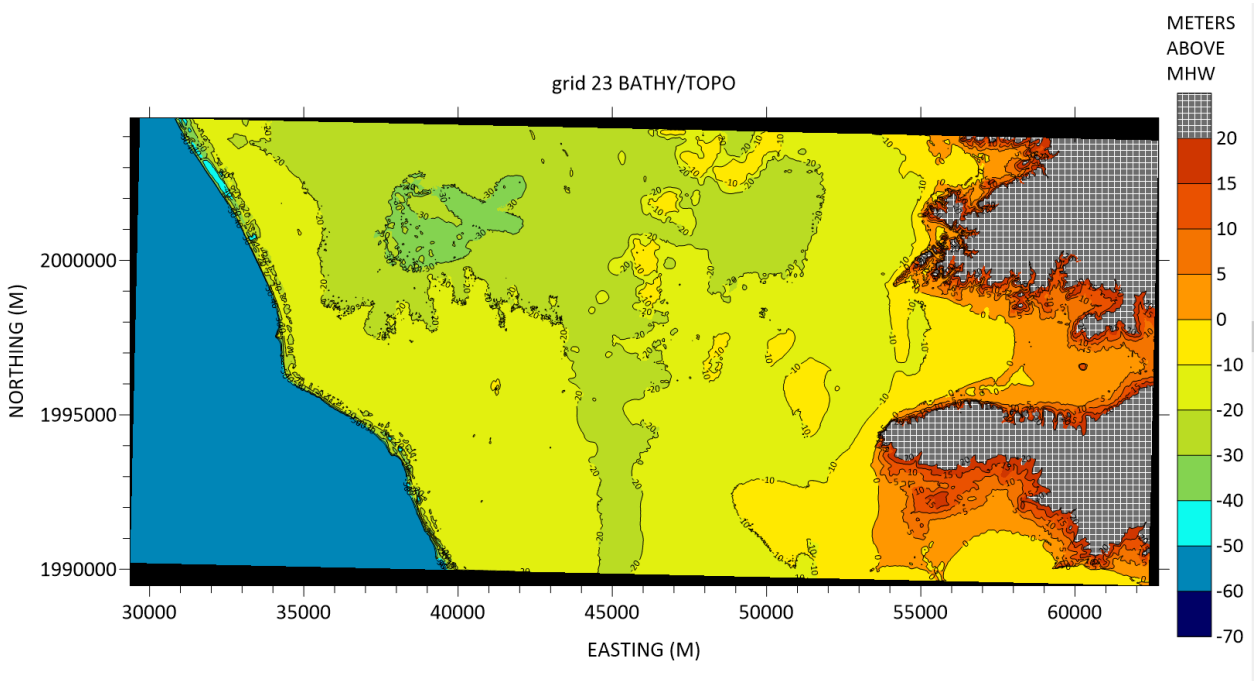

Figure 113 - 2D plot of bathymetry/topography supplied to Grid 23. Red curve is the MSL shoreline. Wavemaker is at the left boundary and waves propagate eastward.

GRID 24 (CABO ROJO TO MAYAGUEZ)

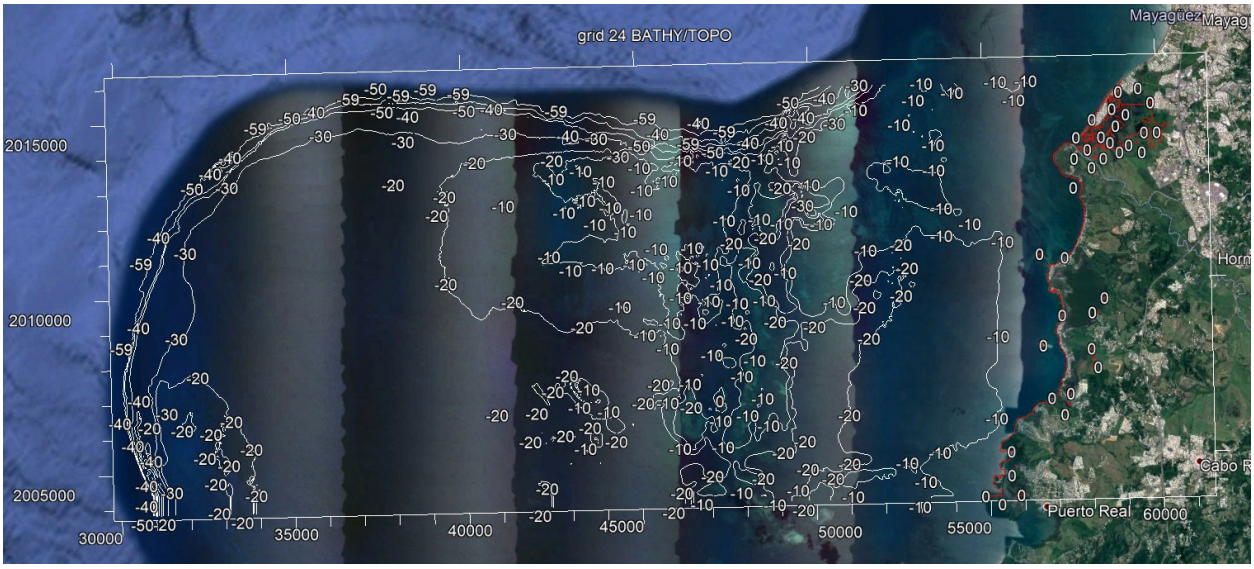

Figure 114 – Outline of computational Grid 24 overlaid on top of Google Earth, showing depth contours, in meters. Mean Sea Level Shoreline is outlined by the red curve. Contours up to 59 m are shown. Deeper waters are set to a constant depth of 60 m. The wavemaker is located at the left boundary and waves propagate eastward (to the right).

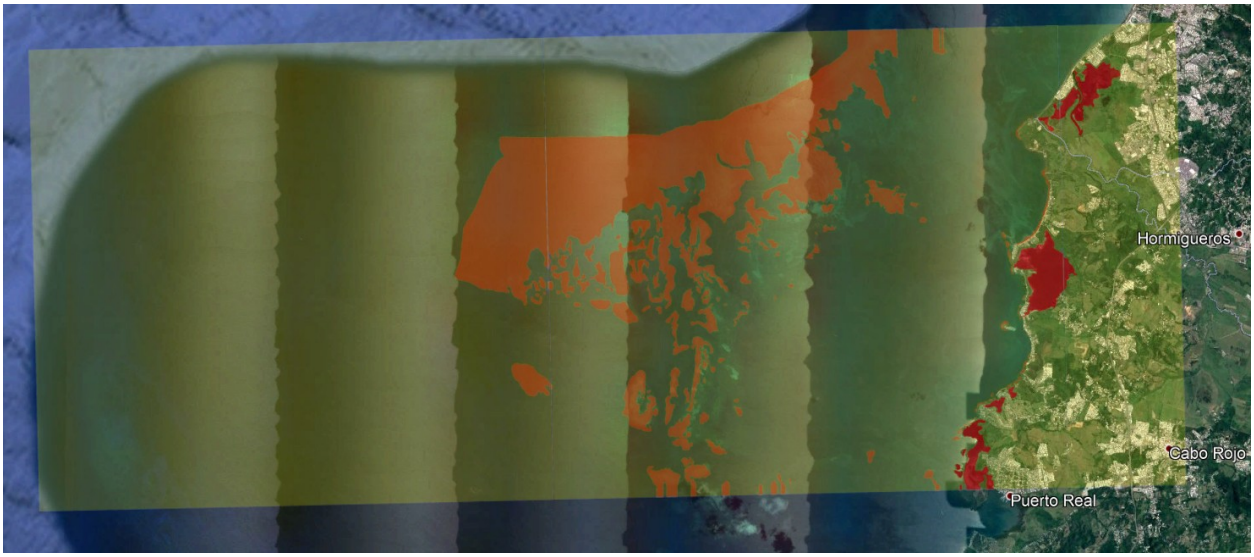

Figure 115 - Image of color-classified frictional Manning coefficients for Grid 24. Red are mangroves (Manning = 0.145), orange are reefs (Manning = 0.05), and the rest of the grid is painted with a yellow hue where the Manning coefficient is set at 0.03.

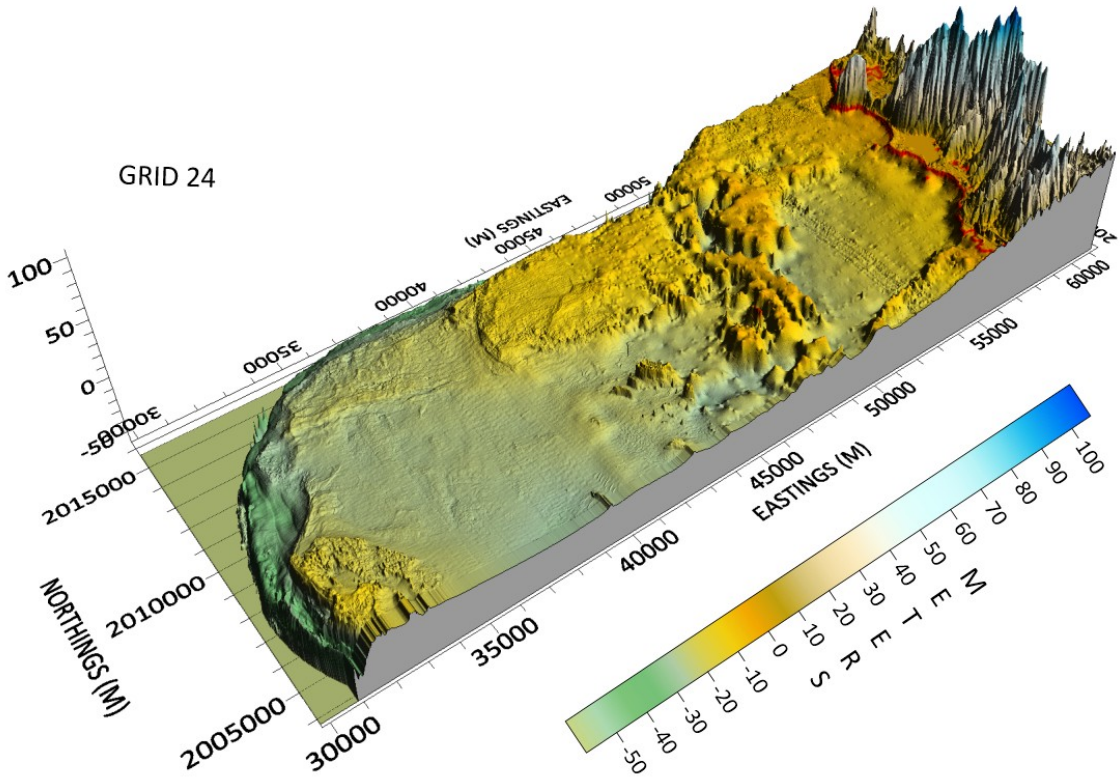

Figure 116 – 3D plot of bathymetry/topography supplied to Grid 24. Red curve is the MSL shoreline.

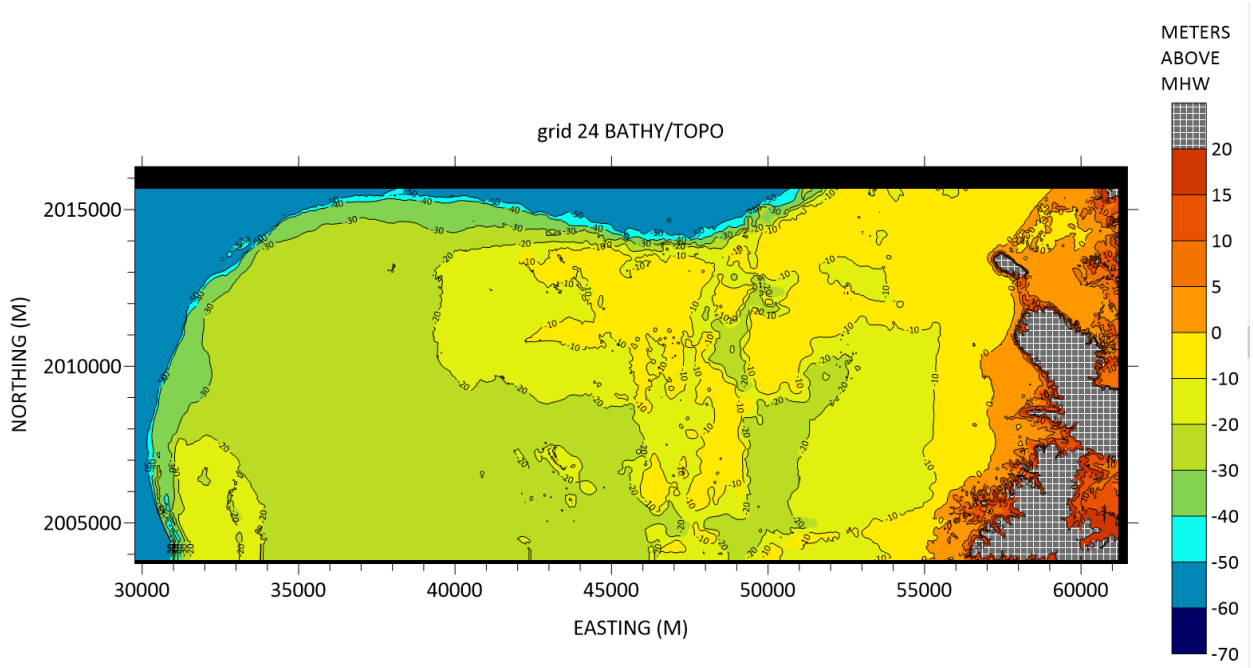

Figure 117 – 2D plot of bathymetry/topography supplied to Grid 24. Red curve is the MSL shoreline. Wavemaker is at the left boundary and waves propagate eastward.

GRID 25 (MAYAGUEZ TO AÑASCO)

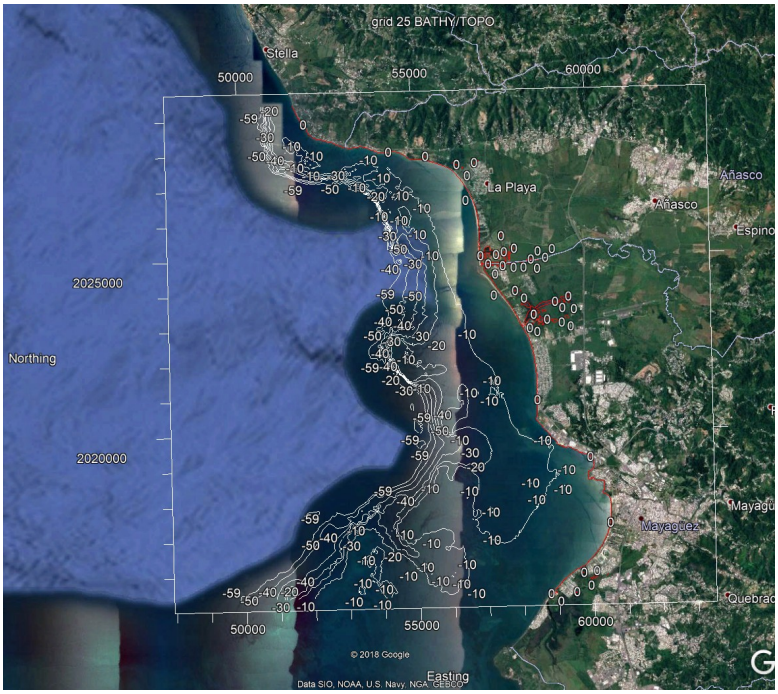

Figure 118 – Outline of computational Grid 25 overlaid on top of Google Earth, showing depth contours, in meters. Mean Sea Level Shoreline is outlined by the red curve. Contours up to 59 m are shown. Deeper waters are set to a constant depth of 60 m. The wavemaker is located at the left boundary and waves propagate eastward (to the right).

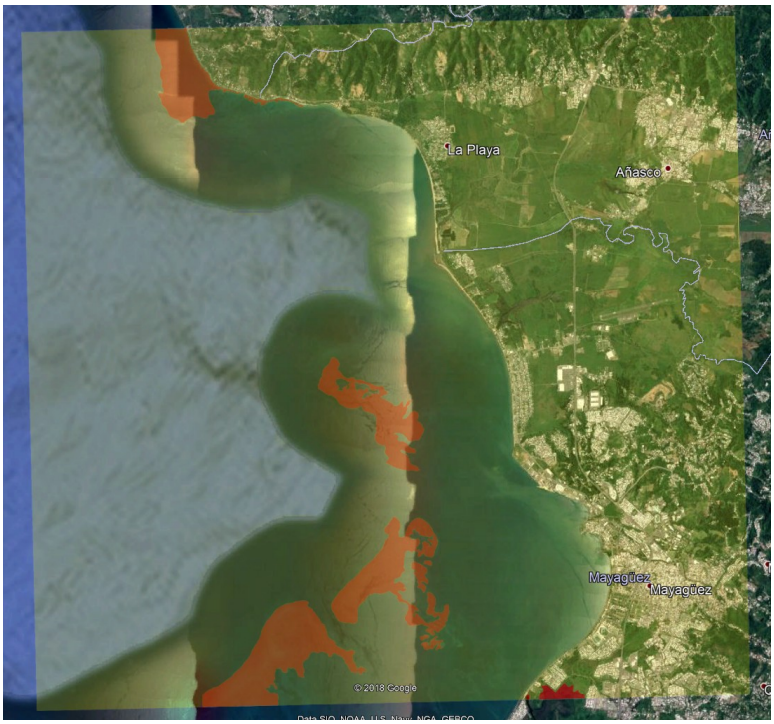

Figure 119 - Image of color-classified frictional Manning coefficients for Grid 25. Red are mangroves (Manning = 0.145), orange are reefs (Manning = 0.05), and the rest of the grid is painted with a yellow hue where the Manning coefficient is set at 0.03.

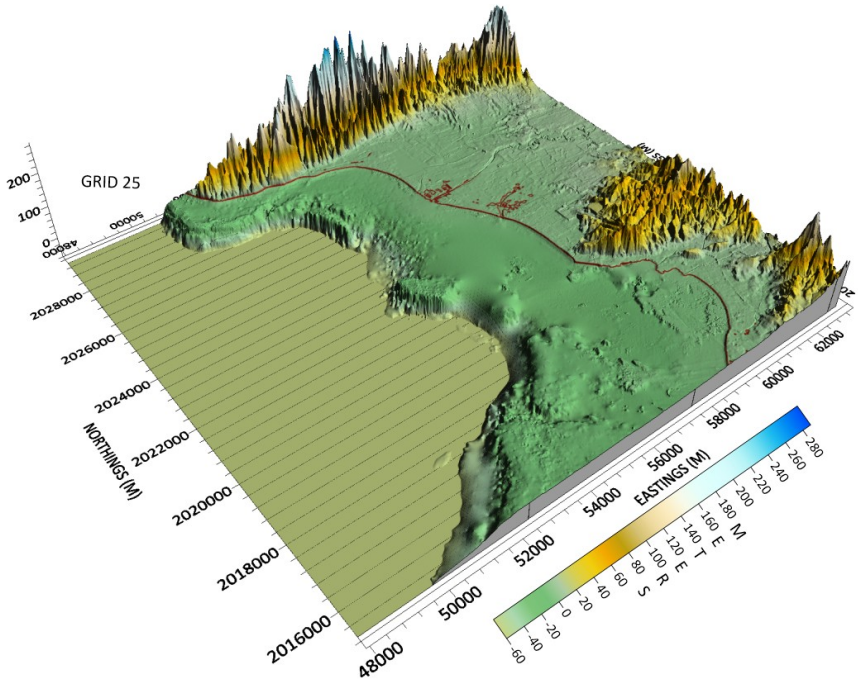

Figure 120 – 3D plot of bathymetry/topography supplied to Grid 25. Red curve is the MSL shoreline.

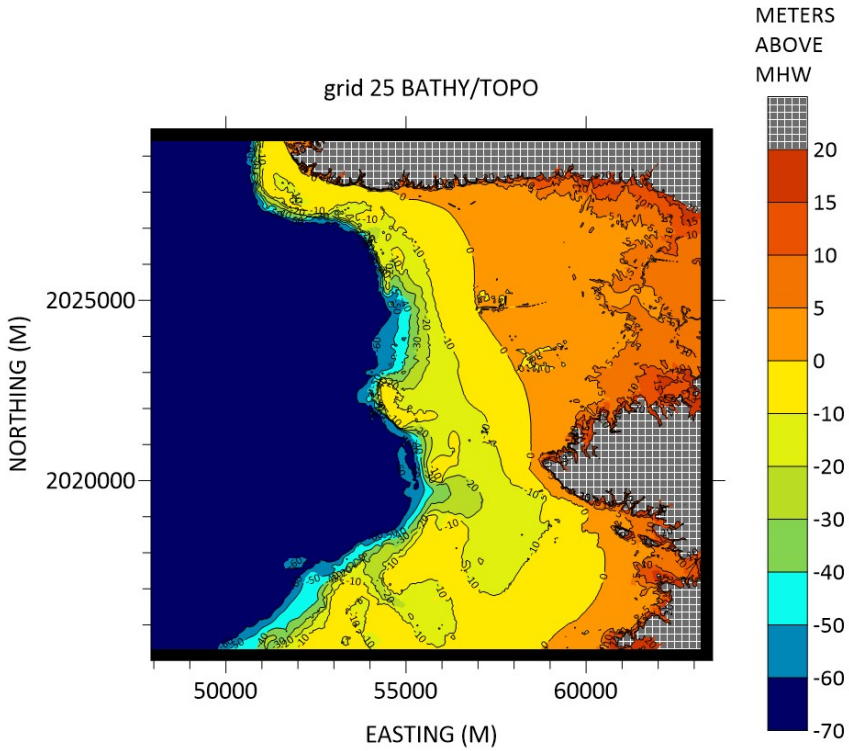

Figure 121 – 2D plot of bathymetry/topography supplied to Grid 25. Red curve is the MSL shoreline. Wavemaker is at the left boundary and waves propagate eastward.

GRID 26 (RINCON TO AGUADA)

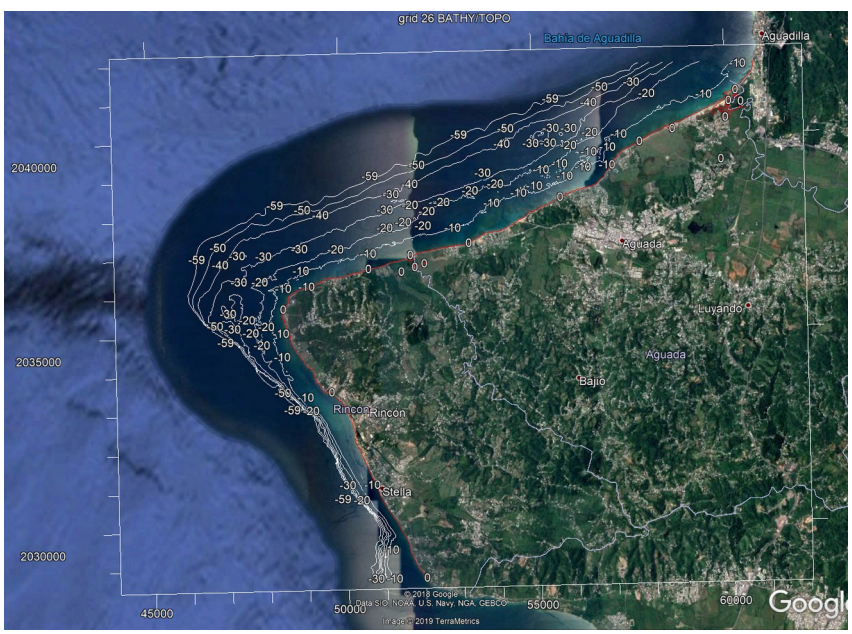

Figure 122– Outline of computational Grid 26 overlaid on top of Google Earth, showing depth contours, in meters. Mean Sea Level Shoreline is outlined by the red curve. Contours up to 59 m are shown. Deeper waters

are set to a constant depth of 60 m. The wavemaker is located at the left boundary and waves propagate eastward (to the right).

Figure 123 - Image of color-classified frictional Manning coefficients for Grid 26. Red are mangroves (Manning = 0.145), orange are reefs (Manning = 0.05), and the rest of the grid is painted with a yellow hue where the Manning coefficient is set at 0.03.

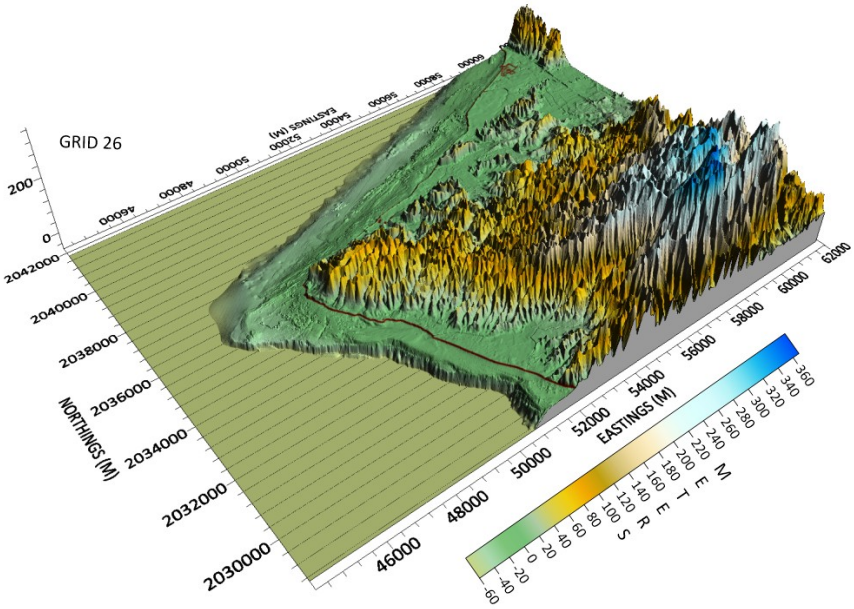

Figure 124 – 3D plot of bathymetry/topography supplied to Grid 26. Red curve is the MSL shoreline.

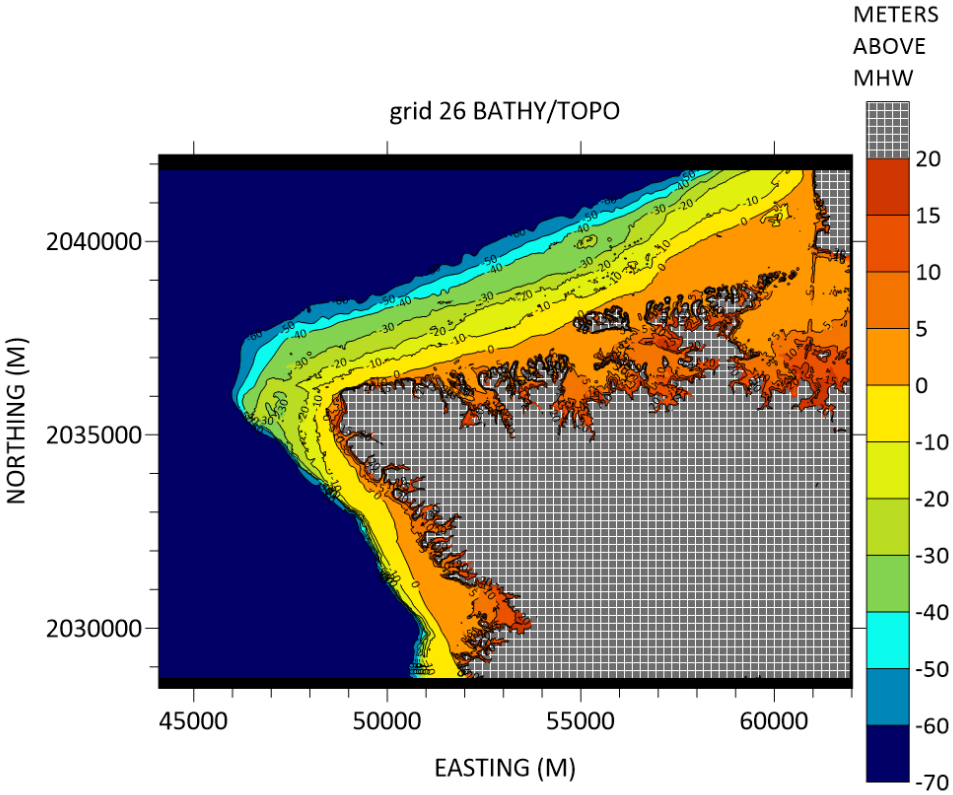

Figure 125 – 2D plot of bathymetry/topography supplied to Grid 26. Red curve is the MSL shoreline. Wavemaker is at the left boundary and waves propagate eastward.

GRID 27 (AGUADILLA)

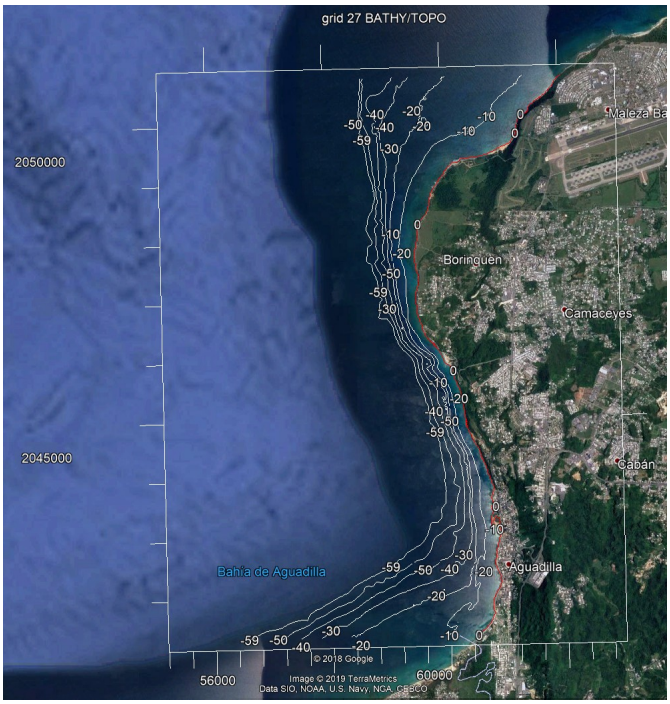

Figure 126– Outline of computational Grid 27 overlaid on top of Google Earth, showing depth contours, in meters. Mean Sea Level Shoreline is outlined by the red curve. Contours up to 59 m are shown. Deeper waters are set to a constant depth of 60 m. The wavemaker is located at the left boundary and waves propagate eastward (to the right).

Figure 127- Image of color-classified frictional Manning coefficients for Grid 27. Red are mangroves (Manning = 0.145), orange are reefs (Manning = 0.05), and the rest of the grid is painted with a yellow hue where the Manning coefficient is set at 0.03.

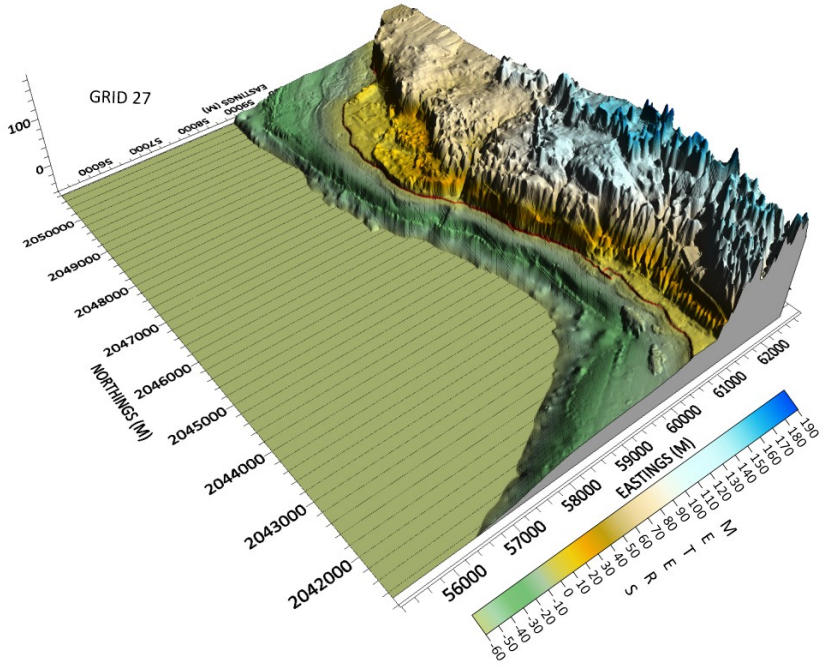

Figure 128 – 3D plot of bathymetry/topography supplied to Grid 27. Red curve is the MSL shoreline.

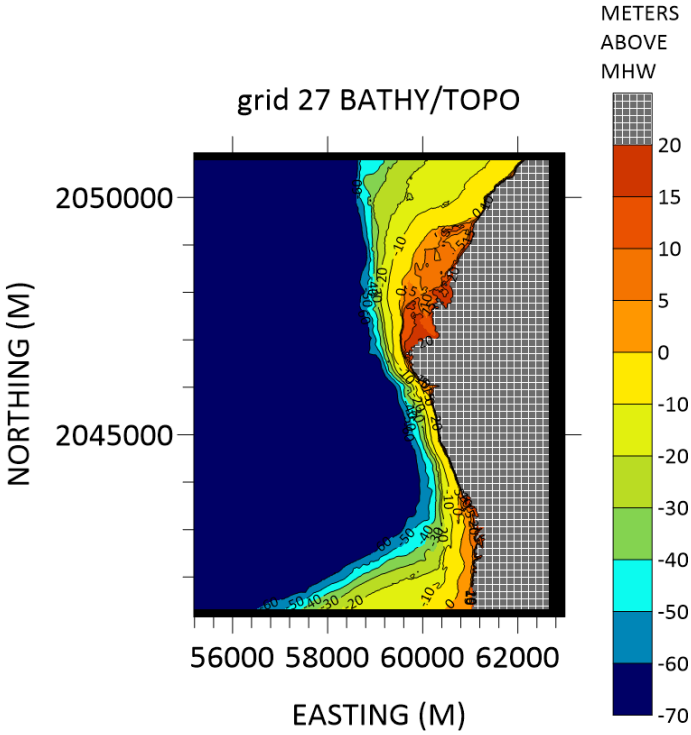

Figure 129 – 2D plot of bathymetry/topography supplied to Grid 27. Red curve is the MSL shoreline. Wavemaker is at the left boundary and waves propagate eastward.

RESULTS

1. The model outputs its results in the netcdf format. Among several output variables included in the netcdf file there is one called ***zs_max***, which represents the maximum sea surface elevation having occurred at each computational cell, irrespective of the time when it occurred (see Figure 130). This is the variable which we will be analyzing. It represents the elevation of the maximum wave crest that propagated through that computational cell during program execution, and this elevation is given relative to MSL. As will be mentioned below, this elevation will be brought to relative to the local terrain elevation (the elevation of the topography of the computational cell). This is done by subtracting the elevation of the topography from *zs_max*. The result will be the depth of the water column at each computational cell, having set all computational cells lying in the sea prior to the "storm" to NaN. This is similar to FEMAs Base Flood Elevation, which gives the maximum elevation of the crests of the waves propagating over the 100-year stillwater elevation, in this case relative to MSL.

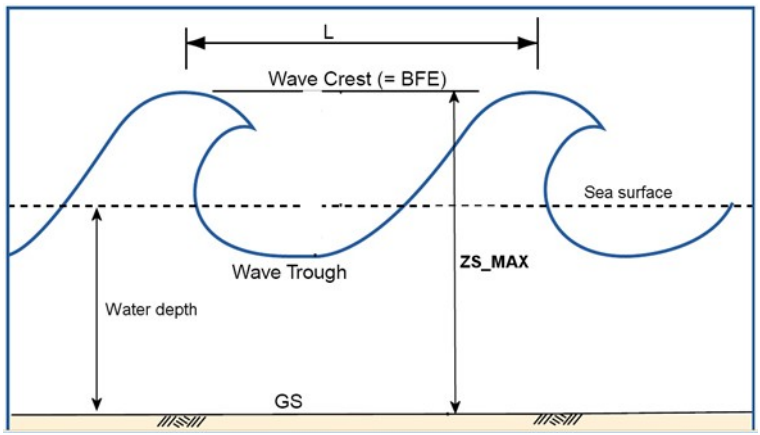

Figure 130 - Schematic showing the meaning of the output variable zs_max. This is a conceptual image since the sea surface will consist of an irregular superimposition of waves.

   The model also outputs the variable ***zs_mean***, which is the mean of the of the water surface elevation, the mean taken over the length of the computation time. This variable may contain useful information, and it will be examined in a separate study.

2. The results in the post-processing will be output in both kmz and shapefile formats. In the kmz images it was decided to limit the colorbar to 10 meters (see discussion below). That is, all elevations above 10 meters were painted in red. But contours, and its values, for those elevations are shown.

3. As is standard in preparing inundation maps, the images show inland inundation depth starting right from the tidal MHW line. That is, no sea surface elevations will be shown seaward of the MHW line (that is, in what is the sea originally). This is done in the post-processing by setting all computational nodes initially lying below MHW equal to a NaN (Not a Number). A consequence of this is that no rivers for which the river bed at the start of the simulation lies below MHW will be shown as flooded in the post-processed images (kmz and shapefiles) since the river will be considered as part of the sea. A good example is the Rio Hondo and Bayamon rivers east of Levittown, in Vega Baja. The main channel is not painted (as if not flooded), but its banks are painted. Where the river bed lies above MHW the image will show it painted.
   Also, the elevations shown in the maps are of the sea surface relative to the local terrain elevation. That is why it is called *inundation depth*. But in contradistinction to regular storm surge maps which show the stillwater elevation (the pressure+wind+static wave setups), the elevations *zs_max* represent the elevation of the wave crests above the local terrain elevation. That is, *zs_max* is the elevation of the crest of the wind waves, and possibly infragravity waves (whichever is higher – see Figure 3), that propagate over the stillwater elevation. It is not the elevation of the stillwater (the typical storm surge), which is what the Benitez and Mercado (2015) maps show. In a way, these new maps are similar to the FEMA maps, which show the so-called Base Flood Elevation at a given location, which is the crest elevation of the maximum wave that can propagate over that location without breaking. But FEMA's Base Flood Elevation values are relative to MSL, while in our case the elevations are relative to the elevation of the local terrain, which are relative to MHW. If we want to compare this report's values to the FEMA's BFE's we need to add to our values the terrain elevation.

4. A decision had to be made of whether to include (or "paint") all of the area flooded areas or to limit the areas to be "painted" as flooded. Once the waves overtop the highest elevation along a profile, the water will flow downhill, driven by gravity, and it can cover large areas, especially so if the Manning coefficient used does not dissipate the flow (recall that in this study all inland areas – initially dry areas – are assumed to have a Manning of 0.03, a typical value for tsunami flood mapping). So, in order to limit the flood extension, it was decided to "paint' only the areas covered with a water depth greater than 0.1 meters. This is in accord with Moftakhari et al. (2018),

   > "Nuisance flooding (NF) refers to low levels of inundation that do not pose significant threats to public safety or cause major property damage, but can disrupt routine day-to-day activities, put added strain on infrastructure systems such as roadways and sewers, and cause minor property damage."

> They continue with "Here a simple, quantitative definition of NF is proposed based on established flood intensity thresholds for flood consequences (e.g., pedestrian safety, property damage, and health risks). Based on a wide range of literature including hydrology, transportation, public health risk, and safety impacts, we define NF based on depth >3 cm and <10 cm, regardless of the source. This definition of NF is not limited to high tide flooding but rather is inclusive of all possible flood drivers including pluvial, fluvial, and oceanic and can capture trends in NF resulting from trends in, and compounding effects of, flood drivers."

If we had not restricted the "painted" areas to be those whose local depth was larger than, or equal, to 10 cm the maps would show much more flooding.

5. XBeach accepts as initial input a sea surface elevation that is present prior to the wave's arrival. We want to have XBeach compute the storm surge (the pressure + wind + (static) wave setups), in addition to the waves that propagate over the storm surge, be it wind waves, or infragravity waves, or both. XBeach can simulate all of the above with the exception of the pressure setup. In order to include pressure setup in the calculations what we did was to use the storm surge values produced by Benitez and Mercado (2015) given at the deep water (offshore) boundary of each XBeach computational grid. The Benitez & Mercado (2015) results contain the pressure, wind, and static wave setups for each hurricane category (the superMOMs – the MOM of the MOMs, where MOM stands for Maximum of the Maximums), of which XBeach also computes the wind and static wave setup. But this apparent double contribution from ADCIRC+SWAN is believed to be very negligible since it is reasonable to assume that, since the XBeach offshore boundary lies in relatively deep waters (60 m), the wind setup and the (static) wave setup there are negligible (wave setup starts where wave breaking starts). Therefore, at the offshore boundary of XBeach we are practically providing just the pressure setup, which can be assumed not to vary over the XBeach computational grid. XBeach takes care of computing all the other setups and higher frequency stuff.

6. As discussed in the Methodology section above, each run was started with an initial sea surface elevation spatially uniform based on the storm surge values obtained by Benitez and Mercado (2015). This initial sea surface elevation, zs0, that is given to XBeach is taken at the offshore boundary of each computational grid (where the wavemaker is located), and we have already discussed that, to a good approximation, it corresponds to the pressure setup corresponding to the hurricane category intensity being modeled. This initial sea surface elevation will "passively" flood all terrain elevations lying below it (zs0). That is, before the

waves reach the shoreline there will be low-lying areas already flooded. For those areas that are flooded areas by this process, and that one can see a hydraulic connection with the sea, one can assume that the flooding comes from the sea. But there are some inland low-lying areas that appear initially flooded and which one cannot see any hydraulic connection to the sea. We will assume that those areas are flooded because the water table has been elevated and it has surpassed the ground elevation.

7. A caveat. No surge/river discharge interaction is being simulated. As far as the model is concerned, the rivers are seen as low-lying terrain (bathymetry), and the storm surge will flood them accordingly. In real life one should expect some type of storm surge (trying to move up river) and river discharge interaction (river discharge moving seaward), that could increase the flood elevations in the vicinity of river mouths. This interaction will make waves to break more intensely, thus generating larger wave setups. At the same time, the storm surge will impose a higher downriver boundary condition on the river hydraulics. It should be stated that XBeach is capable of simulating this effect as far as the effect it has on the sea surface elevations. You just impose a river mouth discharge rate and let the model run. This is beyond the scope of this project and is left for future efforts. In the same way, no riverine, nor rainfall, flooding is included.

8. For each grid and hurricane category a panoramic view of the results will be shown (no zoom). For some grids a zoom will be shown of some areas of interest as a proof of concept. These are shown in Figures 131 to 270.

GRID 1: Cat 1

Figure 131 – Grid 1, category 1, maximum sea surface elevation (meters), relative to local terrain elevation, during 1 hour of simulation after spin up of 300 seconds.

GRID 1: Cat 2

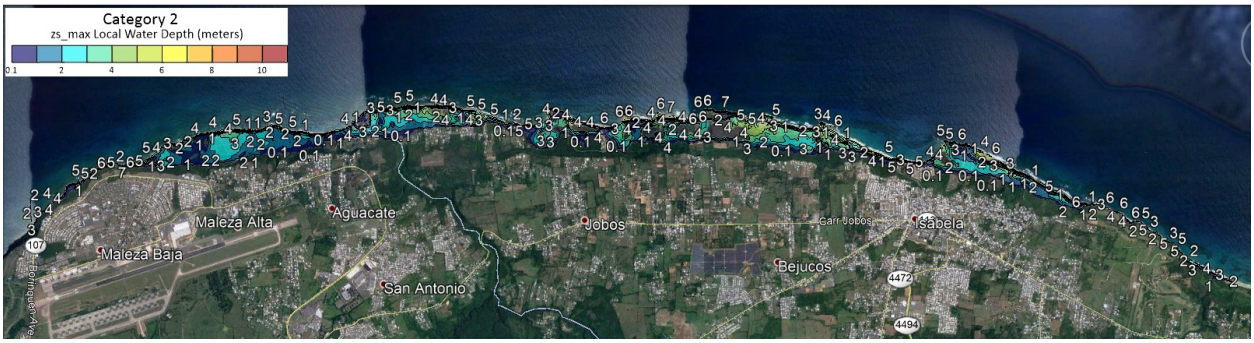

Figure 132 – Grid 1, category 2, maximum sea surface elevation (meters), relative to local terrain elevation, during 1 hour of simulation after spin up of 300 seconds.

GRID 1: Cat 3

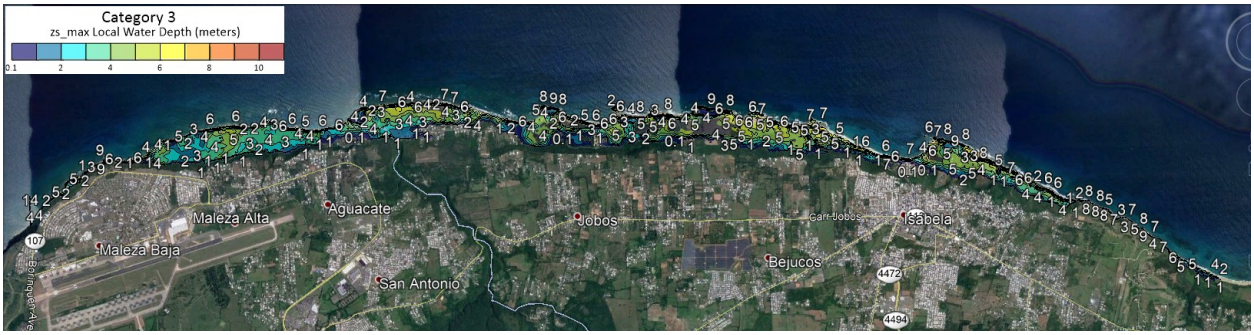

Figure 133 – Grid 1, category 3, maximum sea surface elevation (meters), relative to local terrain elevation, during 1 hour of simulation after spin up of 300 seconds.

GRID 1: Cat 4

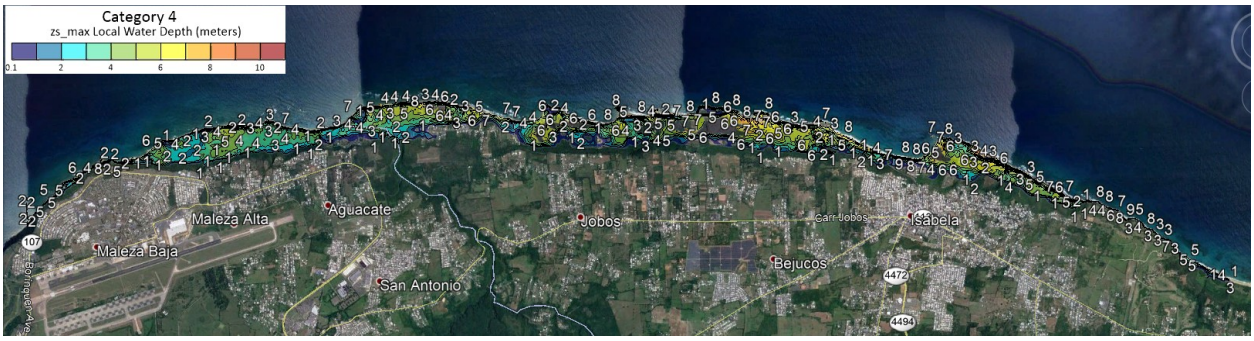

Figure 134 – Grid 1, category 4, maximum sea surface elevation (meters), relative to local terrain elevation, during 1 hour of simulation after spin up of 300 seconds.

GRID 1: Cat 5

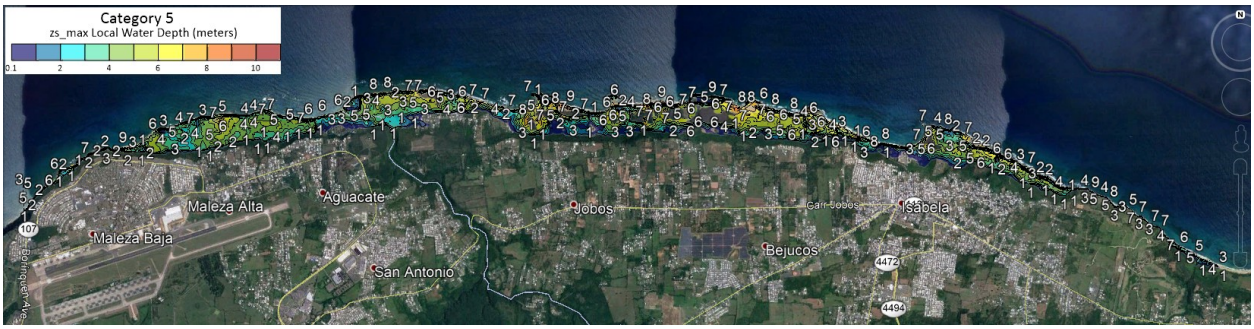

Figure 135 – Grid 1, category 5, maximum sea surface elevation (meters), relative to local terrain elevation, during 1 hour of simulation after spin up of 300 seconds.

GRID 2: CAT 1

Figure 136 – Grid 2, category 1, maximum sea surface elevation (meters), relative to local terrain elevation, during 1 hour of simulation after spin up of 300 seconds.

GRID 2: CAT 2

Figure 137 – Grid 2, category 2, maximum sea surface elevation (meters), relative to local terrain elevation, during 1 hour of simulation after spin up of 300 seconds.

GRID 2: CAT 3

Figure 138 – Grid 2, category 3, maximum sea surface elevation (meters), relative to local terrain elevation, during 1 hour of simulation after spin up of 300 seconds.

GRID 2: CAT 4

Figure 139 – Grid 2, category 4, maximum sea surface elevation (meters), relative to local terrain elevation, during 1 hour of simulation after spin up of 300 seconds.

GRID 2: CAT 5

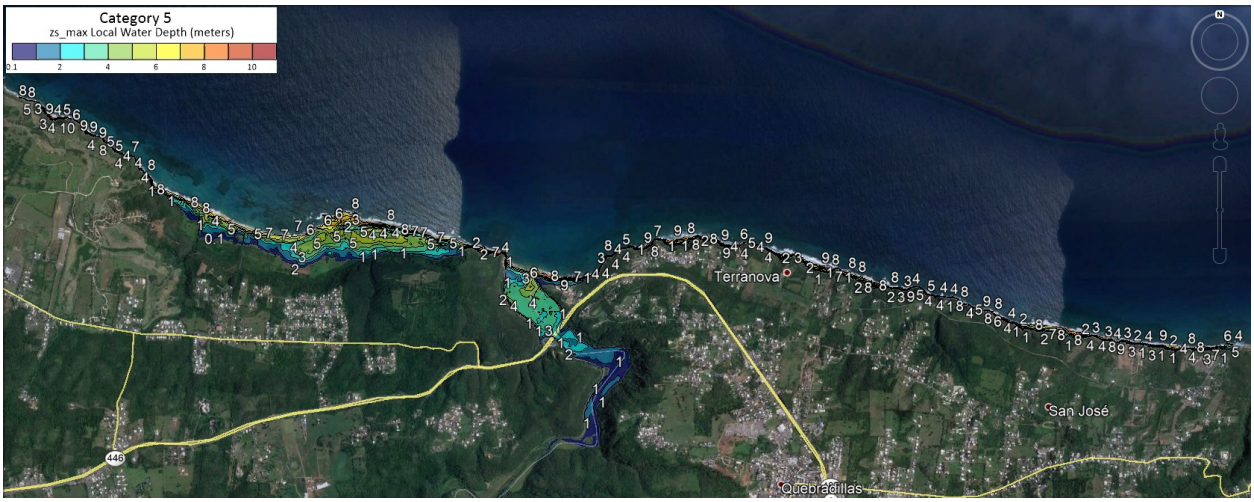

Figure 140 – Grid 2, category 5, maximum sea surface elevation (meters), relative to local terrain elevation, during 1 hour of simulation after spin up of 300 seconds.

GRID 3: CAT 1

Figure 141 – Grid 3, category 1, maximum sea surface elevation (meters), relative to local terrain elevation, during 1 hour of simulation after spin up of 300 seconds.

GRID 3: CAT 2

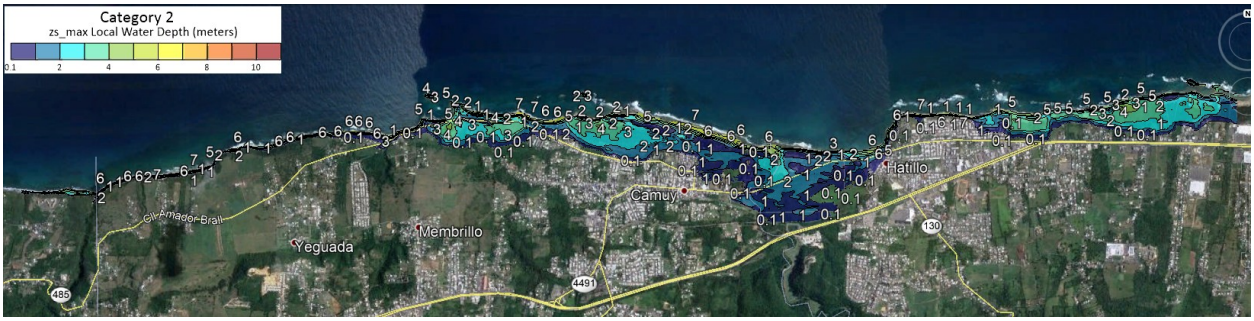

Figure 142 – Grid 3, category 2, maximum sea surface elevation (meters), relative to local terrain elevation, during 1 hour of simulation after spin up of 300 seconds.

GRID 3: CAT 3

Figure 143 – Grid 3, category 3, maximum sea surface elevation (meters), relative to local terrain elevation, during 1 hour of simulation after spin up of 300 seconds.

GRID 3: CAT 4

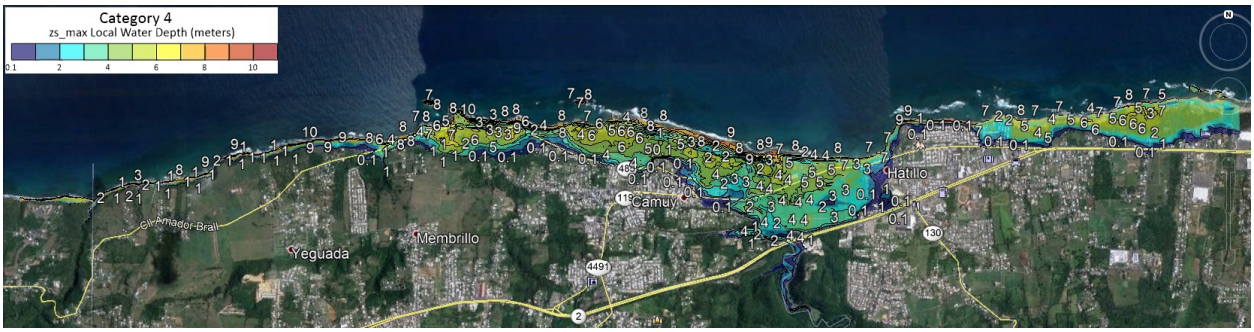

Figure 144 - Grid 3, category 4, maximum sea surface elevation (meters), relative to local terrain elevation, during 1 hour of simulation after spin up of 300 seconds.

GRID 3: CAT 5

Figure 145 – Grid 3, category 5, maximum sea surface elevation (meters), relative to local terrain elevation, during 1 hour of simulation after spin up of 300 seconds.

GRID 4: CAT 1

Figure 146 – Grid 4, category 1, maximum sea surface elevation (meters), relative to local terrain elevation, during 1 hour of simulation after spin up of 300 seconds.

GRID 4: CAT 2

Figure 147 – Grid 4, category 2, maximum sea surface elevation (meters), relative to local terrain elevation, during 1 hour of simulation after spin up of 300 seconds.

GRID 4: CAT 3

Figure 148 – Grid 4, category 3, maximum sea surface elevation (meters), relative to local terrain elevation, during 1 hour of simulation after spin up of 300 seconds.

GRID 4: CAT 4

Figure 149 – Grid 4, category 4, maximum sea surface elevation (meters), relative to local terrain elevation, during 1 hour of simulation after spin up of 300 seconds.

GRID 4: CAT 5

Figure 150 – Grid 4, category 5, maximum sea surface elevation (meters), relative to local terrain elevation, during 1 hour of simulation after spin up of 300 seconds.

GRID 5: CAT 1

Figure 151 – Grid 5, category 1, maximum sea surface elevation (meters), relative to local terrain elevation, during 1 hour of simulation after spin up of 300 seconds.

GRID 5: CAT 2

Figure 152 – Grid 5, category 2, maximum sea surface elevation (meters), relative to local terrain elevation, during 1 hour of simulation after spin up of 300 seconds.

GRID 5: CAT 3

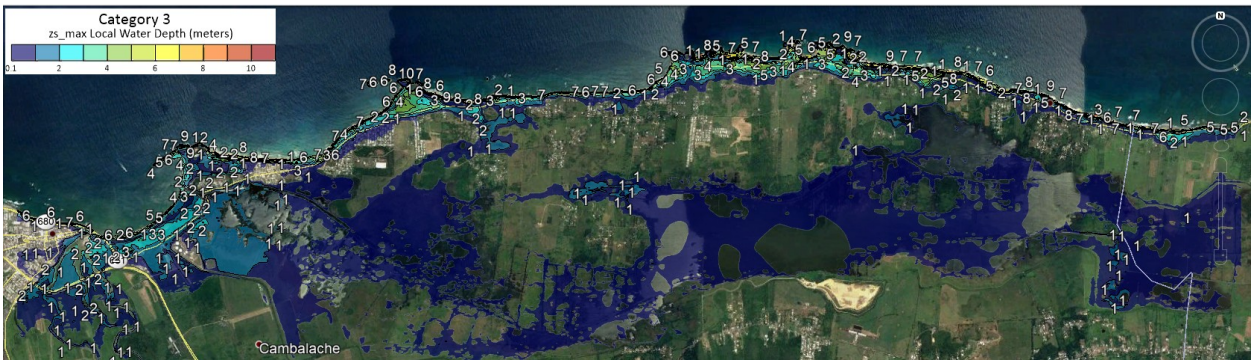

Figure 153 – Grid 5, category 3, maximum sea surface elevation (meters), relative to local terrain elevation, during 1 hour of simulation after spin up of 300 seconds.

GRID 5: CAT 4

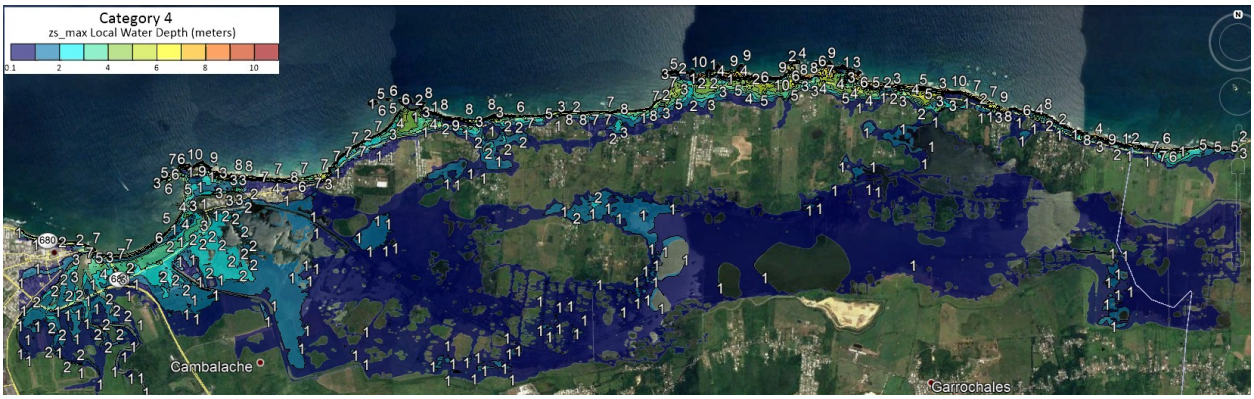

Figure 154 – Grid 5, category 4, maximum sea surface elevation (meters), relative to local terrain elevation, during 1 hour of simulation after spin up of 300 seconds.

GRID 5: CAT 5

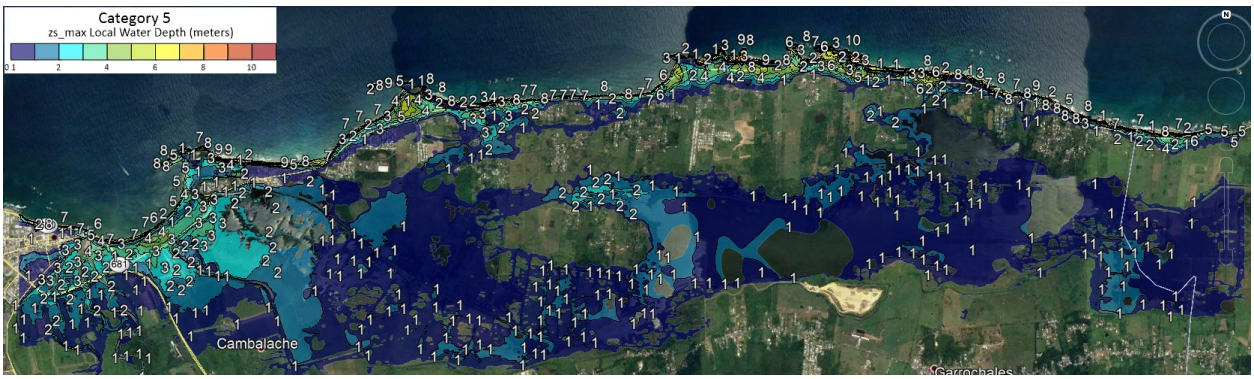

Figure 155 – Grid 5, category 5, maximum sea surface elevation (meters), relative to local terrain elevation, during 1 hour of simulation after spin up of 300 seconds.

GRID 6: CAT 1

Figure 156 – Grid 6, category 1, maximum sea surface elevation (meters), relative to local terrain elevation, during 1 hour of simulation after spin up of 300 seconds.

GRID 6: CAT 2

Figure 157 – Grid 6, category 2, maximum sea surface elevation (meters), relative to local terrain elevation, during 1 hour of simulation after spin up of 300 seconds.

GRID 6: CAT 3

Figure 158 – Grid 6, category 3, maximum sea surface elevation (meters), relative to local terrain elevation, during 1 hour of simulation after spin up of 300 seconds.

GRID 6: CAT 4

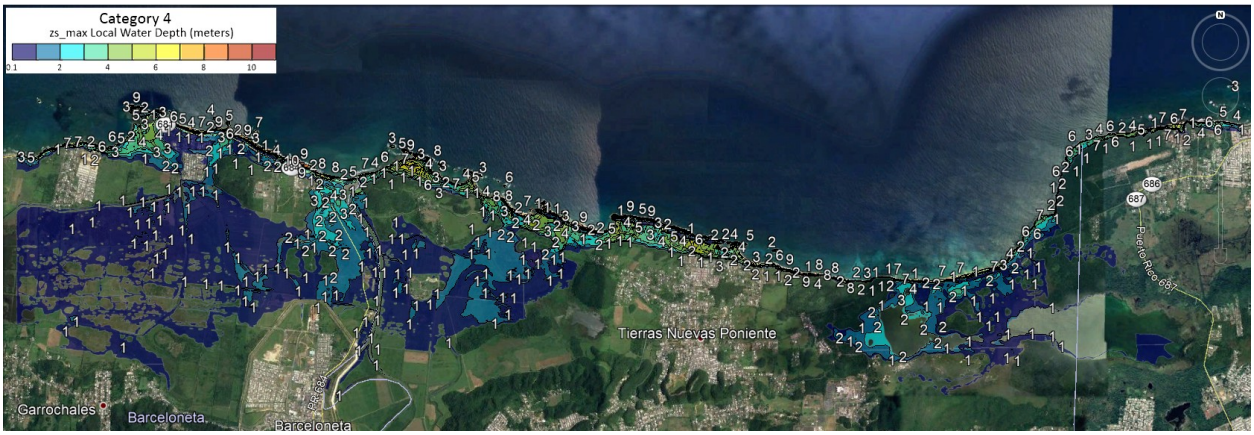

Figure 159 – Grid 6, category 4, maximum sea surface elevation (meters), relative to local terrain elevation, during 1 hour of simulation after spin up of 300 seconds.

GRID 6: CAT 5

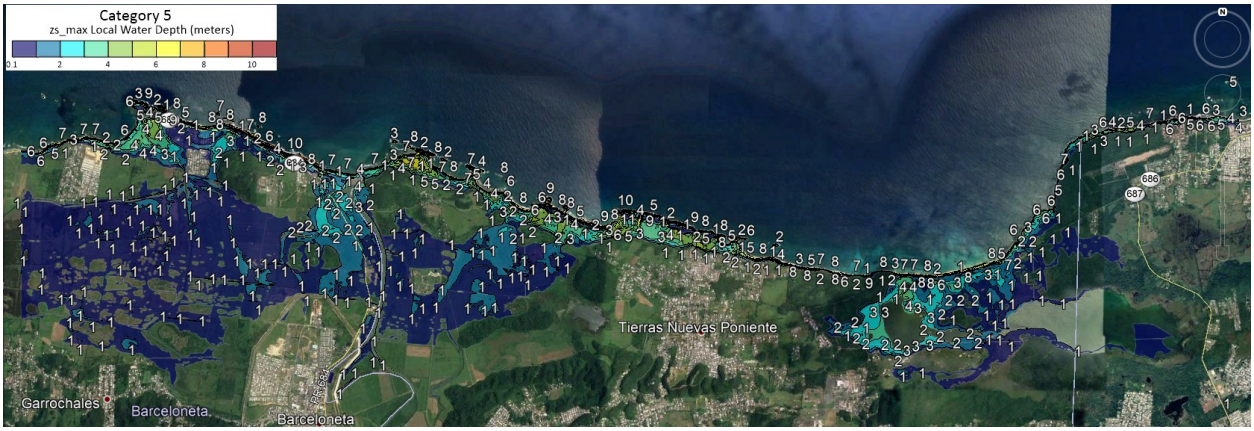

Figure 160 – Grid 6, category 5, maximum sea surface elevation (meters), relative to local terrain elevation, during 1 hour of simulation after spin up of 300 seconds.

GRID 7: CAT 1

Figure 161 – Grid 7, category 1, maximum sea surface elevation (meters), relative to local terrain elevation, during 1 hour of simulation after spin up of 300 seconds.

GRID 7: CAT 2

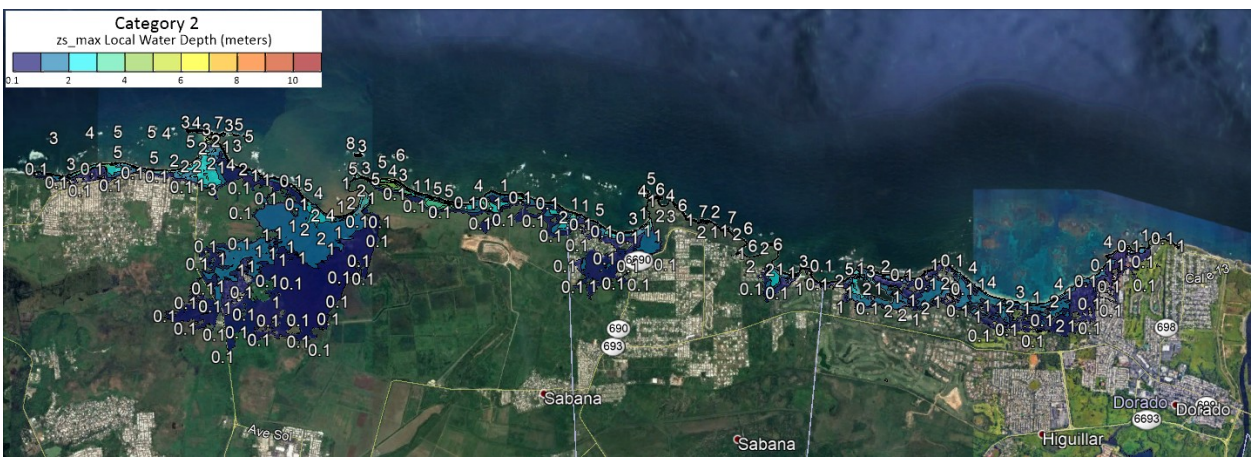

Figure 162 – Grid 7, category 2, maximum sea surface elevation (meters), relative to local terrain elevation, during 1 hour of simulation after spin up of 300 seconds.

GRID 7: CAT 3

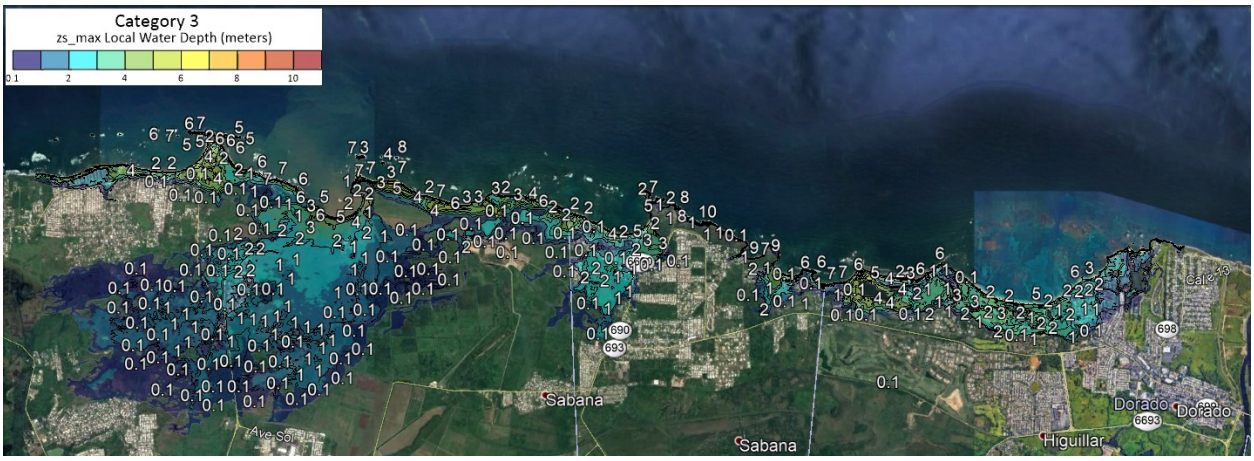

Figure 163 – Grid 7, category 3, maximum sea surface elevation (meters), relative to local terrain elevation, during 1 hour of simulation after spin up of 300 seconds.

GRID 7: CAT 4

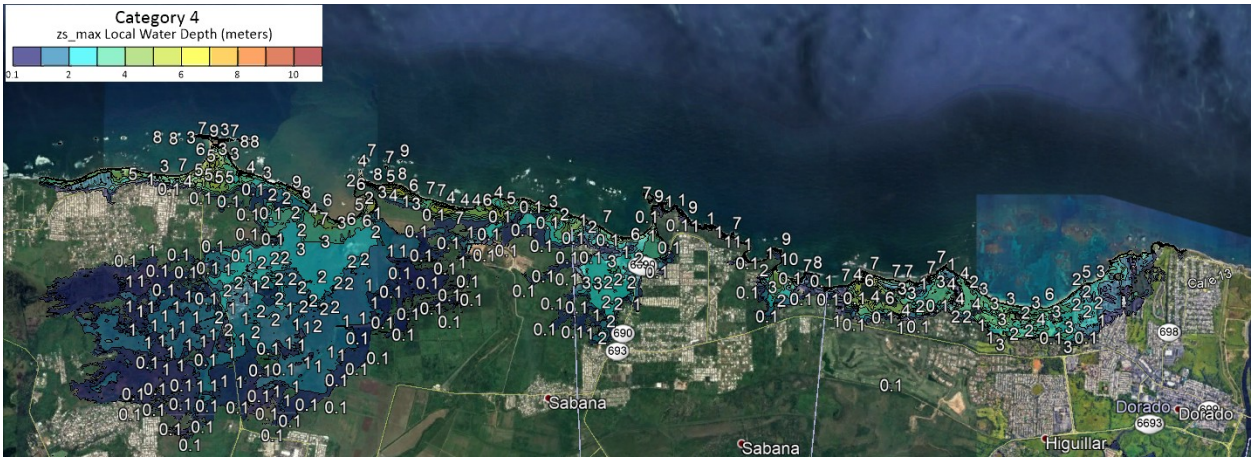

Figure 164 – Grid 7, category 4, maximum sea surface elevation (meters), relative to local terrain elevation, during 1 hour of simulation after spin up of 300 seconds.

GRID 7: CAT 5

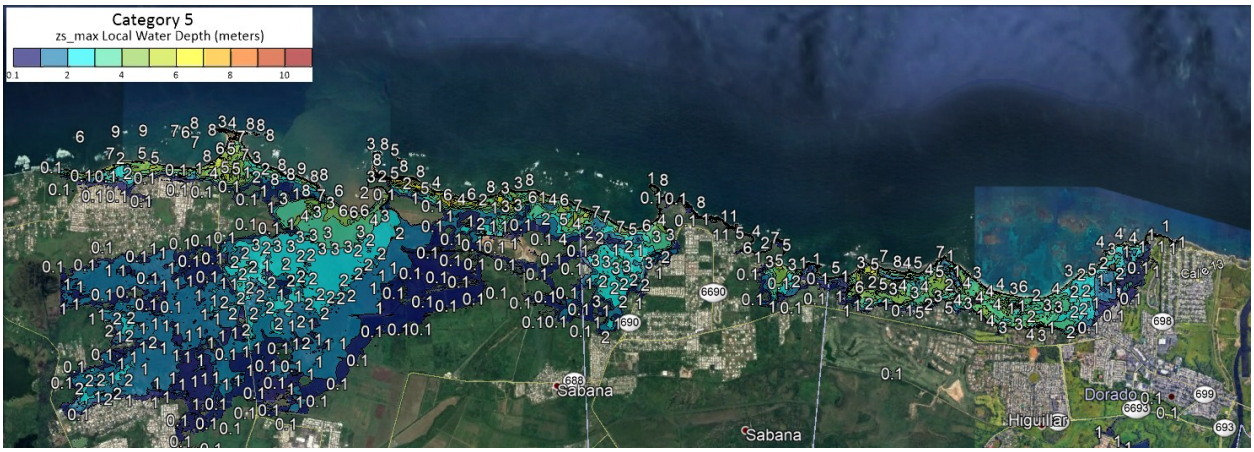

Figure 165 – Grid 7, category 5, maximum sea surface elevation (meters), relative to local terrain elevation, during 1 hour of simulation after spin up of 300 seconds.

GRID 8: CAT 1

Figure 166 - Grid 8, category 1, maximum sea surface elevation (meters), relative to local terrain elevation, during 1 hour of simulation after spin up of 300 seconds.

GRID 8: CAT 2

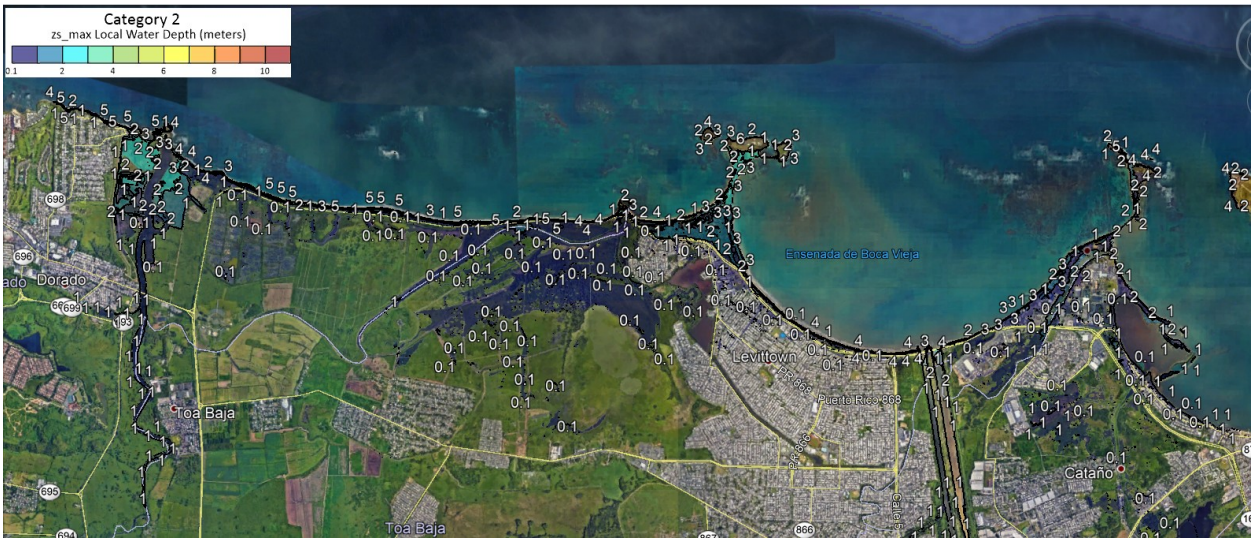

Figure 167 - Grid 8, category 2, maximum sea surface elevation (meters), relative to local terrain elevation, during 1 hour of simulation after spin up of 300 seconds.

GRID 8: CAT 3

Figure 168 - Grid 8, category 2, maximum sea surface elevation (meters), relative to local terrain elevation, during 1 hour of simulation after spin up of 300 seconds.

GRID 8: CAT 4

Figure 169 - Grid 8, category 4, maximum sea surface elevation (meters), relative to local terrain elevation, during 1 hour of simulation after spin up of 300 seconds.

GRID 8: CAT 5

Figure 170 - Grid 8, category 5, maximum sea surface elevation (meters), relative to local terrain elevation, during 1 hour of simulation after spin up of 300 seconds.

GRID 9: CAT 1

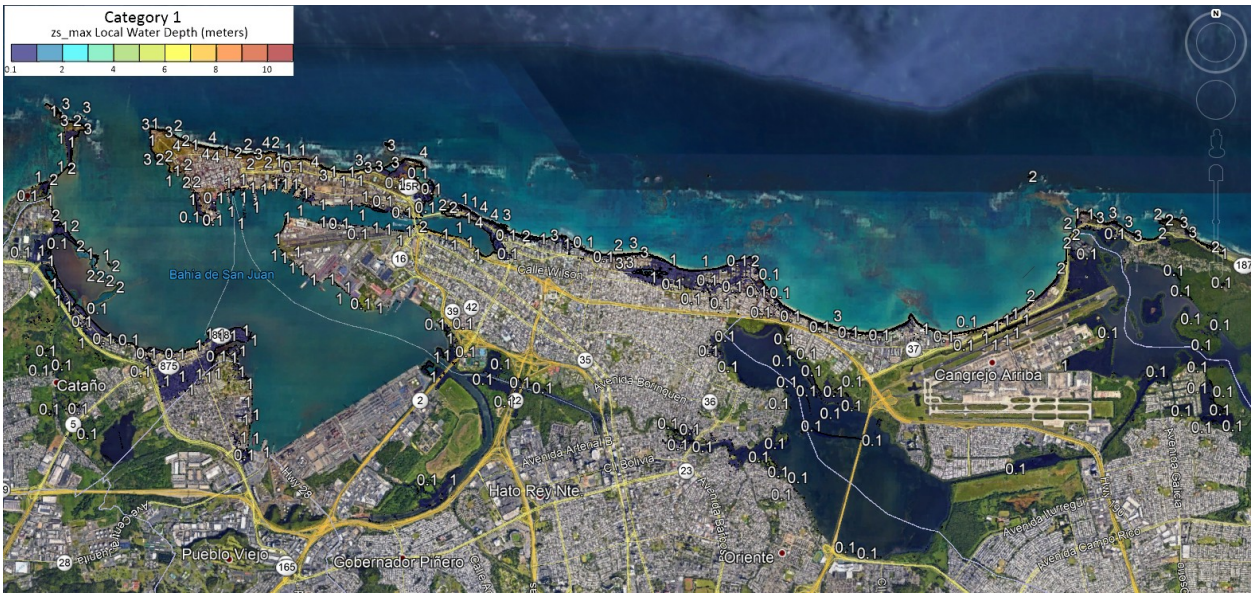

Figure 171 - Grid 9, category 1, maximum sea surface elevation (meters), relative to local terrain elevation, during 1 hour of simulation after spin up of 300 seconds.

GRID 9: CAT 2

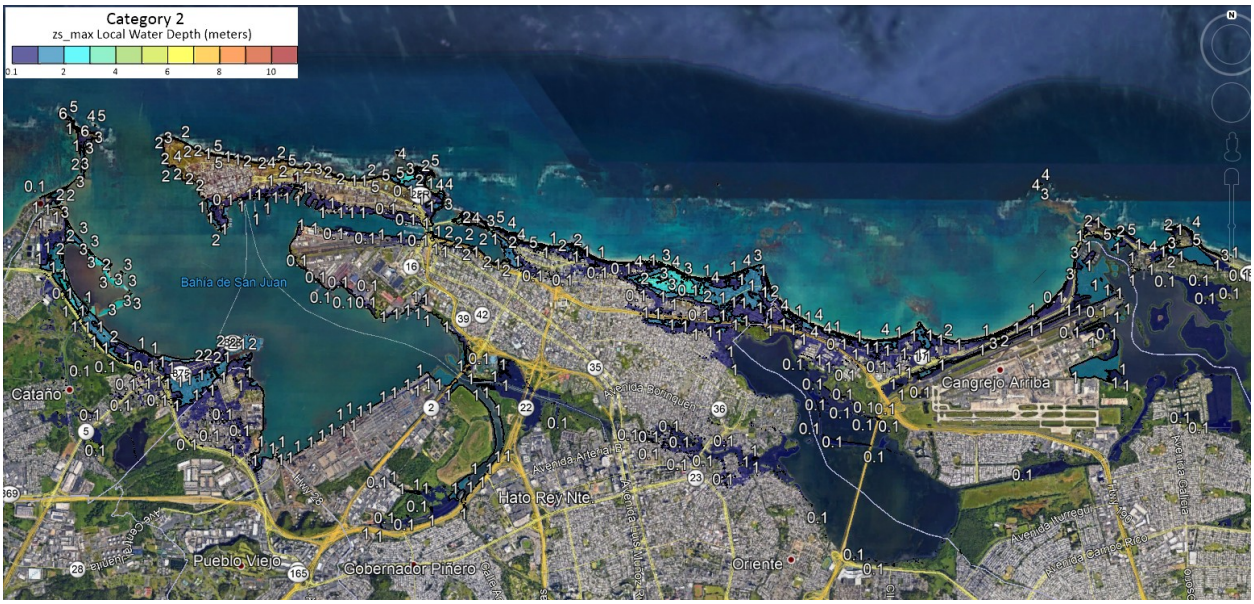

Figure 172 - Grid 9, category 2, maximum sea surface elevation (meters), relative to local terrain elevation, during 1 hour of simulation after spin up of 300 seconds.

GRID 9: CAT 3

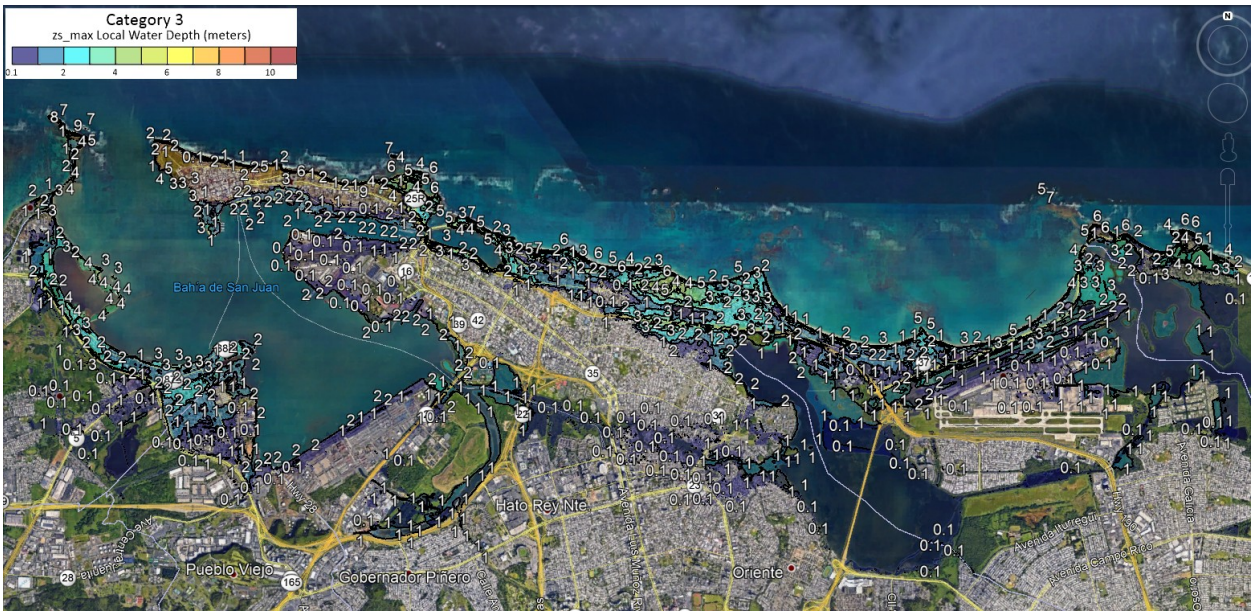

Figure 173 - Grid 9, category 3, maximum sea surface elevation (meters), relative to local terrain elevation, during 1 hour of simulation after spin up of 300 seconds.

GRID 9: CAT 4

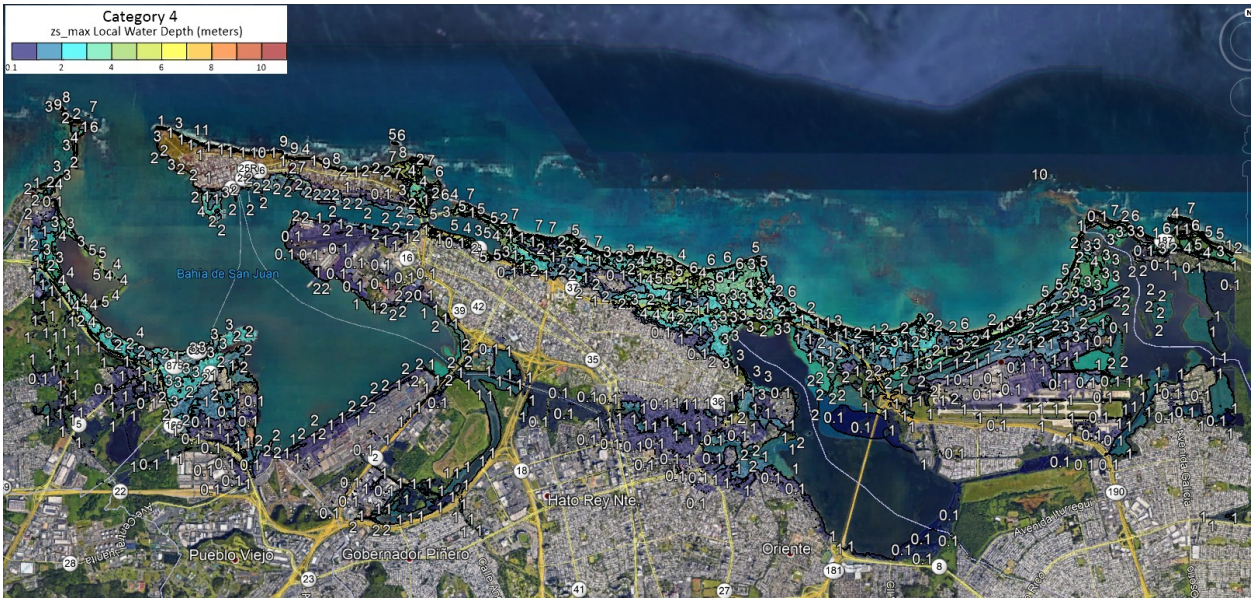

Figure 174 - Grid 9, category 4, maximum sea surface elevation (meters), relative to local terrain elevation, during 1 hour of simulation after spin up of 300 seconds.

GRID 9: CAT 5

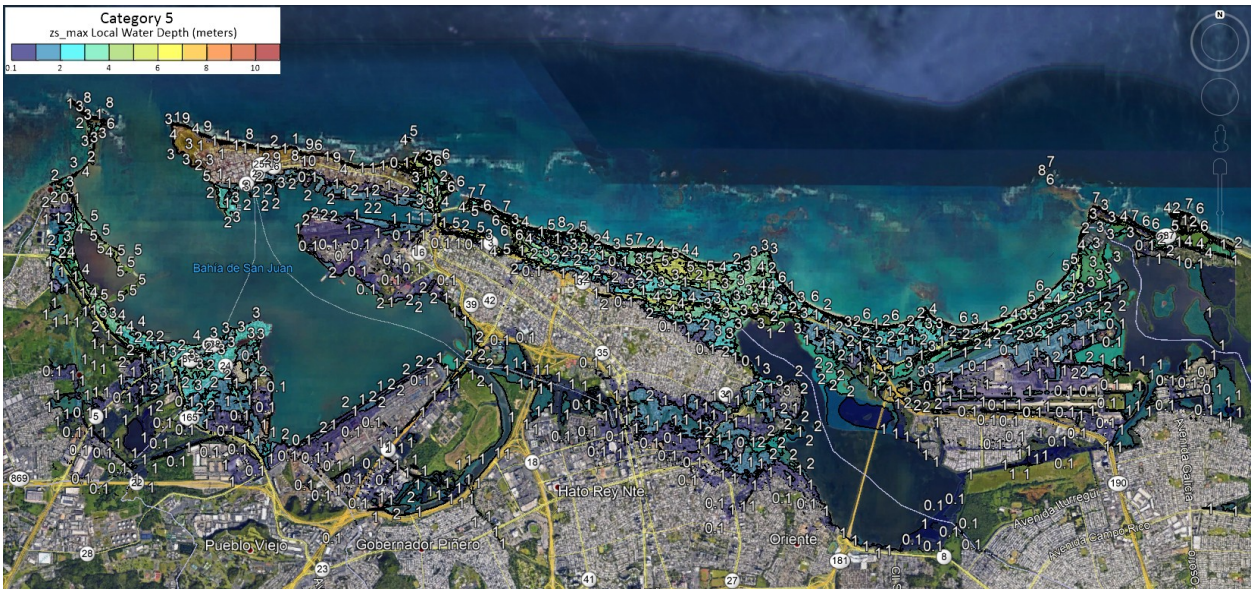

Figure 175 - Grid 9, category 5, maximum sea surface elevation (meters), relative to local terrain elevation, during 1 hour of simulation after spin up of 300 seconds.

GRID 10: CAT 1

Figure 176 - Grid 10, category 1, maximum sea surface elevation (meters), relative to local terrain elevation, during 1 hour of simulation after spin up of 300 seconds.

GRID 10: CAT 2

Figure 177 - Grid 10, category 2, maximum sea surface elevation (meters), relative to local terrain elevation, during 1 hour of simulation after spin up of 300 seconds.

GRID 10: CAT 3

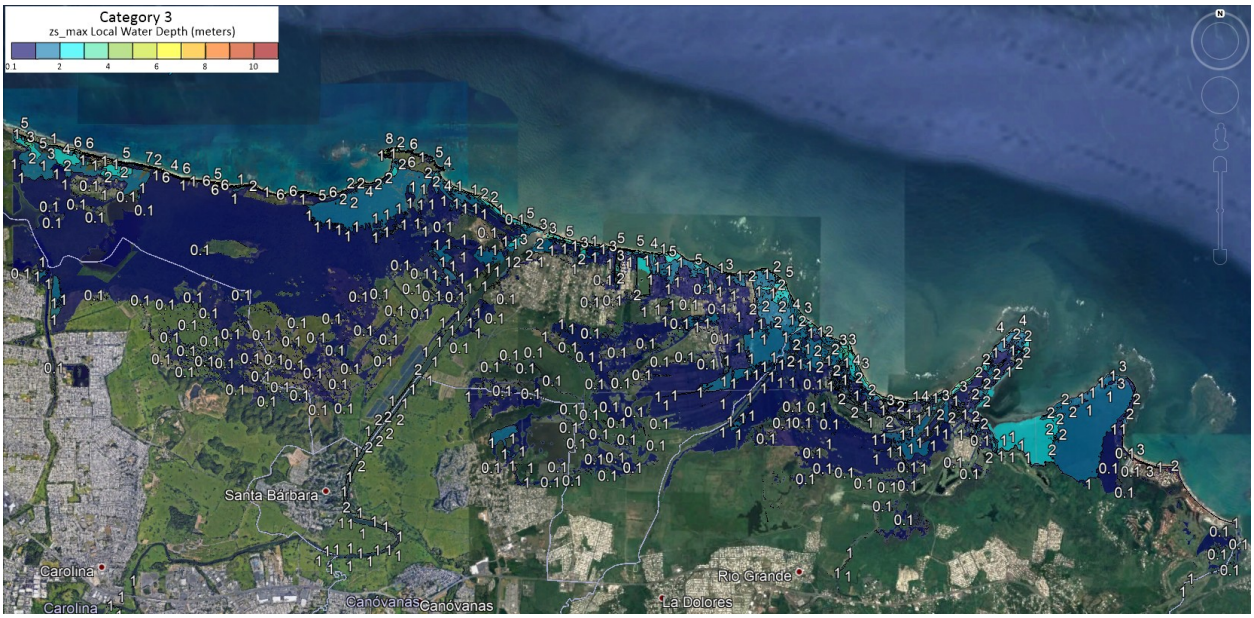

Figure 178 - Grid 10, category 3, maximum sea surface elevation (meters), relative to local terrain elevation, during 1 hour of simulation after spin up of 300 seconds.

GRID 10: CAT 4

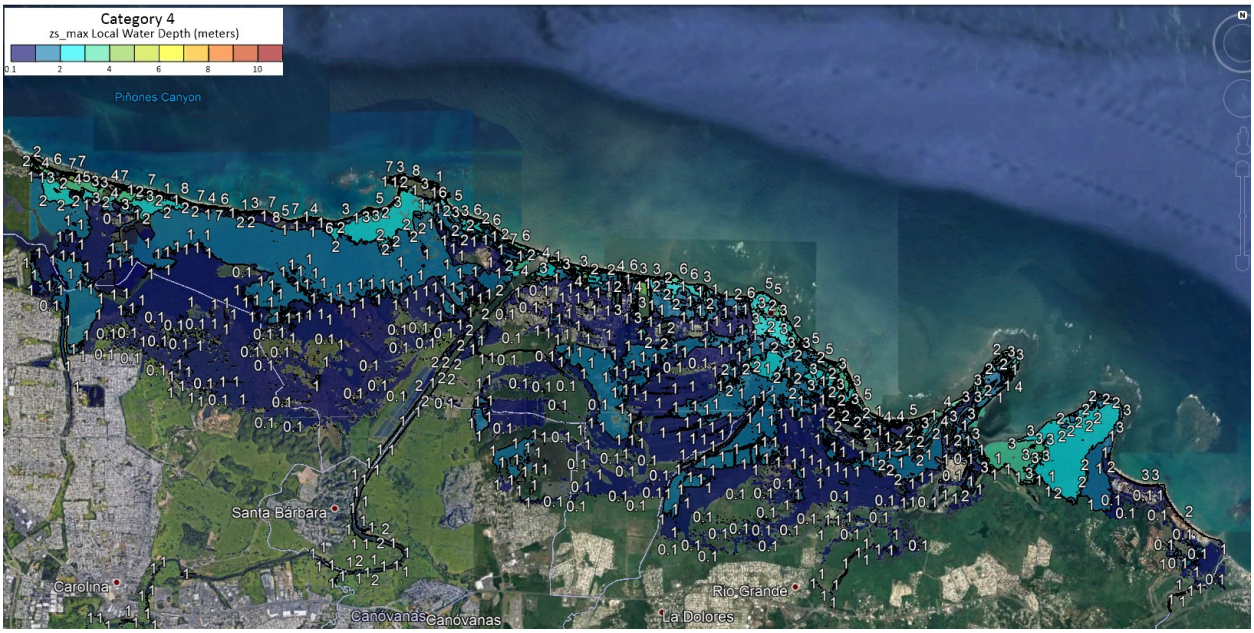

Figure 179 - Grid 10, category 4, maximum sea surface elevation (meters), relative to local terrain elevation, during 1 hour of simulation after spin up of 300 seconds.

GRID 10: CAT 5

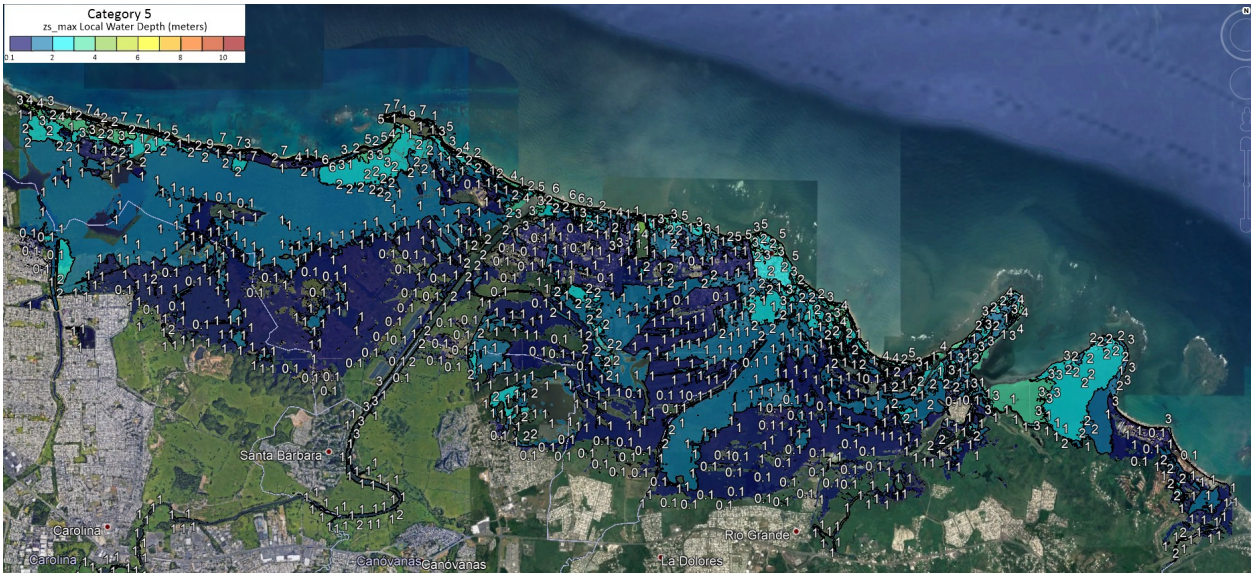

Figure 180 - Grid 10, category 5, maximum sea surface elevation (meters), relative to local terrain elevation, during 1 hour of simulation after spin up of 300 seconds.

GRID 11: CAT 1

Figure 181 - Grid 11, category 1, maximum sea surface elevation (meters), relative to local terrain elevation, during 1 hour of simulation after spin up of 300 seconds.

GRID 11: CAT 2

Figure 182 - Grid 11, category 2, maximum sea surface elevation (meters), relative to local terrain elevation, during 1 hour of simulation after spin up of 300 seconds.

GRID 11: CAT 3

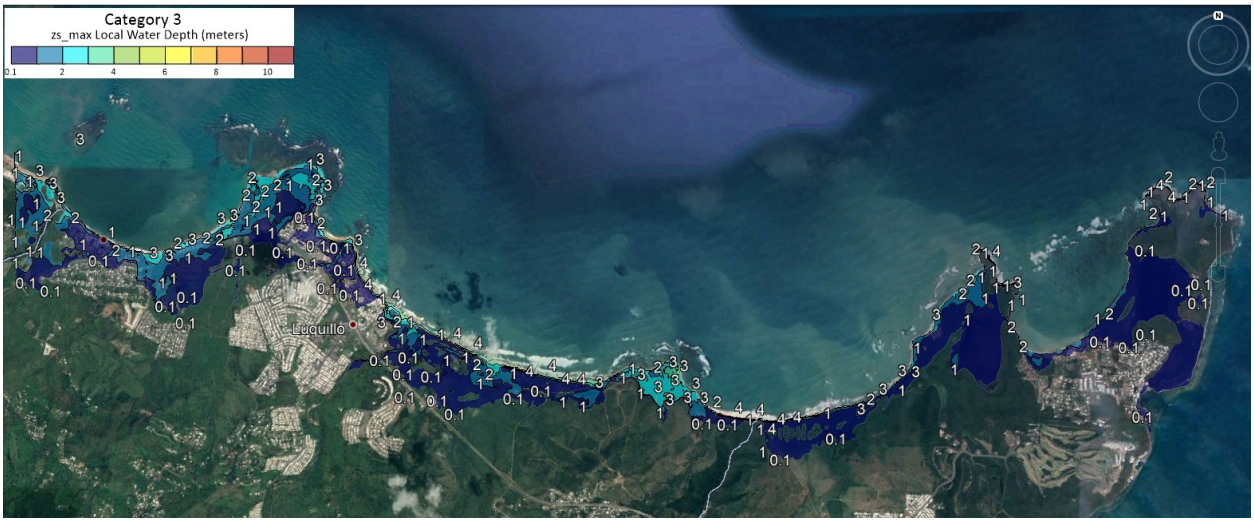

Figure 183 - Grid 11, category 3, maximum sea surface elevation (meters), relative to local terrain elevation, during 1 hour of simulation after spin up of 300 seconds.

GRID 11: CAT 4

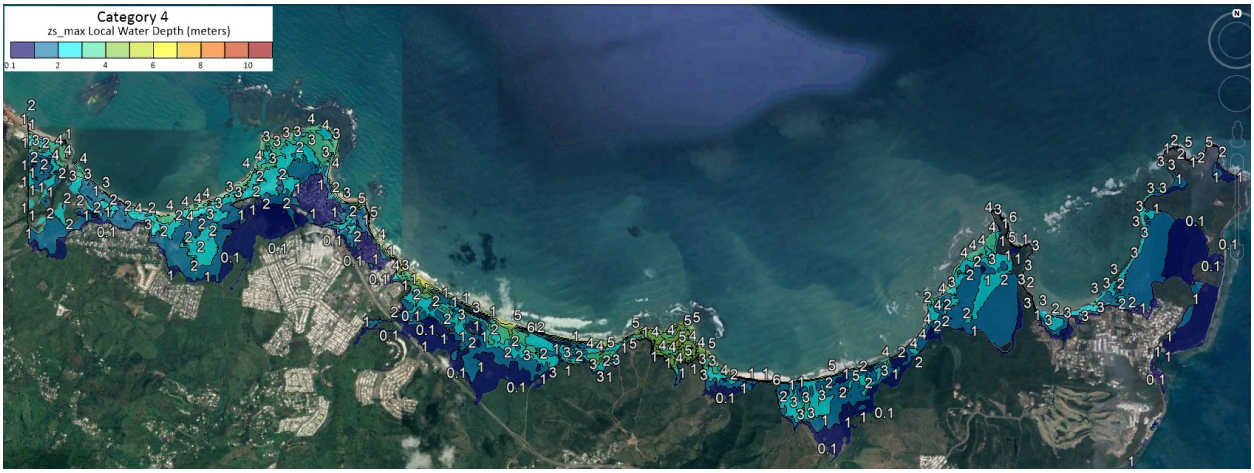

Figure 184 - Grid 11, category 4, maximum sea surface elevation (meters), relative to local terrain elevation, during 1 hour of simulation after spin up of 300 seconds.

GRID 11: CAT 5

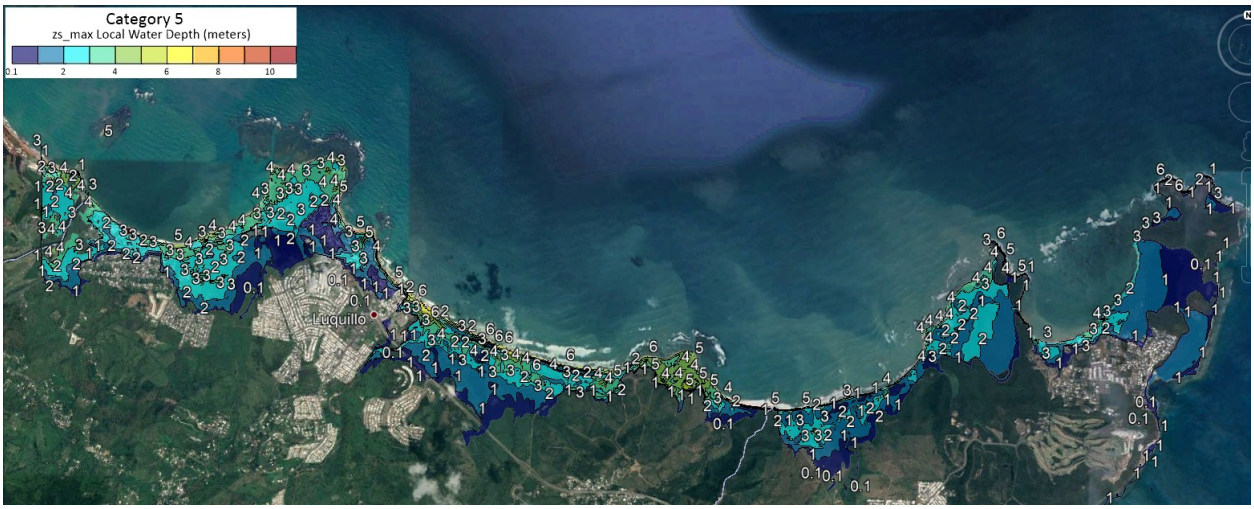

Figure 185 - Grid 11, category 5, maximum sea surface elevation (meters), relative to local terrain elevation, during 1 hour of simulation after spin up of 300 seconds.

GRID 12: CAT 1

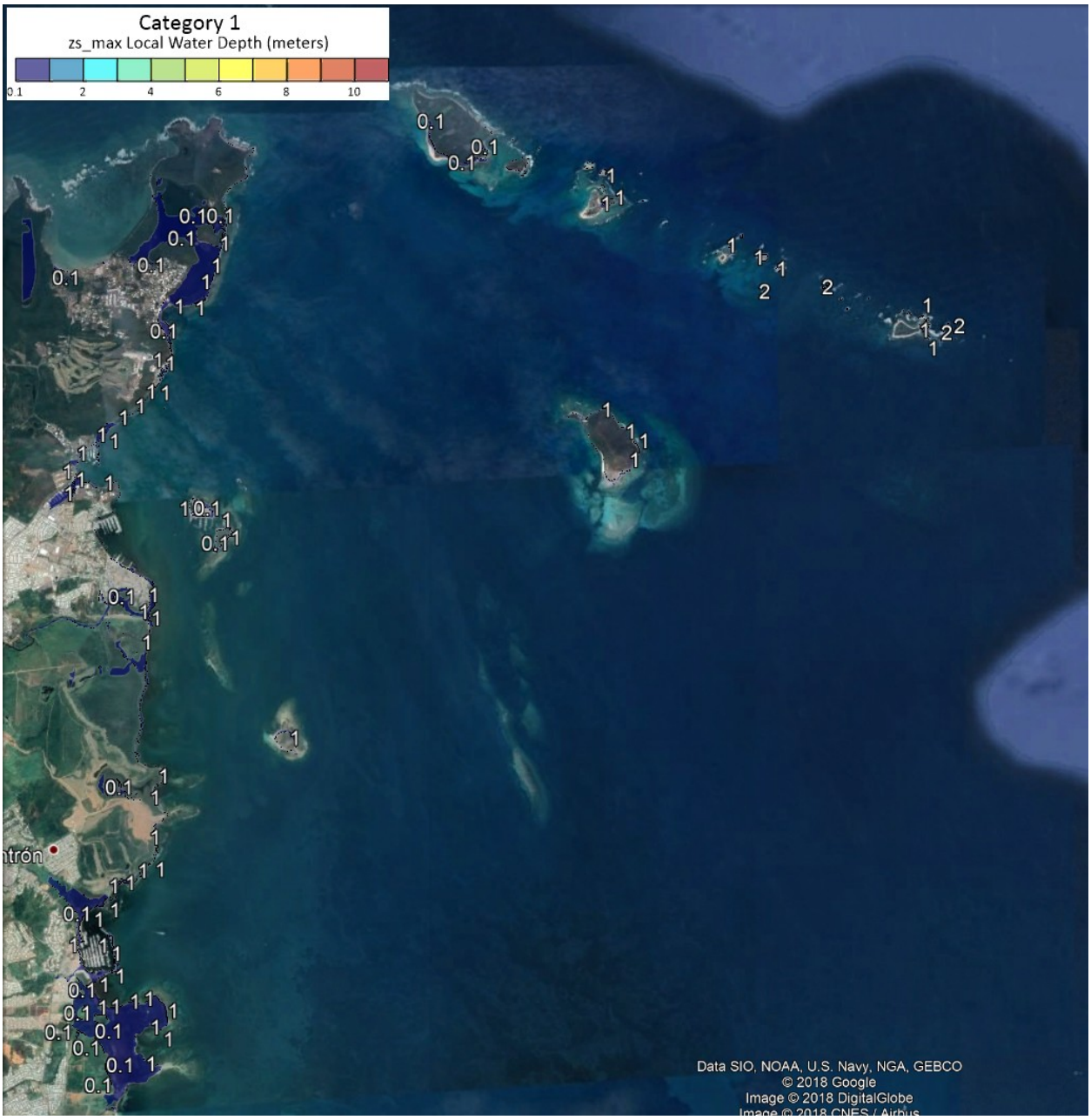

Figure 186 - Grid 12, category 1, maximum sea surface elevation (meters), relative to local terrain elevation, during 1 hour of simulation after spin up of 300 seconds.

GRID 12: CAT 2

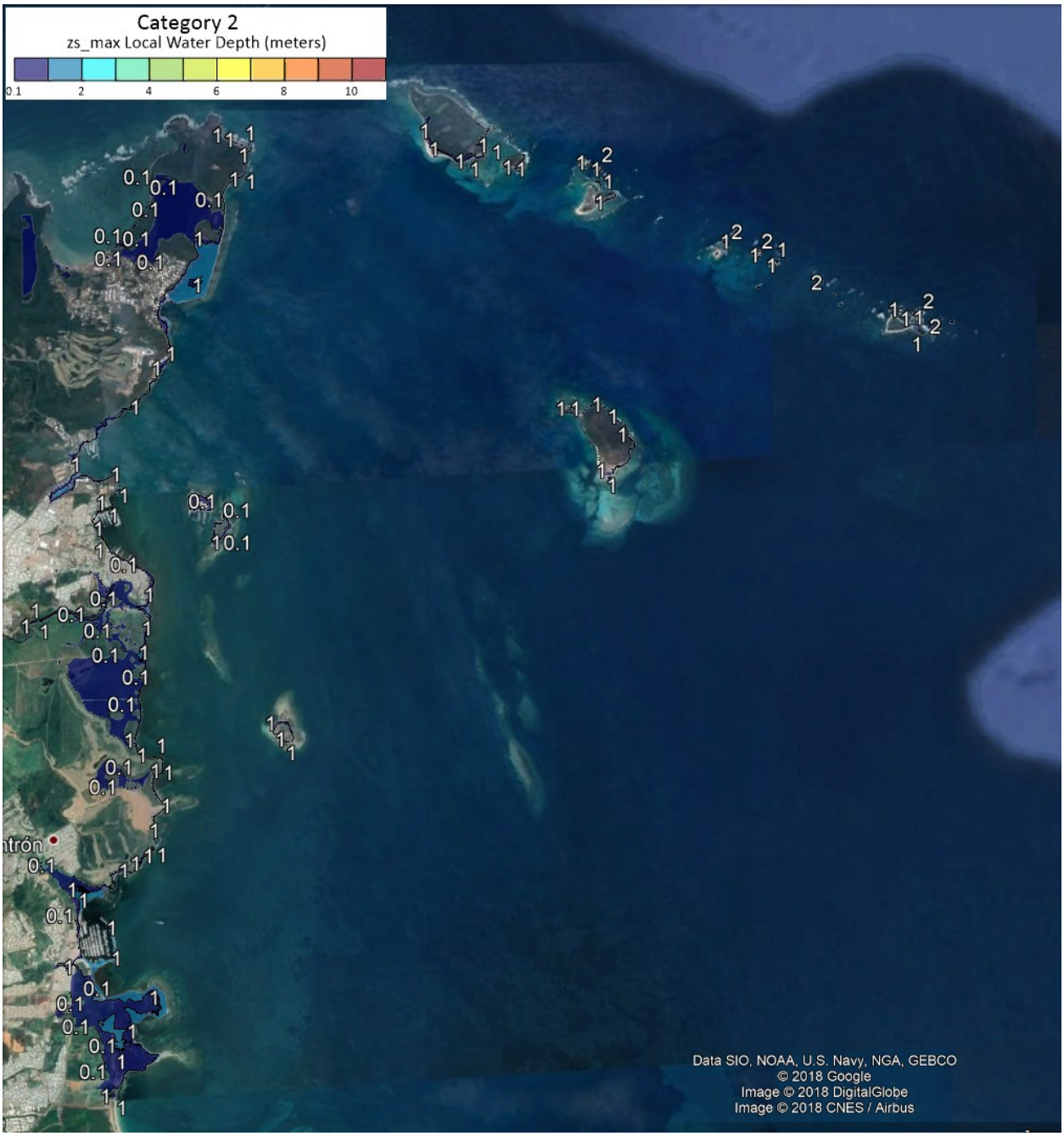

Figure 187 - Grid 12, category 2, maximum sea surface elevation (meters), relative to local terrain elevation, during 1 hour of simulation after spin up of 300 seconds.

GRID 12: CAT 3

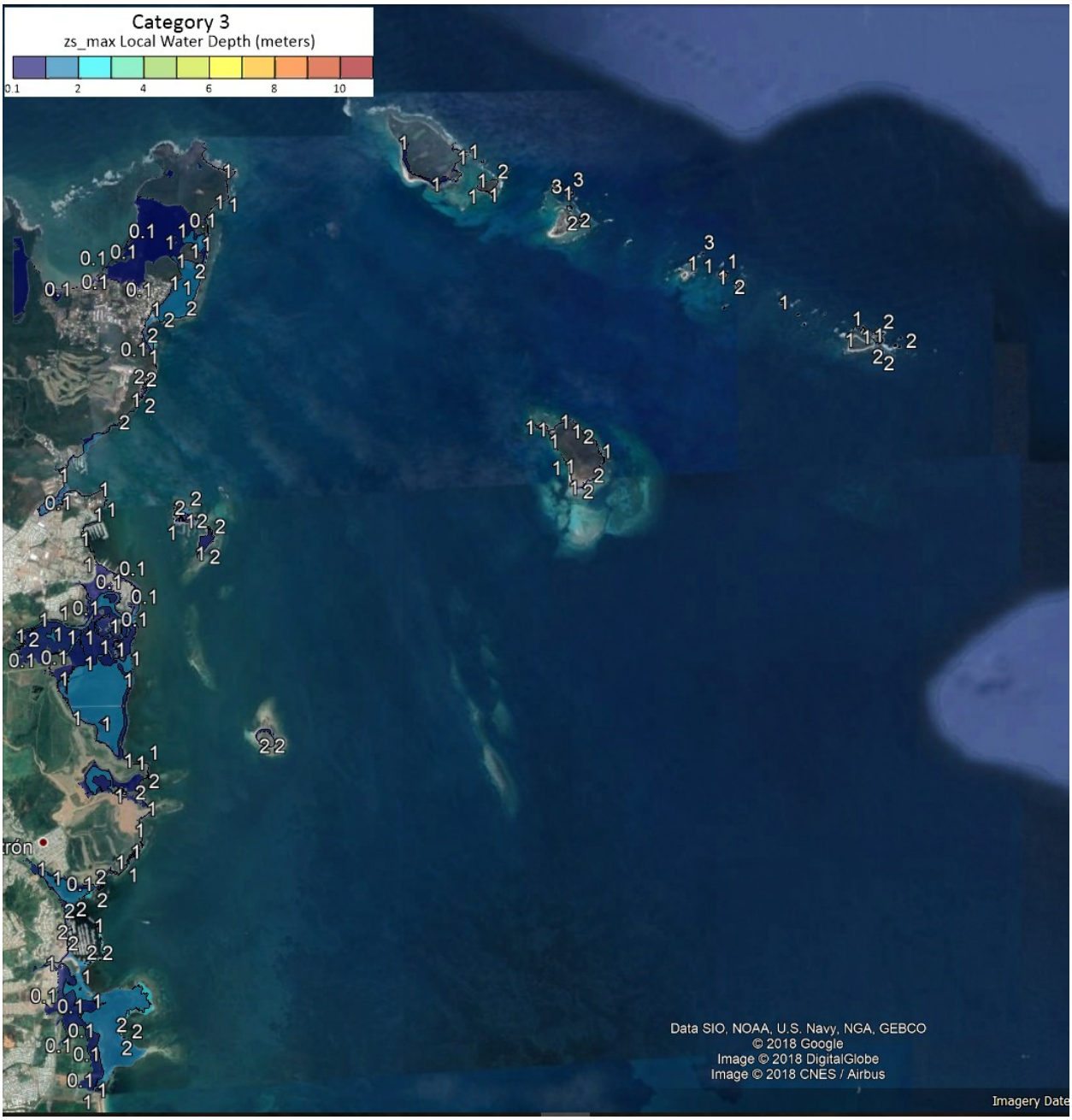

Figure 188- Grid 12, category3, maximum sea surface elevation (meters), relative to local terrain elevation, during 1 hour of simulation after spin up of 300 seconds.

GRID 12: CAT 4

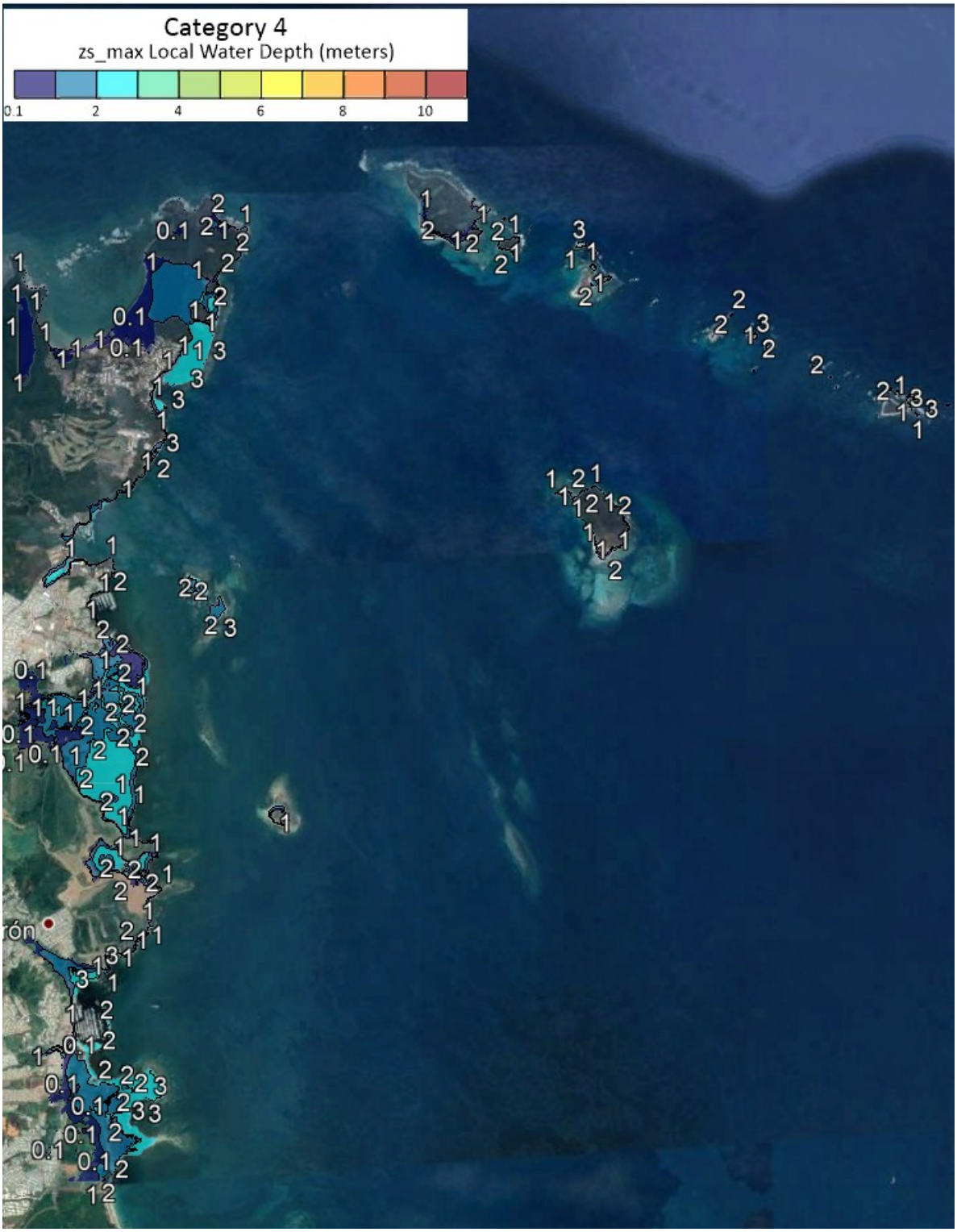

Figure 189 - Grid 12, category 4, maximum sea surface elevation (meters), relative to local terrain elevation, during 1 hour of simulation after spin up of 300 seconds.

GRID 12: CAT 5

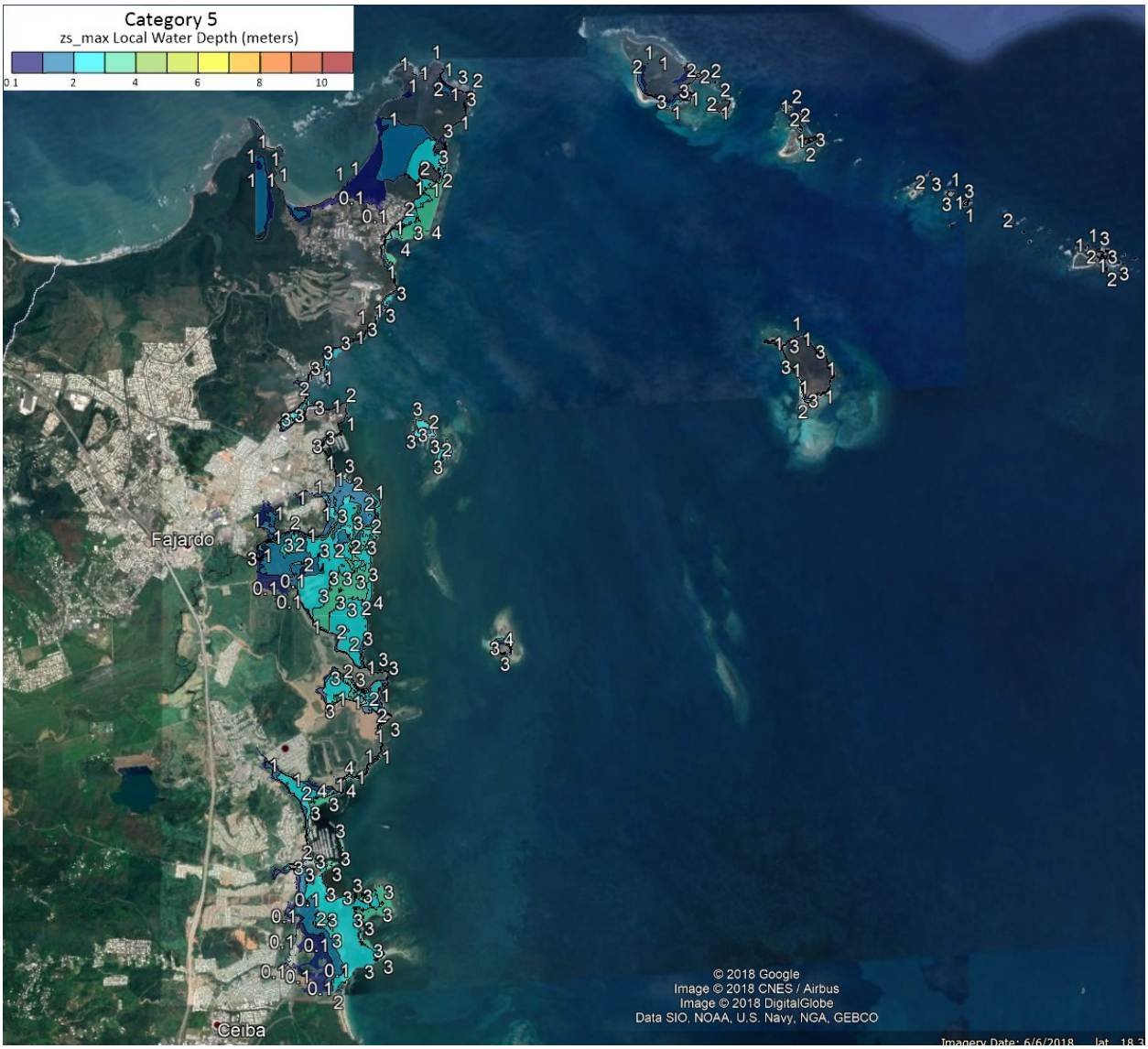

Figure 190 - Grid 12, category 5, maximum sea surface elevation (meters), relative to local terrain elevation, during 1 hour of simulation after spin up of 300 seconds.

GRID 13: CAT 1

Figure 191 - Grid 13, category 1, maximum sea surface elevation (meters), relative to local terrain elevation, during 1 hour of simulation after spin up of 300 seconds.

GRID 13: CAT 2

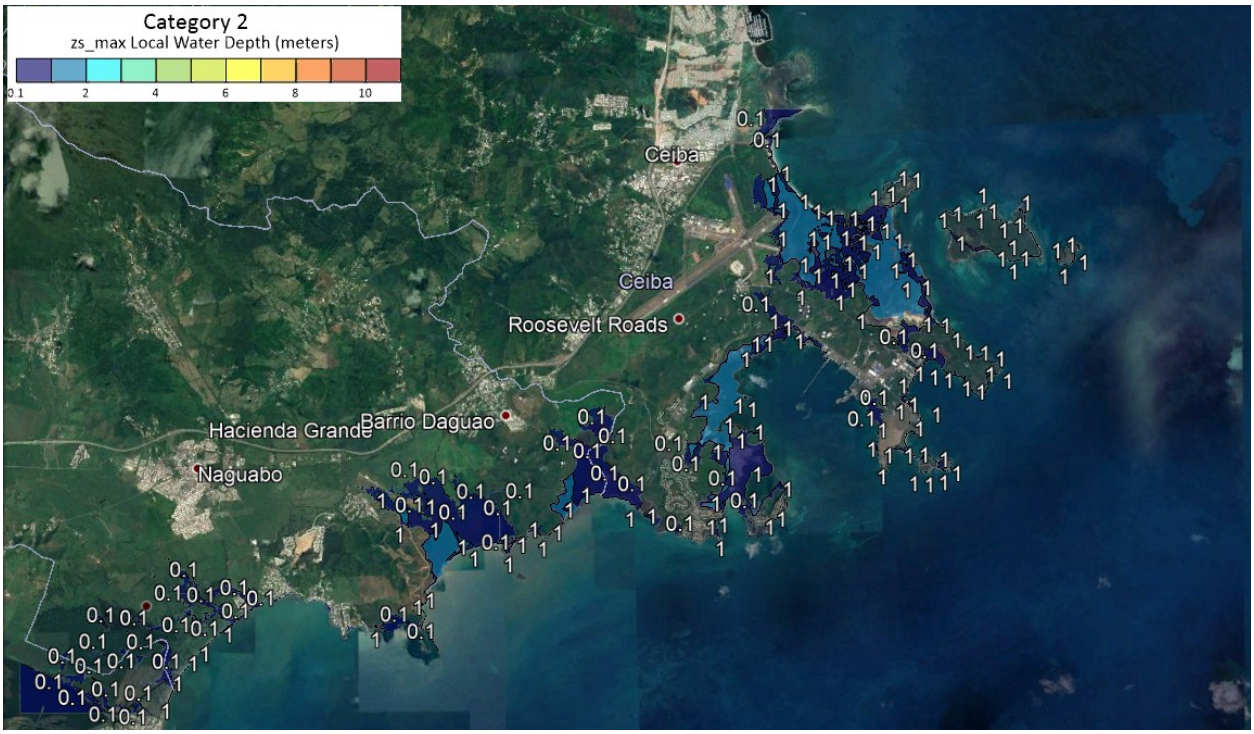

Figure 192 - Grid 13, category 2, maximum sea surface elevation (meters), relative to local terrain elevation, during 1 hour of simulation after spin up of 300 seconds.

GRID 13: CAT 3

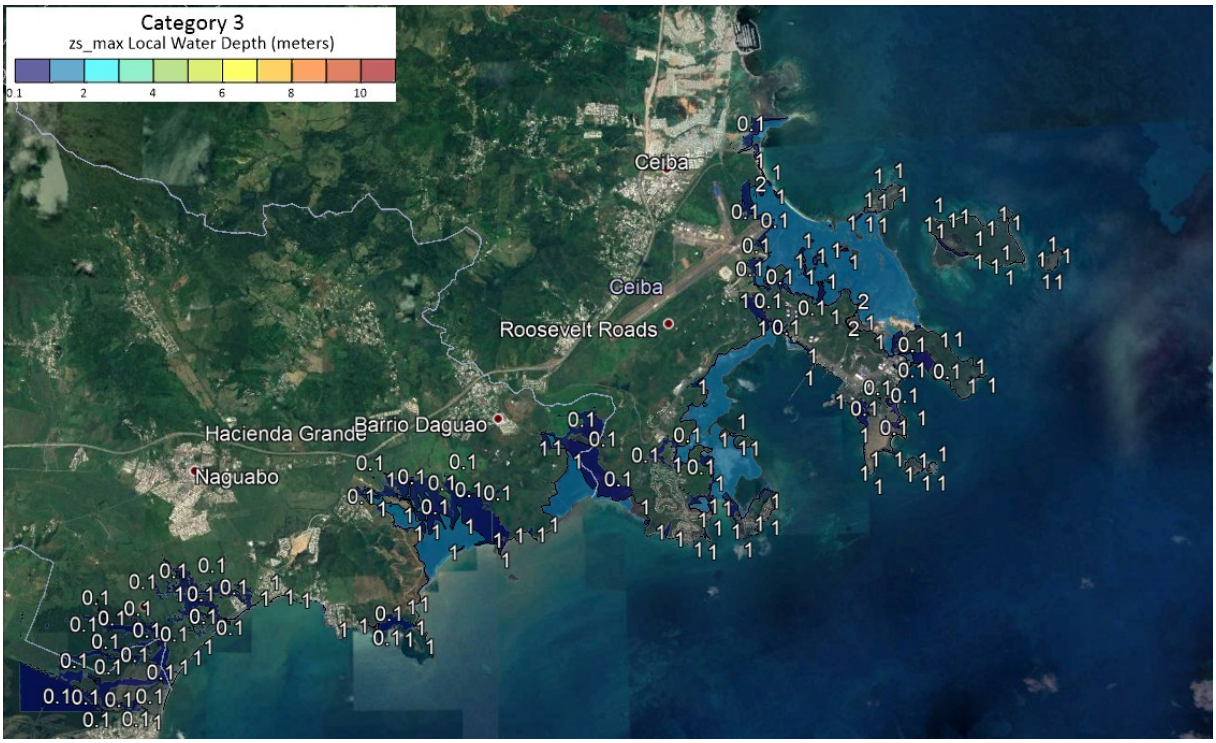

Figure 193 - Grid 13, category 3, maximum sea surface elevation (meters), relative to local terrain elevation, during 1 hour of simulation after spin up of 300 seconds.

GRID 13: CAT 4

Figure 194 - Grid 13, category 4, maximum sea surface elevation (meters), relative to local terrain elevation, during 1 hour of simulation after spin up of 300 seconds.

GRID 13: CAT 5

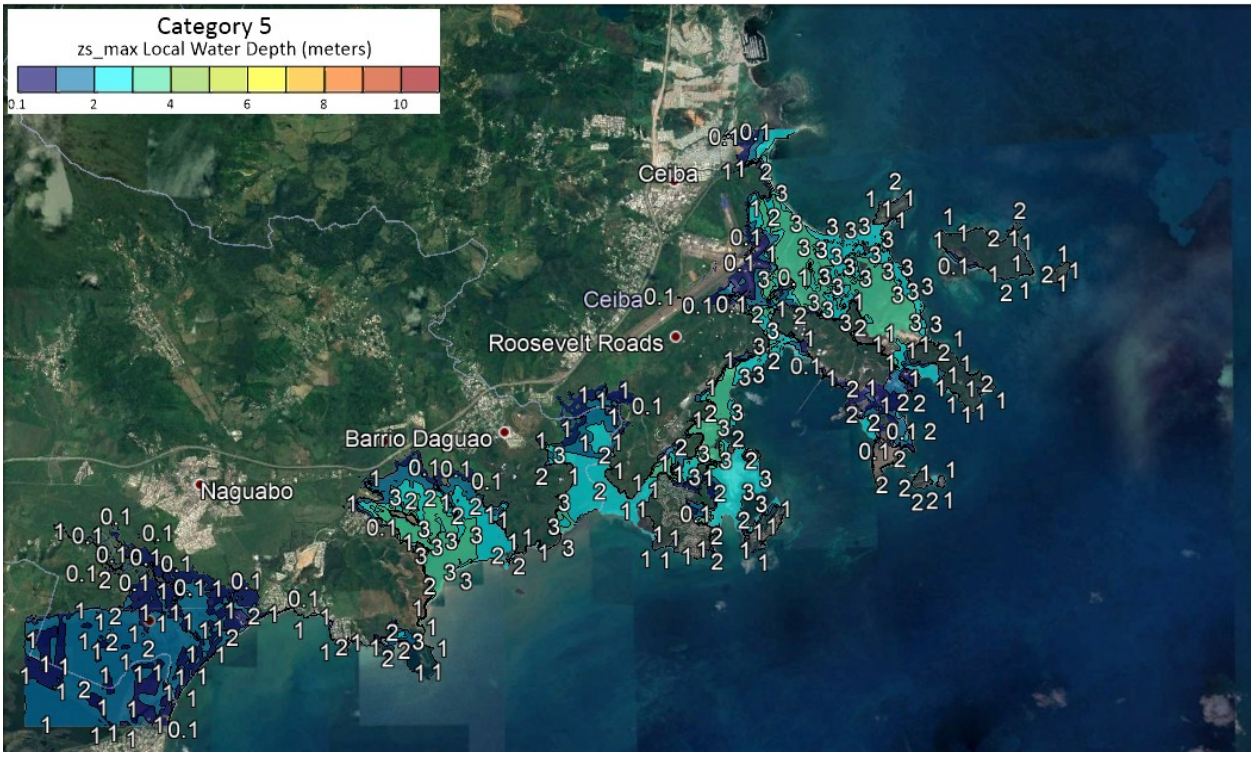

Figure 195 - Grid 13, category 5, maximum sea surface elevation (meters), relative to local terrain elevation, during 1 hour of simulation after spin up of 300 seconds.

GRID 14: CAT 1

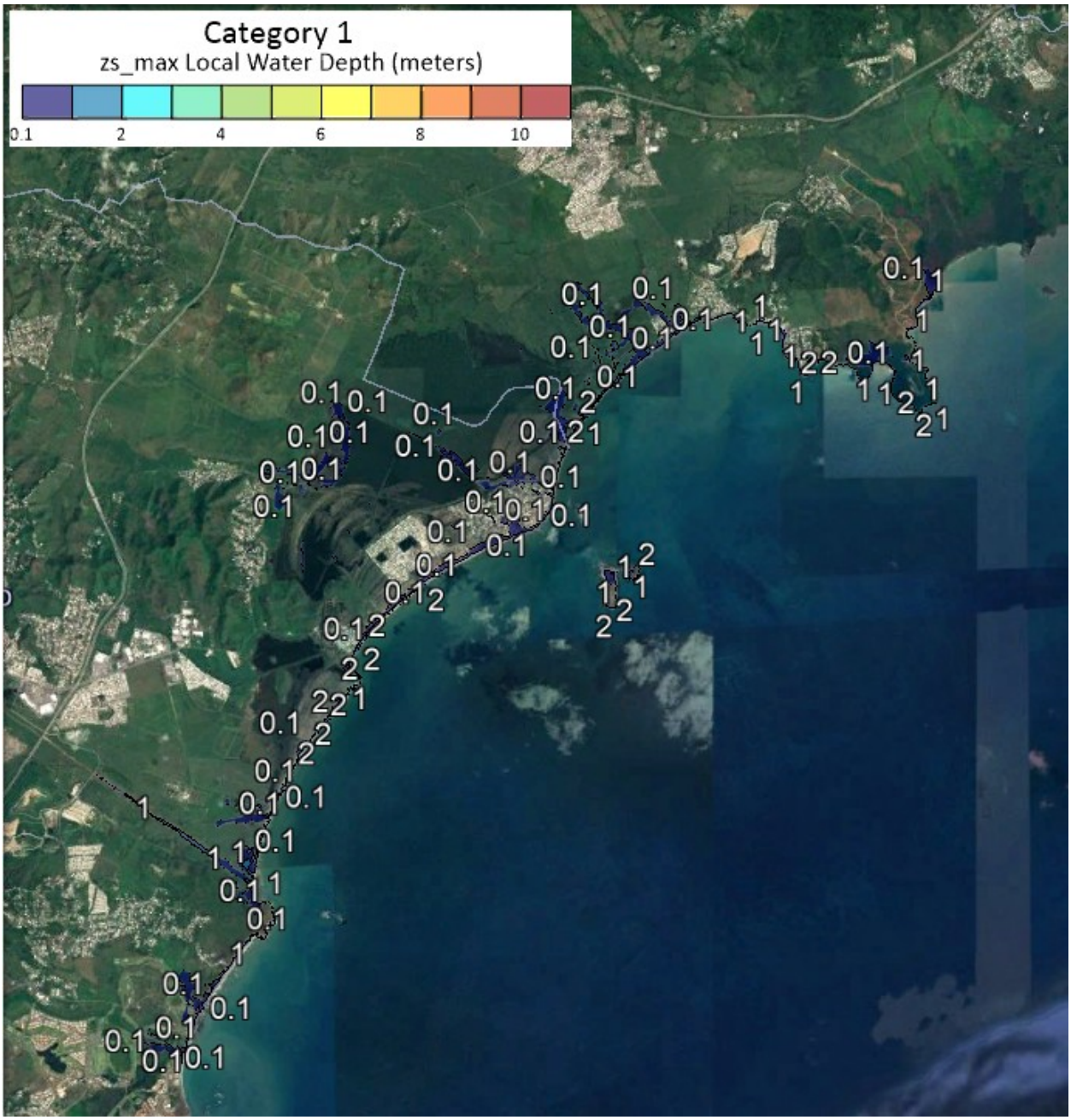

Figure 196 - Grid 14, category 1, maximum sea surface elevation (meters), relative to local terrain elevation, during 1 hour of simulation after spin up of 300 seconds.

GRID 14: CAT 2

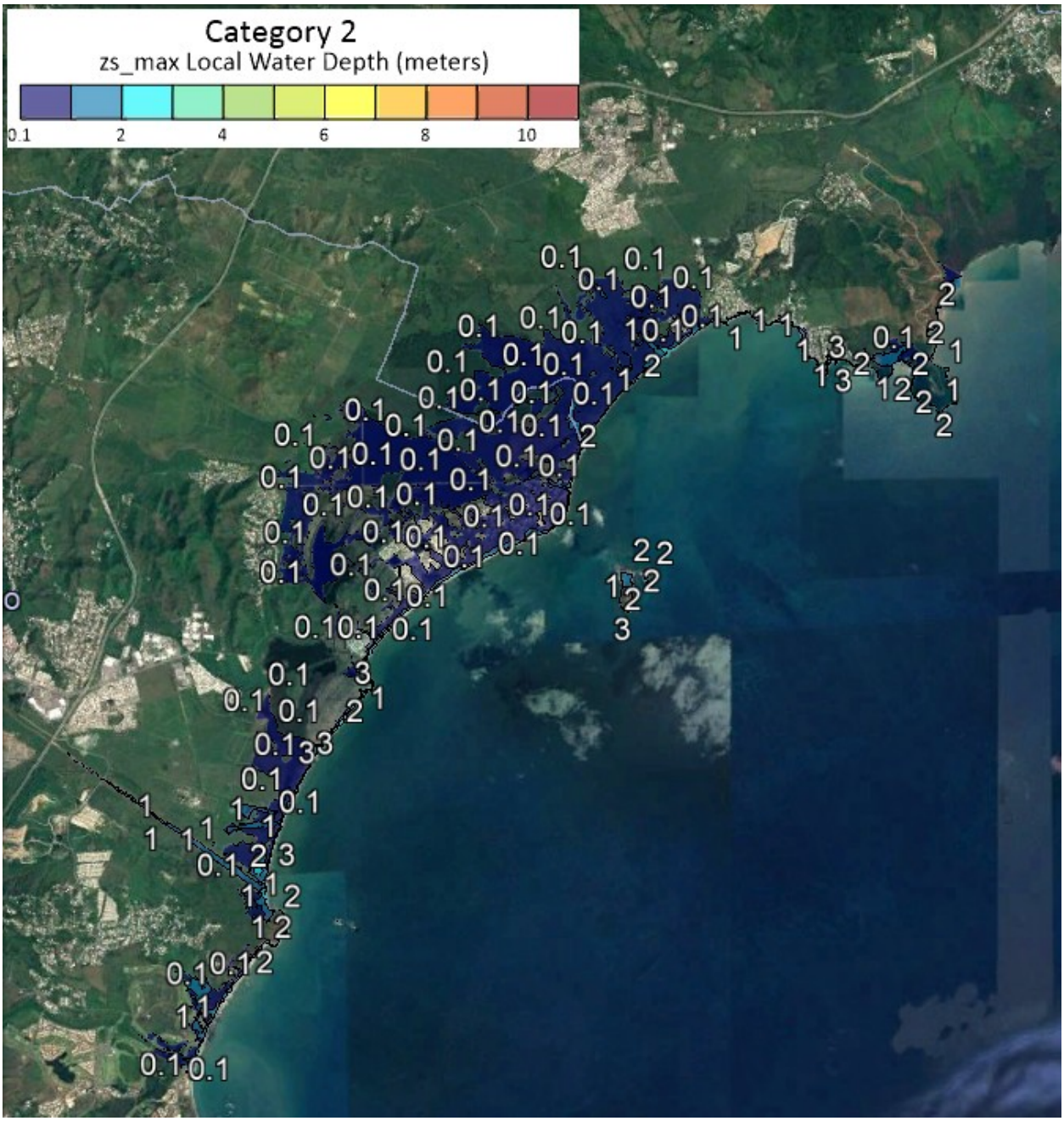

Figure 197 - Grid 14, category 2, maximum sea surface elevation (meters), relative to local terrain elevation, during 1 hour of simulation after spin up of 300 seconds.

GRID 14: CAT 3

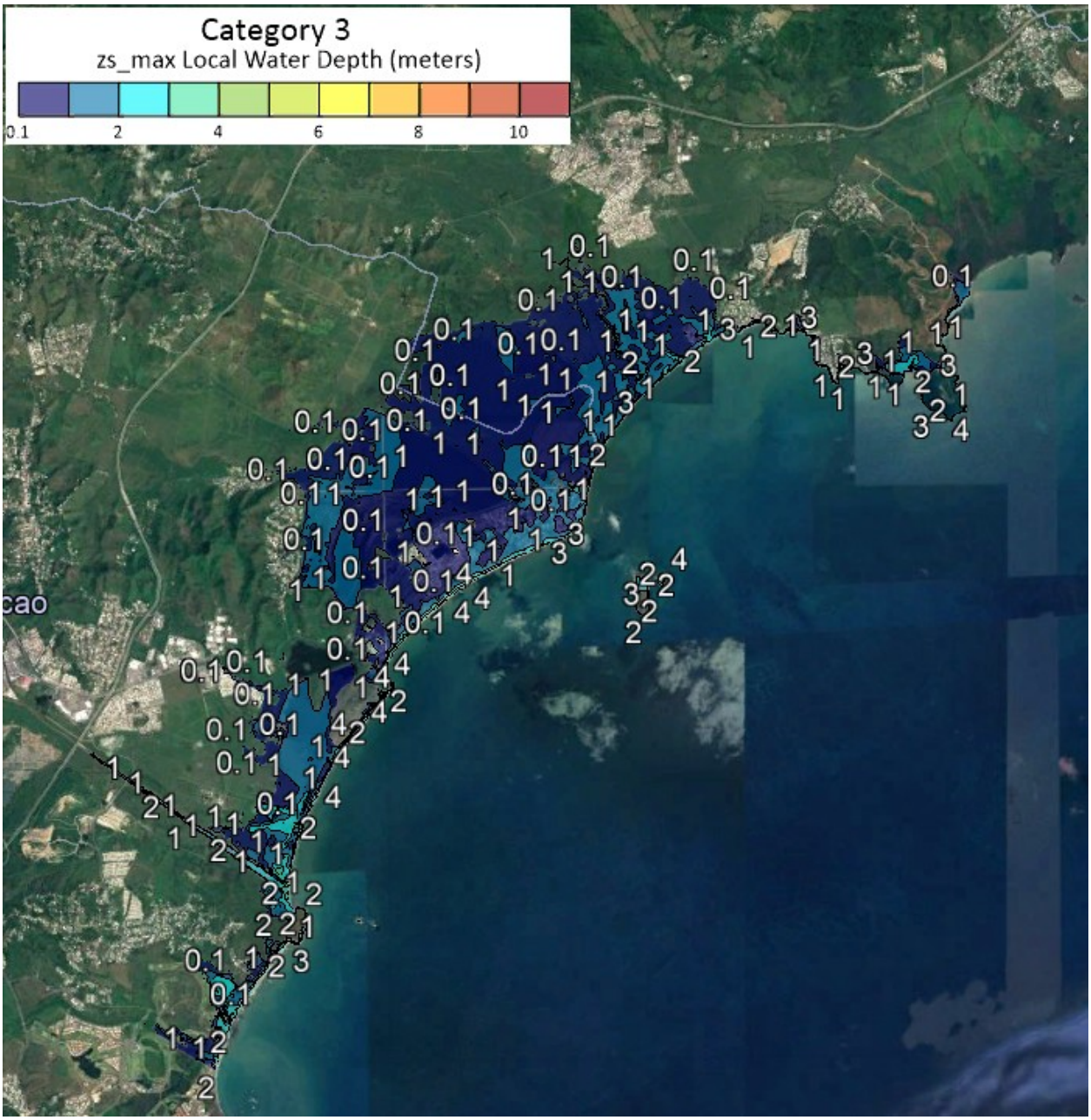

Figure 198- Grid 14, category 3, maximum sea surface elevation (meters), relative to local terrain elevation, during 1 hour of simulation after spin up of 300 seconds.

GRID 14: CAT 4

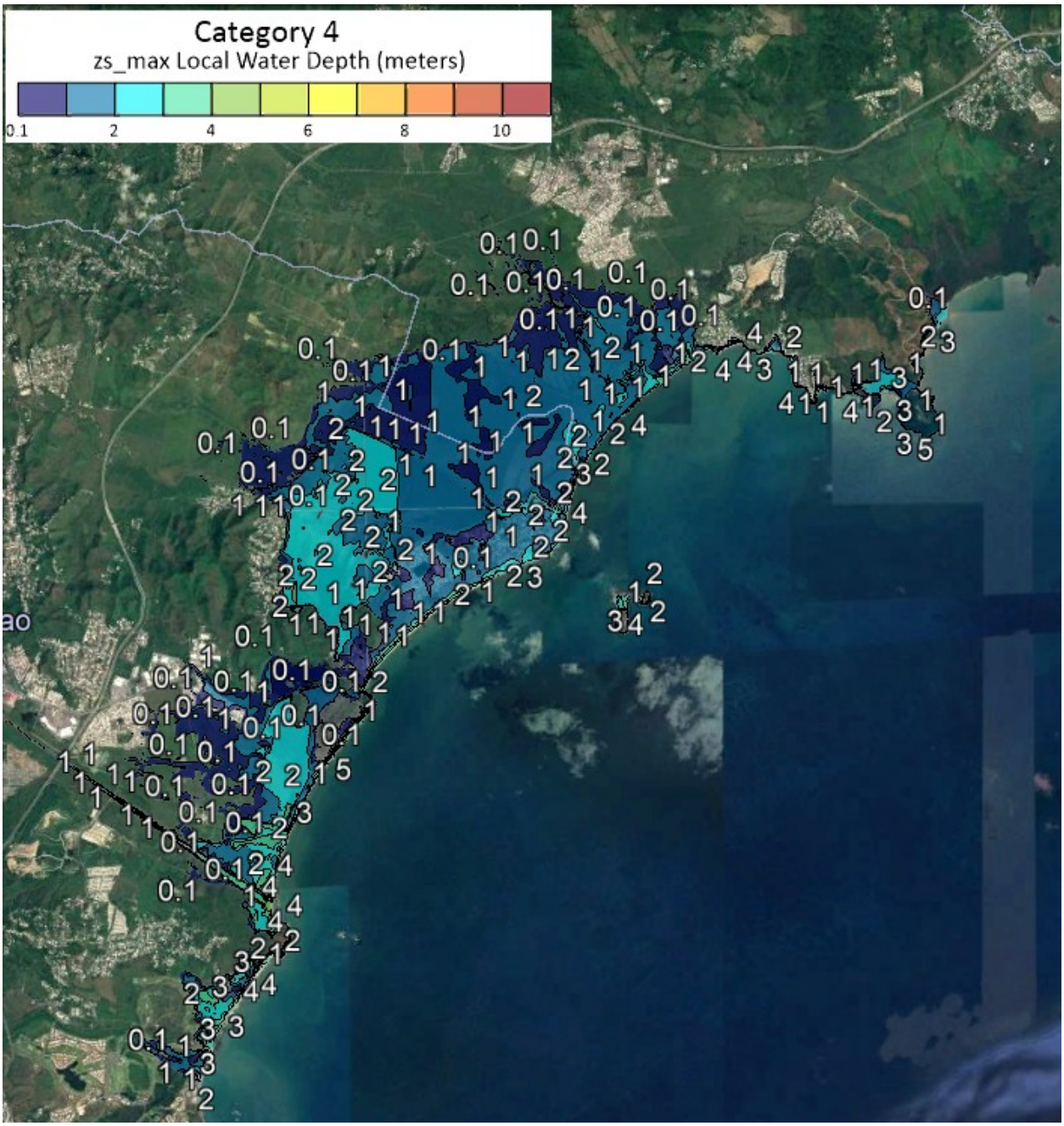

Figure 199 - Grid 14, category 4, maximum sea surface elevation (meters), relative to local terrain elevation, during 1 hour of simulation after spin up of 300 seconds.

GRID 14: CAT 5

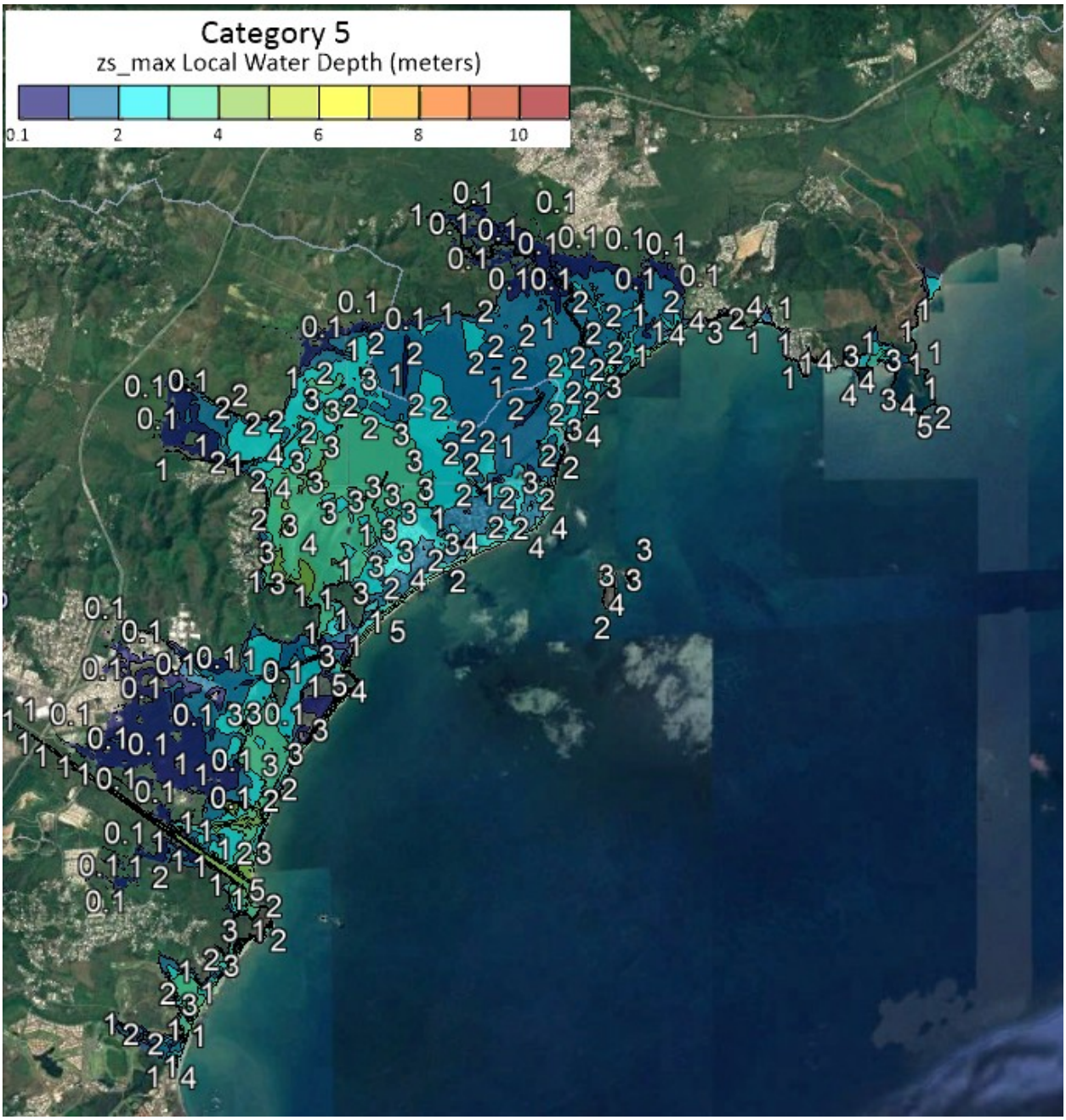

Figure 200 - Grid 14, category 5, maximum sea surface elevation (meters), relative to local terrain elevation, during 1 hour of simulation after spin up of 300 seconds.

GRID 15: CAT 1

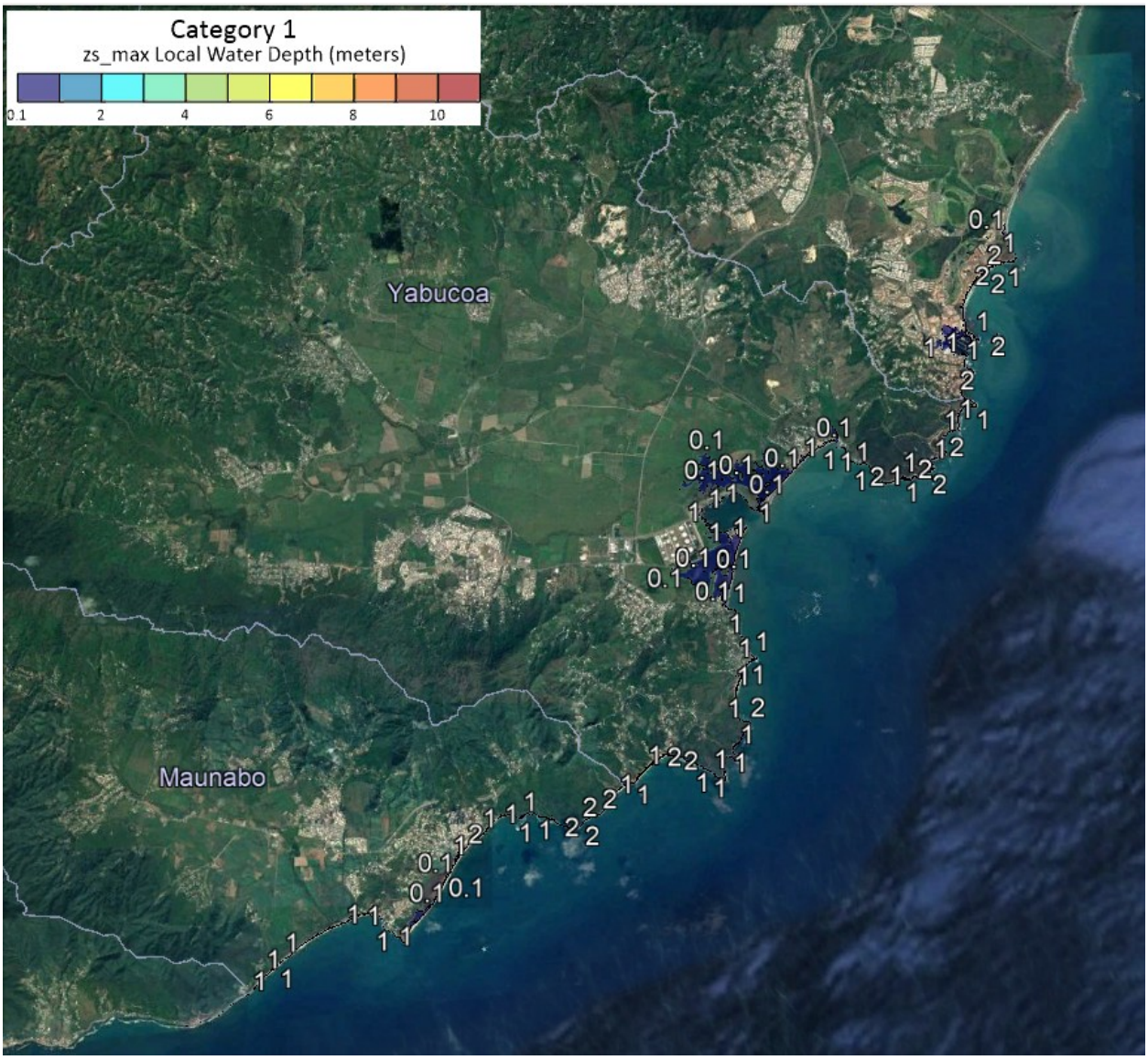

Figure 201 - Grid 15, category 1, maximum sea surface elevation (meters), relative to local terrain elevation, during 1 hour of simulation after spin up of 300 seconds.

GRID 15: CAT 2

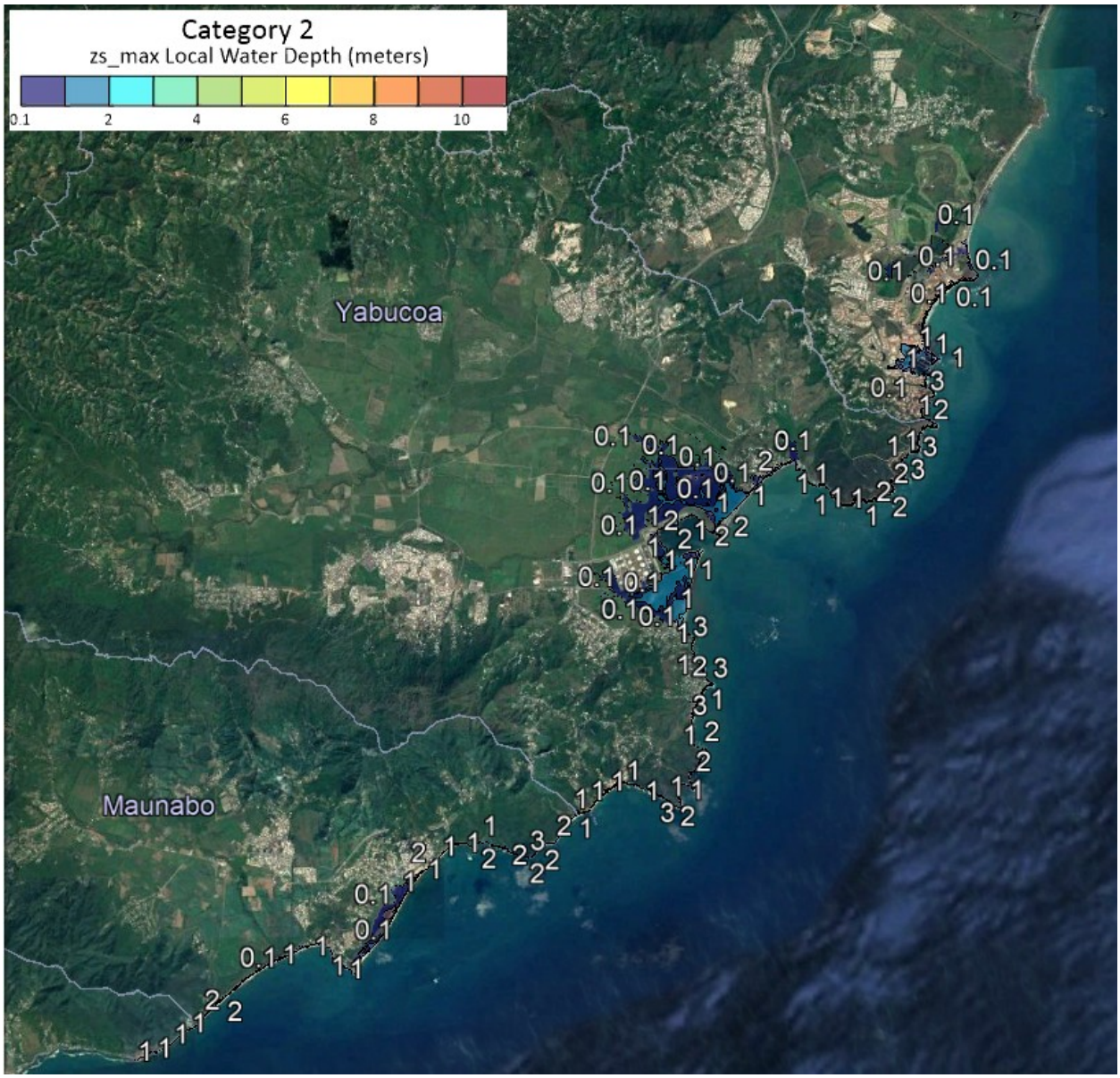

Figure 202 - Grid 15, category 2, maximum sea surface elevation (meters), relative to local terrain elevation, during 1 hour of simulation after spin up of 300 seconds.

GRID 15: CAT 3

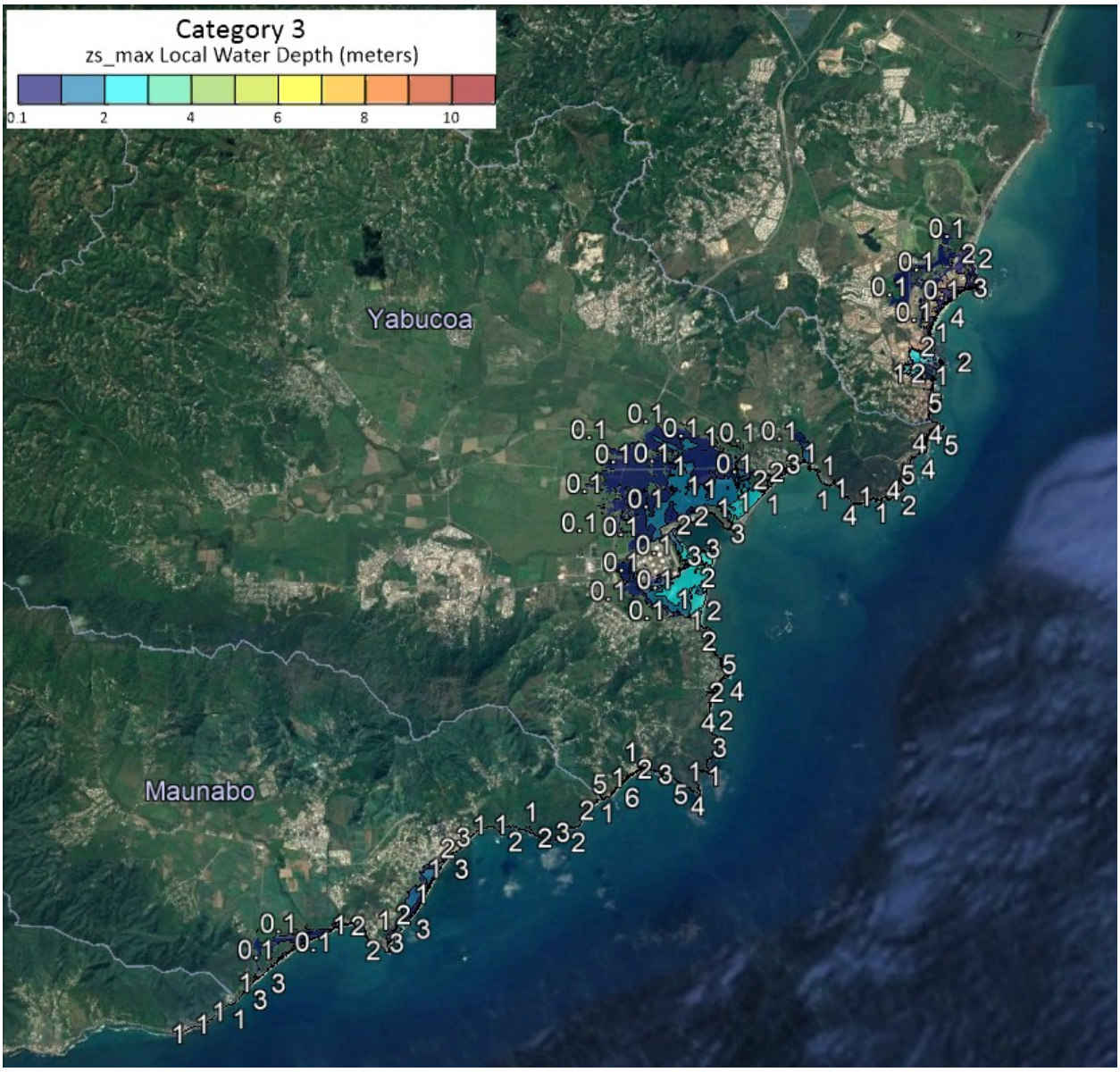

Figure 203 - Grid 15, category 3, maximum sea surface elevation (meters), relative to local terrain elevation, during 1 hour of simulation after spin up of 300 seconds.

GRID 15: CAT 4

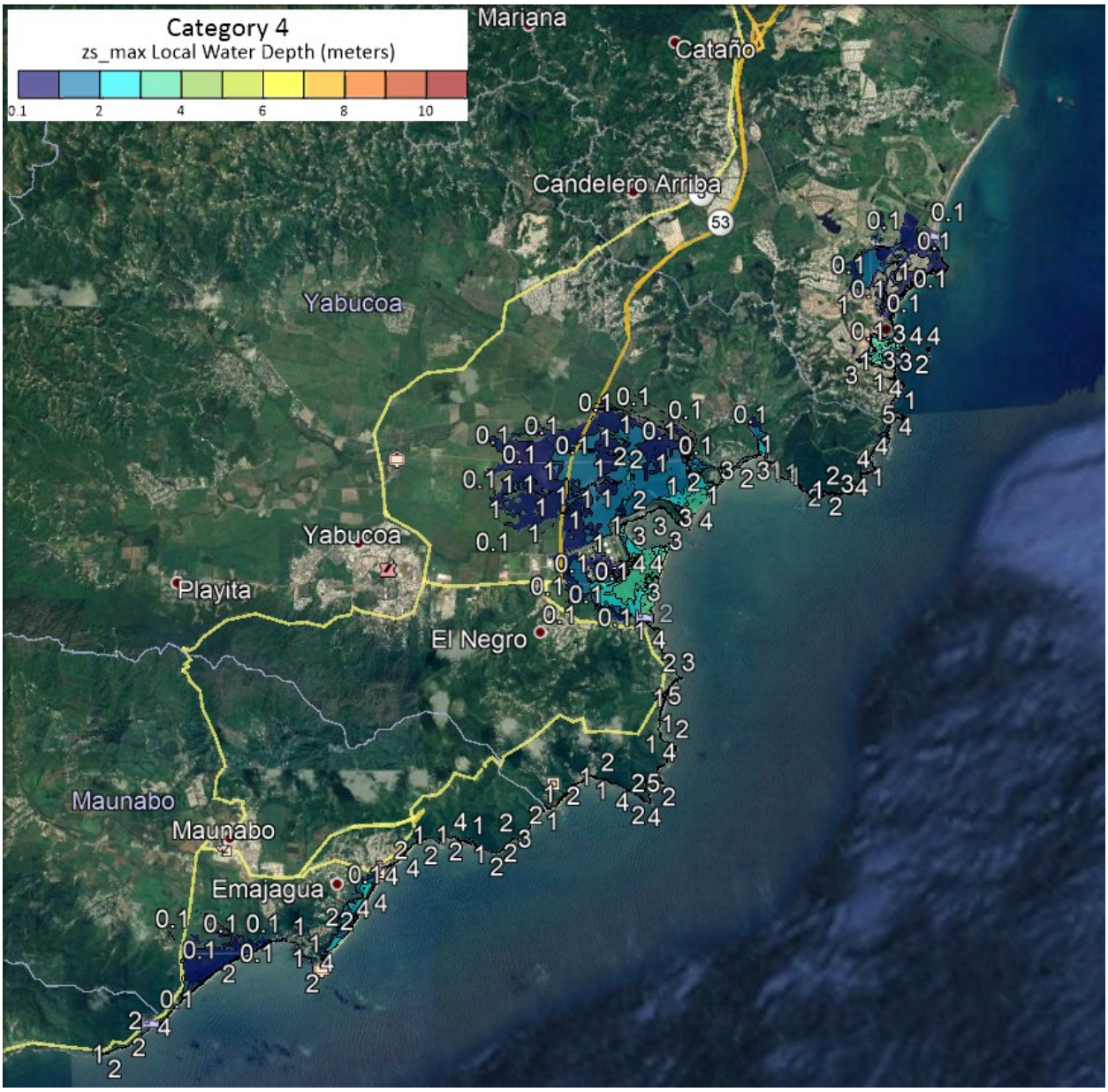

Figure 204 - Grid 15, category 4, maximum sea surface elevation (meters), relative to local terrain elevation, during 1 hour of simulation after spin up of 300 seconds.

GRID 15: CAT 5

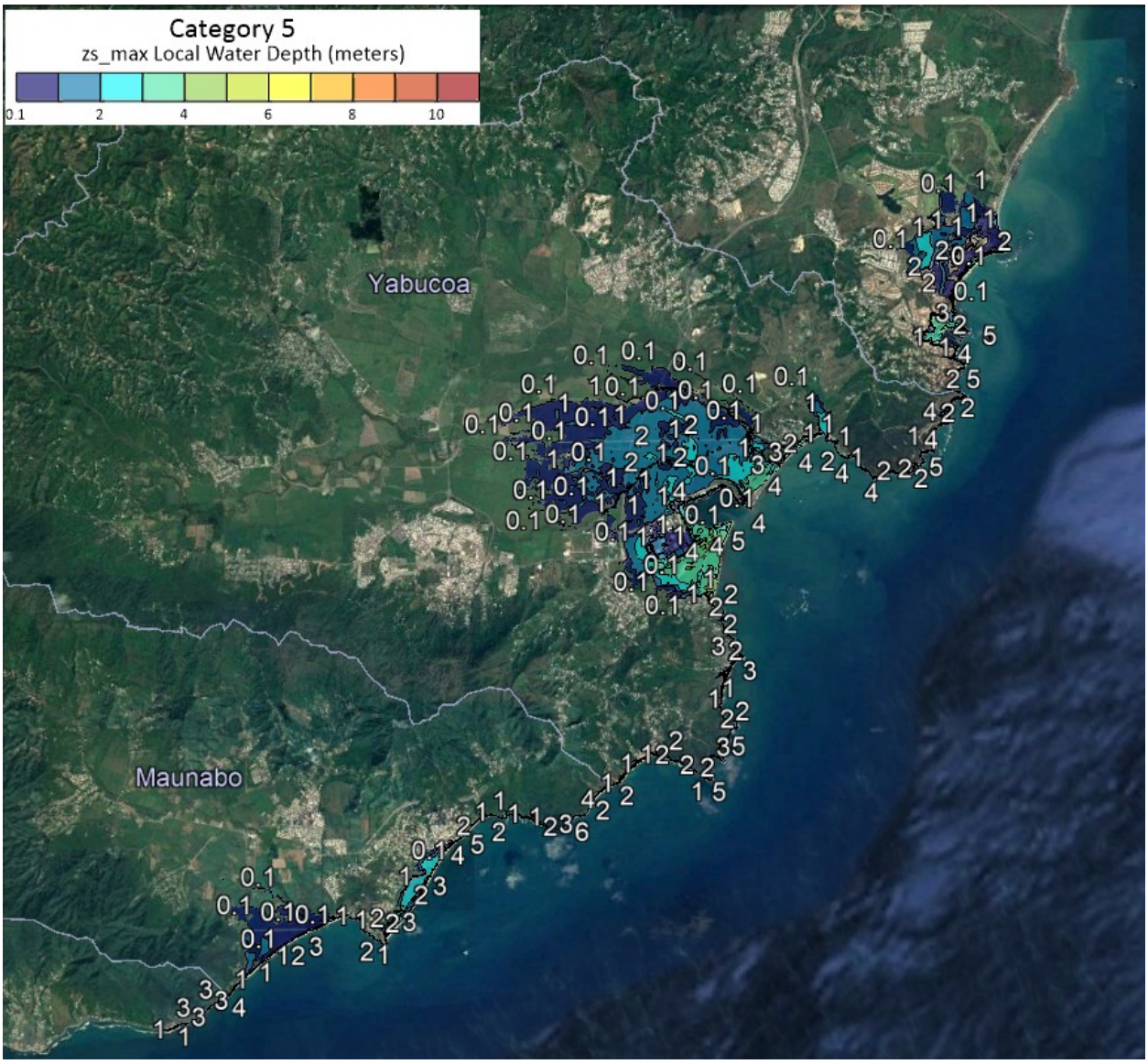

Figure 205 - Grid 15, category 5, maximum sea surface elevation (meters), relative to local terrain elevation, during 1 hour of simulation after spin up of 300 seconds.

GRID 16: CAT 1

Figure 206 - Grid 16, category 1, maximum sea surface elevation (meters), relative to local terrain elevation, during 1 hour of simulation after spin up of 300 seconds.

GRID 16: CAT 2

Figure 207 - Grid 16, category 2, maximum sea surface elevation (meters), relative to local terrain elevation, during 1 hour of simulation after spin up of 300 seconds.

GRID 16: CAT 3

Figure 208 - Grid 16, category 3, maximum sea surface elevation (meters), relative to local terrain elevation, during 1 hour of simulation after spin up of 300 seconds.

GRID 16: CAT 4

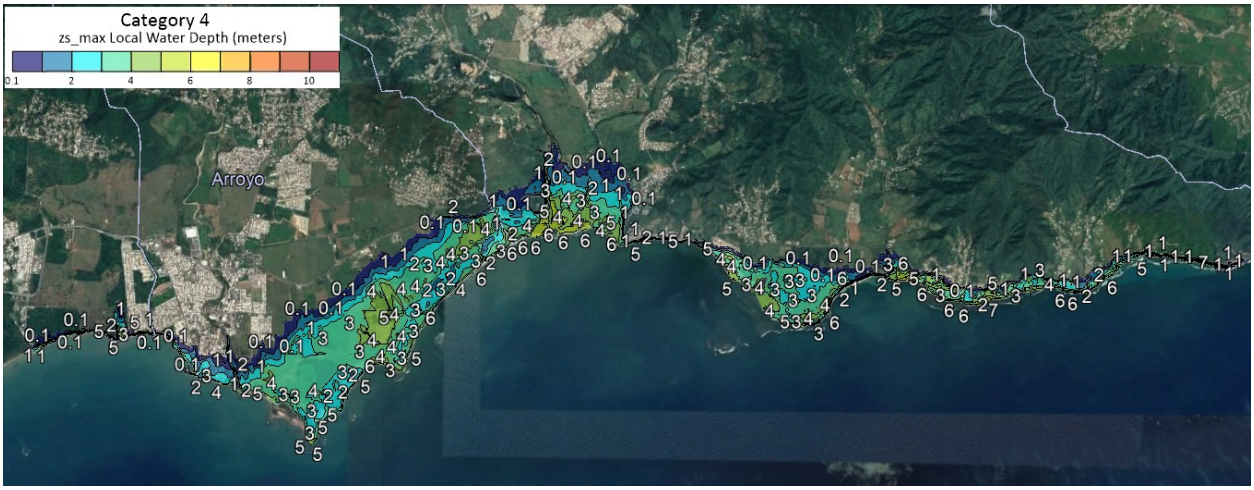

Figure 209 - Grid 16, category 4, maximum sea surface elevation (meters), relative to local terrain elevation, during 1 hour of simulation after spin up of 300 seconds.

GRID 16: CAT 5

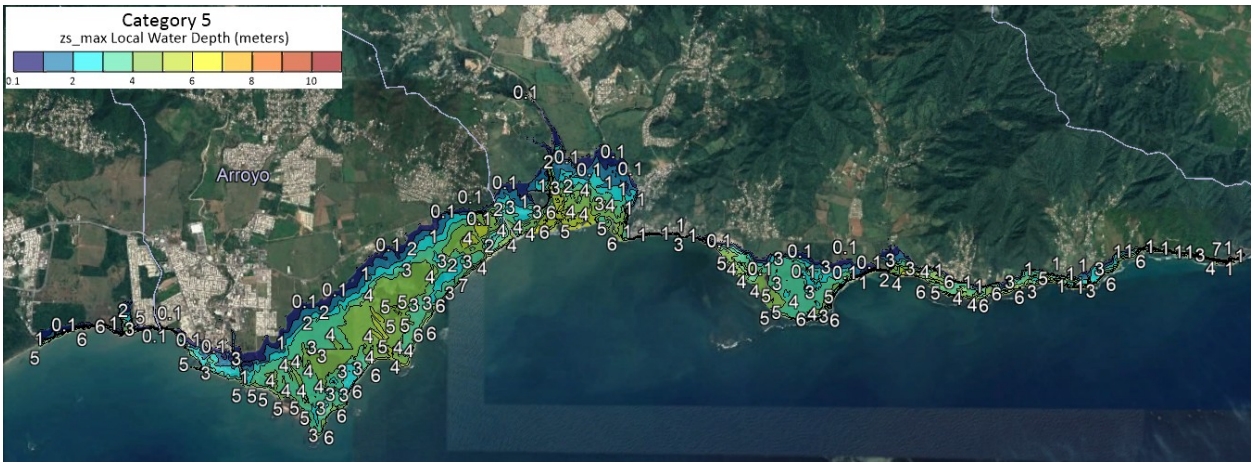

Figure 210 - Grid 16, category 5, maximum sea surface elevation (meters), relative to local terrain elevation, during 1 hour of simulation after spin up of 300 seconds.

GRID 17: CAT 1

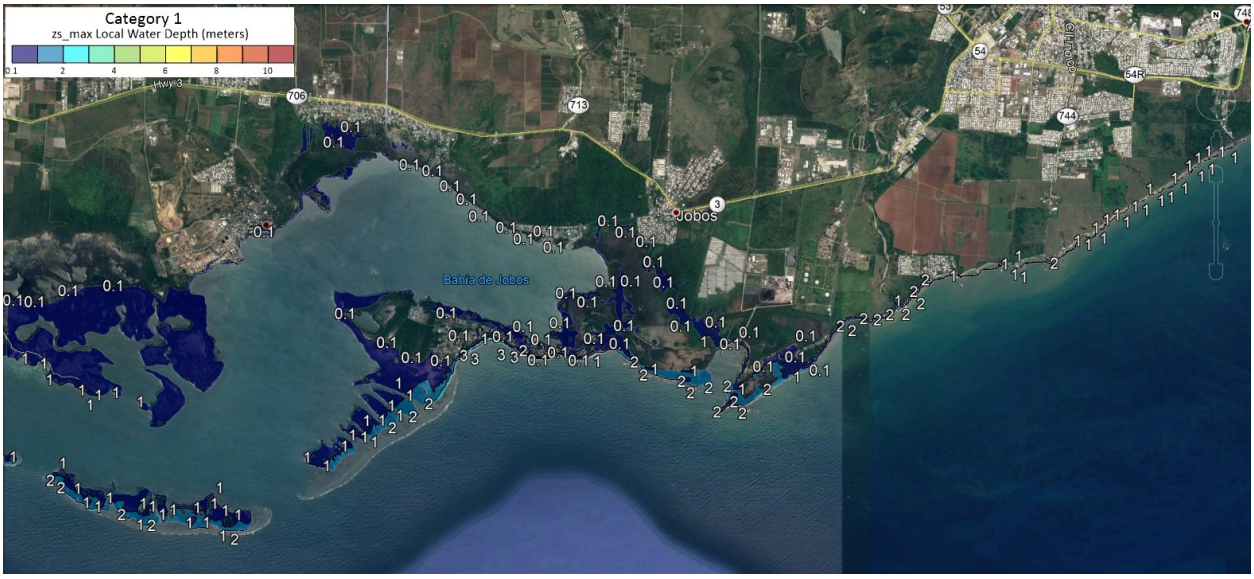

Figure 211 - Grid 17, category 1, maximum sea surface elevation (meters), relative to local terrain elevation, during 1 hour of simulation after spin up of 300 seconds.

GRID 17: CAT 2

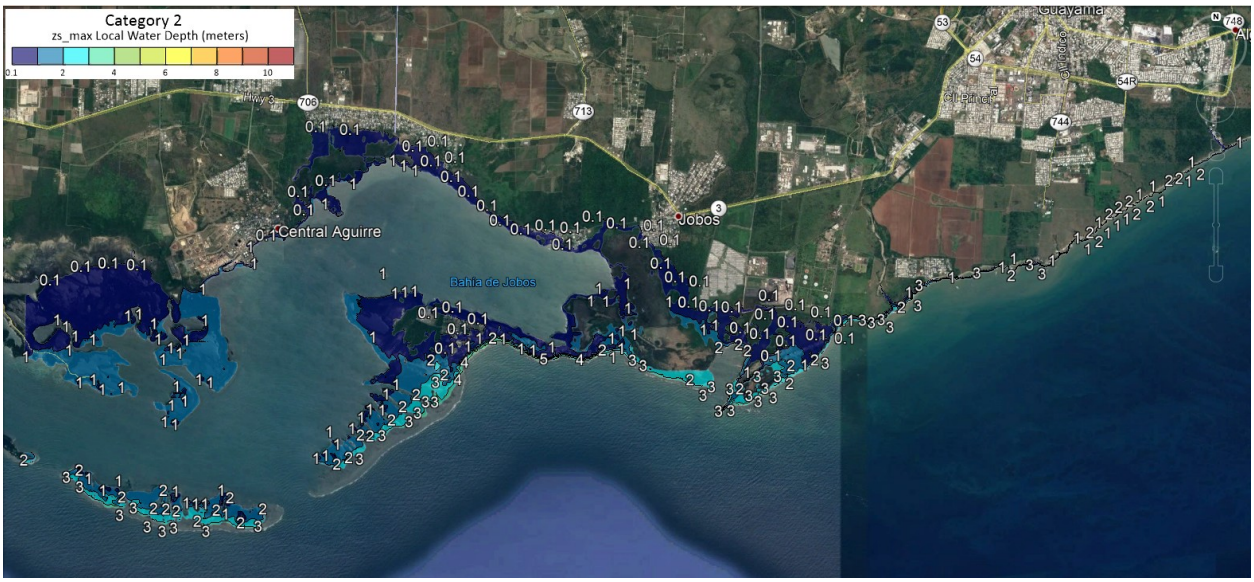

Figure 212 - Grid 17, category 2, maximum sea surface elevation (meters), relative to local terrain elevation, during 1 hour of simulation after spin up of 300 seconds.

GRID 17: CAT 3

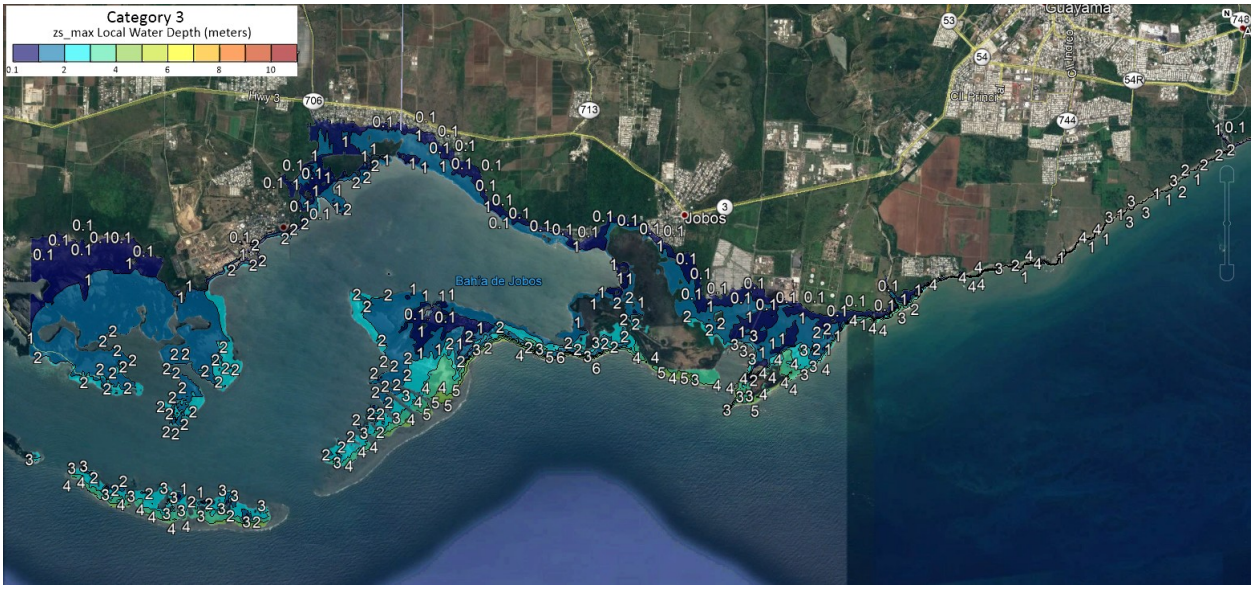

Figure 213- Grid 17, category 3, maximum sea surface elevation (meters), relative to local terrain elevation, during 1 hour of simulation after spin up of 300 seconds.

GRID 17: CAT 4

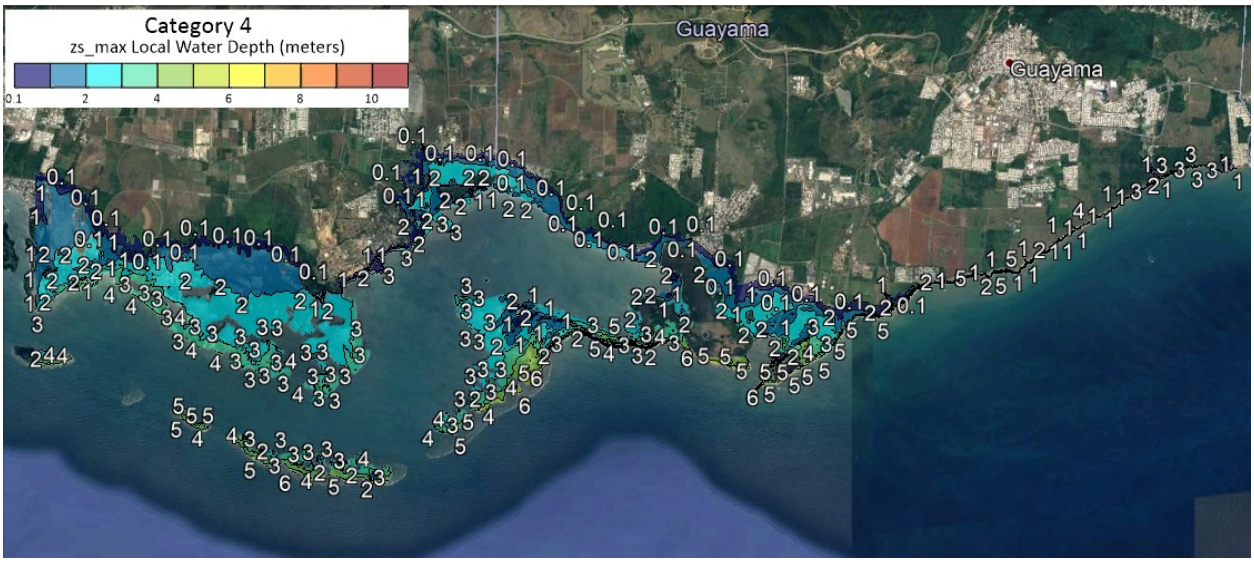

Figure 214- Grid 17, category 4, maximum sea surface elevation (meters), relative to local terrain elevation, during 1 hour of simulation after spin up of 300 seconds.

GRID 17: CAT 5

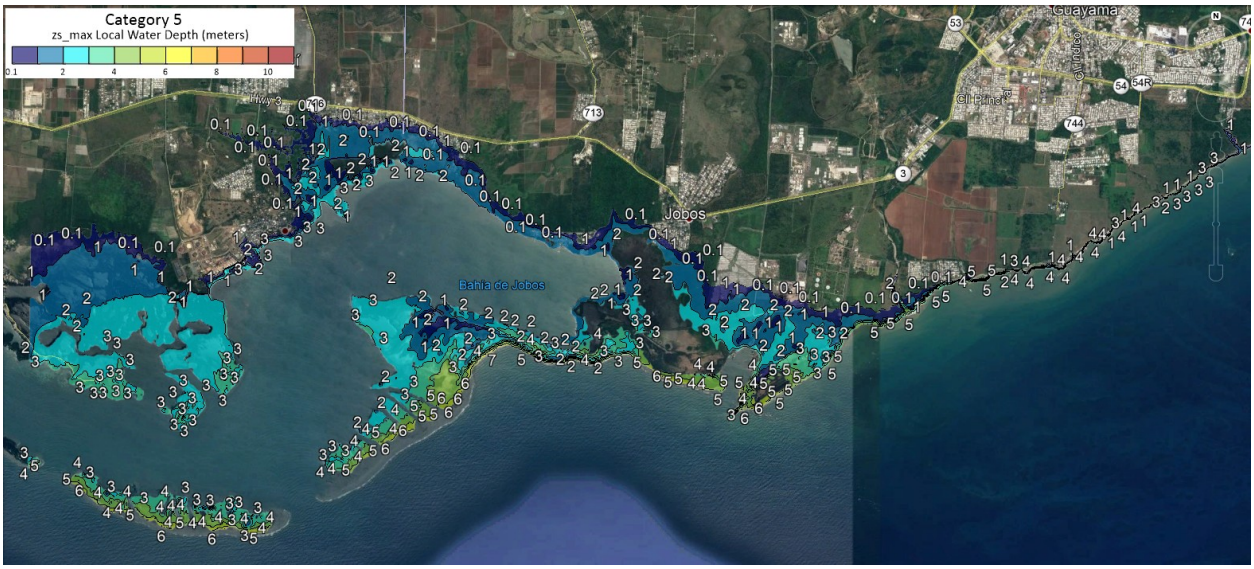

Figure 215 - Grid 17, category 5, maximum sea surface elevation (meters), relative to local terrain elevation, during 1 hour of simulation after spin up of 300 seconds.

GRID 18: CAT 1

Figure 216 - Grid 18, category 1, maximum sea surface elevation (meters), relative to local terrain elevation, during 1 hour of simulation after spin up of 300 seconds.

GRID 18: CAT 2

Figure 217 - Grid 18, category 2, maximum sea surface elevation (meters), relative to local terrain elevation, during 1 hour of simulation after spin up of 300 seconds.

GRID 18: CAT 3

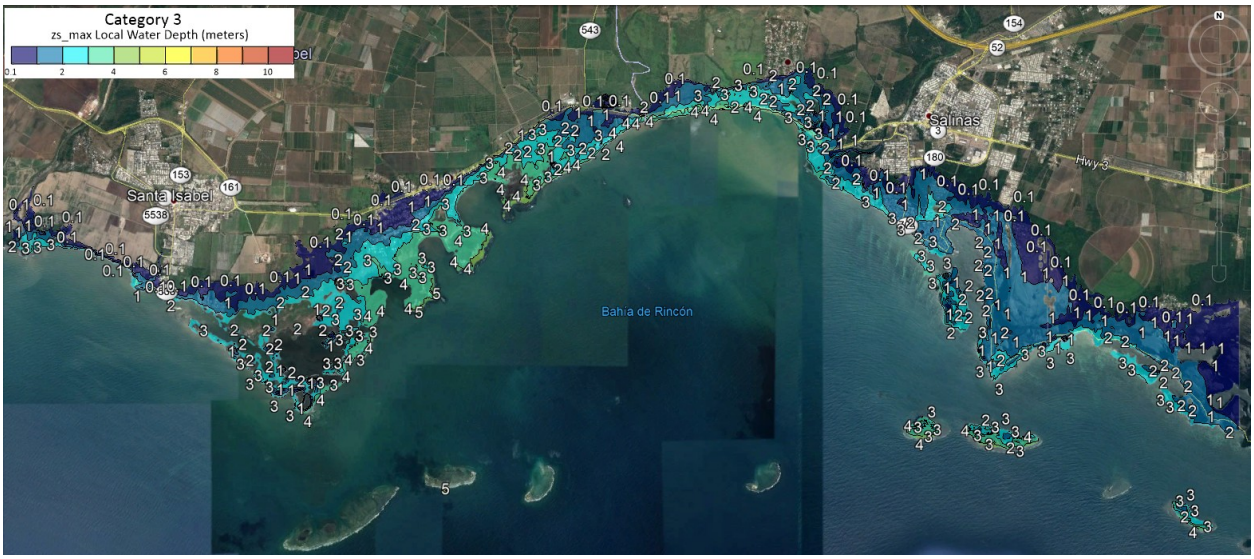

Figure 218 - Grid 18, category 3, maximum sea surface elevation (meters), relative to local terrain elevation, during 1 hour of simulation after spin up of 300 seconds.

GRID 18: CAT 4

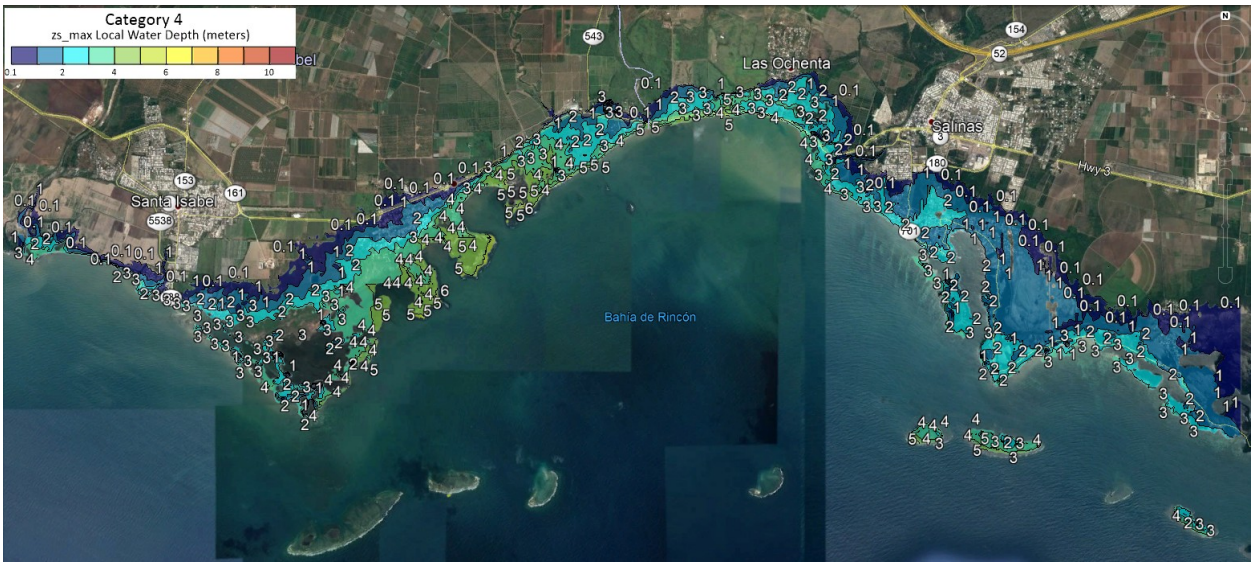

Figure 219 - Grid 18, category 4, maximum sea surface elevation (meters), relative to local terrain elevation, during 1 hour of simulation after spin up of 300 seconds.

GRID 18: CAT 5

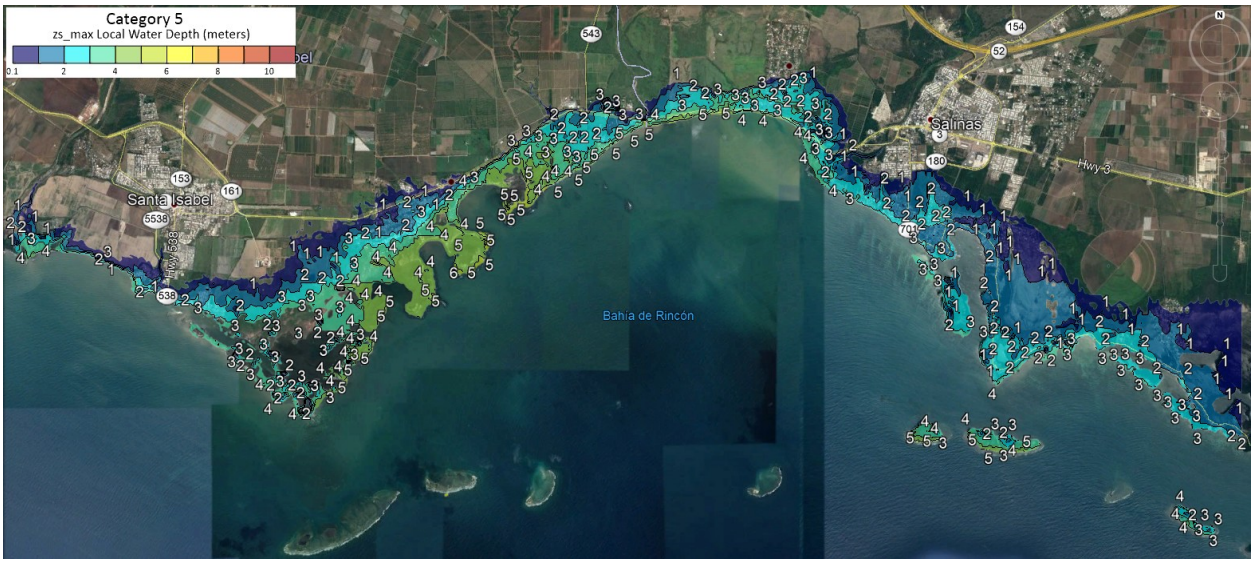

Figure 220 - Grid 18, category 5, maximum sea surface elevation (meters), relative to local terrain elevation, during 1 hour of simulation after spin up of 300 seconds.

GRID 19: CAT 1

Figure 221 - Grid 19, category 1, maximum sea surface elevation (meters), relative to local terrain elevation, during 1 hour of simulation after spin up of 300 seconds. Isla Caja de Muertos is shown as a separate image.

GRID 19: CAT 1

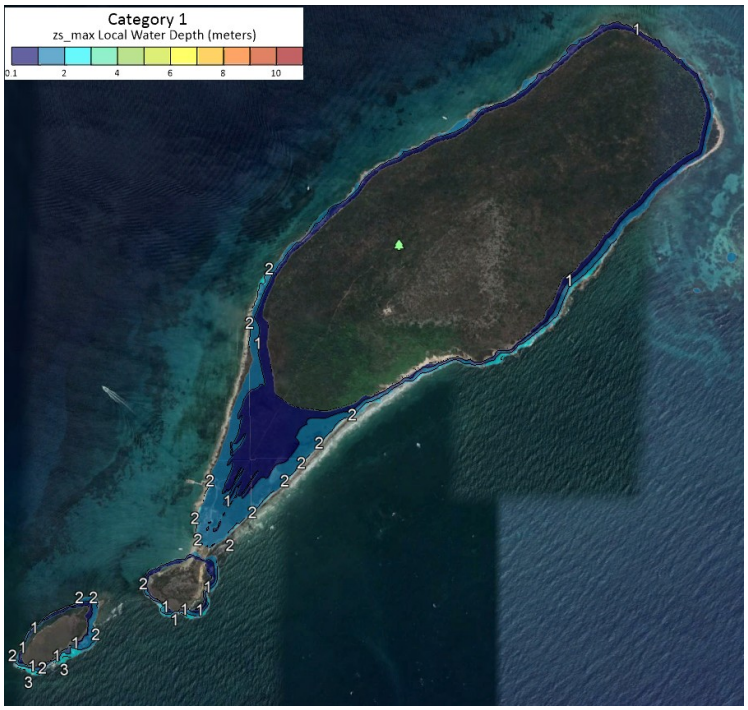

Figure 222 – Isla Caja de Muertos. Grid 19, category 1, maximum sea surface elevation (meters), relative to local terrain elevation, during 1 hour of simulation after spin up of 300 seconds.

GRID 19: CAT 2

Figure 223 - Grid 19, category 2, maximum sea surface elevation (meters), relative to local terrain elevation, during 1 hour of simulation after spin up of 300 seconds. Isla Caja de Muertos is shown as a separate image.

GRID 19: CAT 2

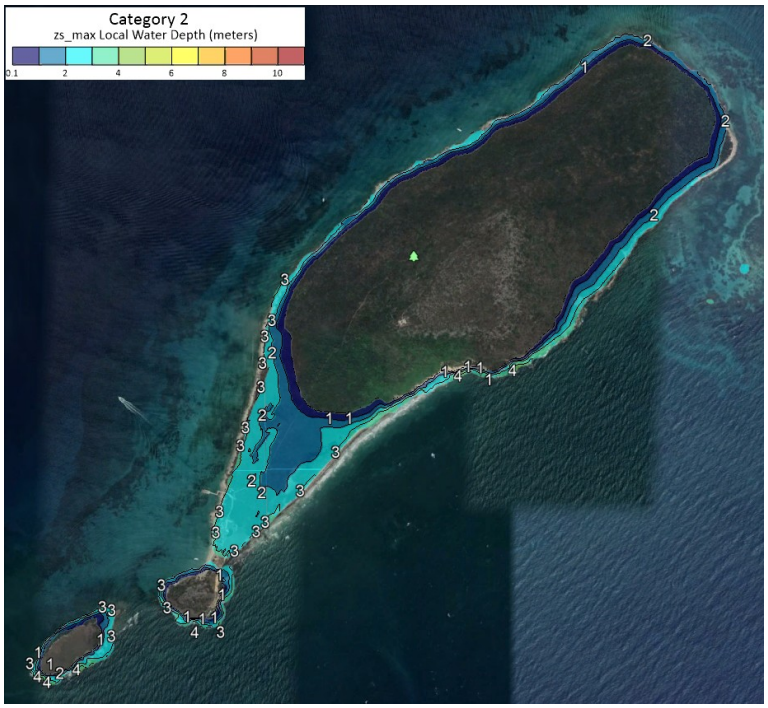

Figure 224 – Isla Caja de Muertos. Grid 19, category 2, maximum sea surface elevation (meters), relative to local terrain elevation, during 1 hour of simulation after spin up of 300 seconds.

GRID 19: CAT 3

Figure 225 - Grid 19, category 3, maximum sea surface elevation (meters), relative to local terrain elevation, during 1 hour of simulation after spin up of 300 seconds. Isla Caja de Muertos is shown as a separate image.

GRID 19: CAT 3

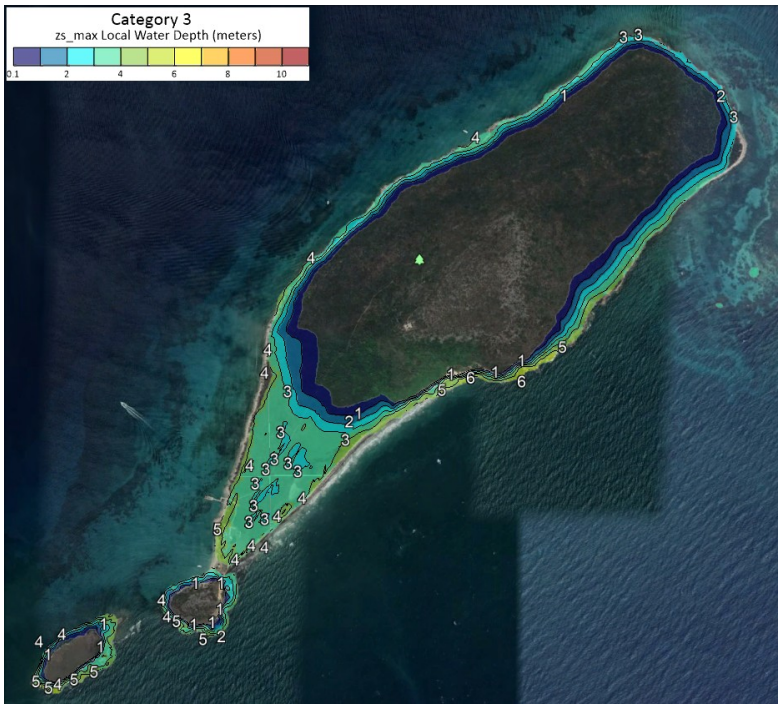

Figure 226 – Isla Caja de Muertos. Grid 19, category 3, maximum sea surface elevation (meters), relative to local terrain elevation, during 1 hour of simulation after spin up of 300 seconds.

GRID 19: CAT 4

Figure 227 - Grid 19, category 4, maximum sea surface elevation (meters), relative to local terrain elevation, during 1 hour of simulation after spin up of 300 seconds. Isla Caja de Muertos is shown as a separate image.

GRID 19: CAT 4

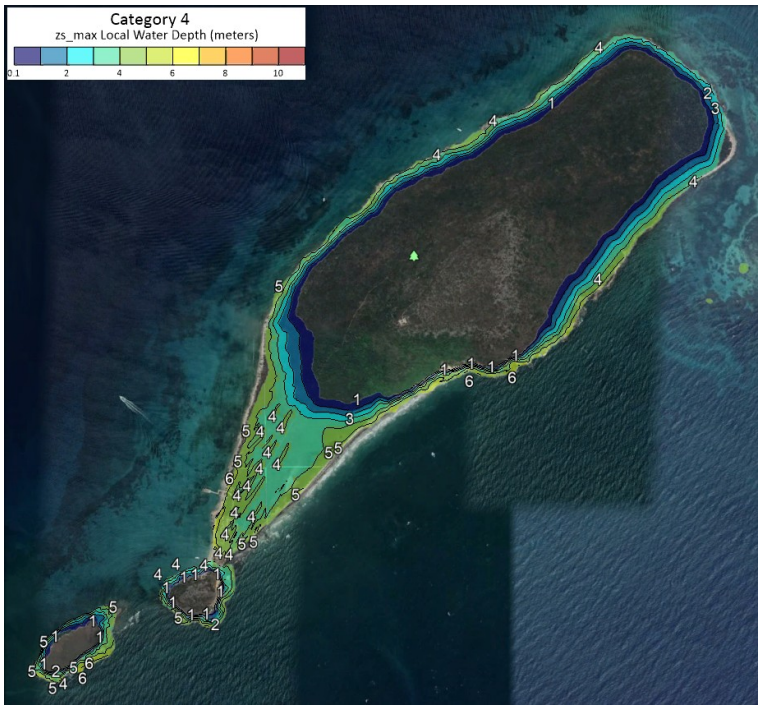

Figure 228 – Isla Caja de Muertos. Grid 19, category 4, maximum sea surface elevation (meters), relative to local terrain elevation, during 1 hour of simulation after spin up of 300 seconds.

GRID 19: CAT 5

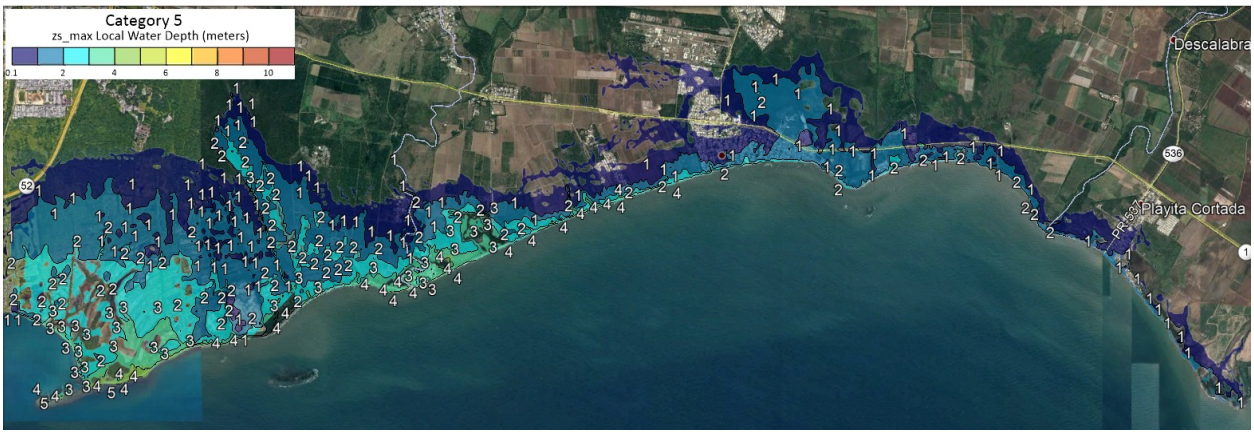

Figure 229 - Grid 19, category 5, maximum sea surface elevation (meters), relative to local terrain elevation, during 1 hour of simulation after spin up of 300 seconds. Isla Caja de Muertos is shown as a separate image.

GRID 19: CAT 5

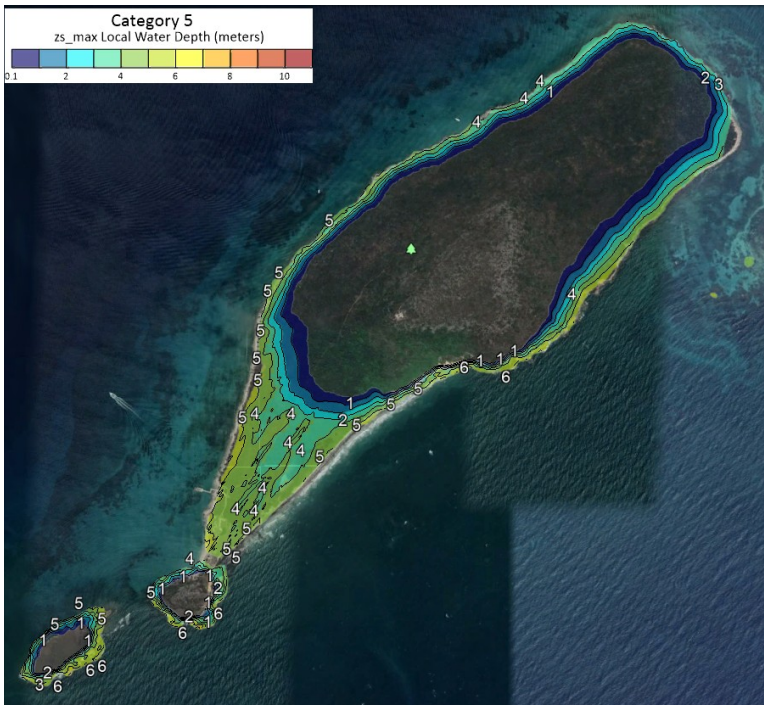

Figure 230 – Isla Caja de Muertos. Grid 19, category 5, maximum sea surface elevation (meters), relative to local terrain elevation, during 1 hour of simulation after spin up of 300 seconds.

GRID 20: CAT 1

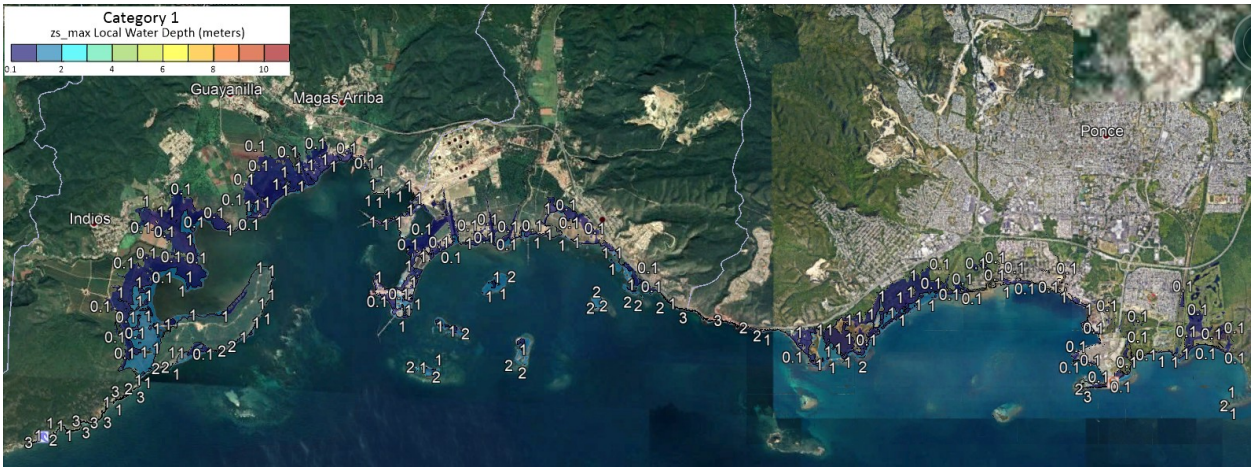

Figure 231 - Grid 20, category 1, maximum sea surface elevation (meters), relative to local terrain elevation, during 1 hour of simulation after spin up of 300 seconds.

GRID 20: CAT 2

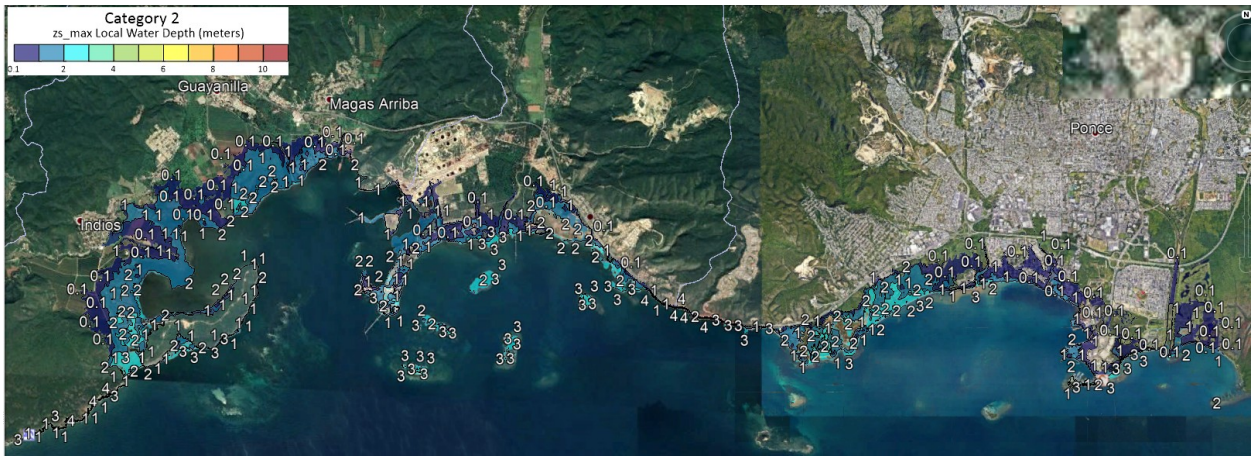

Figure 232 - Grid 20, category 2, maximum sea surface elevation (meters), relative to local terrain elevation, during 1 hour of simulation after spin up of 300 seconds.

GRID 20: CAT 3

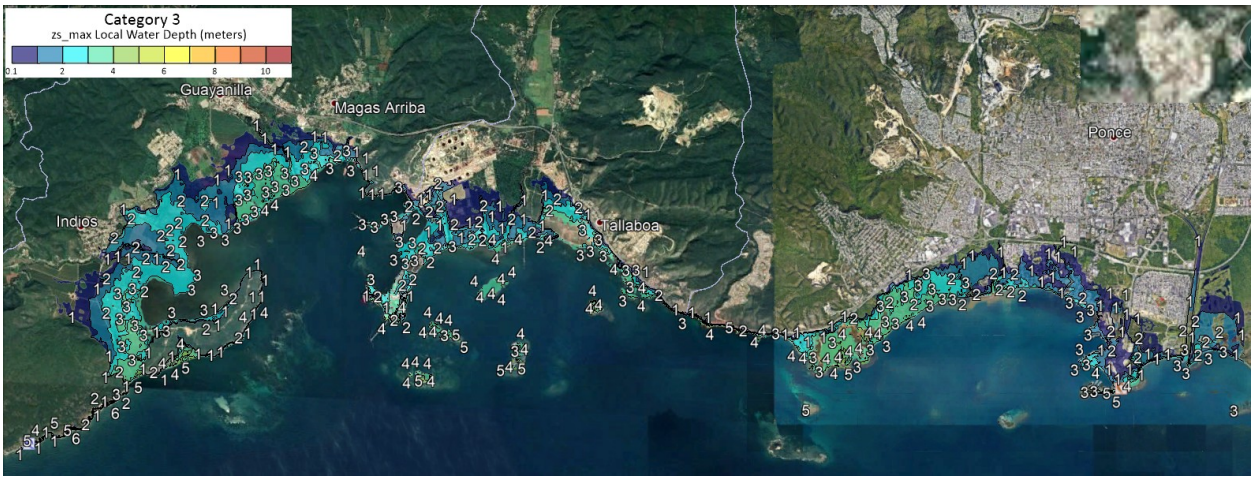

Figure 233 - Grid 20, category 3, maximum sea surface elevation (meters), relative to local terrain elevation, during 1 hour of simulation after spin up of 300 seconds.

GRID 20: CAT 4

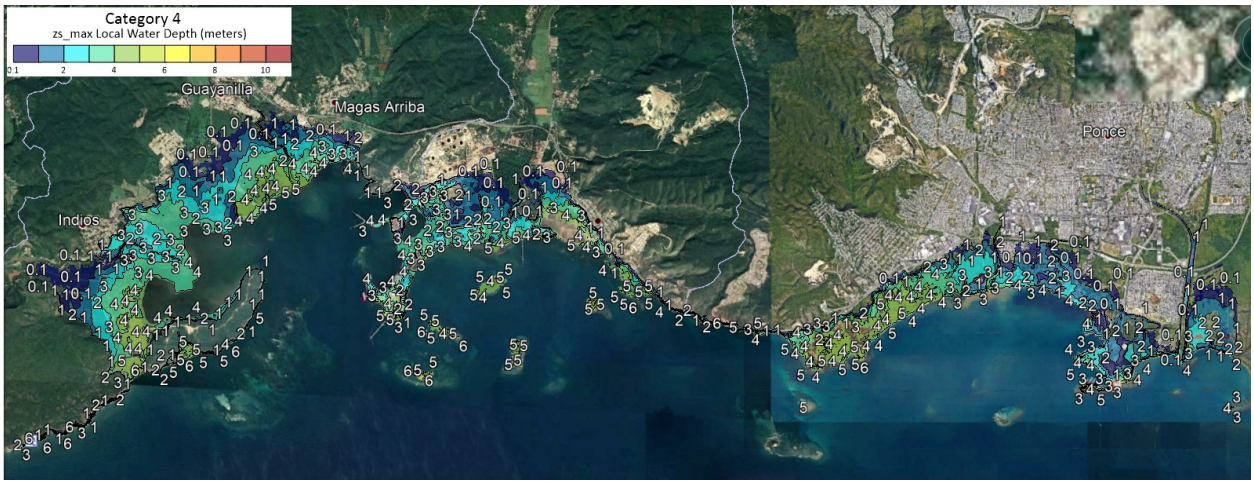

Figure 234 - Grid 20, category 4, maximum sea surface elevation (meters), relative to local terrain elevation, during 1 hour of simulation after spin up of 300 seconds.

GRID 20: 5

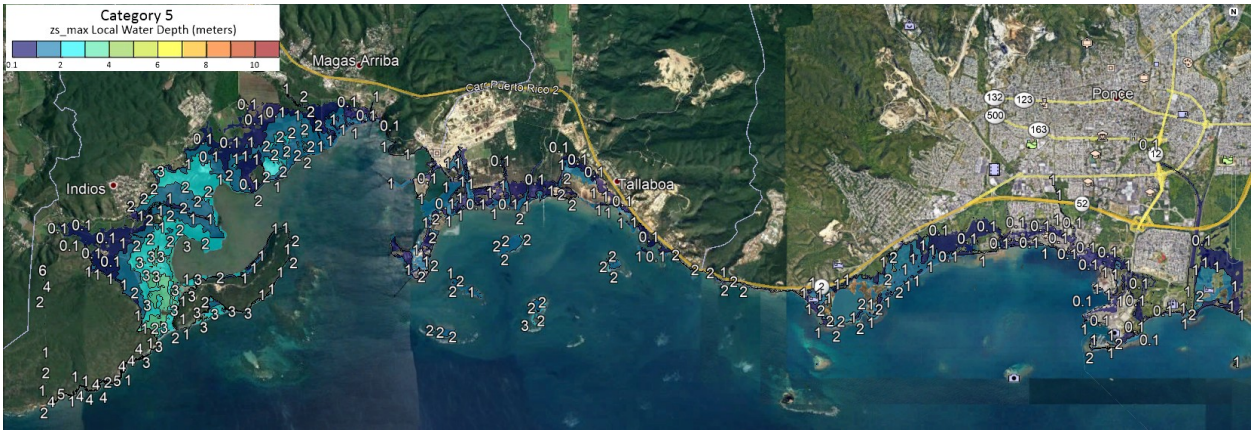

Figure 235 - Grid 20, category 1, maximum sea surface elevation (meters), relative to local terrain elevation, during 1 hour of simulation after spin up of 300 seconds.

GRID 21: CAT 1

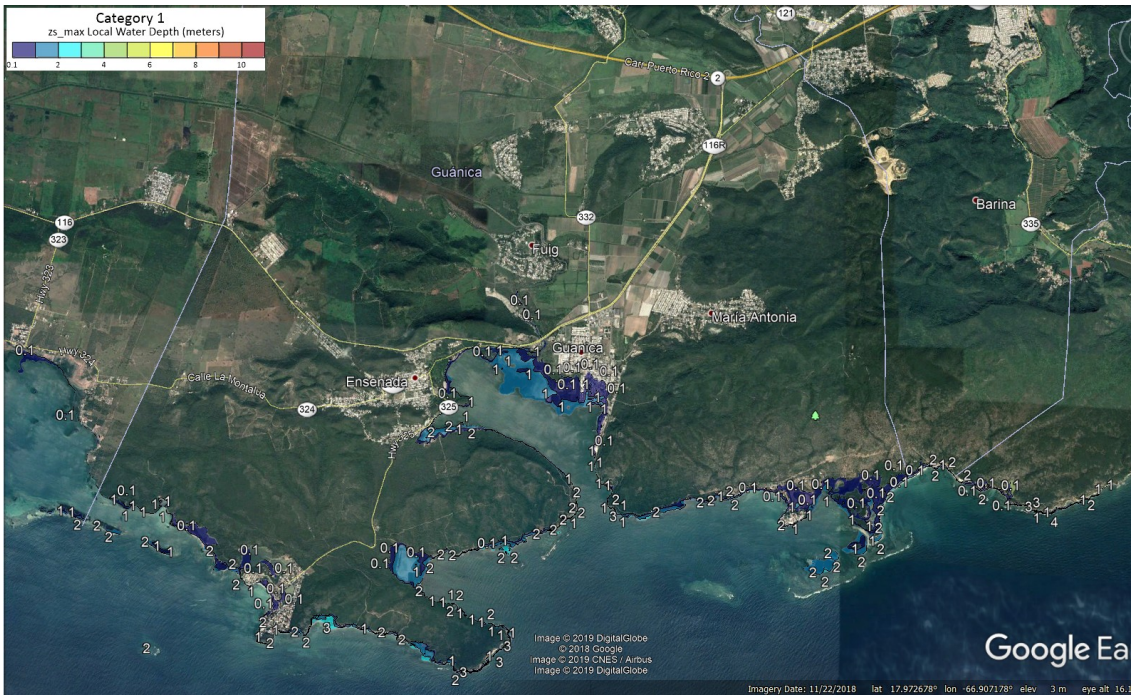

Figure 236 - Grid 21, category 1, maximum sea surface elevation (meters), relative to local terrain elevation, during 1 hour of simulation after spin up of 300 seconds.

GRID 21: CAT 2

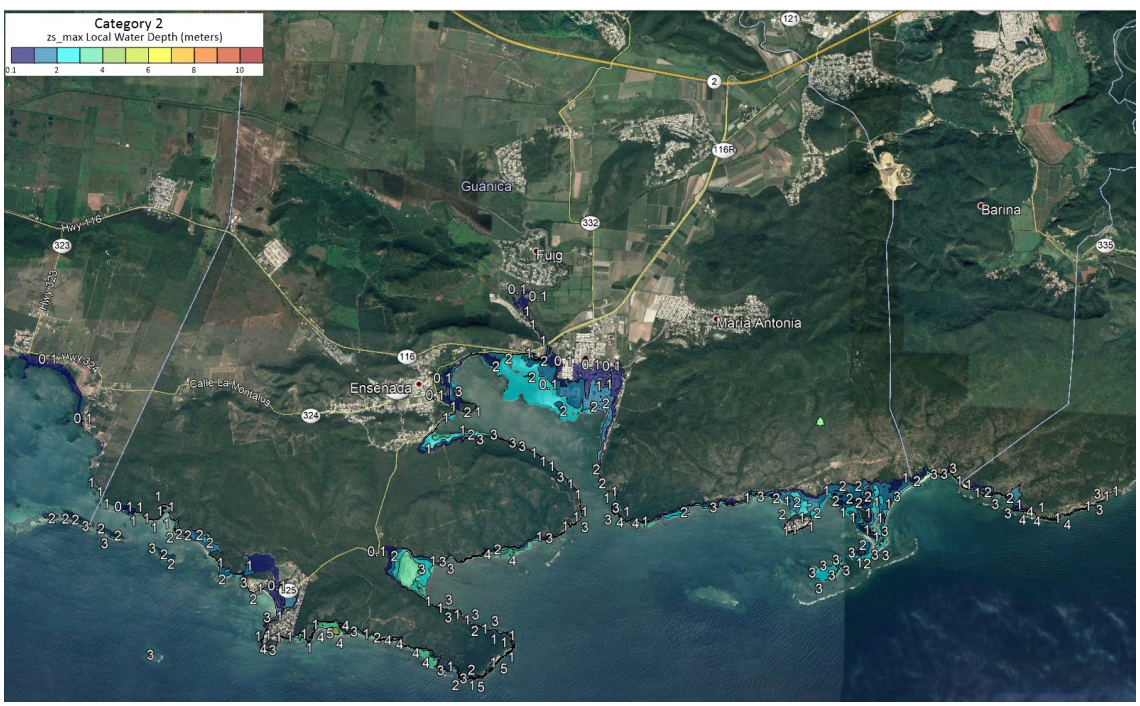

Figure 237 - Grid 21, category 2, maximum sea surface elevation (meters), relative to local terrain elevation, during 1 hour of simulation after spin up of 300 seconds.

GRID 21: CAT 3

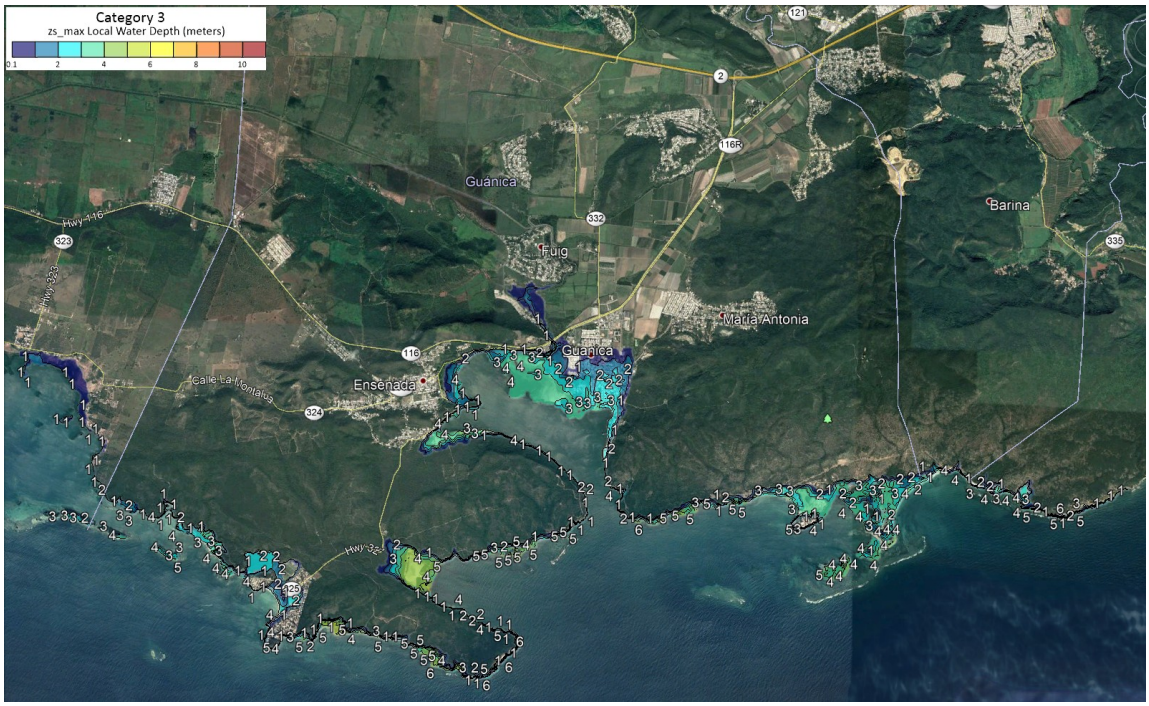

Figure 238 - Grid 21, category 3, maximum sea surface elevation (meters), relative to local terrain elevation, during 1 hour of simulation after spin up of 300 seconds.

GRID 21: CAT 4

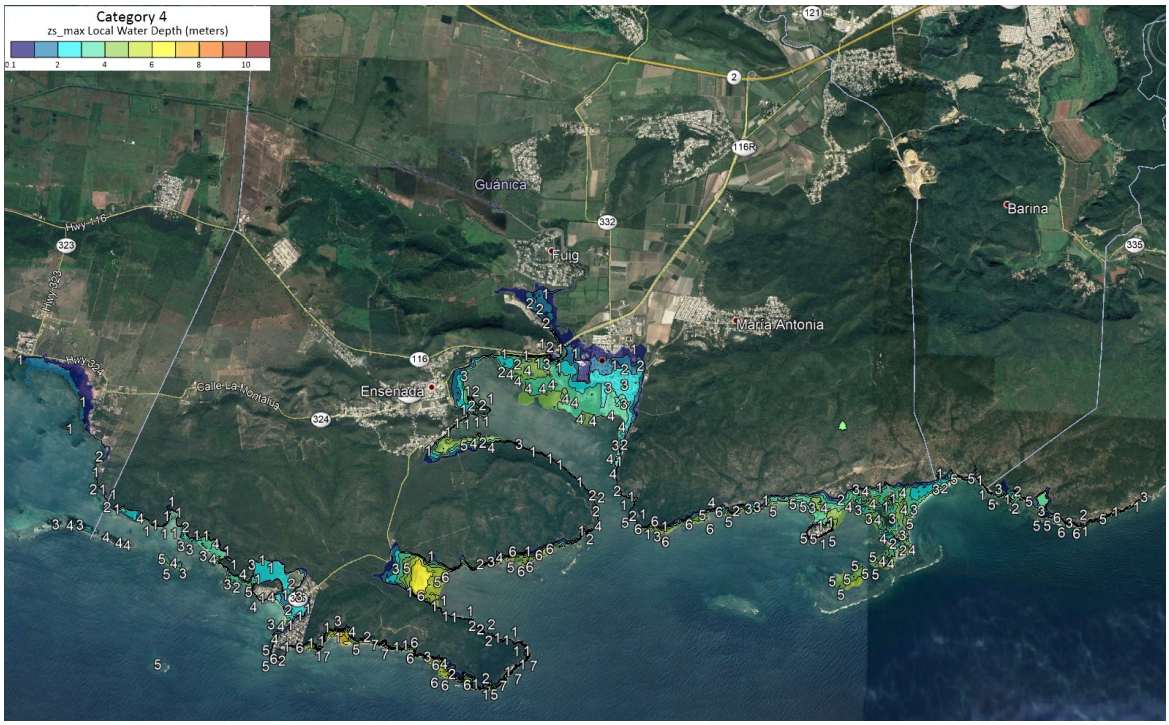

Figure 239 - Grid 21, category 4, maximum sea surface elevation (meters), relative to local terrain elevation, during 1 hour of simulation after spin up of 300 seconds.

GRID 21: CAT 5

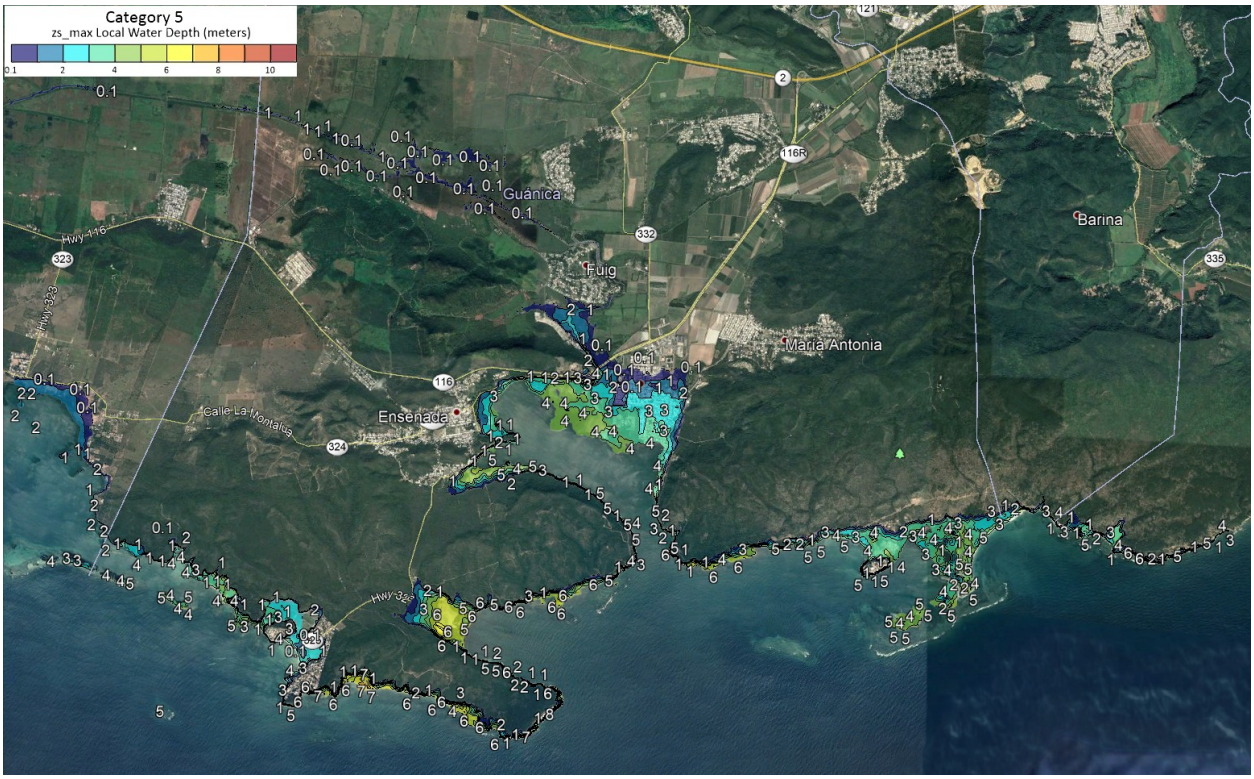

Figure 240 - Grid 21, category 5, maximum sea surface elevation (meters), relative to local terrain elevation, during 1 hour of simulation after spin up of 300 seconds.

GRID 22: CAT 1 (LAJAS TO CABO ROJO)

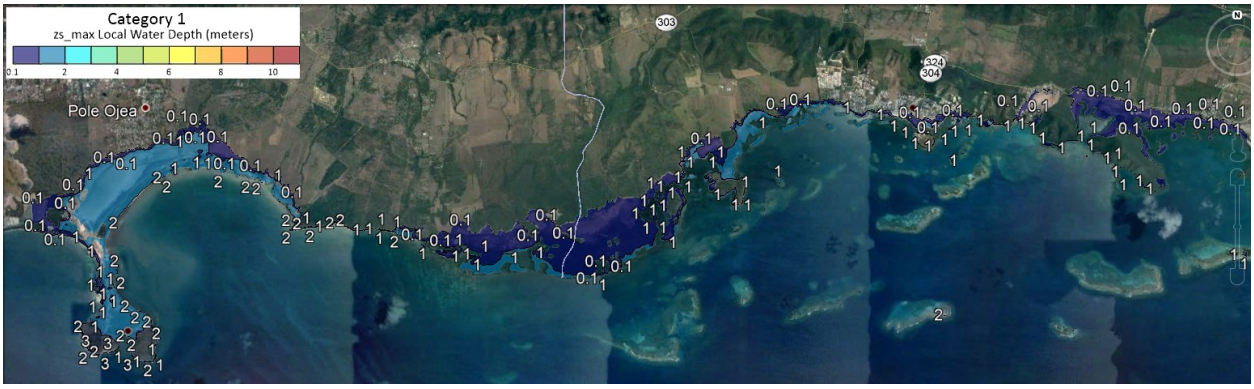

Figure 241 - Grid 22, category 1, maximum sea surface elevation (meters), relative to local terrain elevation, during 1 hour of simulation after spin up of 300 seconds. Waves propagating from the south.

GRID 22: CAT 2 (LAJAS TO CABO ROJO)

Figure 242 - Grid 22, category 2, maximum sea surface elevation (meters), relative to local terrain elevation, during 1 hour of simulation after spin up of 300 seconds. Waves propagating from the south.

GRID 22: CAT 3 (LAJAS TO CABO ROJO)

Figure 243 - Grid 22, category 3, maximum sea surface elevation (meters), relative to local terrain elevation, during 1 hour of simulation after spin up of 300 seconds. Waves propagating from the south.

GRID 22: CAT 4 (LAJAS TO CABO ROJO)

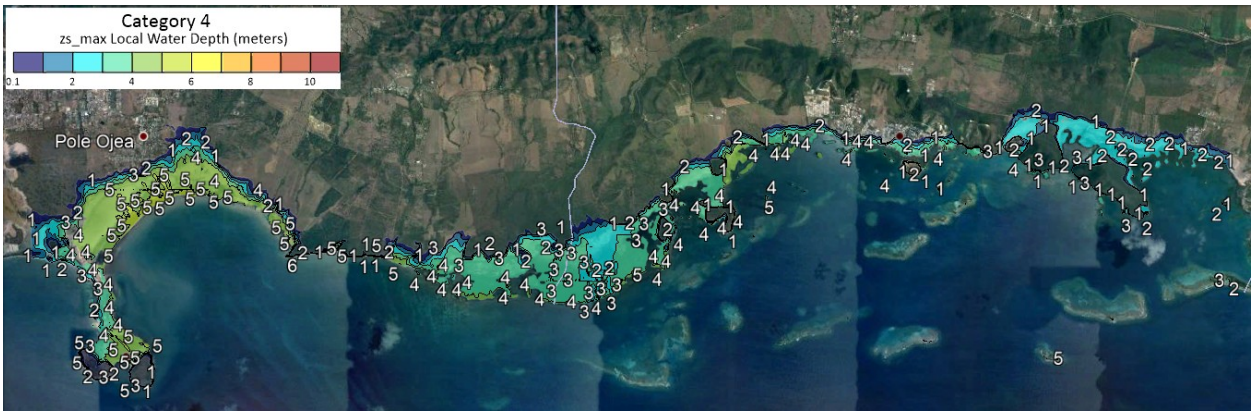

Figure 244 - Grid 22, category 4, maximum sea surface elevation (meters), relative to local terrain elevation, during 1 hour of simulation after spin up of 300 seconds. Waves propagating from the south.

GRID 22: CAT 5 (LAJAS TO CABO ROJO)

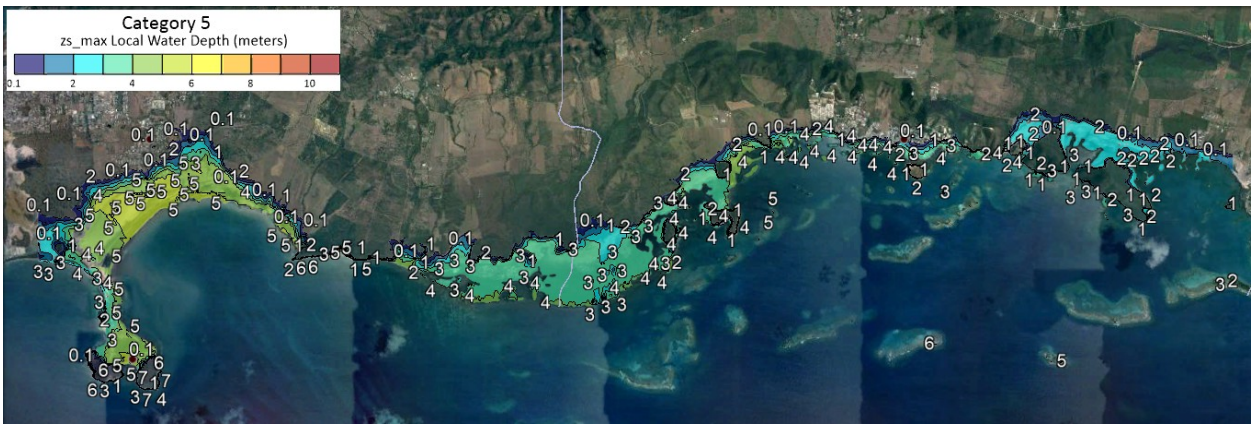

Figure 245 - Grid 22, category 5, maximum sea surface elevation (meters), relative to local terrain elevation, during 1 hour of simulation after spin up of 300 seconds. Waves propagating from the south.

GRID 23: CAT 1 (CABO ROJO)

Figure 246 - Grid 23, category 1, maximum sea surface elevation (meters), relative to local terrain elevation, during 1 hour of simulation after spin up of 300 seconds. Waves propagating from the west.

GRID 23: CAT 2 (CABO ROJO)

Figure 247 - Grid 23, category 2, maximum sea surface elevation (meters), relative to local terrain elevation, during 1 hour of simulation after spin up of 300 seconds. Waves propagating from the west.

GRID 23: CAT 3 (CABO ROJO)

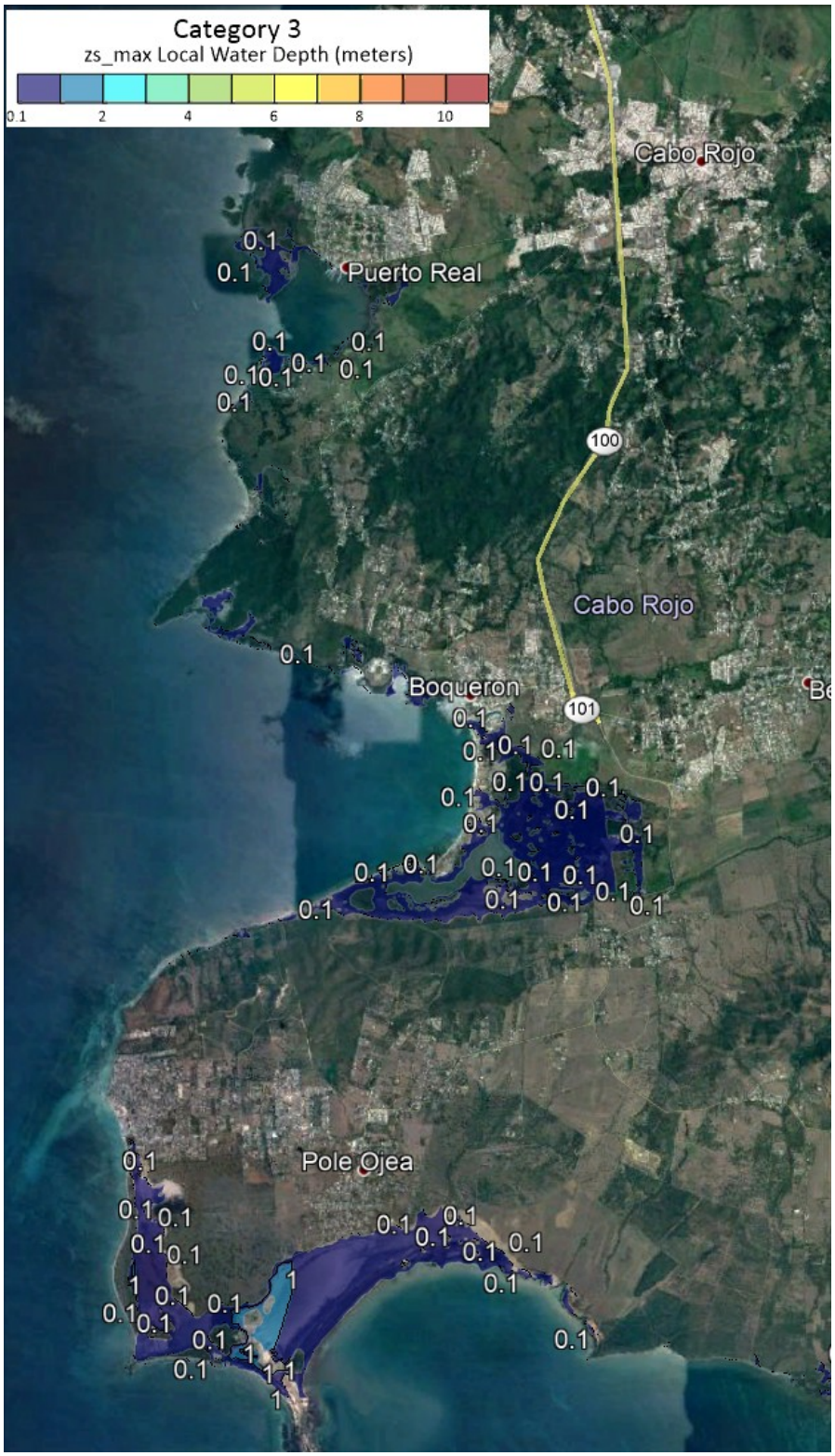

Figure 248 - Grid 23, category 3, maximum sea surface elevation (meters), relative to local terrain elevation, during 1 hour of simulation after spin up of 300 seconds. Waves propagating from the west.

GRID 23: CAT 4 (CABO ROJO)

Figure 249 - Grid 23, category 4, maximum sea surface elevation (meters), relative to local terrain elevation, during 1 hour of simulation after spin up of 300 seconds. Waves propagating from the west.

GRID 23: CAT 5 (CABO ROJO)

Figure 250 - Grid 23, category 5, maximum sea surface elevation (meters), relative to local terrain elevation, during 1 hour of simulation after spin up of 300 seconds. Waves propagating from the west.

GRID 24: CAT 1 (CABO ROJO TO MAYAGUEZ)

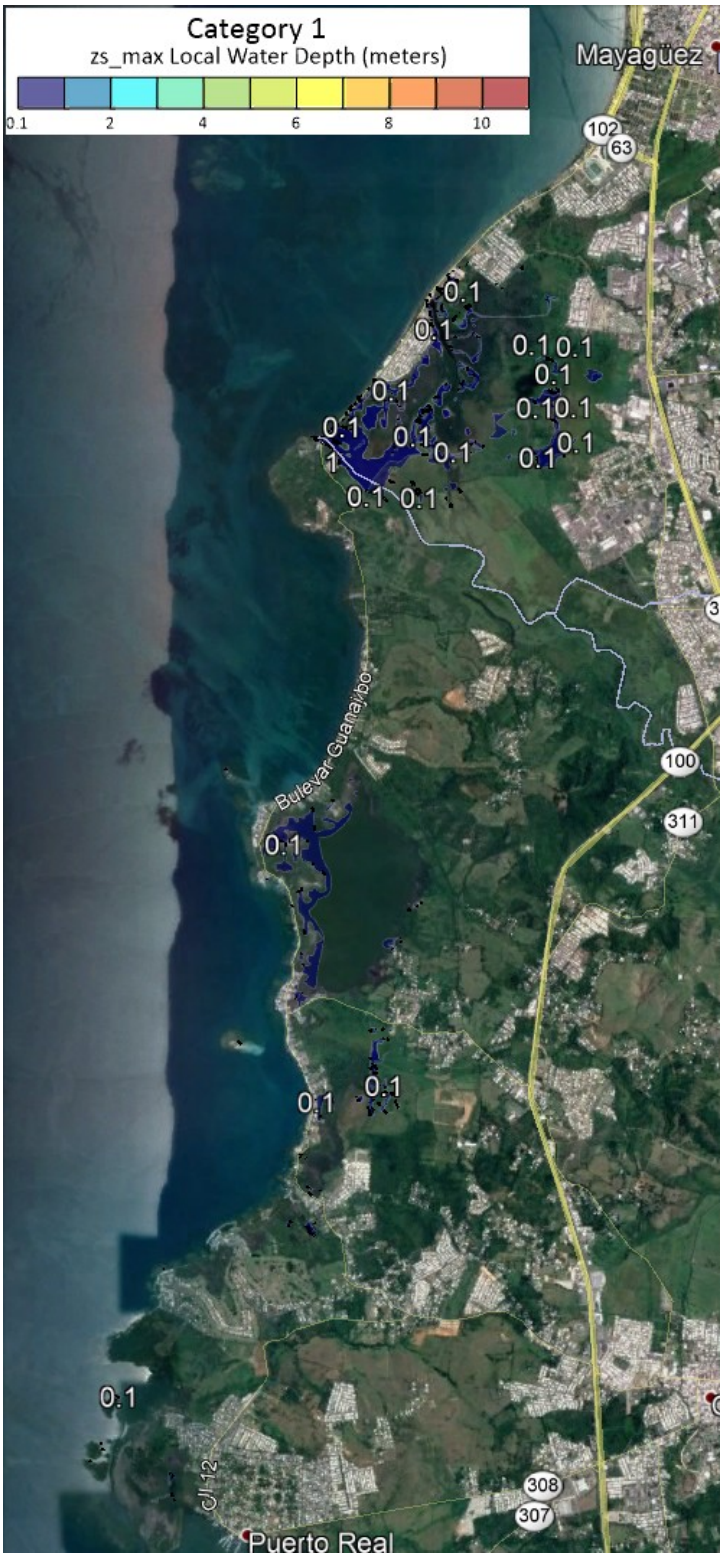

Figure 251 - Grid 24, category 1, maximum sea surface elevation (meters), relative to local terrain elevation, during 1 hour of simulation after spin up of 300 seconds. Waves propagating from the west.

GRID 24: CAT 2 (CABO ROJO TO MAYAGUEZ)

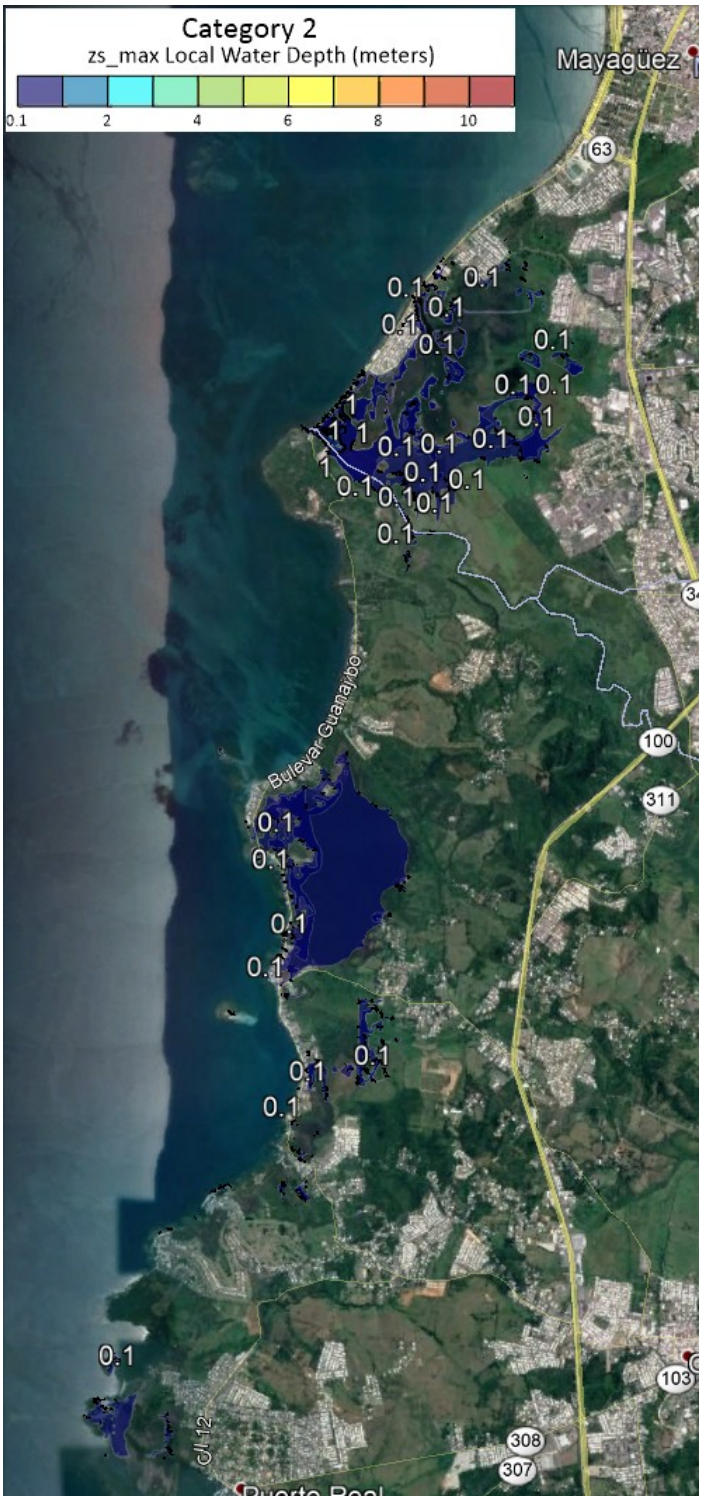

Figure 252 - Grid 24, category 2, maximum sea surface elevation (meters), relative to local terrain elevation, during 1 hour of simulation after spin up of 300 seconds. Waves propagating from the west.

GRID 24: CAT 3 (CABO ROJO TO MAYAGUEZ)

Figure 253 - Grid 24, category 3, maximum sea surface elevation (meters), relative to local terrain elevation, during 1 hour of simulation after spin up of 300 seconds. Waves propagating from the west.

GRID 24: CAT 4 (CABO ROJO TO MAYAGUEZ)

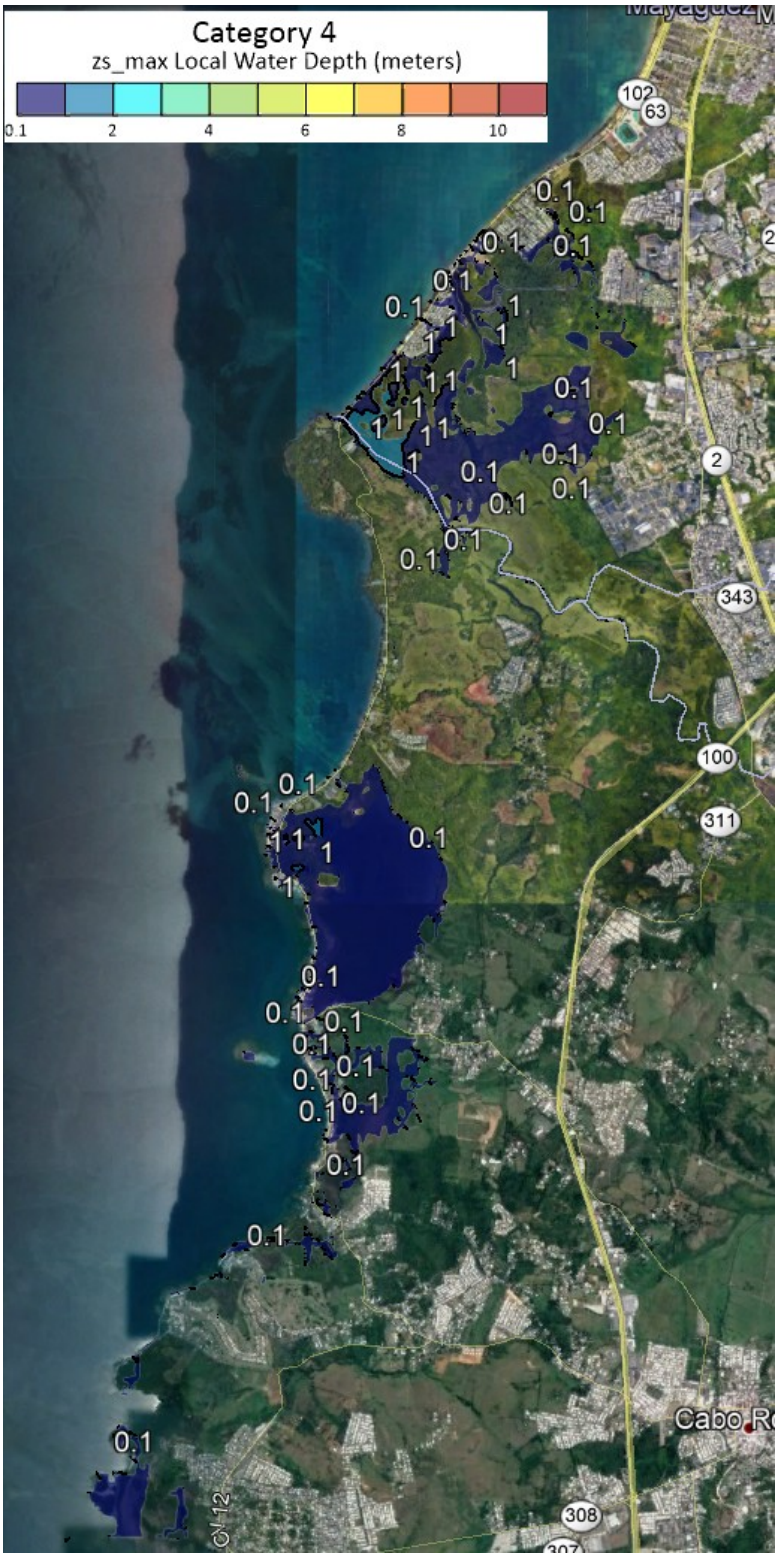

Figure 254 - Grid 24, category 4, maximum sea surface elevation (meters), relative to local terrain elevation, during 1 hour of simulation after spin up of 300 seconds. Waves propagating from the west.

GRID 24: CAT 5 (CABO ROJO TO MAYAGUEZ)

Figure 255 - Grid 24, category 5, maximum sea surface elevation (meters), relative to local terrain elevation, during 1 hour of simulation after spin up of 300 seconds. Waves propagating from the west.

GRID 25: CAT 1 (MAYAGUEZ TO RINCON)

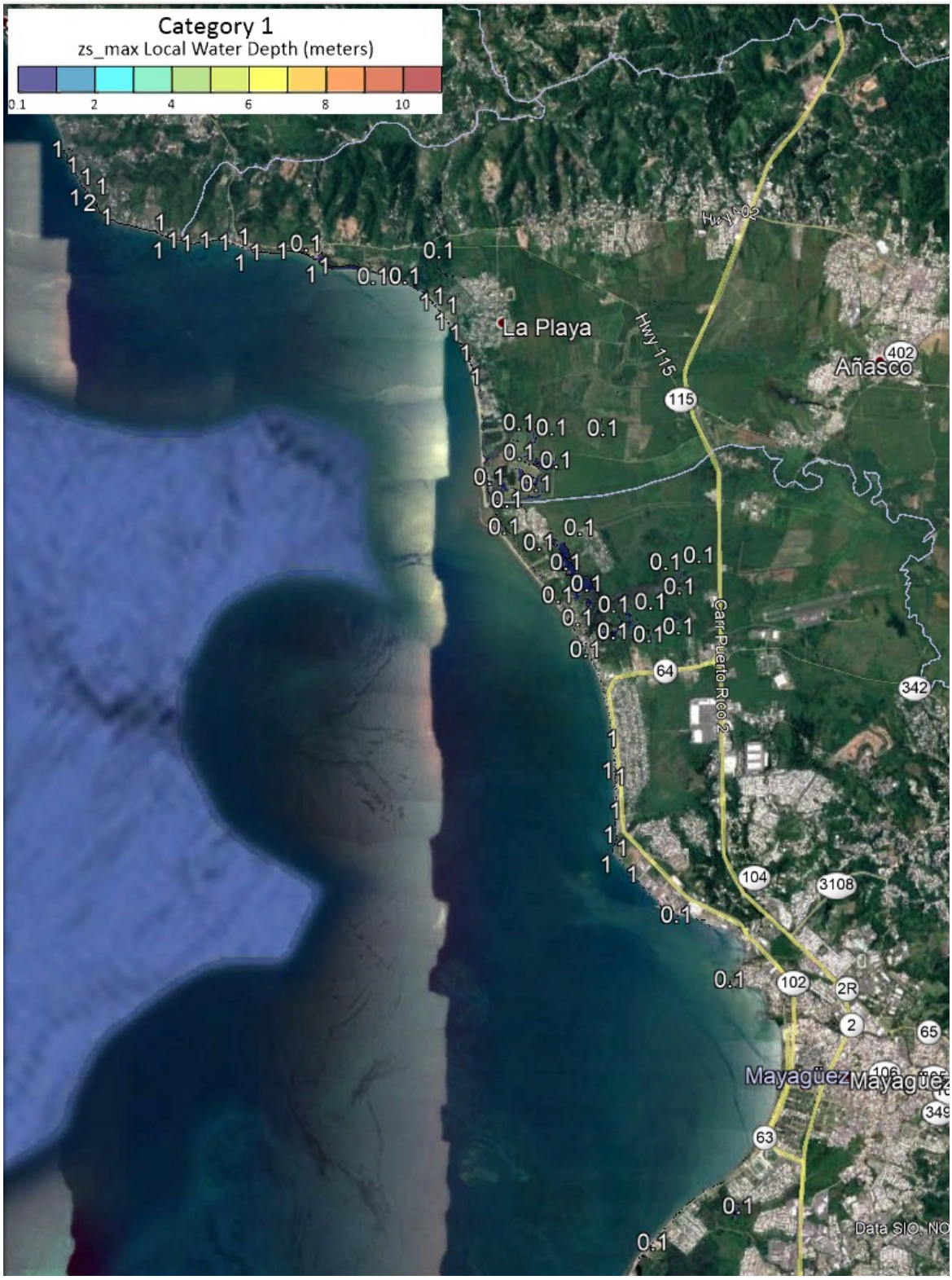

Figure 256 - Grid 25, category 1, maximum sea surface elevation (meters), relative to local terrain elevation, during 1 hour of simulation after spin up of 300 seconds. Waves propagating from the west.

GRID 25: CAT 2 (MAYAGUEZ TO RINCON)

Figure 257 - Grid 25, category 2, maximum sea surface elevation (meters), relative to local terrain elevation, during 1 hour of simulation after spin up of 300 seconds. Waves propagating from the west.

GRID 25: CAT 3 (MAYAGUEZ TO RINCON)

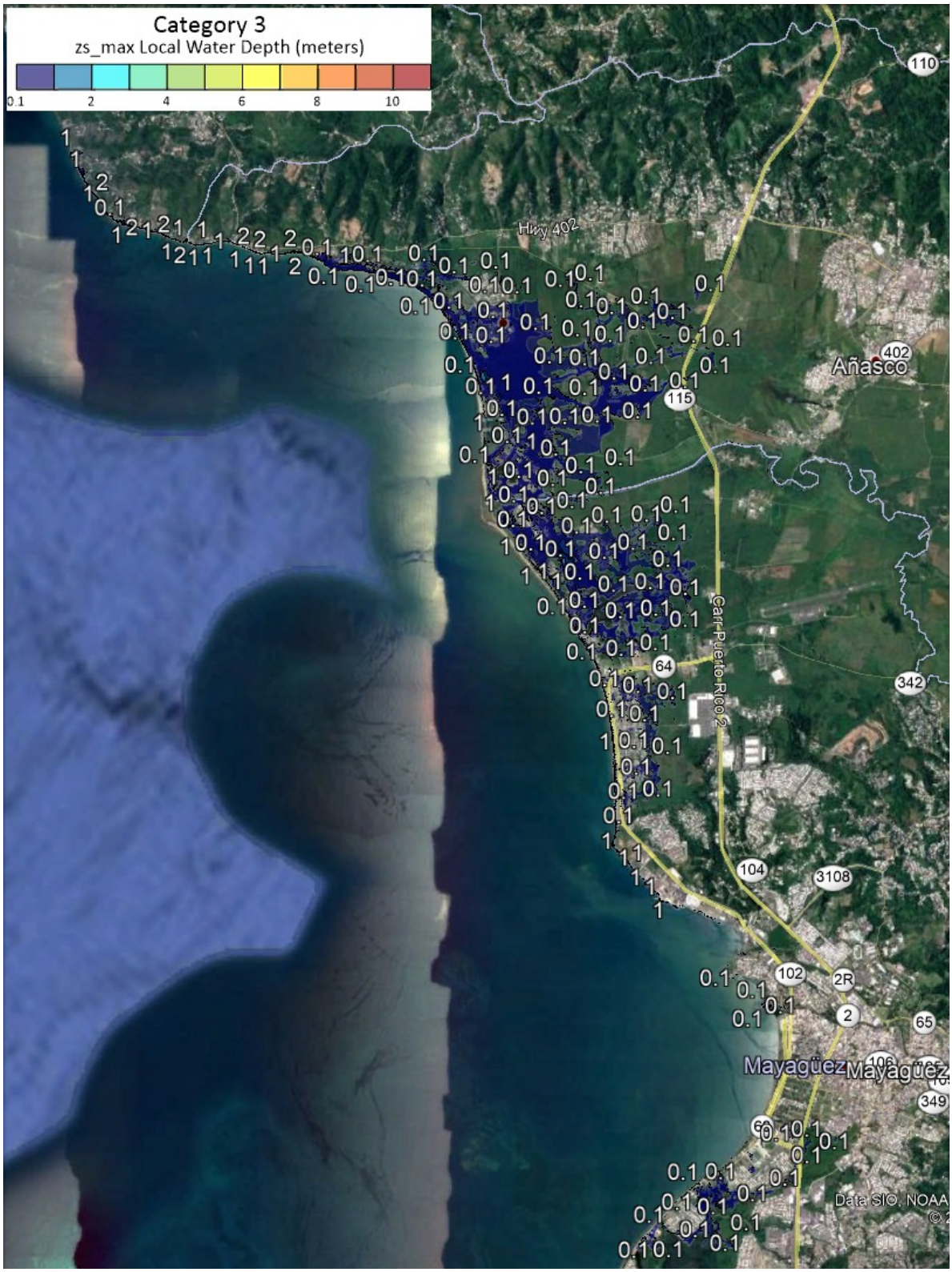

Figure 258 - Grid 25, category 3, maximum sea surface elevation (meters), relative to local terrain elevation, during 1 hour of simulation after spin up of 300 seconds. Waves propagating from the west.

GRID 25: CAT 4 (MAYAGUEZ TO RINCON)

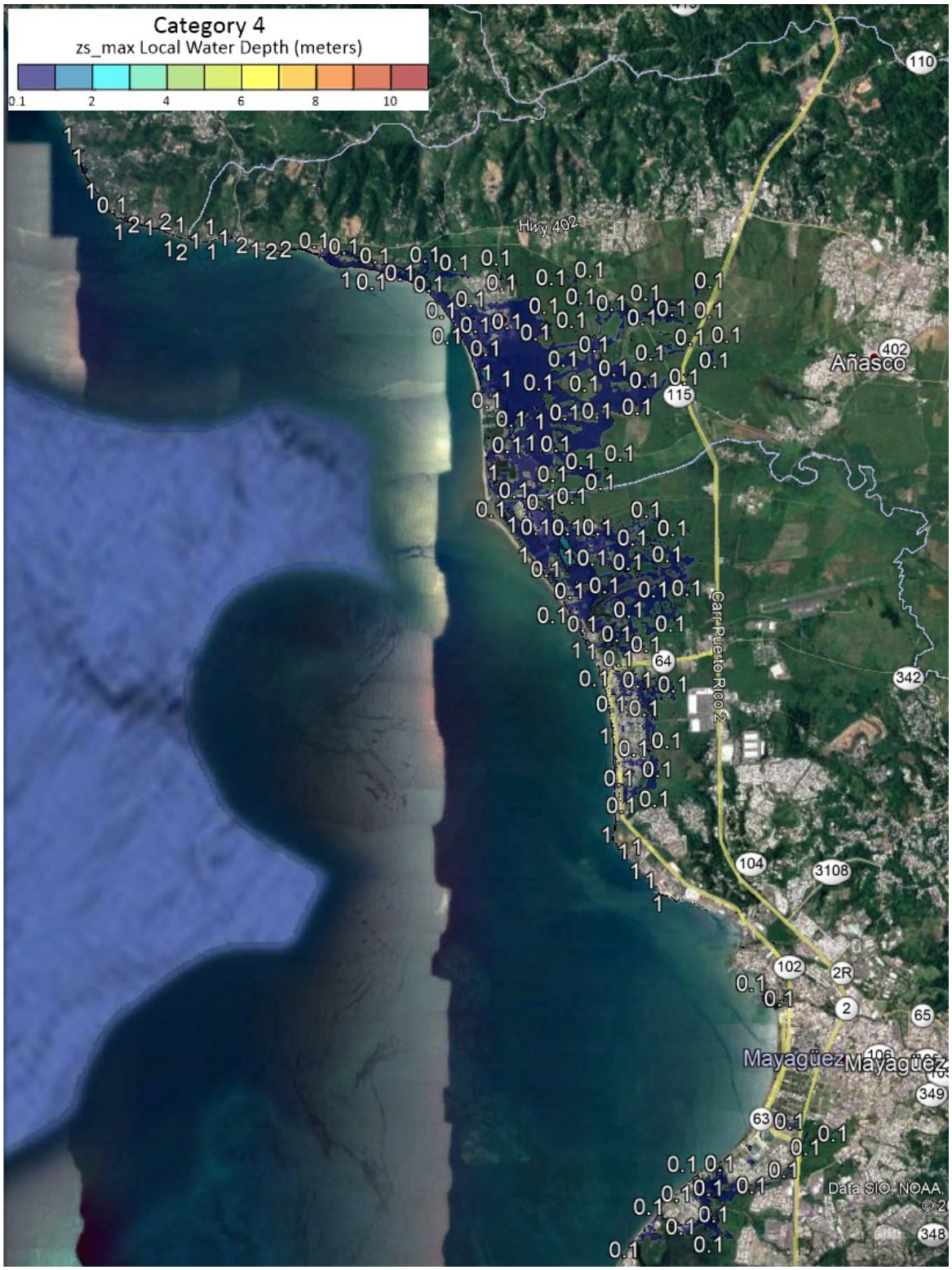

Figure 259 - Grid 25, category 4, maximum sea surface elevation (meters), relative to local terrain elevation, during 1 hour of simulation after spin up of 300 seconds. Waves propagating from the west.

GRID 25: CAT 5 (MAYAGUEZ TO RINCON)

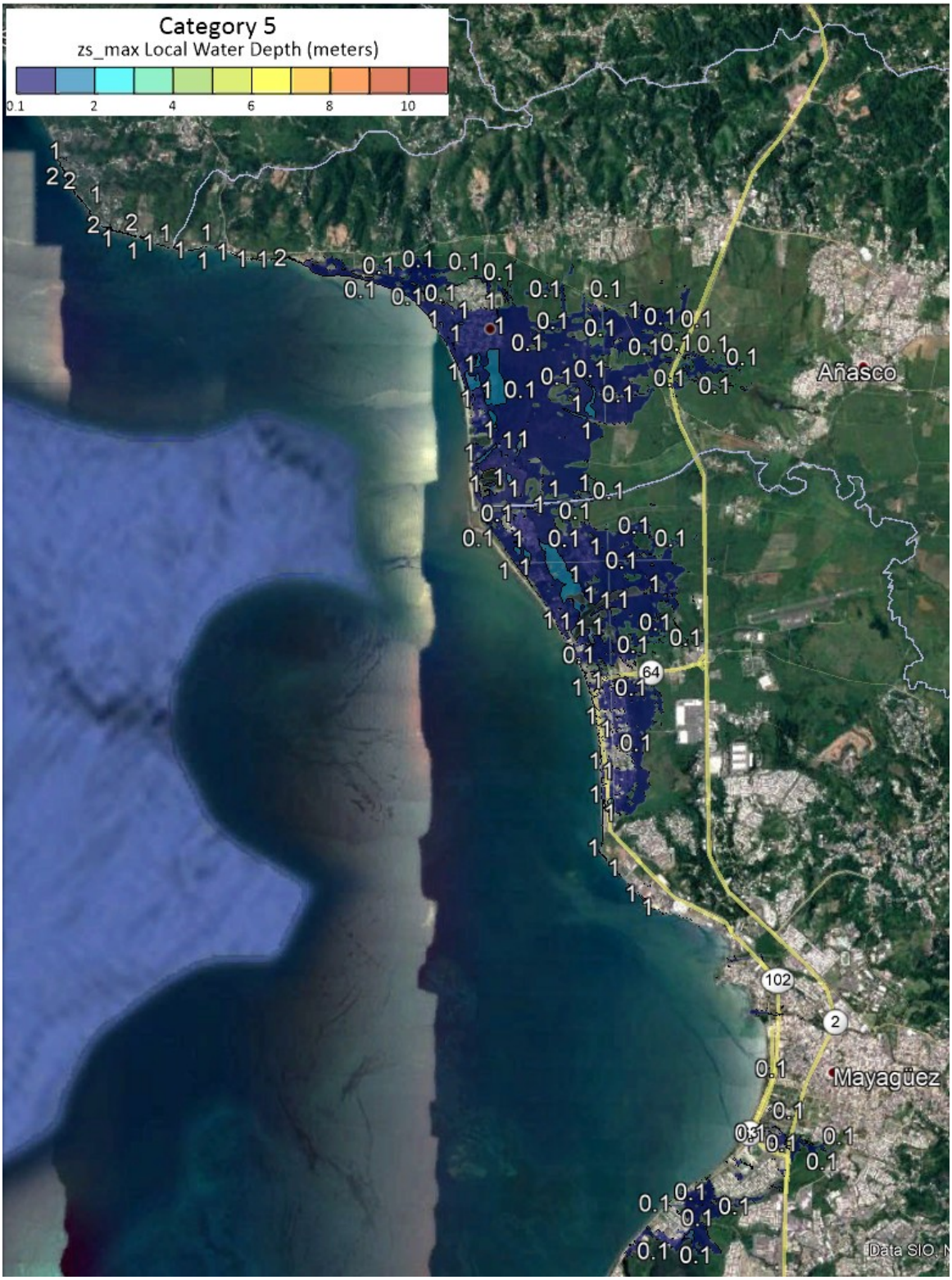

Figure 260- Grid 25, category 5, maximum sea surface elevation (meters), relative to local terrain elevation, during 1 hour of simulation after spin up of 300 seconds. Waves propagating from the west.

GRID 26: CAT 1 (RINCON TO AGUADA)

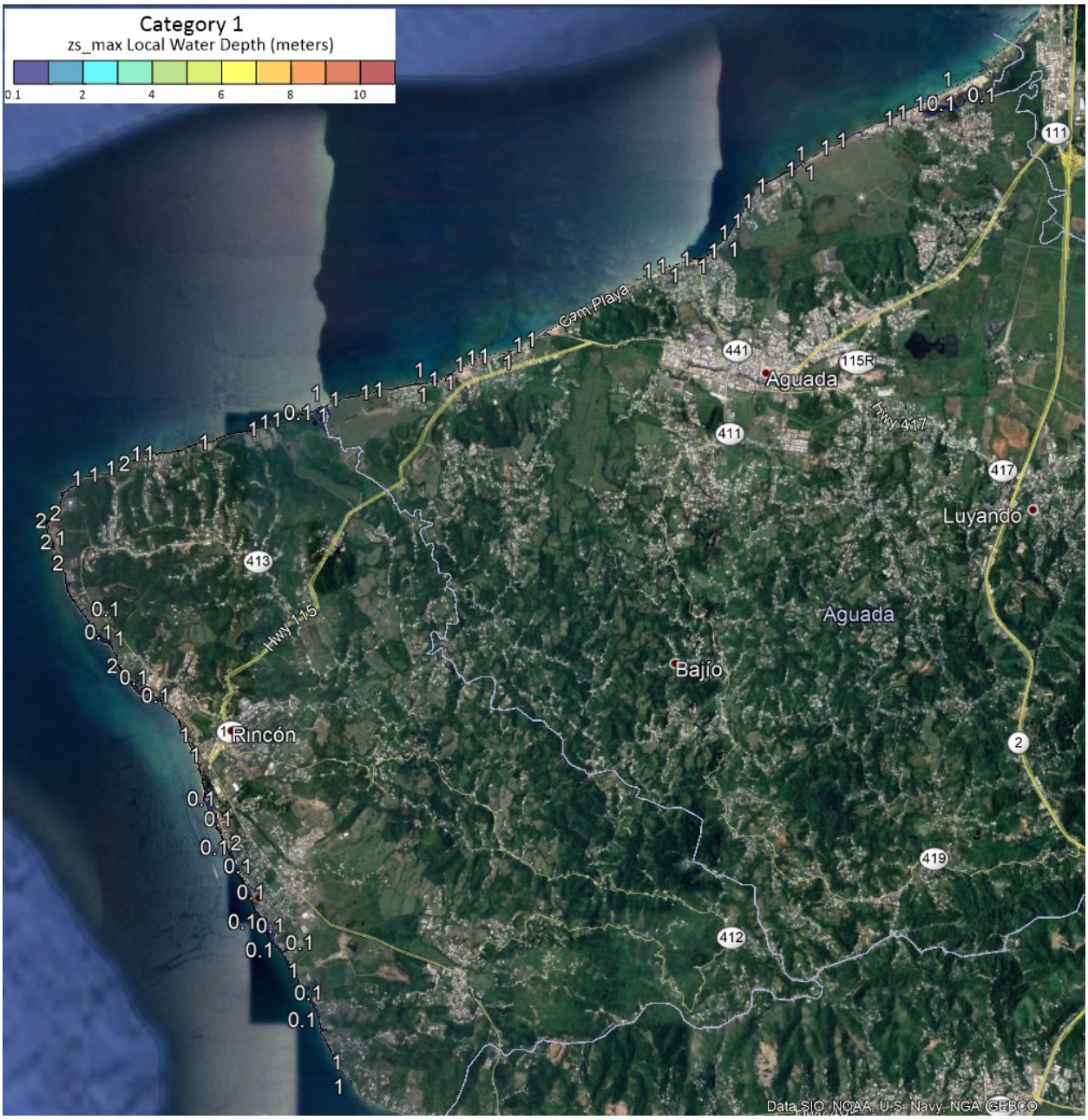

Figure 261 - Grid 26, category 1, maximum sea surface elevation (meters), relative to local terrain elevation, during 1 hour of simulation after spin up of 300 seconds. Waves propagating from the west.

GRID 26: CAT 2 (RINCON TO AGUADA)

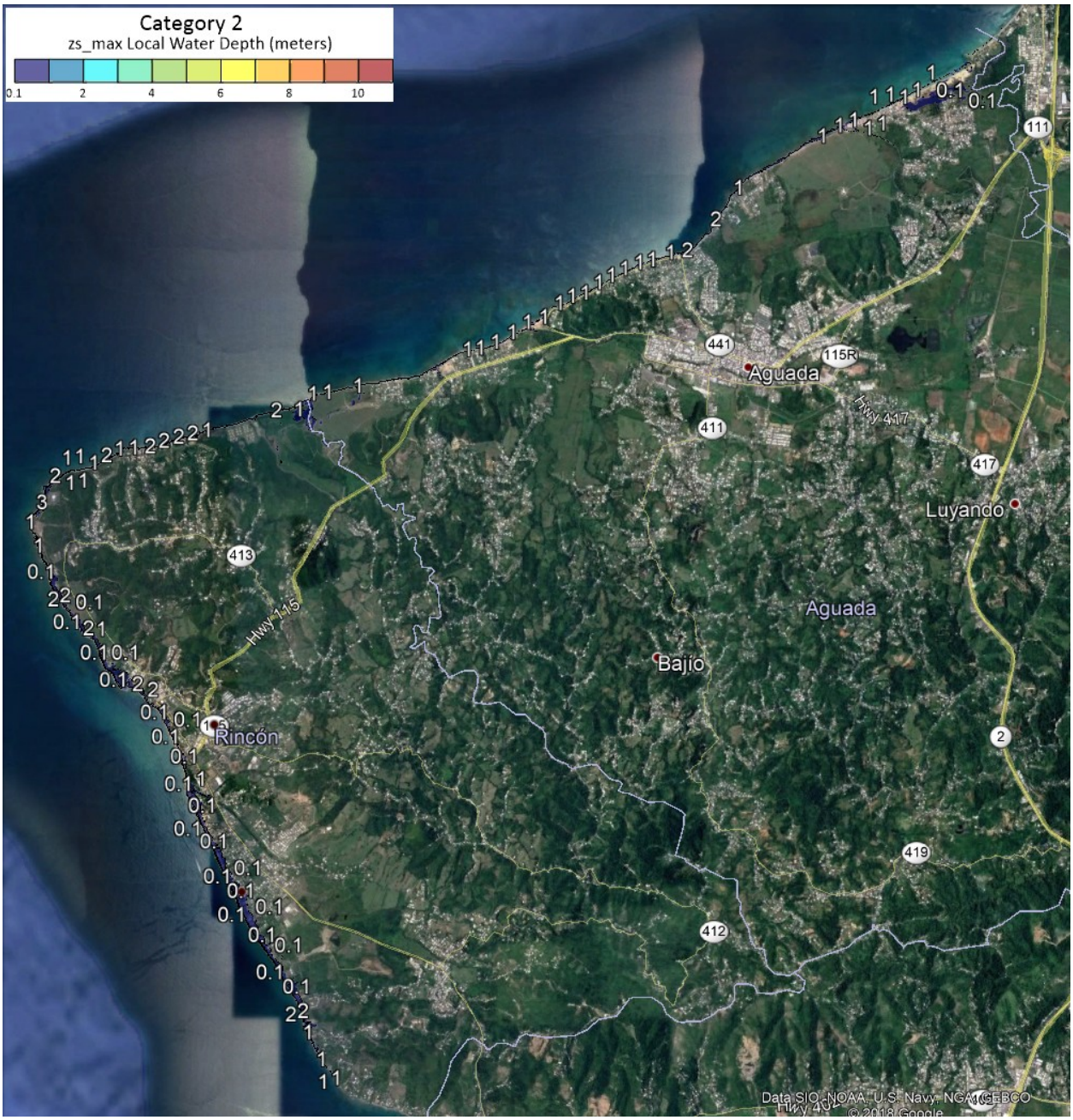

Figure 262 - Grid 26, category 2, maximum sea surface elevation (meters), relative to local terrain elevation, during 1 hour of simulation after spin up of 300 seconds. Waves propagating from the west.

GRID 26: CAT 3 (RINCON TO AGUADA)

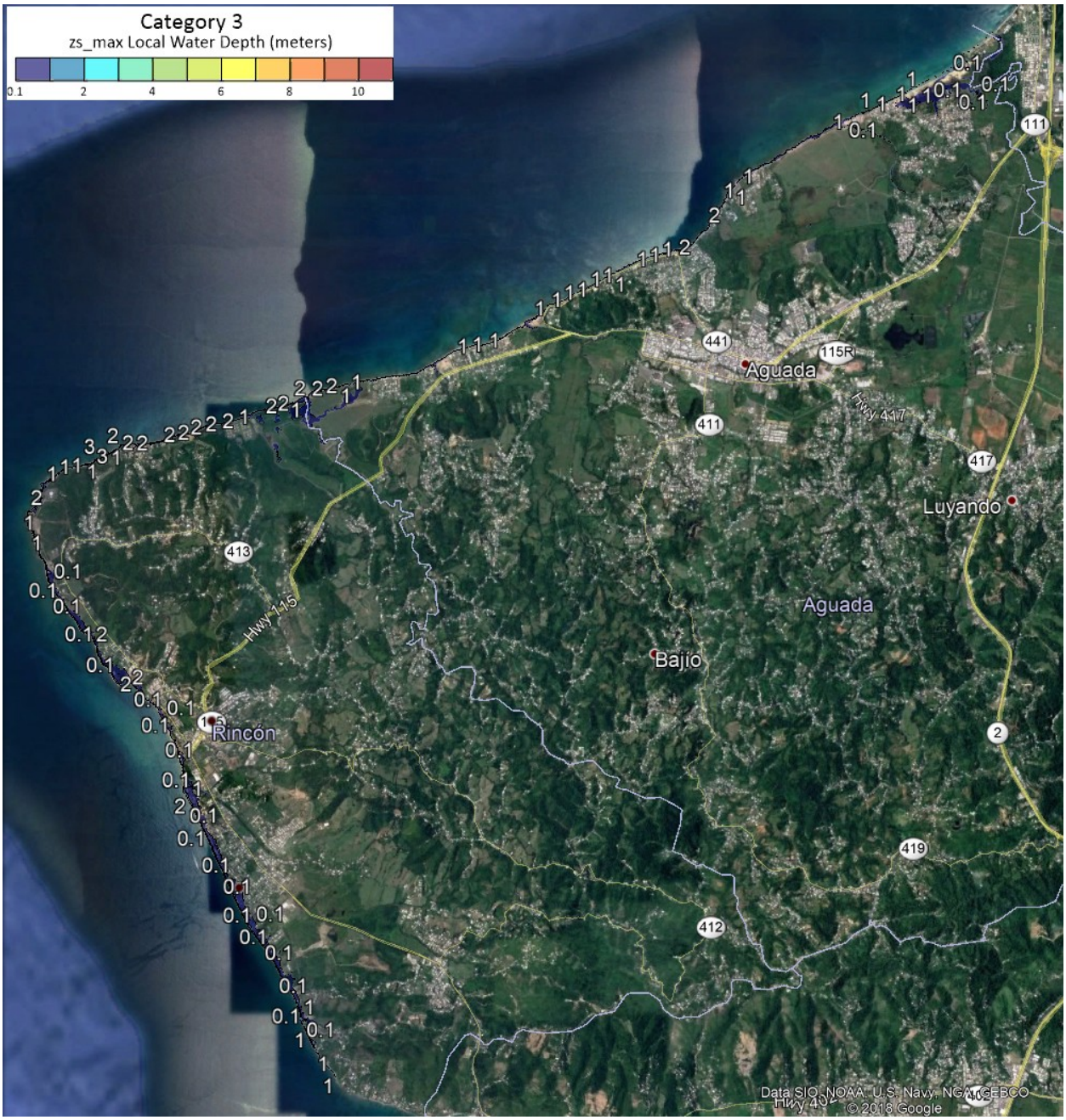

Figure 263 - Grid 26, category 3, maximum sea surface elevation (meters), relative to local terrain elevation, during 1 hour of simulation after spin up of 300 seconds. Waves propagating from the west.

GRID 26: CAT 4 (RINCON TO AGUADA)

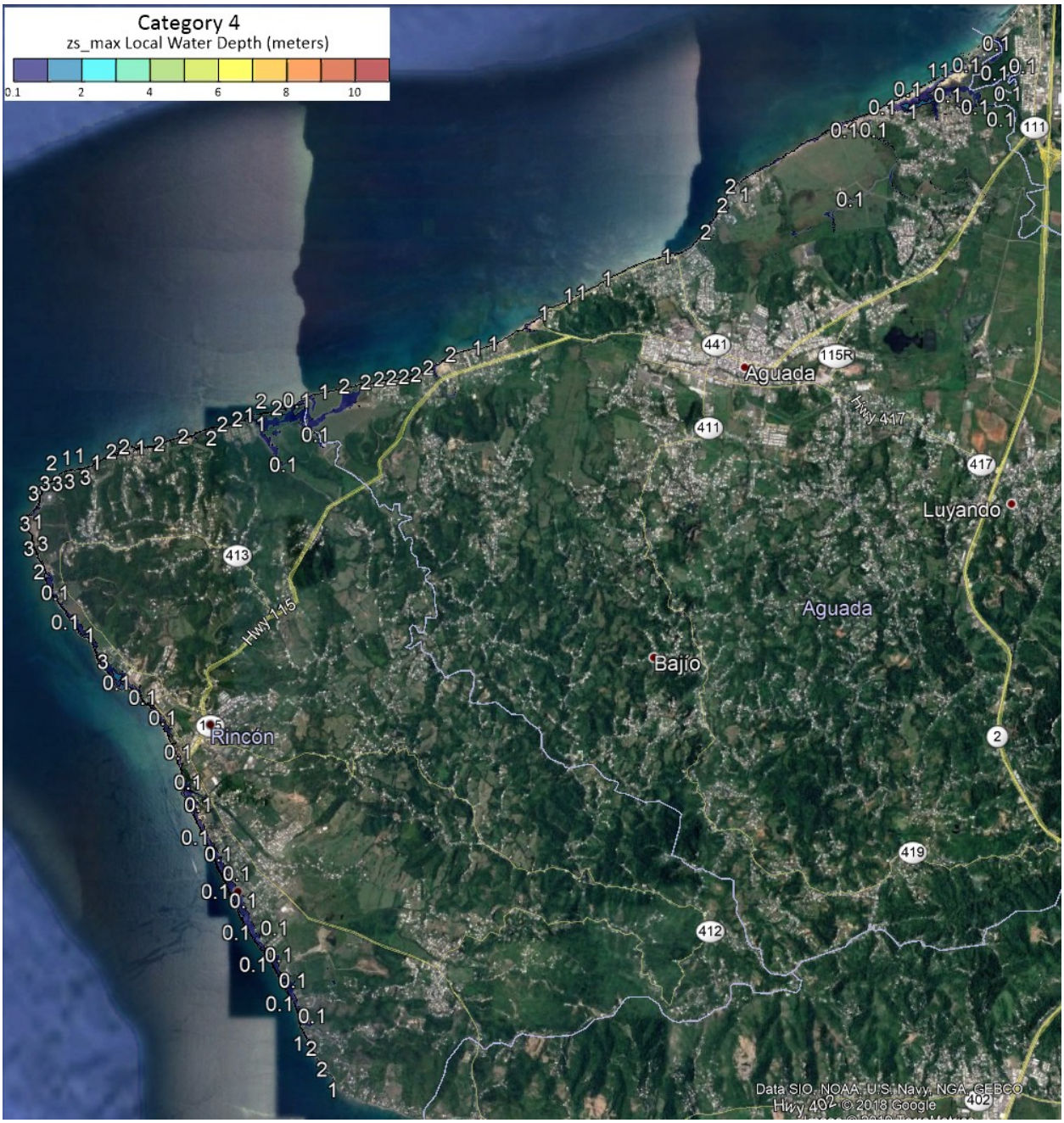

Figure 264 - Grid 26, category 4, maximum sea surface elevation (meters), relative to local terrain elevation, during 1 hour of simulation after spin up of 300 seconds. Waves propagating from the west.

GRID 26: CAT 5 (RINCON TO AGUADA)

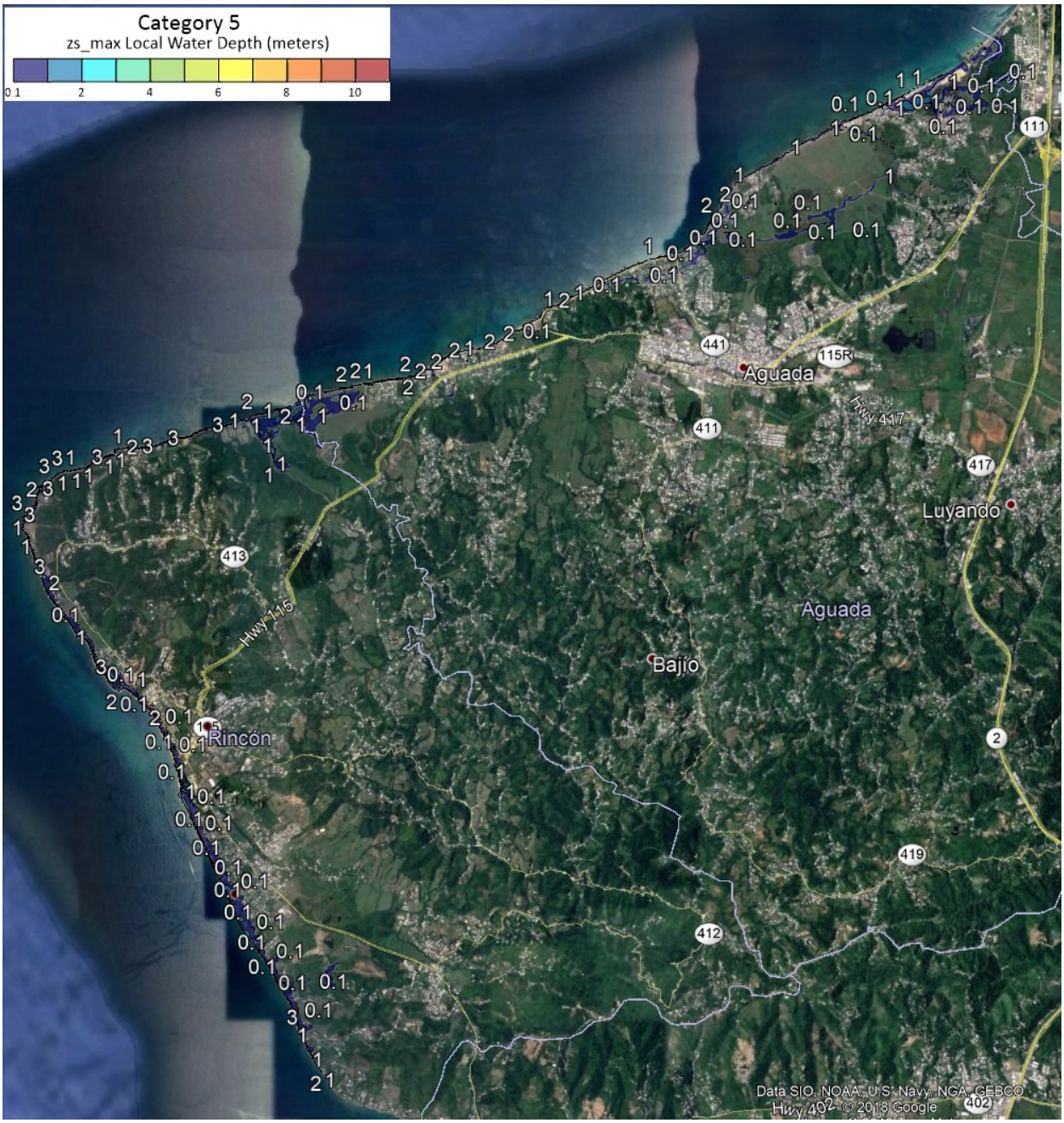

Figure 265 - Grid 26, category 5, maximum sea surface elevation (meters), relative to local terrain elevation, during 1 hour of simulation after spin up of 300 seconds. Waves propagating from the west.

GRID 27: CAT 1 (AGUADILLA)

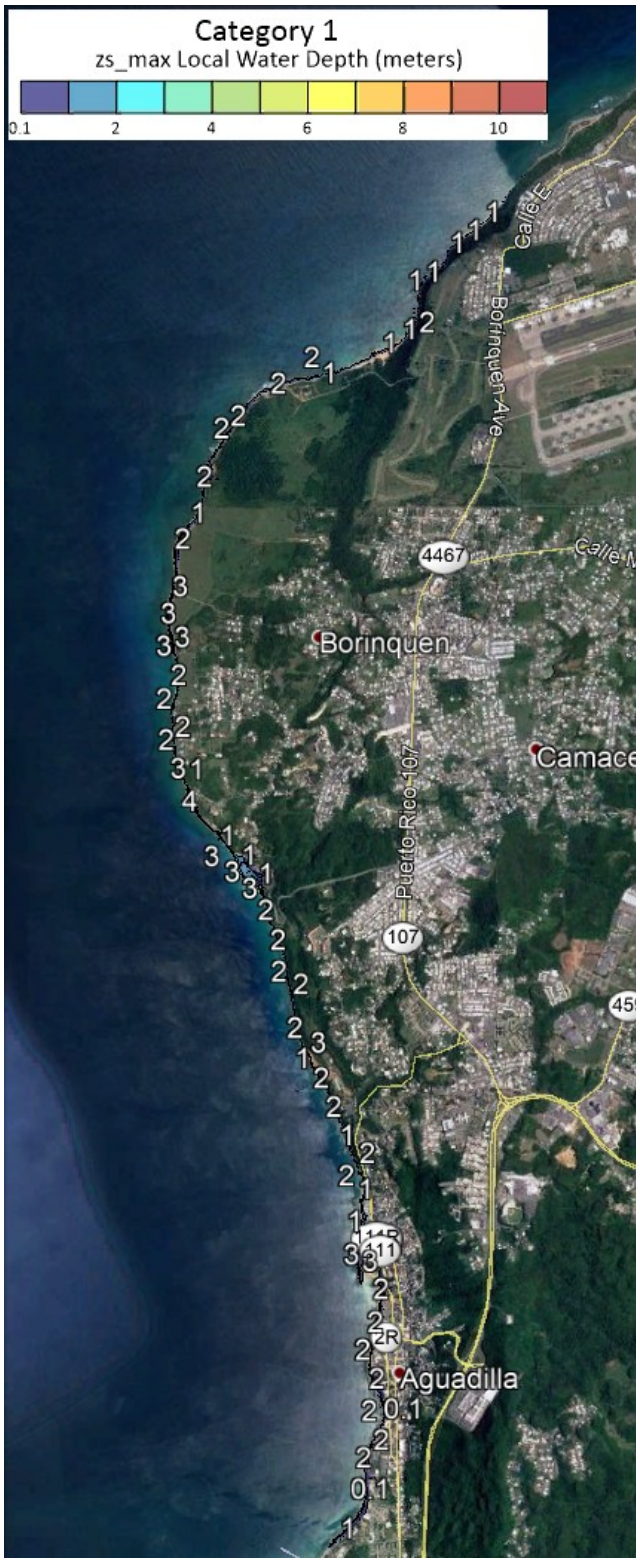

Figure 266 - Grid 27, category 1, maximum sea surface elevation (meters), relative to local terrain elevation, during 1 hour of simulation after spin up of 300 seconds. Waves propagating from the west.

GRID 27: CAT 2 (AGUADILLA)

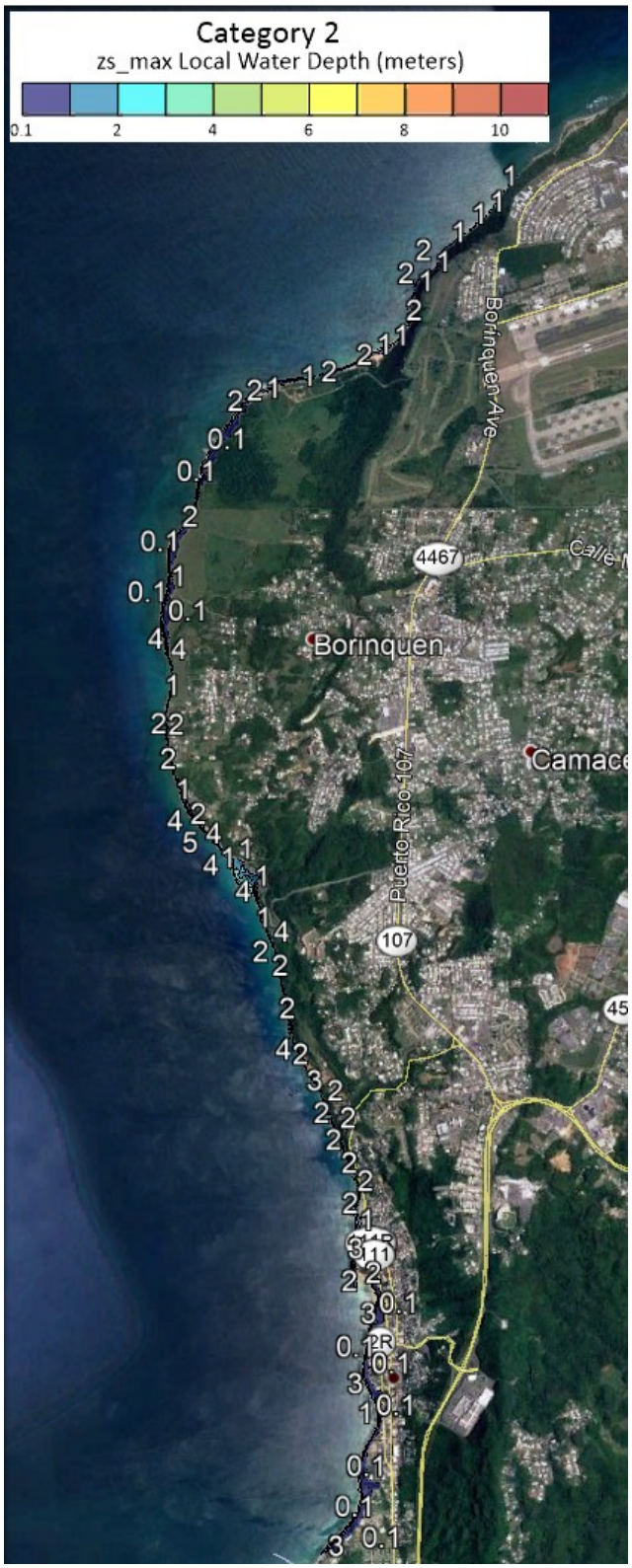

Figure 267 - Grid 27, category 2, maximum sea surface elevation (meters), relative to local terrain elevation, during 1 hour of simulation after spin up of 300 seconds. Waves propagating from the west.

GRID 27: CAT 3 (AGUADILLA)

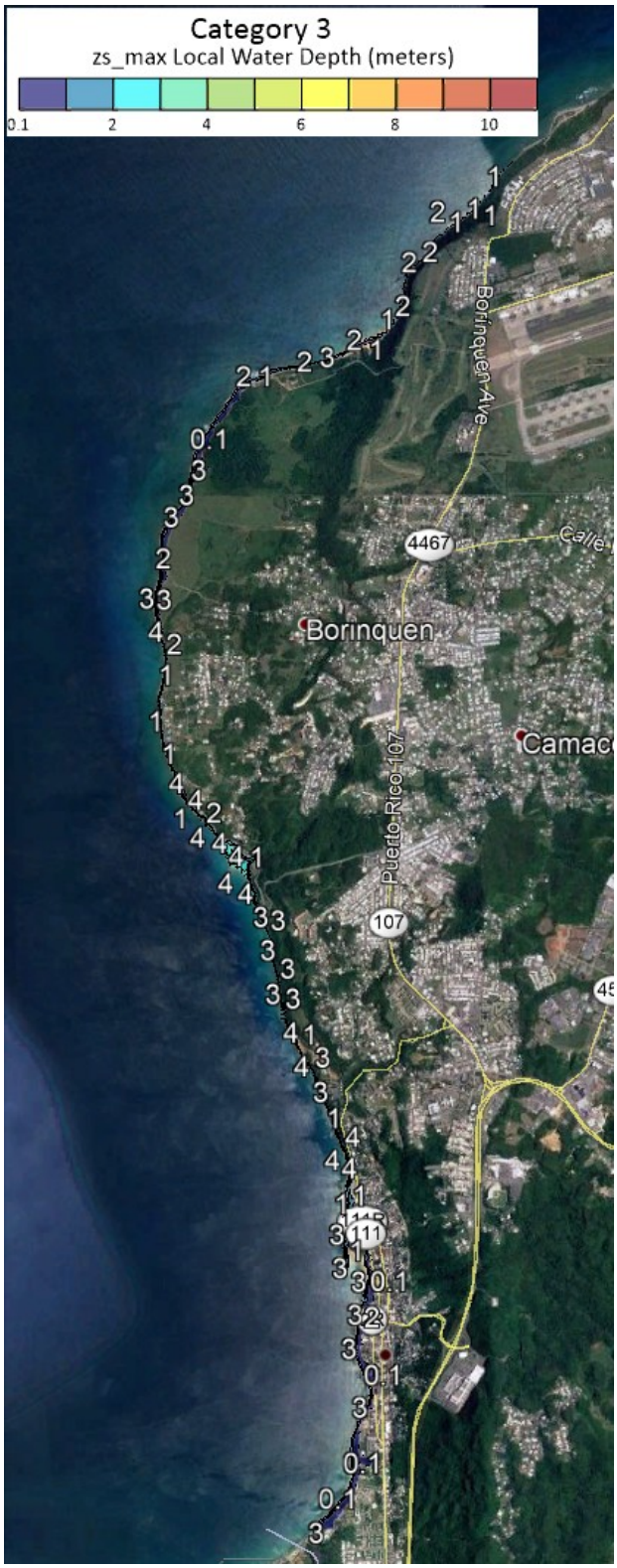

Figure 268 - Grid 27, category 3, maximum sea surface elevation (meters), relative to local terrain elevation, during 1 hour of simulation after spin up of 300 seconds. Waves propagating from the west.

GRID 27: CAT 4 (AGUADILLA)

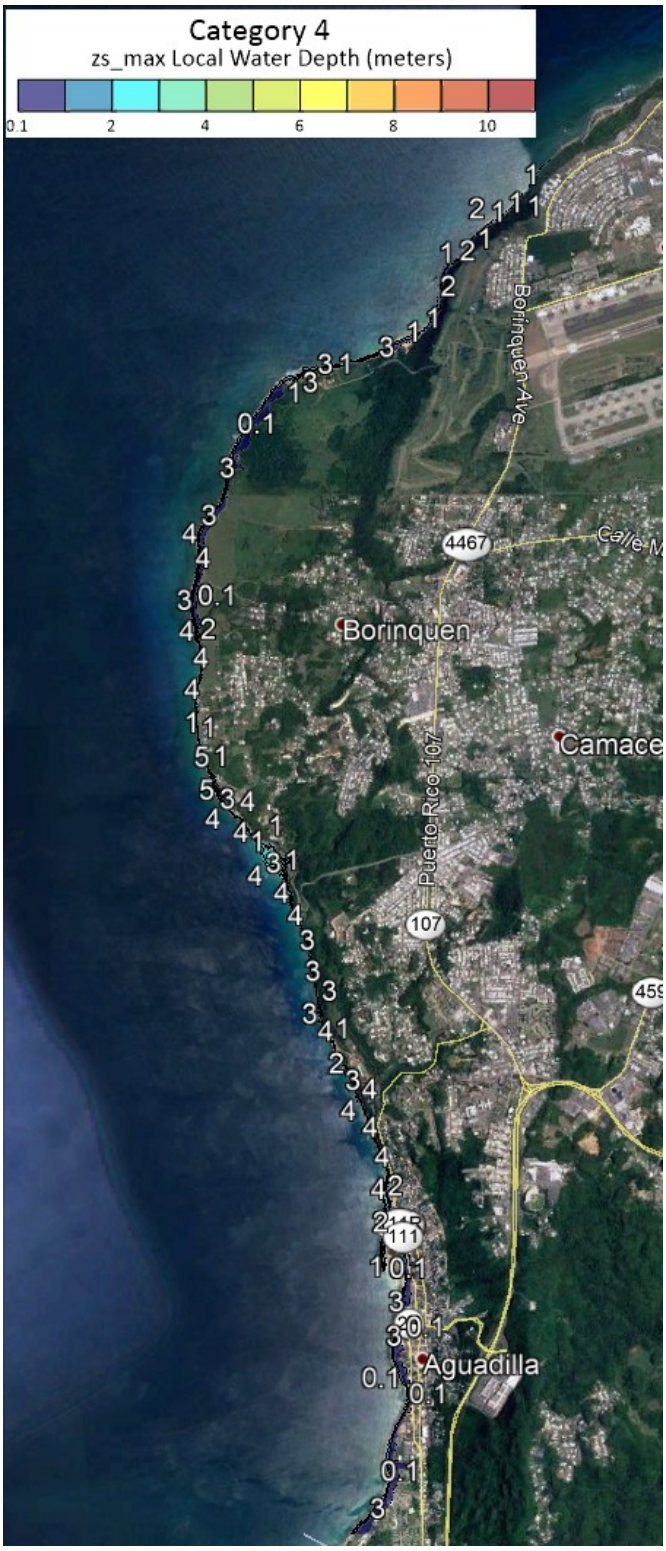

Figure 269 - Grid 27, category 4, maximum sea surface elevation (meters), relative to local terrain elevation, during 1 hour of simulation after spin up of 300 seconds. Waves propagating from the west.

GRID 27: 5 (AGUADILLA)

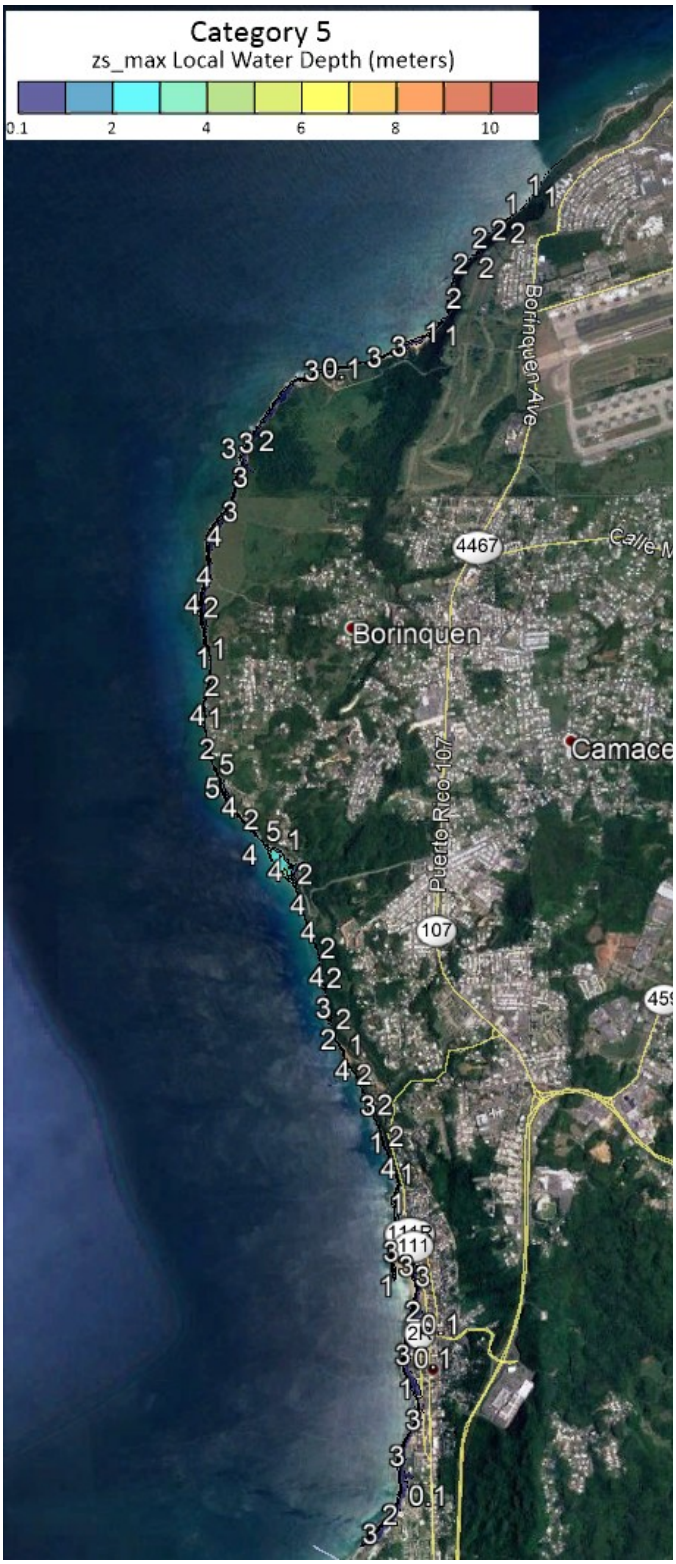

Figure 270 - Grid 27, category 5, maximum sea surface elevation (meters), relative to local terrain elevation, during 1 hour of simulation after spin up of 300 seconds. Waves propagating from the west.

RECOMMENDATIONS FOR FUTURE RESEARCH

1. Include in the modeling effort the effect of river discharge on the storm surge flooding near river mouths.
2. The availability of 1/9 arc seconds (approximately 3.33 meters) DEMs for a large portion of the north coast (see Figure 13) allowed us to model wave runup by high frequency waves (25 seconds, or smaller, periods) with a computational resolution of 3 meters for Grids 2 to 10. At this very high resolution it might be better to work with DEMs for which infrastructure is retained, but vegetation cover is eliminated. So that should be a next step.
3. Related with the above point, according to personal communication from the National Centers for Environmental Information, the 1/9 arc seconds DEMs (approximately 3 meters) will be extended for the rest of the island (besides the five boxes shown in Figure 13). Meanwhile what was done was to interpolate the 1/3 arc seconds resolution DEMs (approximately 10 meters) available for the rest of the island (Mayaguez, Fajardo, Guayama, and Ponce) to 1/9 arc seconds and prepare the computational grids based on that interpolation. It is acknowledged that this is not the best way of proceeding, but we think it is better than decreasing the resolution to 10 meters. When all of the island is available at 1/9 arc seconds the computations can be repeated, if so desired and funds are available.

ACKNOWLEDGMENTS

It is acknowledged the invaluable help provided by Mr. Carlos Andrade von Hillebrandt and Mr. Harry Justiniano. Without them this work would have taken much longer. Also Mr. Ernesto Diaz, Manager of the Puerto Rico Coastal Zone Management Program of NOAA. Finally, the support of Dr. Ernesto Diaz, director of the Department of Marine Sciences of the University of Puerto Rico at Mayaguez.

REFERENCES

Benítez, J. and A. Mercado, 2015. "Storm Surge Modeling in Puerto Rico in Support of Emergency Response, Risk Assessment, Coastal Planning and Climate Change Analysis'. Report prepared for the Caribbean Coastal Ocean Observing System (CariCOOS)/NOAA, University of Puerto Rico/Mayaguez, P.R. and the Puerto Rico Coastal Zone Management Program, Department of Natural and Environmental Resources, Puerto Rico.

Bertin, X., K. Li, A. Roland, Y. Zhang, J. F. Breilh, and R. Chaumillon, 2014. A modeling-based analysis of the flooding associated with Xynthia, central Bay of Biscay. Coastal Engineering, 94: 80-89.

Dietrich, J. C., S Tanaka, JJ Westerink, CN Dawson, RA Luettich, M Zijlema, LH Holthuijsen, JM Smith,

LG Westerink, HJ Westerink (2012). “Performance of the Unstructured-Mesh, SWAN+ADCIRC Model in Computing Hurricane Waves and Surge.” Journal of Scientific Computing, 52(2), 468-497, DOI:10.1007/s10915-011-9555-6.

Hoeke, R. K., K. L. McInnes and J. G. O’Grady, 2015. Wind and wave setup contributions to extreme sea levels at a tropical high island: a stochastic cyclone simulation study for Apia, Samoa. Journal of Marine Science and Engineering 3:1117-1135.

Kim, S. Y., T. Yasuda ad H. Mase, 2010. Wave set-up in the storm surge along open coasts during Typhoon Anita. Coastal Engineering 57: 631-642.

Moftakhari, H. R., A. AghaKouchak, B. F. Sanders, M. Allaire, and R. A. Matthew, 2018. What Is Nuisance Flooding? Defining and Monitoring an Emerging Challenge. Water Resources Research, 54: 4218–4227. https://doi.org/10.1029/2018WR022828

Rahdarian, A. and M. H. Niksokhan, 2017. Numerical modeling of storm surge attenuation by mangroves in protected area of mangroves of Qheshm Island. Ocean Engineering, 145: 304-315.

Soloviev, A., V., R. Lukas, M. A. Donelan, B. K. Haus, and I. Ginis, 2017. Is the state of the air-sea interface a factor in rapid intensification and rapid decline of tropical cyclones? J. Geophys. Res., 122:10,174-10,183. doi:10.1002/2017JC013435.

APPENDIX I

In this appendix we will present the input parameter files (PARAMS.TXT) used for all computer runs. It will be presented as a separate volume.